ON INVESTIGATION OF CONTACT MODELS IN DEM SIMULATION OF ROCKFALLS

by

Houshin Nejati

A Thesis

in

The Department

of

Building, Civil, and Environmental Engineering

Presented in Partial Fulfillment of the Requirements
for the Degree of Master of Applied Science (Civil Engineering) at
CONCORDIA UNIVERSITY
Montreal, Quebec, Canada

July, 2008

Your file Votre référence
ISBN: 978-0-494-42489-6
Our file Notre référence
ISBN: 978-0-494-42489-6

Abstract

On Investigation of Contact Models in DEM Simulation of Rockfalls

Houshin Nejati

Simulation of rockfall allows us to protect infrastructures and forests along rock slopes against the impacts of rockfall. In this thesis, a computer program based on 3D Discrete Element Method (DEM) is developed by the author for rockfall simulation and fundamental investigation of physics of a rockfall event. Each rock is modeled as a sphere and impact surfaces are generated by numbers of 3D triangles.

Contacts in DEM between objects are modeled using a mass-damper model. Different contact models of DEM produce different contact stiffnesses for springs and therefore different contact forces. Since contact forces have essential effect on dynamic behaviour of particles; hence a comparative study is performed to investigate the effect of each contact model on dynamic of rocks contacts. The five chosen contact models are: linear model, Hertz-Mindlin, Ng model, elastic-inelastic power function model and combination of Hertz model and Ng model (Hertz-Ng model).

Energy in linear, Hertz-Mindlin, Hertz-Ng and Ng model is dissipated using linear normal and shear dashpots. Also, the coefficient of restitution is a concept that defines the energy level of a rock after contact with a surface. To relate the concept of coefficient of restitution and damping ratio for each contact model, the correlations of damping ratio and coefficient of restitution are determined for contact of a spherical rock and horizontal wall as well as the correlation of coefficient of restitution and damping ratio for sloped walls for linear contact model.

An has developed a 2D elastic-inelastic power function for modeling of normal contact of rocks and surfaces. In this research, 3D modeling of this contact model is produced, and the effects of the input parameters on dynamic behaviours of a rock are studied and the correlation between transition force and coefficient of restitution is determined.

Finally, for a 3D slope, a sensitivity analysis is performed and the effect of seven input parameters on horizontal travel distance of a rock is investigated.

ACKNOWLEGMENTS

ARISE, oh Cup-bearer, rise! And bring
To lips that are thirsting the bowl they praise,
For it seemed that love was an easy thing,
But my feet have fallen on difficult ways.
Hafez Shirazi (14th century), translation by G. Bell (19th century).

My Passionate for science started when I was just four years. I was impressed with a movie of Marie Curie's life (Nobel 1911, Laureate in Chemistry), afterward I told myself "I am going to be a scientist ". This dream never left me and lead me the way (path of the love), which was not easy but full of joy and adventure.

This thesis has been written with help, advice and moral support of many people whom I am greatly in dept:

I would like to thank my supervisor Dr. A. M. Zsaki who provided the initial idea for this thesis and for his trust to giving me freedom to try my ideas. Also I would like to express my gratitude to members of my committee, Dr. Ramamurthy, Dr. Pekau, Dr. Galal and Dr. Paraschivoiu.

I would like to thank my friends Zahra Fakhraai and Sina Valadkhan for their continuous friendships, without their helps I could not come and live in Canada. My special thanks to Hojjat Izadi for his continuous friendship and support during my Masters. Without whom this thesis would not possible. I would like to thank Parham Ashayer for his valuables advices which open my eyes to this filed.

I would like to thank my friends, who accompanied me to succeed during the hard periods. I would like to thank Ronak Mosaivi Zanani, Hoori Moghbeli, Elham Yektaee, Toba Yektaee, Marilyn Trudel, Celest Flores, Kamyar Gordnian, François M. Nadeau, Hoda Moteshafi , Ali Azimi, Hossein Azzimi and Bhasker Dubey.

Finally, I wish to thank my mother Marzie Hosseini, my Father Mehdi Nejati, my brothers Ali and Amin and my sister Ila. Without their life time love, supports and encouragements, I had nothing in my life. They had essential roles in every single minute of my life. I believe, words are not capable to express my love and thankfulness to them and I never can thank enough.

This thesis is dedicated to my mother·

TABLE OF CONTENTS

LIST OF TABLES V

LIST OF FIGURES VI

LIST OF APPENDICES XII

LIST OF SYMBOLS XIII

1. INTRODUCTION AND OUTLINE 1

1.1. NATURAL FACTORS FOR OCCURRENCE OF A ROCKFALL EVENT 2

1.2. NUMERICAL ANALYSIS OF ROCKFALL 3

1.3. OBJECTIVES 4

1.4. ORGANIZATION OF THE THESIS 6

2. REVIEW OF CONTACT MECHANICS 9

2.1. COEFFICIENT OF RESTITUTION 10

2.1.1. Coefficient of Restitution Scaling in Rockfall Simulation *12*

2.2. REVIEW OF HERTZ AND MINDLIN STUDIES FOR CALCULATION OF CONTACT FORCES . 13

2.2.1. Tangential Contact Force *15*

2.3. DISCRETE ELEMENT METHOD (DEM) 18

2.4. INTRODUCTION TO LINEAR, HERTZ-MINDLIN, NG, HERTZ-NG, AN AND MODIFIED DISCRETE ELEMENT MODEL (MDEM) CONTACT MODELS FOR APPLICATION IN DEM SIMULATION 20

2.4.1. Contact Stiffness in Linear Model *20*

2.4.2. Contact Stiffness in Hertz- Mindlin Contact Model *21*

2.4.3. Viscous Damping for Linear and Hertz-Mindlin Model *22*

2.4.4. Ng Model *24*

2.4.5. Hertz-Ng Model *25*

2.4.6. Elastic-Inelastic Power Function Contact Model (An Model) *26*

2.4.7. Modified Discrete Element Model (MDEM) *32*

3. REVIEW OF CURRENT APPROACHES FOR SIMULATION OF ROCKFALL 34

3.1. CALCULATION PROCEDURE IN ROCFALL 35

3.2. COEFFICIENT OF RESTITUTION IN ROCFALL 38

3.3. DISCRETE ELEMENT METHOD FORMULATION 38

3.3.1. Calculating Time Step *38*

3.3.2. Detection of Contacts *41*

3.3.3. Calculation of Contact Forces (Force-Displacement Law) *43*
3.3.4. Law of Motion *46*
3.4. COMPARISON ROCFALL ALGORITHM AND A PROGRAM BASED ON DEM 48

4. HARAZ: OVERVIEW AND DETAILS 50

4.1. CALCULATION CYCLE 50
4.1.1. Generation of Balls *50*
4.1.2. Ball's Initial Conditions *51*
4.1.3. Generation of Walls *51*
4.1.4. Determination of the Time Step *53*
4.1.5. Force-Displacement Law *53*
4.2. NEWTON'S SECOND LAW OF MOTION 61

5. NONLINEAR NORMAL AND SHEAR STIFFNESS FOR DIFFERENT ROCK TYPES 63

5.1. HERTZ – MINDLIN MODEL 64
5.2. NG NORMAL AND SHEAR STIFFNESS FOR DIFFERENT ROCK TYPES 67
5.3. HERTZ-NG MODEL 70
5.4. SUMMARY 73

6. INFLUENCE OF THE CONTACT MODELS ON DYNAMIC RESPONSES OF FALLING BALL ON A HORIZONTAL WALL 74

6.1. COMPARISON OF CONTACT MODELS 74
6.2. THE EFFECT OF VISCOUS DAMPING ON BALL MOTION 80
6.2.1. Ball's Motion *81*
6.2.2. Ball's Velocity *83*
6.2.3. Contact Normal Force *86*
6.2.4. Normal Displacement (Overlap) *91*
6.2.5. Force–Displacement Relation *96*
6.3. COEFFICIENT OF RESTITUTION 99
6.4. COMPARING THE BALL'S MOTION IN HARAZ AND ROCFALL 103
6.5. SUMMARY 104

7. STUDY OF 3D ELASTIC-INELASTIC POWER FUNCTION CONTACT MODEL AND COMPARISON WITH OTHER CONTACT MODELS 106

7.1. THE EFFECT OF THE EXPONENT (b) ON MOTION OF BALL 106
7.2. THE EFFECT OF THE TRANSITION FORCE ON THE MOTION 108

7.3. The Effect of Transition Force and Exponent on Coefficient of Restitution 113
7.4. Comparison of Elastic-Inelastic Power Function Model and Other Contact Models 115
7.5. Summary 117
8. COEFFICIENT OF RESTITUTION OF SLOPES USING LINEAR MODEL 119
8.1. Coefficient of Restitution for a 120 Degree Slope Angle (slope ratio -1:1.73) 121
8.2. Coefficient of Restitution for a 135 Degree Slope Angle (slope ratio -1:1) 124
8.3. Summary 128
9. ESTIMATION OF THE HORIZONTAL TRAVEL DISTANCE OF A ROCK USING ARTIFICIAL NEURAL NETWORKS (ANN) 129
9.1. Intelligent Modeling 132
9.1.1. Basics of Artificial Neural Network 132
9.1.2. Artificial Neural Network Based Approximation 133
9.2. Sensitivity Analysis Based on Neural Network Model 134
9.3. Summary 139
10. SUMMARY AND RECOMMENDATIONS FOR FURTHER RESEARCH 140
10.1. Conclusion 140
10.2. Future Work 143
APPENDIX 1 145
Inroduction to Computer Program "Haraz" 145
List of Input and Output Files in Haraz 146
Data 146
Wallpoints 147
Wallstiffness 148
Points 149
Location_out 149
Force_out.txt 149
Fn_Un_wall.txt 150
Contact_velocity.txt 150
APPENDIX 2 151
List of Samples for Estimation of Horizontal Travel Distance of a Rock 151
APPENDIX 3 155

MATLAB CODE FOR ARTIFICIAL NEURAL NETWORK 155

REFERENCES 160

LIST OF TABLES

TABLE 1-1: CLASSIFICATION OF THE WIDESPREAD ROCKFALL CAUSES (AND, MORE GENERALLY SLOPE MOVEMENT CAUSES) [15]. 2
TABLE 1-2: NUMERICAL METHODS OF ANALYSIS [14,16] 4
TABLE 2-1: TRANSITION FORCE FOR VARIOUS PARTICLE SIZE SAMPLES AT DIFFERENT NORMAL STIFFNESS [20]. 28
TABLE 3-1: DIFFERENT COMPUTER SIMULATION FOR ROCKFALLS CATEGORIZED BASED ON THEIR MAIN CHARACTERISTICS, AFTER GUZZETTI ET AL. (2002) [11]. 34
TABLE 5-1: PROPERTIES OF SOME ROCK TYPES [40]. 63
TABLE 5-2: INPUTS FOR THE MODEL. 64
TABLE 5-3: THE RATIO OF MAXIMUM NORMAL STIFFNESS TO SHEAR STIFFNESS 64
TABLE 5-4: THE RATIO OF MAXIMUM NORMAL STIFFNESS TO SHEAR STIFFNESS USING 68
TABLE 5-5: RATIO OF MAXIMUM NORMAL STIFFNESS TO SHEAR STIFFNESS 71
TABLE 6-1: INPUTS FOR THE MODEL. 74
TABLE 6-2: WALL STIFFNESS OF HORIZONTAL WALL. 75
TABLE 6-3: INPUTS OF SIMULATION 80
TABLE 6-4: THE VALUES OF VISCOUS DAMPING RATIO FOR CONTACT OF A BALL AND A WALL WITH DIFFERENT MATERIALS. 100
TABLE 7-1: THE INPUTS FOR MODEL A SYSTEM OF A BALL AND A HORIZONTAL WALL. 109
TABLE 7-2: COEFFICIENT OF RESTITUTION FOR SOME WALL'S MATERIAL. 114
TABLE 7-3: COEFFICIENT OF RESTITUTION FOR SOME WALL 115
TABLE 8-1: INPUTS FOR THE MODEL. 119
TABLE 8-2: COEFFICIENT OF RESTITUTION WITH RESPECT TO "Z" FOR DIFFERENT DAMPING RATIO FOR A 120 DEGREE SLOPE. 122
TABLE 8-3: COEFFICIENT OF RESTITUTION FOR DIFFERENT DAMPING RATIO FOR HORIZONTAL WALL. 124
TABLE 8-4: COEFFICIENT OF RESTITUTION WITH RESPECT TO "Z" FOR DIFFERENT DAMPING RATIO FOR A 135 DEGREE SLOPE. 126
TABLE 8-5: COEFFICIENT OF RESTITUTION FOR DIFFERENT DAMPING RATIO FOR A HORIZONTAL WALL AFTER A 135 DEGREE SLOPE. 127

LIST OF FIGURES

FIGURE 2.1: DEFORMATION DURING THE IMPACT [21]. 9
FIGURE 2.2: THE VARIATION OF COEFFICIENT OF FRICTION VERSUS INITIAL TANGENTIAL VELOCITY [21] 10
FIGURE 2.3: RELATION BETWEEN SCALING FACTOR AND IMPACT VELOCITY [20]. 13
FIGURE 2.4: TWO SPHERES IN NORMAL CONTACT [28]. 13
FIGURE 2.5: CONTACT AREA AND HERTZ PRESSURE. (A) CIRCULAR CONTACT-AREA (VIEWED FROM +Z).SECTION B-B IS CONTACT-AREA DIAMETER. (B) HERTZ NORMAL PRESSURE AT SECTION B-B [28]. 14
FIGURE 2.6: TWO FRICTIONAL SPHERES SUBJECTED TO NORMAL FORCES [28]. 16
FIGURE 2.7: SLIP REGION AND TANGENTIAL STRESS DISTRIBUTION. (A) ANNULUS OF SLIP. SECTION A-A IS ALIGNED WITH A CONTACT-AREA DIAMETER. (B) TANGENTIAL STRESS ON THE CONTACT-AREA, AT SECTION A-A [29]. 16
FIGURE 2.8: SCHEMATIC DIAGRAM ILLUSTRATING DEM AND FEM ANALOGY. (A) ELEMENTS AND NODES (FEM). (B) PARTICLES AND CONTACTS [38]. 19
FIGURE 2.9: THE VOIGT-KELVIN ELEMENT CONSISTS OF A SPRING AND A DASHPOT (DAMPER) CONNECTED IN PARALLEL [11]. 19
FIGURE 2.10: ELASTIC-INELASTIC POWER FUNCTION MODEL [20] 26
FIGURE 2.11: DIFFERENT FORMS OF ELASTIC-INELASTIC POWER FUNCTION MODEL [20]. 28
FIGURE 2.12: TRANSITION FORCE VS. PARTICLE RADIUS (MODELS WITH VARIOUS NORMAL STIFFNESS) [20]. 29
FIGURE 2.13: EXPONENT VS. IMPACT VELOCITY AND VARIOUS RADII [20]. 29
FIGURE 2.14: SCHEMATIC OF ENERGY DISSIPATION OF ELASTIC-PERFECTLY PLASTIC POWER FUNCTION MODEL [20]. 30
FIGURE 2.15: COEFFICIENT OF NORMAL RESTITUTION VERSUS EXPONENT FOR VARYING AMOUNTS OF INELASTIC DEFORMATION [20]. 31
FIGURE 2.16: SCALING FACTOR FOR COEFFICIENT OF NORMAL RESTITUTION (AS v_i INCREASES R_n DECREASES) [20]. 32
FIGURE 2.17: NORMAL AND TANGENTIAL MODULES IN MODIFIED DEM (MDEM) [11]. 32
FIGURE 3.1: CALCULATION OF CRITICAL TIME FOR MULTIPLE MASS-SPRING SYSTEM [18]. 40
FIGURE 3.2: COLLISION NOTATION (A): BALL-WALL CONTACT. (B): BALL-WALL CONTACT [18]. 42
FIGURE 4.1: FLOWCHART REPRESENTATION OF MAIN BLOCK IN HARAZ. 52

FIGURE 4.2: FLOWCHART REPRESENTATION OF FUNCTION CFORCE: CALCULATION OF CONTACT FORCES BETWEEN TWO BALLS. 54
FIGURE 4.3: FLOWCHART REPRESENTATION OF FUNCTION CFORCE_WALL: CALCULATION OF CONTACT FORCES BETWEEN A BALL AND A TRIANGLE. 55
FIGURE 4.4: FLOWCHART REPRESENTATION OF CALCULATION HERTZ-MINDLIN NORMAL FORCES. 56
FIGURE 4.5: FLOWCHART REPRESENTATIONS OF HERTZ-MINDLIN SHEAR STIFFNESS. 56
FIGURE 4.6: FLOWCHART REPRESENTATION OF CALCULATION OF NG NORMAL AND SHEAR STIFFNESS. 57
FIGURE 4.7: FLOWCHART REPRESENTATION OF CALCULATION OF POWER FUNCTION FORCES ("AN" NORMAL CONTACT FORCES). 58
FIGURE 4.8: FLOWCHART REPRESENTATION OF CALCULATION OF VISCOUS DAMPING FORCES. 59
FIGURE 4.9: NORMAL UNIT VECTOR IN BALL-WALL CONTACT [18]. 60
FIGURE 4.10: FLOWCHART REPRESENTATION OF CALCULATION OF THE SHORTEST DISTANCE BETWEEN A BALL AND A TRIANGLE. 61
FIGURE 4.11: FLOWCHART REPRESENTATION OF COMPUTE NEW POSITION OF AN OBJECT USING THE LAW OF MOTION. 62
FIGURE 5.1: THE NORMAL STIFFNESS PRODUCED BY HERTZ-MINDLIN MODEL FOR DIFFERENT ROCK TYPES. 65
FIGURE 5.2: THE SHEAR STIFFNESS PRODUCED BY HERTZ-MINDLIN MODEL FOR DIFFERENT ROCK TYPES. 65
FIGURE 5.3:THE VARIATION OF NORMAL CONTACT FORCE VERSUS TIME. 66
FIGURE 5.4: THE VARIATION OF NORMAL CONTACT FORCE VERSUS NORMAL DISPLACEMENT. 67
FIGURE 5.5: THE VARIATION OF NG NORMAL STIFFNESS VERSUS TIME FOR DIFFERENT ROCK TYPES. 68
FIGURE 5.6: THE VARIATIONS OF NG SHEAR STIFFNESS VERSUS TIME FOR DIFFERENT MATERIAL. 69
FIGURE 5.7: THE VARIATION OF NG NORMAL FORCES VERSUS TIME DURING FIRST CONTACT. 69
FIGURE 5.8: THE VARIATION OF NG NORMAL FORCES VERSUS NORMAL DISPLACEMENT FOR DIFFERENT ROCK TYPES. 70
FIGURE 5.9: THE VARIATION OF HERTZ-NG CONTACT NORMAL FORCES VERSUS TIME FOR DIFFERENT ROCK TYPES. 71
FIGURE 5.10: THE VARIATIONS OF HERTZ-NG SHEAR STIFFNESS VERSUS TIME FOR DIFFERENT ROCK TYPES. 72

FIGURE 5.11: THE VARIATION OF NORMAL CONTACT FORCES VERSUS NORMAL DISPLACEMENT FOR DIFFERENT ROCK TYPES. 72
FIGURE 6.1 : CONFIGURATION OF THE MESH OF THE HORIZONTAL WALL. 75
FIGURE 6.2: BALL TRAJECTORY IN FREE FALL ON HORIZONTAL WALL WHEN DAMPING RATIO EQUAL TO ZERO. 76
FIGURE 6.3: BALL'S MOTION IN RESPECT WITH TIME IN IDEAL SITUATION FOR DIFFERENT CONTACT MODEL. 77
FIGURE 6.4: BALL'S VELOCITY IN FREE FALL IN IDEAL SITUATION USING LINEAR, HERTZ- MINDLIN AND NG MODEL. 78
FIGURE 6.5: FORCE-DISPLACEMENT RELATION IN IDEAL SITUATION FOR DIFFERENT CONTACT MODELS. 78
FIGURE 6.6: NORMAL CONTACT FORCE VERSUS TIME IN IDEAL SITUATION FOR LINEAR, HERTZ-MINDLIN AND NG CONTACT MODELS AT FIRST CONTACT. 79
FIGURE 6.7: THE VARIATION OF NORMAL DISPLACEMENT VERSUS TIME AT FIRST CONTACT USING LINEAR, HERTZ –MINDLIN AND NG CONTACT MODELS IN IDEAL SITUATION. 80
FIGURE 6.8: BALL'S DAMPED MOTION USING LINEAR MODEL. 81
FIGURE 6.9: BALL'S DAMPED MOTION IN RESPECT TO TIME USING HERTZ-MINDLIN MODEL. 82
FIGURE 6.10: BALL'S DAMPED MOTION USING HERTZ-NG MODEL. 82
FIGURE 6.11: BALL'S DAMPED MOTION USING NG MODEL. 83
FIGURE 6.12: THE VARIATION OF CONTACT VELOCITY VERSUS TIME FOR VARIOUS DAMPING RATIO USING LINEAR MODEL. 84
FIGURE 6.13: THE VARIATION OF CONTACT VELOCITY VERSUS TIME FOR VARIOUS DAMPING RATIO USING HERTZ-MINDLIN MODEL. 84
FIGURE 6.14: THE VARIATION OF CONTACT VELOCITY VERSUS TIME FOR VARIOUS DAMPING RATIO USING HERTZ-NG MODEL. 85
FIGURE 6.15: THE VARIATION OF CONTACT VELOCITY VERSUS TIME FOR VARIOUS DAMPING RATIO USING NG MODEL. 85
FIGURE 6.16: THE VARIATION OF NORMAL CONTACT FORCE VERSUS TIME USING LINEAR MODEL. 87
FIGURE 6.17: THE VARIATION OF NORMAL CONTACT FORCE VERSUS TIME USING LINEAR MODEL AT FIRST CONTACT. 87
FIGURE 6.18: THE VARIATION OF NORMAL CONTACT FORCE VERSUS TIME USING HERTZ-MINDLIN. 88
FIGURE 6.19: THE VARIATION OF NORMAL CONTACT FORCE VERSUS TIME USING HERTZ-MINDLIN MODEL AT FIRST CONTACT. 88

FIGURE 6.20: THE VARIATION OF NORMAL CONTACT FORCE VERSUS TIME USING HERTZ-NG MODEL. 89
FIGURE 6.21: THE VARIATION OF NORMAL CONTACT FORCE VERSUS TIME USING HERTZ-NG MODEL AT FIRST CONTACT. 90
FIGURE 6.22: THE VARIATION OF NORMAL CONTACT FORCE VERSUS TIME USING NG MODEL. 90
FIGURE 6.23: THE VARIATION OF NORMAL CONTACT FORCE VERSUS TIME USING NG MODEL AT FIRST CONTACT. 91
FIGURE 6.24: THE VARIATION OF NORMAL DISPLACEMENT VERSUS TIME USING LINEAR MODEL. 92
FIGURE 6.25: THE VARIATION OF NORMAL DISPLACEMENT VERSUS TIME USING LINEAR MODEL AT FIRST CONTACT. 92
FIGURE 6.26: THE VARIATION OF NORMAL DISPLACEMENT VERSUS TIME USING HERTZ-MINDLIN MODEL. 93
FIGURE 6.27: THE VARIATION OF NORMAL DISPLACEMENT VERSUS TIME USING HERTZ-MINDLIN MODEL AT FIRST CONTACT. 93
FIGURE 6.28: THE VARIATION OF NORMAL DISPLACEMENT VERSUS TIME USING HERTZ-NG MODEL. 94
FIGURE 6.29: THE VARIATION OF NORMAL DISPLACEMENT VERSUS TIME USING HERTZ-NG MODEL AT FIRST CONTACT. 94
FIGURE 6.30: THE VARIATION OF NORMAL DISPLACEMENT VERSUS TIME USING NG MODEL. 95
FIGURE 6.31: THE VARIATION OF NORMAL DISPLACEMENT VERSUS TIME USING NG MODEL AT FIRST CONTACT. 95
FIGURE 6.32: THE VARIATION OF NORMAL CONTACT FORCE VERSUS NORMAL DISPLACEMENT USING LINEAR MODEL. 96
FIGURE 6.33 : THE VARIATION OF NORMAL CONTACT FORCE VERSUS NORMAL DISPLACEMENT USING HERTZ-MINDLIN MODEL. 97
FIGURE 6.34: THE VARIATION OF NORMAL CONTACT FORCE VERSUS NORMAL DISPLACEMENT USING HERTZ-NG MODEL. 98
FIGURE 6.35: THE VARIATION OF NORMAL CONTACT FORCE VERSUS NORMAL DISPLACEMENT USING NG MODEL. 98
FIGURE 6.36: THE CORRELATION OF COEFFICIENT OF RESTITUTION AND DAMPING RATIO FOR LINEAR MODEL. 101
FIGURE 6.37: THE CORRELATION OF COEFFICIENT OF RESTITUTION AND DAMPING RATIO FOR HERTZ-MINDLIN CONTACT MODEL. 102

FIGURE 6.38: THE CORRELATION OF COEFFICIENT OF RESTITUTION AND DAMPING RATIO FOR NG MODEL. 102
FIGURE 6.39: BALLS TRAJECTORIES FOR DIFFERENT WALL'S MATERIAL IN ROCFALL. 103
FIGURE 6.40: COMPARISON BALL'S MOTION COMES FROM LINEAR, HERTZ-MINDLIN AND NG MODEL AND THE MODEL IN ROCFALL. 104
FIGURE 7.1: BALL'S MOTION IN "AN" MODEL WHEN EXPONENT IS VARIABLE. 107
FIGURE 7.2: THE VARIATION OF NORMAL CONTACT FORCE VERSUS TIME WHEN EXPONENT IS VARIABLE. 108
FIGURE 7.3: THE VARIATION OF BALL'S BOUNCING VERSUS TIME WHEN TRANSITION FORCES VARY FROM 4.0 KN TO 16.0 KN. 110
FIGURE 7.4: THE VARIATION OF BALL'S VELOCITY VERSUS TIME WHEN TRANSITION FORCES VARY FROM 4.0 N TO 16.0 N. 110
FIGURE 7.5: THE LINEAR RELATIONSHIP BETWEEN COEFFICIENT OF RESTITUTION AND TRANSITION FORCE. 111
FIGURE 7.6: THE VARIATION OF NORMAL CONTACT FORCES VERSUS TIME WHEN TRANSITION FORCES VARY FROM 4.0-16.0 KN. 112
FIGURE 7.7: THE VARIATION OF NORMAL CONTACT FORCES VERSUS NORMAL DISPLACEMENT WHEN TRANSITION FORCES VARY FROM 4.0 TO 16.0 KN. 113
FIGURE 7.8: BALL'S MOTION IN RESPECT TO TIME FOR VARIOUS TRANSITION FORCES AND EXPONENTS. 114
FIGURE 7.9:BALL'S MOTION USING DIFFERENT CONTACT MODEL WHEN COEFFICIENT OF RESTITUTION IS 0.53. 116
FIGURE 7.10: THE VARIATION OF CONTACT VELOCITY VERSUS TIME USING DIFFERENT CONTACT MODELS WHEN COEFFICIENT OF RESTITUTION IS 0.53. 117
FIGURE 8.1: THE VARIATION OF BALL'S TRAJECTORY FOR VARIOUS DAMPING RATIO FOR A 120 DEGREE SLOPE ANGLE. 120
FIGURE 8.2: THE VARIATION OF BALL'S TRAJECTORY FOR VARIOUS DAMPING RATIO FOR A 135 DEGREE SLOPE ANGLE. 121
FIGURE 8.3: THE VARIATION OF COEFFICIENT OF RESTITUTION VERSUS DAMPING RATIO FOR A SLOPE WITH SLOPE RATIO OF -1:1.73. 122
FIGURE 8.4: THE VARIATION OF COEFFICIENT OF RESTITUTION WITH RESPECT TO "Z" VERSUS DAMPING RATIO FOR A SLOPE WITH SLOPE RATIO OF -1 : 1.73. 123
FIGURE 8.5: CORRELATION OF COEFFICIENT OF RESTITUTION AND DAMPING RATIO FOR HORIZONTAL WALL AFTER A 120 DEGREE SLOPE. 124
FIGURE 8.6: CORRELATION OF COEFFICIENT OF RESTITUTION AND DAMPING RATIO FOR A SLOPE WITH SLOPE RATIO -1:1. 125

FIGURE 8.7: CORRELATION OF COEFFICIENT OF RESTITUTION WITH RESPECT TO "Z" AND DAMPING RATIO FOR A 135 DEGREE SLOPE. 126
FIGURE 8.8: CORRELATION OF COEFFICIENT OF RESTITUTION AND DAMPING RATIO FOR HORIZONTAL WALL AFTER A SLOPE WITH SLOPE RATIO -1:1. 127
FIGURE 9.1: SOME OF THE POSSIBLE TRAJECTORIES FOR A ROCK AT TOP OF THE SLOPE. 130
FIGURE 9.2: THE VARIATION OF BALL'S TRAJECTORIES WHEN BALL'S DAMPING RATIO IS VARIABLE USING LINEAR MODEL. 131
FIGURE 9.3: THE VARIATION OF BALL'S TRAJECTORT WHEN BALL'S DAMPING RATIO CHANGE USING LINEAR MODEL. 131
FIGURE 9.4: BASIC STRUCTURE OF ARTIFICIAL NEURAL NETWORK [44]. 132
FIGURE 9.5: TRAINING OF NEURAL NETWORK ESTIMATOR 133
FIGURE 9.6: THE EFFECT OF DENSITY OF A FREEFALLING BALL ON HORIZONTAL TRAVEL DISTANCE USING LINEAR MODEL. 135
FIGURE 9.7: THE EFFECT OF RADIUS OF A FREEFALLING BALL ON HORIZONTAL TRAVEL DISTANCE USING LINEAR MODEL. 136
FIGURE 9.8: THE EFFECT OF DAMPING RATIO OF A FREEFALLING BALL ON HORIZONTAL TRAVEL DISTANCE USING LINEAR MODEL. 136
FIGURE 9.9: THE EFFECT OF HORIZONTAL INITIAL POSITION OF A FREEFALLING BALL ON HORIZONTAL TRAVEL DISTANCE USING LINEAR MODEL. 137
FIGURE 9.10: THE EFFECT OF VERTICAL INITIAL POSITION (Z) OF A FREEFALLING BALL ON HORIZONTAL TRAVEL DISTANCE USING LINEAR MODEL. 138
FIGURE 9.11: THE EFFECT OF INITIAL VELOCITY (WITH RESPECT TO X) OF A FREEFALLING BALL ON HORIZONTAL TRAVEL DISTANCE USING LINEAR MODEL. 138
FIGURE 9.12: THE EFFECT OF VERTICAL INITIAL POSITION (Z) OF A FREEFALLING BALL ON HORIZONTAL TRAVEL DISTANCE USING LINEAR MODEL. 139

LIST OF APPENDICES

Appendix 1: Computer program "Haraz" Demonstration.....145

Appendix 2: List of Samples for Estimation of Endpoint of a Rock 151

Appendix 3: Matlab Code for Artificial Neural Networks Model.....155

LIST OF SYMBOLS

Roman Symbols

a	radius of contact
b	an exponent for An contact model
B	maximum overlap displacement
c	slip radius
c_T	tangential compliance
C_n, C_s	normal and tangential damping coefficient
C_i^{crit}	critical damping constant
COR	coefficient of restitution
d	the minimum distance between two contact bodies
e	energy coefficient of restitution
E	modulus of elasticity
E^*	equivalent elastic modulus
$F_n, F_i^n, F_i^n\_wall$	normal contact force
F_t, F_i^s	tangential (shear) contact forces
F_n^d, F_s^d	normal and tangential contact forces
$\left\|F_i^n\right\|$	magnitude of the normal contact force
F_i	resultant force on center of particle
g	gravitational acceleration
G	equivalent shear modulus, equivalent shear modulus for colliding particles
G	ratio of elastic to inelastic deformation in An contact model
$\{F_i^s\}_{rot.1}$	shear force due to rotation about unit normal of old contact plane
$\{F_i^s\}_{rot.2}$	shear force due to rotation about unit normal of new contact plane
I	moment of inertia around the axis perpendicular to surface
J	polar moment of inertia

k	spring stiffness in the system of one degree of freedom
$K^n, K_n, k_n^{[A]}, k_n^{[B]}$	normal contact stiffness, normal stiffness of ball A, normal stiffness of ball B
$K_T, K^s, K_S, k_s^{[A]}, k_s^{[B]}$	tangential stiffness, shear contact stiffness, shear stiffness of ball A, shear stiffness of ball B
k^{tran}	translational stiffness
k^{rot}	rotational stiffness
m	particle's mass or equivalent mass of system
n_i	unit normal of the contact plane
n_m^{old}	old unit normal
$p(r)$	normal pressure for a point with distance of r from center in contact area
P	normal contact force
q	tangential stress
Q	applied tangential force
q	the slope of line segment
$R^{[A]}, R^{[B]},$	radii of ball A and ball B
R^b, R	radius of ball.
R_N	normal coefficient of restitution
R_T	tangential coefficient of restitution
$1/R_e$	equivalent contact curvature
$R_n(scaled)$	scaled coefficient of restitution for rockfall simulation
s	scaling factor
$t, t_{critical}$	time, critical time of a system
T	natural period of a system
T	transition force
U^n	normal overlap in ball-ball contact
U_w^n	normal overlap in ball-wall contact
V_i	contact velocity, impact velocity

V_i^n	normal component of velocity
V_i^s	shear component of velocity
$V_{0.5}$	velocity at scaling factor of 0.5
V_{X0}, V_{Y0}	the initial velocity of the rock
V_{NB}, V_{TB}	normal and tangential components of the rock velocity
V_{XA}, V_{YA}	velocity components of the rock, before impact
V_{XB}, V_{YB}	velocity components of the rock, after impact
$V_i^{(t+\Delta t)}$	new velocity of particle (velocity at primary intervals $(t+\Delta t)$)
V_{rn}, V_{out}	normal component of rebounding velocity
V_{rt}	tangential component of rebounding velocity
V_{in}	normal component of incoming velocity
V_{it}	tangential component of incoming velocity
x_i^A	coordinates of centre of ball A at ball-ball contact
$x_i^{[b]}$	coordinates of ball centre at ball-wall contact
$x_i^{[c]}$	contact point coordinates
$\dot{x}_i^{(t+\Delta t/2)}, \dot{x}_i^{(t-\Delta t/2)}$	translational velocity of ball
$\ddot{x}_i^t$	translation acceleration at time t
X_0, Y_0	initial position of a rock

Greek Symbols

α	coefficient of critical time
α'	safety factor
γ	Density
Δt_0	time step without viscous damping
Δt	time step
β_i	damping ratio
μ	coefficient of friction
μ_s	coefficient of static friction
μ_d	coefficient of dynamic friction
υ	Poisson ratio, equivalent Poisson's ratio for colliding particles
θ	slope angle of the line segment
η	ratio of tangential and normal springs stiffness at contact
σ_c	uniaxial compressive strength
ω_{ni}	natural frequency of a system
ω_k	angular velocity of two contact bodies about new normal direction
$\omega_i^{[A]}, \omega_i^{[B]}$	rotational velocity of ball A, rotational velocity of ball B
$\dot{\omega}_i^t$	rotational acceleration at time t

1. Introduction and Outline

A rockfall is a sudden freefall or down slope bounce (sliding/rolling) of detached blocks of rocks from bedding planes or joints in rock slopes. Rockfall can cause loss of life and economic impact. Rockfalls are a major hazard for infrastructures in mountainous area [1,2]. "In the 20th century, disasters caused by massive rockslope failure have killed 50'000 people" [1]. Several people lost their lives during rockfalls in Canada such as the rockfall of 1889 in Quebec, which killed 50 people, and the rock avalanche in 1903 in Alberta that killed 75 people and buried the CP railway [3]. In 1980, 8 miners were killed because of the triggering flow of lacustrine sediments from a roof in Belmoral Mine, Val D'Or, Quebec [3]. In January 1995 after contact of a 125 feet rock cliff and a freight train, the locomotive engineer and a trainman were drowned in Kootonay Lake at British Colombia [4]. Based on the Transportation Safety Board of Canada (TSB) report, three locomotives and first two cares behind of the locomotive of freight train derailed and plunged in Lake [4]. Some other examples of economic impacts of rockfalls are traffic disruptions, delays in roads or stoppage of production in mines like the shortfall in gold production after some rockfalls in La Ronde gold mine in Quebec in 2003[5]. According to Transportation Development Centre (TDC) report, 12 percents of the direct costs are spent for ground hazards such as rockfall in Canada while these accidents contain only 2 percents of train-related accidents [6].

In respond to safety issues, a considerable amount of money is spent every year for maintenance and protection of infrastructures from rockfall in many countries [7]. Since the preventive maintenances can decrease the long term maintenance cost by

decreasing the rehabilitation cost, by evaluating the rock slope stability and potential hazards further decisions for monitoring or stabilization of rock slope can be made [8].

Rockfall simulation is one of the existing methods for assess the rockfall hazards. Rockfall simulation is performed in order to predict the rockfall hazards, prepare rockfall hazard mapping in mountainous area specially along roads [9,10] and design appropriate remedial measures such as ditches, cable nets, rockfall shelters, rock fences [8,11,12,13] and design safe or functional excavated slopes [14]. It also contributes to ensuring the stability of tunnels during construction, and providing safety in open pit mines by stabilizing the mine's slopes during exploration, construction, maintenance or normal production blasting or during earthquakes [14]. Also, rockfall simulation can decreases the maintenances costs by decreases the rehabilitations costs.

This thesis is concerned with fundamental investigation of physics and not practical application of rockfall simulation.

1.1. Natural Factors for Occurrence of a Rockfall Event

In addition to critical slope gradient reasons for instability of slopes, there are other natural reasons for occurrence of rockfall. Table 1-1 demonstrates some of the natural reasons for the occurrence of rockfalls in rock slopes [15].

Table 1-1: Classification of the widespread rockfall causes (and, more generally slope movement causes) [15].

	Predisposition factors	Preparatory factors	Trigger fracture
Mechanical	Steep-sided valley Well –developed fracture network Neotectonics stresses	Rise in slope steepness to valley incision Regular seismic activity Damage process fatigue	High-magnitude earthquake Freezing and thawing of water in fractures
Hydrological and meteorological	Climate with precipitation rate	Regular rainfall regime	Heavy rainfall episode Rapid snowmelt
Thermal	Climate with a sharp temperature contrast	Daily a seasonal surface temperature oscillations	?
Geo-chemical	Mineralogical content of the rocks prone to weathering	Progressive weathering	?

1.2. Numerical Analysis of Rockfall

Numerical analysis is widely used for the study of stability of slopes, including analysis of rockfall. Generally, numerical methods for rock slope simulation can use three different types of models: continuum models, discontinuum models, and hybrid models (which is a combination of continuum and discontinuum). Table 1-2 describes different numerical approaches for analysis of stability of slopes [14,16].

Currently, discontinuum modeling of geomaterial (such as soil and rock) increases because of their discontinuum nature and the simplicity and significance of micromechanics of soil and rock's particles on overall behaviour of the system. Discrete Element Method (DEM) is one of the widely used discontinuum methods for the dynamic simulation of macroscopic and microscopic behaviours of soil and rocks. In this thesis, the DEM is utilized for simulation of rockfall in order to avoid the complexities within the nature of continuum models and also to take advantage of emergent properties of macroscopic systems that come automatically from discontinuum model i.e., transition from brittle to ductile behaviour, hysteresis and nonlinear mechanism in deformation [17]. In addition to the advantages that come from discontinnum methods, for the following reasons Discrete Element Method is potentially appropriate for modeling rockfall and studying contacts in rockfall simulation:

1. Rocks can be modeled with more details of their material properties, sizes and shapes.
2. The effect of contact of between of rocks on each other is considered as well as effect of contacts between rocks and sloped surfaces.

3. Microscopic behaviours of rocks can be tracked, as well as macroscopic behaviours.

4. Since a surface can be defined with several triangles (mesh) and each triangle has its own material properties and stiffness, surfaces can be modeled very closely to real field conditions.

It can be seen that the Discrete Element Method may be very appropriate for rockfall simulation; however the run time for complex model can be very long.

Table 1-2: Numerical methods of analysis [14,16]

Analysis method	Critical input parameters	Advantages	Limitations
Continuum Modeling (e.g. Finite Element, Finite Difference)	Representative slope geometry, constitutive criteria (e.g. elastic, elasto-plastic, creep, etc.), ground water characteristics; shear strength of surfaces; in situ stress state.	Allows for material deformation and failure. Can model complex behaviour and mechanisms. Capability of 3D modeling. Can model effects of groundwater and pore pressures. Able to assess effects of parameter variations on instability. Recent advantages in computing hardware allow complex models to be solved on PC's with reasonable run times. Can incorporate creep deformation. Can incorporate dynamic analysis.	Users must be well trained, experienced and can observe good modelling practice. Need to be aware of mode / software limitations (e.g. boundary effects, mesh aspect ratios, symmetry, hardware memory restrictions). Availiability of input data generally poor. Required input parameters not routinely measured. Inability to model effects of highly jointed rock. Can be difficult to be performing sensitivity analysis due to run time constraints.
Discontinuum Modeling (e.g. Distinct Element Method, Discrete Element Method)	Representative slope and discontinuity geometry; intact constitutive criteria; discontinuity stiffness and shear strength; ground water characteristic; in situ stress state.	Allows for bed block deformation and movement of blocks relative to each other. Can model complex behaviour and mechanism (combined material and discontinuity behaviour coupled with hydro-mechanical and dynamic analysis). Able to assess effects of parameter variations on instability.	As above experienced user required to observe good modeling practice. General limitations similar to those listed above. Need to be aware of scale effects. Need to simulate repetitive discontinuity geometry (spacing, persistence, etc.) Limited data on joint properties are available.
Hybrid/ Coupled Modeling	Combination of input parameters listed above for stand-alone models	Coupled finite element/ distinct element modls able to simulate intact fracture propagation and fragmentation of jointed and bedded media	Complex problem require high memory capacity. Comparatively little practical experience in use. Requires ongoing calibration and constraints

1.3. Objectives

Most of the previous studies for rockfall analysis were based on macroscopic behaviour of rocks in a rockfall, determination of a conservative range for trajectory of falling rocks, as well as the kinetic energy level of the rocks at position of mitigation

devices [12,13]. This research is concerned with microscopic behaviour of rocks during the rockfall as well as macroscopic behaviour of the system.

The first objective of this research is a comparative study to find the best contact model for simulation of rockfall. Several contact models have been developed based on DEM. Each contact model defines a method for calculation of contact forces based on force-displacement relationship between colliding bodies. Since contact forces have essential effect on overall behaviour of rockfall simulation, it is necessary to investigate effect of each contact model on dynamic behaviour of rocks. Five contact models are obtained through DEM, three of which were successfully used for the modeling of soil grains: linear model [18], Hertz-Mindlin [18] and Ng model [19]. The forth contact model is called elastic-inelastic power function [20], which was originally proposed for simulation of rockfall by An, and finally, a combination of Hertz and Ng model is performed. The effect of using each model on macroscopic result of rockfall is investigated by building some simple models and comparing the microscopic properties (contact stiffnessess, contact forces, and deformations) and macroscopic behaviours (trajectories, motions and velocities).

The second objective of this research is to determine the correlation between the microscopic properties of rock types and their macroscopic behaviour in a contact. In this research the relation between damping ratio (microscopic) and coefficient of restitution (macroscopic) are discussed, as well as the relation between material properties such as mass, density, Poisson ratio, Young modulus and uniaxial compressive strength for certain rock types.

The third objective of this research is to determine the effect of input factors on horizontal travel distance of a rock in a probable rockfall. Estimating the horizontal travel distance (endpoints) of a rock is an important outcome of the rockfall simulation. Knowing the trajectories of balls allows engineers to design appropriate remedial measures with a reasonable factor of safety at an appropriate position for reducing the impact of rockfall on infrastructures. An intelligent model (the neural network model) is utilized to estimate the possible end points of a rock and study the effect of initial conditions in a probable rockfall. A sensitivity analysis is performed for seven factors that are ball's radius, ball's density, damping ratio, initial position of the ball (horizontal and vertical coordinates with respect to X and Z) and initial velocity of the ball (horizontal component of the velocity with respect to "X" direction and vertical component of the velocity with respect to "Z" direction). Using this analysis the effect of seven parameters on horizontal travel distance of a spherical rock is investigated.

To achieve the objectives of this research a computer program is developed by the author for simulation and numerical analysis of rockfalls based on 3D Discrete Element Method (DEM). This code is capable of modeling numerous rocks of various sizes and properties some of which are mass, moment of inertia, Poisson ratio, Young modulus and friction coefficient. Also, it is capable of realistically modeling the geometry and material properties of the impact surfaces.

1.4. Organization of the Thesis

The contents of this dissertation are organized as follow:

Chapter 2 provides the literature review covering the essential and relevant parts of contact mechanics theory, an introduction to DEM, as well as the contact models of DEM.

Chapter 3 provides an overview of the analysis of rockfall, and determination of rocks' trajectories method in RocFall software. It also provides a better insight about calculation cycle in Discrete Element Method and general formula of DEM.

Chapter 4 presents an overview and details of the "Haraz" code, based on 3D DEM for simulation of rockfall.

Chapter 5 compares the magnitude and configuration of the nonlinear normal and shear stiffness of Hertz-Mindlin, Hertz-Ng and Ng model during a freefalling contact and compares the ratio of normal stiffness to shear stiffness of each contact model for different rock types and discusses the force-displacement configuration of each contact model.

Chapter 6 presents the dynamic behaviour of a free falling ball made of different rock types when colliding with a flat and horizontal surface for each contact model with and without damping ratio. Relation between coefficient of restitution and damping ratio is discussed as well.

Chapter 7 investigates 3D elastic–inelastic power function contact model. A simple model (A freefalling ball on a horizontal and flat wall) is utilized to study the variation of dynamic properties of a rock for different values of transition forces, exponents and linear stiffness. In this chapter, the correlation of coefficient of restitution and transition forces that represent different rock types (transition forces are depend upon unaxial compressive strength of the material) is determined, also.

Chapter 8 presents a discussion about correlation of coefficient of restitution and damping ratio using linear model in slopes.

Chapter 9 presents an estimation of horizontal travel distance for a 3D case study using an Intelligent Modelling Method (Artificial Neural Network) and a discussion of the effects of seven factors on horizontal travel distance of a rock in a probable rockfall.

Chapter 10 presents conclusions, limitations of the proposed methods, and main research contributions, and recommendations for future research work.

2. Review of Contact Mechanics

When two bodies collide, their velocities change and reaction forces and contact elastic and/or plastic deformation of bodies take place with some energy dissipation [21]. There are two main approaches to analyse contacts. "The first approach assumes that the interaction between the objects occurs in a very short time and that the configuration of the impacting bodies does not change significantly"[21]. "The second approach is based on the fact that the forces of interaction act in a continuous manner during impact" [21]. Therefore, the contact forces are added into the equations of motion during contact [21]. Figure 2.1 describes the contact according to the second approach [21]. Contact occurs in two phases [21]: The first phase is called compression (impact or loading), which starts at point O, where two bodies come in contact with each other and deformation (displacement or overlap) starts to increase. After reaching a maximum deformation (displacement) at point A the first phase ends. The second phase called restitution (rebound or unloading), during which deformation (displacement) decreases until two bodies separate and the deformation return to zero at point B, C or D [21].

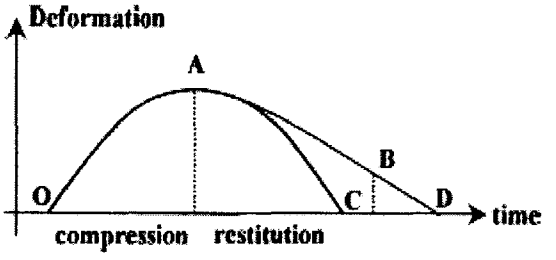

Figure 2.1: Deformation during the impact [21].

Friction in the system will stop and/or reverse the motion and will dissipate energy [21]. According to Coulomb's law, the magnitude of frictional force depends upon normal contact forces and act in opposite directions of the tangential motion [21].

The contacts are categorized as "sticking" and sliding. Sticking contacts occur when $F_t < \mu_s F_n$, and "sliding" contacts occur when $F_t = \mu_d F_n$ [21,22].

where:

F_t is tangential contact force.

F_n is normal contact force.

μ_s is coefficient of static friction.

μ_d is coefficient of dynamic friction.

Figure 2.2 illustrates the zones with possibility of sticking and sliding contact [21].

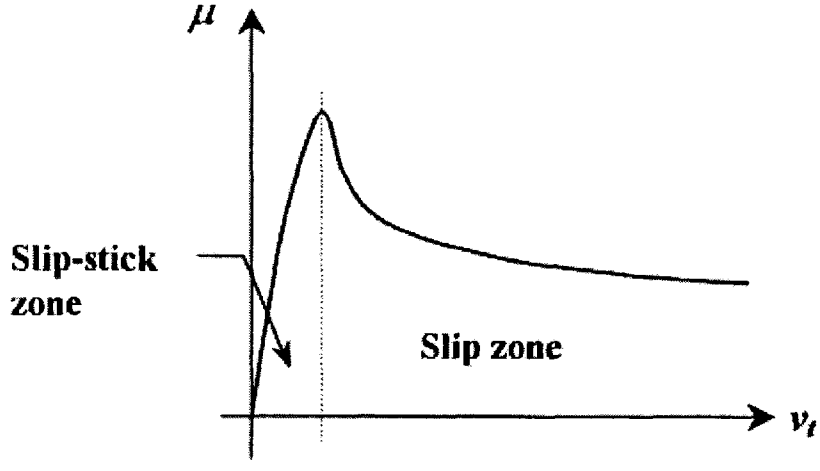

Figure 2.2: the variation of coefficient of friction versus initial tangential velocity [21]

2.1. Coefficient of Restitution

Energy loss during contact due to motion can be expressed in terms of coefficient of restitution [21]. Coefficient of restitution characterizes the energy loss due to *inelastic* deformation during object's contact [11]. One of the most acceptable definitions for calculation of coefficient of restitution which is identified by Newton is given by

Equations (2.1) and (2.2) [11]. At impacts with zero velocity coefficient of restitution is calculated by Equations (2.1) and (2.2) [11].

$$R_n = \frac{V_{rn}}{V_{in}} \tag{2.1}$$

$$R_t = \frac{V_{rt}}{V_{it}} \tag{2.2}$$

where:

R_n and R_t are normal and tangential coefficient of restitution.

V_{rn} and V_{rt} are normal and tangential component of rebounding velocity.

V_{in} and V_{it} are normal and tangential component of incoming velocity.

Another definition based on work done by the normal contact force in first and second phases of contact (impact and rebound respectively) is presented by Strong [23]. Strong defines the square coefficient of restitution *(e^2)*, as "the negative of the ratio of the elastic strain energy released during restitution (rebound, unloading) to the internal energy of deformation absorbed during compression (impact, loading)" [23], which is equal to the enclosed area between the loading (impact) and unloading (rebound) curves [23]. Strong proved that these definitions of coefficient of restitution are the same except for the eccentric contacts, for rough contact's bodies, and also for cases that the direction of slip varies during contact.

$$e^2 = \frac{Area\ under\ unloading\ curve}{Area\ under\ loading\ curve} \tag{2.3}$$

where:

e is energy coefficient of restitution.

For each contact material, the normal coefficient of restitution is not a constant value. Coefficient of restitution depends upon geometry, material of contact bodies and the initial velocity (decreases with increasing the initial impact velocity) [21]. The value of coefficient of restitution for most of the material is much less than unity where the impact is perfectly plastic [12,21,24].

2.1.1. Coefficient of Restitution Scaling in Rockfall Simulation

More local crushing on rock and impact surfaces take place at higher impact velocities [11,20] thus a scaled coefficient of restitution can be found by Equation (2.4) and (2.5) considering the effect of velocity on normal coefficient of restitution [20,25]. The value of velocity at scaling factor 0.5, $(V_{0.5})$ empirically have been determined to be about 9.144m/s [20,25]. Figure 2.3 shows that the scaling factor reduces when impact velocity increases [20].

$$R_n(scaled) = R_n \times Scaling\ factor \tag{2.4}$$

$$Scaling\ factor = \frac{1}{[1+(\frac{V_{rock}}{V_{0.5}})^2]} \tag{2.5}$$

where:

$R_n(scaled)$ is scaled coefficient of restitution for rockfall simulation.

$V_{0.5}$ is velocity at scaling factor of 0.5.

V_{rock} is normal component of rock velocity , immediately before impact.

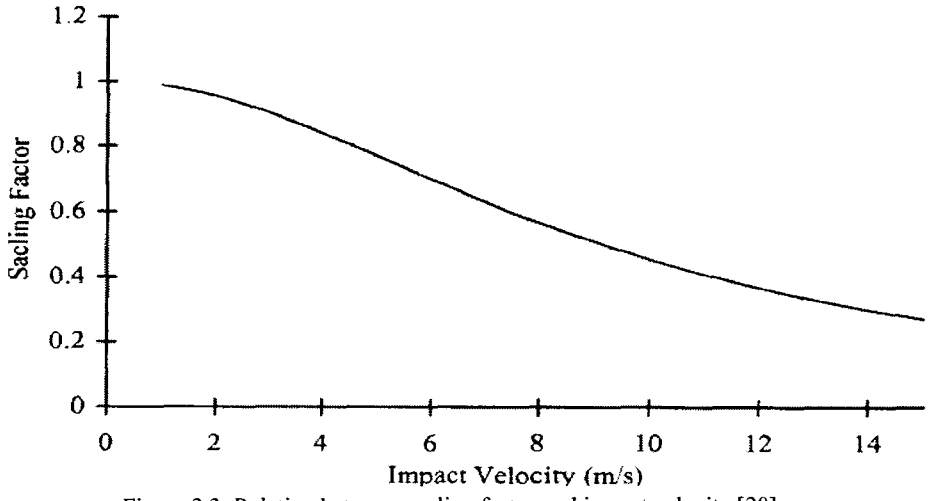

Figure 2.3: Relation between scaling factor and impact velocity [20].

2.2. Review of Hertz and Mindlin Studies for Calculation of Contact Forces

Hertz [26] showed that if two spheres as shown in Figure 2.4, with radius R_i and R_j collide along their centers, the contact surface (as shown in Figure 2.5), is a circle with radius of a, also the distribution of normal pressure which has a half-elliptical configuration is independent of angular coordinates [26].

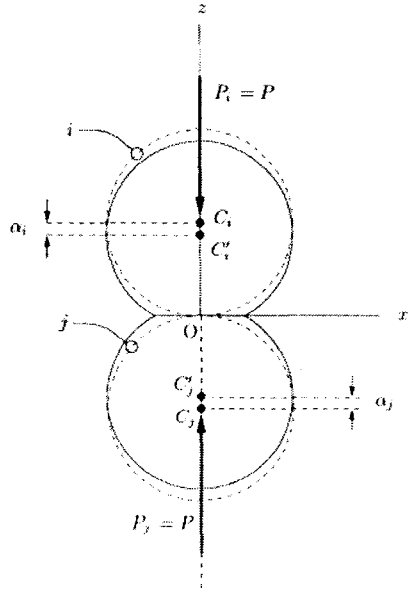

Figure 2.4: Two spheres in normal contact [28].

Therefore, the normal pressure for point A in contact area can be found by Equation (2.6) [28]

$$p(r) = p_m[1-(\frac{r}{a})^2]^{1/2} \tag{2.6}$$

where:

$p(r)$ is normal pressure for a point with distance of r from center in contact area.

r is distance of a point in contact area from center.

P_m is maximum normal pressure.

a is radius of contact area.

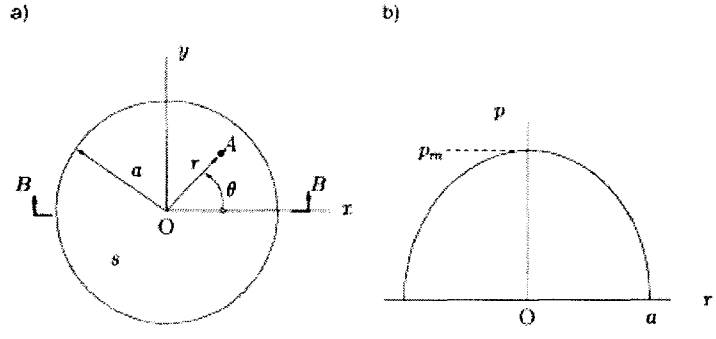

Figure 2.5: Contact area and Hertz pressure. (a) Circular contact-area (viewed from +Z).Section B-B is contact-area diameter. (b) Hertz normal pressure at section B-B [28].

By integrating Equation above with respect to s, the maximum normal pressure, p_m which occur at $r = 0$ can be found by Equation (2.7).

$$p_m = \frac{3p}{2\pi a^2} \tag{2.7}$$

Considering surface displacement and boundary conditions, Hertz determined the contact-area which depends upon normal and distant points in spheres as Equation (2.8). He also found the distant point in spheres (Figure 2.4) is given by Equation (2.9).

$$a = (\frac{3PR^*}{4E^*})^{1/3} \tag{2.8}$$

$$\alpha_{ij} = \alpha_i + \alpha_j = \frac{a^2}{R^*} \tag{2.9}$$

For elastic spheres, α_{ij} is given by the following Equation:

$$\alpha_{ij} = \left(\frac{9P^2}{16R^*(E^*)^2}\right)^{1/3} \tag{2.10}$$

where

E^* is equivalent elastic modulus and is given by Equation (2.11).

$1/R^*$ is equivalent contact curvature is given by Equation (2.12).

$$\frac{1}{E^*} = \frac{1}{E_i} + \frac{1}{E_j} \tag{2.11}$$

$$\frac{1}{R^*} = \frac{1}{R_i} + \frac{1}{R_j} \tag{2.12}$$

Finally, by combination of Equation (2.8) and (2.10) the relation of the maximum contact pressure and spheres' properties is found by:

$$p_m = \left(\frac{6P(E^*)^2}{\pi^3(R^*)^2}\right)^{1/3} \tag{2.13}$$

Where:

P is normal contact force.

Note that Hertz's theory is valid for the contact of hard materials with low initial speed because experimental tests show that Hertz's theory is not valid for perfectly elastic situations [21,24].

2.2.1. Tangential Contact Force

Tangential motion can be divided into sliding, spinning and rolling. Sliding and spinning consist of a relative velocity of the surfaces at their point of contact and stand respectively, for translational and rotational relative velocities. Rolling involves a relative

angular velocity of two bodies about axes parallel to their tangent plane. Rolling and spinning can take place at the same time [28,27,29]. Figure 2.6 shows two identical spheres in frictional contact and subject to normal force P and tangential force Q.

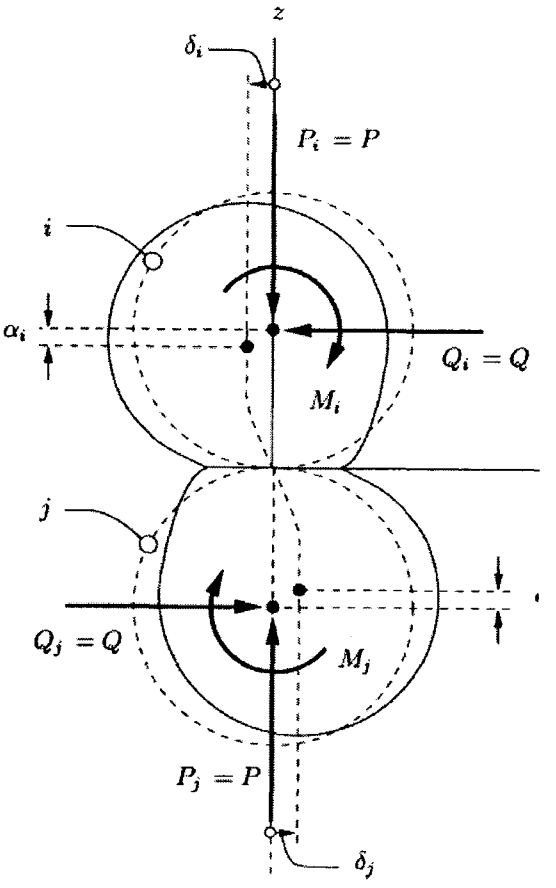

Figure 2.6: Two frictional spheres subjected to normal forces [28].

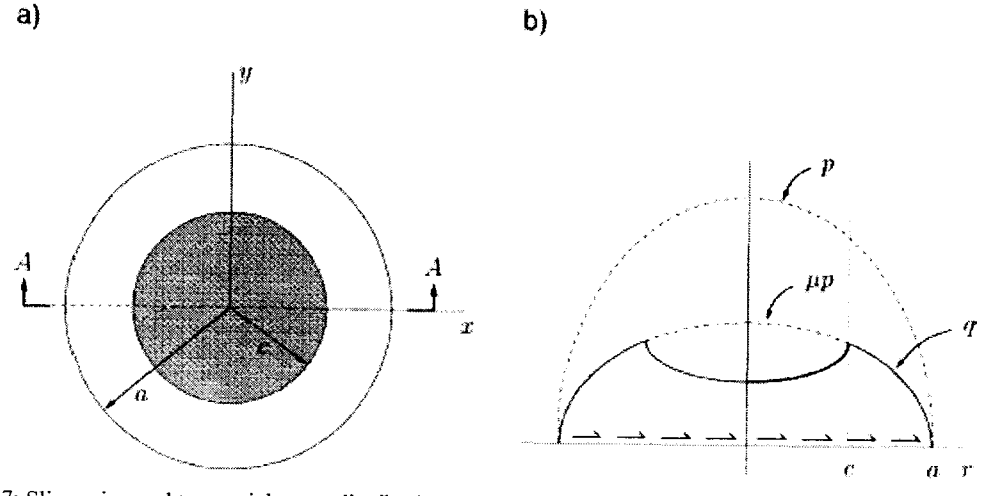

Figure 2.7: Slip region and tangential stress distribution. (a) Annulus of slip. Section A-A is aligned with a contact-area diameter. (b) Tangential stress on the contact-area, at section A-A [29].

Mindlin [27, 28] obtained the relation for tangent stress in case of constant normal force and varying tangential force through Equation (2.14) based on the following three assumptions:

1. Hertzian normal pressure on contact surface is assumed.
2. The effects of normal and tangential force are considered separately.
3. Complete sticking on the contact zone will cause the tangential stress distribution to go to infinity at the edge of contact [28].

The last assumption brings in the concept of slip [28]. Figure 2.7 shows that slip region and tangential stress distribution of cases in cross section of Figure 2.6 [28]. The slip area is an annulus $c \le r \le a$ in which the tangential stress q is the friction limit ($q_m = \mu P$). When c (slip radius) approaches to zero, the applied tangential force (Q) approaches $Q_m = \mu P$ [28]. Mindlin in 1949 [27,28] found the stress profile as Equation (2.14) where P is constant and Q is varying [27,28].

$$q = \begin{cases} \dfrac{3\mu P}{2\pi a^3}(a^2 - r^2)^{1/2}, & c \le r \le a, \\ \dfrac{3\mu P}{2\pi a^3}[(a^2 - r^2)^{1/2} - (c^2 - r^2), & r \le c \end{cases} \tag{2.14}$$

where:

c is slip radius. Slip radius is expressed by Equation (2.15) [27, 28].

$$c = a(1 - \frac{Q}{\mu P})^{1/3} \tag{2.15}$$

It can be seen that when tangential applied force is zero, the slip region disappears. Mindlin calculated the net displacement of spheres relative to contact area

[27,28]. By integrating the above equation, tangential compliance (c_T) was determined as Equation (2.16); hence c_T is the inverse of the tangential stiffness K_T [27,28].

$$c_T = \frac{\partial \delta}{\partial Q} = \frac{2-\upsilon}{8Ga}\left(1-\frac{Q}{\mu P}\right)^{-(1/3)} \qquad \left(P \ constant, Q\uparrow\right) \tag{2.16}$$

K_T is given as follows (Equation (2.17)).

$$K_T = \frac{1}{c_T} = \frac{8Ga}{2-\upsilon}\left(1-\frac{Q}{\mu P}\right)^{1/3} \tag{2.17}$$

Finally, Mindlin and Deressewicz [30] developed a more generalized model for elastic (deformable) spheres in sliding or torsional contact with varying normal force in two cases: when P and Q both increase (loading) in Equation (2.18) and when P and Q decrease (unloading) in Equation (2.19) [28,30]. Because of the complicity of solution, here are the tangential compliance (stiffness):

$$c_T = \frac{2-\upsilon}{8Ga}\left[\mu\frac{dp}{dq} + \left(1-\mu\frac{dp}{dq}\right)\left(1-\frac{Q}{\mu P}\right)^{-(1/3)}\right] \qquad 0 \le \frac{dp}{dQ} \le \frac{1}{Q} \tag{2.18}$$

$$c_T = \frac{2-\upsilon}{8Ga}, \qquad \frac{dp}{dQ} \ge \frac{1}{\mu} \tag{2.19}$$

For case P and Q both decreasing:

$$c_T = \frac{2-\upsilon}{8Ga}\left[-\mu\frac{dp}{dq} + \left(1+\mu\frac{dp}{dq}\right)\left(1-\frac{Q^* - Q}{\mu P}\right)^{-(1/3)}\right] \qquad \frac{dp}{dQ} \ge 0 \tag{2.20}$$

2.3. Discrete Element Method (DEM)

Considering the relation between rigid bodies, Cundall and Strack [31] proposed the Discrete Element Method (DEM), for modeling of geomaterials such as rocks and soils. In this model, soils and rocks are represented as spherical rigid grains. Each grain (particle) is modeled by its trajectory along the system due to the contact forces and external forces acting on each particle, such as gravity.

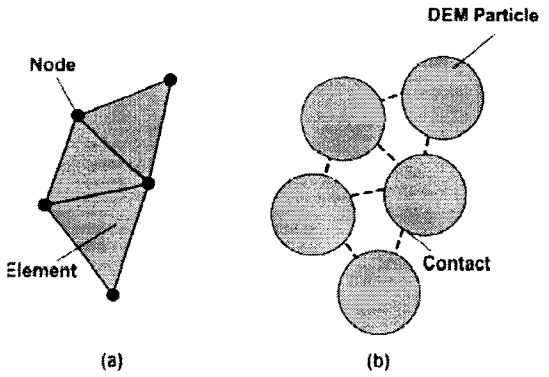

Figure 2.8: Schematic diagram illustrating DEM and FEM analogy. (a) Elements and nodes (FEM). (b) Particles and contacts [38].

The fundamental algorithm of DEM is based on differential equations of motion of contact bodies. In each time step, after detection of colliding objects, contact stiffness, colliding forces and resultant forces on each particle are calculated, and then Newton's second law of motion is utilized in order to update velocity, acceleration and position of each particle. Figure 2.9 demonstrates the Voigt-Kelvin model (mass-spring–damper system with one degree of freedom), which is employed in DEM to model contact between two objects [11,18]. Contact forces are calculated according to force-displacement relationship (Hoek's law). Spring and dampers can be linear or/and nonlinear.

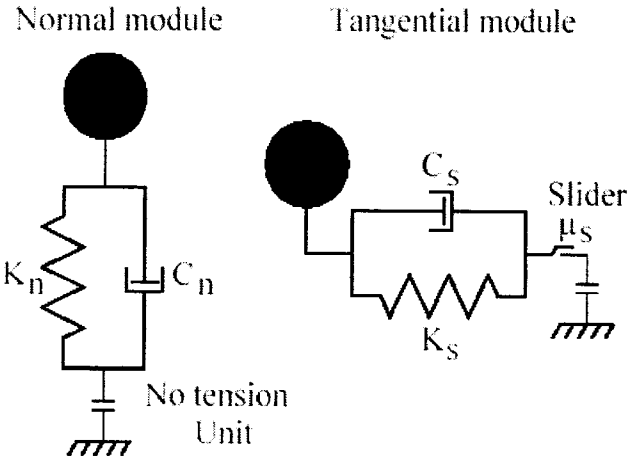

Figure 2.9: The Voigt-Kelvin element consists of a spring and a dashpot (damper) connected in parallel [11].

Discrete Element Method (DEM) [31] is one of the most widely used methods for dynamic simulation of soils and rocks [31,17], whose micromechanical behaviour are discontinuous, thus it helps to have better insight of engineering problems in these fields; for instance, the effect of microfeatures on the overall behaviour [34] and some emergent properties of macroscopic system that come automatically from discontinuum model i.e., "transition from brittle to ductile behaviour, hysteresis and nonlinear mechanism in deformation" [17].

2.4. Introduction to Linear, Hertz-Mindlin, Ng, Hertz-Ng, An and Modified Discrete Element Model (MDEM) Contact Models for Application in DEM Simulation

Several contact models for application of DEM simulation are used. Contact models determine the procedure of calculation of stiffness and contact forces in the model. Generally contact forces are calculated according to the force-displacement relationship; displacements can be found from the geometry of contact's bodies, and the magnitudes of contact stiffnesses are defined in each contact model. Since contact forces have essential effect on overall behaviour of rockfall model, it is necessary to illustrate each contact model. In this chapter, six contact models are introduced: Linear model, Hertz-Mindlin, Ng, Hertz-Ng, elastic-inelastic power function Contact Model (here called An model) and Modified Discrete Element model (MDEM).

2.4.1. Contact Stiffness in Linear Model

The contact stiffness for linear contact model is computed assuming that springs of two contacting bodies act in series. The contact normal secant stiffness is given by the following Equations [18]:

$$K^n = \frac{k_n^{[A]} k_n^{[B]}}{k_n^{[A]} + k_n^{[B]}} \tag{2.21}$$

And the contact shear model shear stiffness is found by [18]:

$$K^s = \frac{k_s^{[A]} k_s^{[B]}}{k_s^{[A]} + k_s^{[B]}} \tag{2.22}$$

where:

$k_n^{[A]}$ and $k_s^{[A]}$ represent linear normal and shear stiffness of ball A.

$k_n^{[B]}$ and $k_s^{[B]}$ represent linear normal and shear stiffness of ball B.

$$k^n \equiv \frac{dF^n}{dU^n} = \frac{d(K^n U^n)}{dU^n} = K^n \tag{2.23}$$

Normal and shear stiffness between two objects should be determined using linear contact model for each contact for each contact i.e., ball-ball or ball-wall normal and shear stiffness for each object should be determined.

2.4.2. Contact Stiffness in Hertz- Mindlin Contact Model

Cundall and Strack [31,33] developed a nonlinear model based on an approximation to the theory of Mindlin and Deresiewicz [30] called "Hertz-Mindlin Model" [18]. According to this model the contact normal secant stiffness and the contact shear tangent is defined as Equation (2.24) and Equation (2.25) [18].

$$K^n = \frac{2G\sqrt{2R^*}}{3(1-\upsilon)}\sqrt{U^n} \tag{2.24}$$

$$K^s = \left(\frac{2G^2 3(1-\upsilon)R^*)^{1/3}}{2-\upsilon}\right)\left|F_i^n\right|^{1/3} \tag{2.25}$$

where:

U^n is the overlap between colliding particles at time of contact.

$\left|F_i^n\right|$ is the magnitude of the normal contact force.

G is equivalent shear modulus for colliding particles given by Equation (2.27).

υ is equivalent Poisson's ratio for colliding particles [dimensionless].

$1/R^*$ is equivalent contact curvature is given by Equation (2.26) for ball-ball contact and Equation (2.27) for ball-wall contact.

where:

$R^{[A]}$ is radius Sphere A.

$R^{[B]}$ is radius Sphere B.

$$\frac{1}{R^*} = \frac{1}{R^{[A]}} + \frac{1}{R^{[B]}} \tag{2.26}$$

$$G = 1/2(G^{[A]} + G^{[B]}) \tag{2.27}$$

$$R^* = R^{[ball]} \tag{2.28}$$

$$G = G^{[ball]} \tag{2.29}$$

$$\upsilon = \upsilon^{[ball]} \tag{2.30}$$

For Hertz model, the normal-secant stiffness k^n is related to the normal-tangent stiffness by the following Equation (2.31) [18].

$$k^n = \frac{dF^n}{dU^n} = \frac{3}{2}K^n \tag{2.31}$$

2.4.3. Viscous Damping for Linear and Hertz-Mindlin Model

Normal and tangential dashpots and friction are the sources of impact energy dissipation in DEM. Several linear and nonlinear damping models were developed. The viscous damping force can be calculated by the following Equations.

$$F_i^d = C_i|V_i| \tag{2.32}$$

$$C_i = \beta_i C_i^{crit} \tag{2.33}$$

where:

F_i^d $(i = n : normal, s : shear)$ is viscous damping force.

C_i $(i = n : normal, s : shear)$ is damping constant.

β_i $(i = n : normal, s : shear)$ is damping ratio.

C_i^{crit} $(i = n : normal, s : shear)$ is critical damping constant.

$$C_i^{crit} = 2m\omega_{ni} = 2\sqrt{mk_i} \tag{2.34}$$

where:

ω_{ni} $(i = n : normal, s : shear)$ is natural frequency of a system.

k_i $(i = n : normal, s : shear)$ is the contact tangent stiffness.

m is the average mass of the two balls in ball-ball contact and m is the ball's mass in ball-wall contact.

Note that time step in damped system should be adjusted by the following Equation [18]:

$$k_i^{'} = \alpha^{'} \frac{k_i}{(\sqrt{1+\lambda^2} - \lambda)^2} \tag{2.35}$$

where:

$k_i^{'}(i = n : normal, s : shear)$ the contact stiffness of a system with viscous damping,

$\alpha^{'}$ is the safety factor.

$\lambda_i (i = n : normal, s : shear)$. λ is a parameter which is given by the following Equation:

$$\lambda_i = \frac{C_i}{2k_i \Delta t_0} \tag{2.36}$$

where:

Δt_0 is the time step without viscous damping.

2.4.4. Ng Model

Ng used Hertzian normal and simplified Mindlin's tangential contact law to find the normal and tangential contact stiffness for ellipsoidal granular materials as follows [19]:

$$K^n = \frac{2Ga}{1-\upsilon} \tag{2.37}$$

$$K^s = \frac{4Ga}{2-\upsilon} \tag{2.38}$$

where:

G is equivalent shear modulus is given by Equation (2.27).

υ is equivalent Poisson's ratio [dimensionless].

a is radius of contact which is dependent upon the normal contact force and can be found by Equation (2.39).

$$a = [\frac{3(1-\upsilon)|F_n|R_e}{8G}]^{1/3} \tag{2.39}$$

where:

$|F_i^n|$ is the magnitude of the normal contact force.

$1/R_e$ is equivalent contact curvature is given by Equation (2.26) for ball-ball contact and Equation (2.27) for ball-wall contact.

The above equations are valid for spheres as well as ellipsoidal particles since sphere is a specific case of ellipsoid in which principle radii of ellipsoid are equal. Ng solved the differential Equation (2.40) [19]. By applying the central difference approximation to the above Equation, the new velocity of particle is found as follows [19]:

$$m\frac{dV_i}{dt} = F_i - cV_i \tag{2.40}$$

where:

m is particle's mass.

F_i is resultant force on center of particle.

V_i is contact velocity.

c is constant damping ratio.

$$V_i^{(t+\Delta t)} = \frac{V_i'(1-\frac{\beta\Delta t}{2}) + \frac{F_i\Delta t}{m}}{(1+\frac{\beta\Delta t}{2})} \tag{2.41}$$

where:

$V_i^{(t+\Delta t)}$ is new velocity of particle.

Δt is the time step.

Calculation of current velocity allows updating the position of particles. Those updated position will be considered step for detection of new contacts between particles in next time.

2.4.5. Hertz-Ng Model

This model is a combination of Hertz-Mindlin model and Ng model. Forces are calculated according to Hertz-Mindlin model. Velocity, acceleration and the positions of particles are updated according to Ng model.

2.4.6. Elastic-Inelastic Power Function Contact Model (An Model)

An proposed a DEM nonlinear contact model for 2D simulation of rockfall [20,37]. In this model, normal dashpot is replaced by a power function to reduce the normal component of the contact force. The power function generates a lower value of coefficient of restitution in each time step. During the impact, at first the normal contact force is calculated in accordance with linear elastic relationship. After reaching the transition force, contact force is set to the transition force until the relative velocity between the objects in contact reaches to zero. In other words, when maximum overlap occurs by rebounding, the contact force is calculated and reduced by power function of

$y = ax^b$ (as shown in Figure 2.10.)

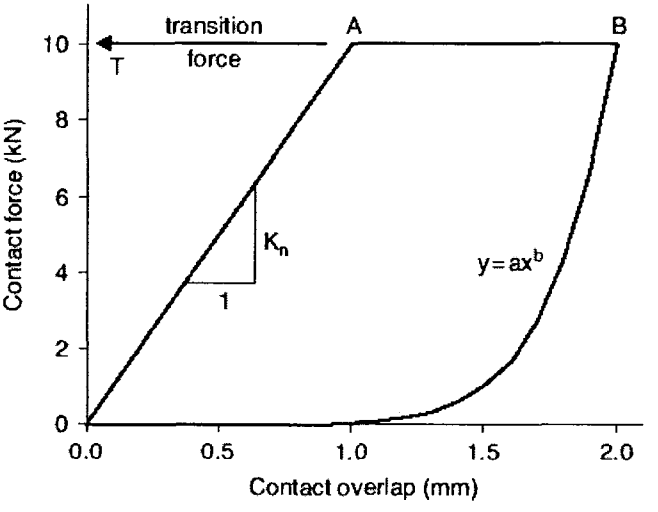

Figure 2.10: Elastic-inelastic power function model [20]

Three parameters are required for elastic-perfectly plastic power function model: transition force, exponent and initial normal contact stiffness. The transition force is a

normal contact force, at which the model transfers form elastic response to perfectly plastic deformation, while undergoing compression. The exponent adjusts the power function to a damping function that is applied to rebound phase of contact. The value of exponent determines the energy loss during the impact.

Point A in Figure 2.10 is found when linear contact force reaches to transition force. Point B is the starting point for rebound phase when contact bodies initiate to move away. In other words, point B is the position of maximum overlap between contact bodies and where relative contact velocity reaches zero. The value of a is determined by Equation (2.42) [20,37].

$$a = \frac{T}{B^b} \tag{2.42}$$

where:

T is transition force.

B is maximum overlap displacement.

b is an exponent.

Using high value of transition force such that the inelastic deformation is prevented, the contact model becomes an elastic-inelastic power function model. Using a low value of transition force and exponent value of 1.0 makes a triangular contact damping model (See Figure 2.11). Low values for transition force cause balls to pass through walls and high values make the model unstable [20].

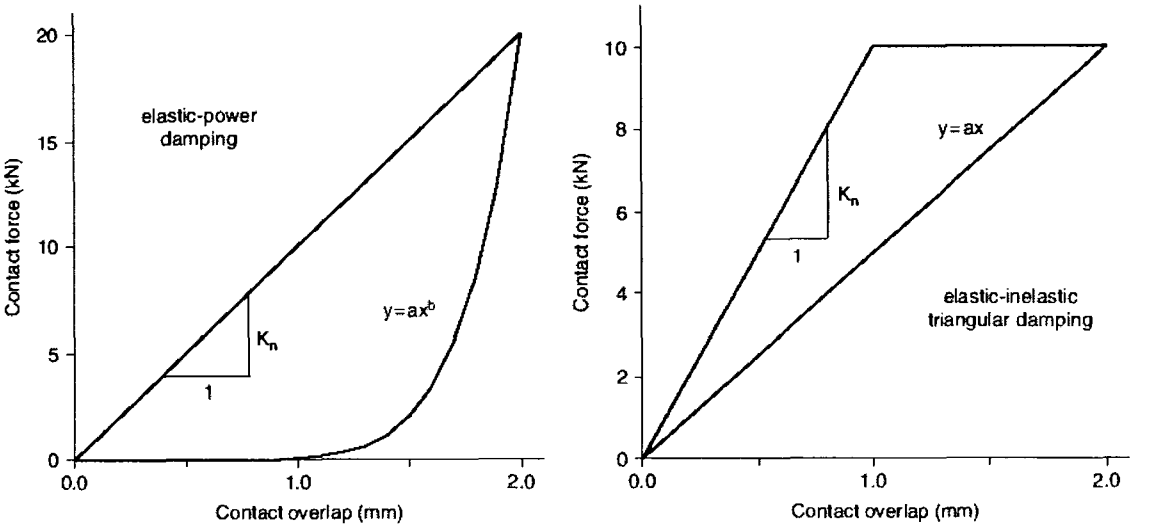

Figure 2.11: Different forms of elastic-inelastic power function model [20].

For a rock under compressive loading, the transition to non-elastic behaviour begins to occur at approximately 75% of the uniaxial compressive strength [20]. An suggests Equation (2.43) to calculate the transition force [20]:

$$T = 0.75\pi(sR)^2\sigma_c \tag{2.43}$$

where:

R is radius of the particle.

σ_c is uniaxial compressive strength.

s is a scaling factor (s<1) that reduces the radius to an effective radius carrying the contact load. Scale factor can be found according to Equation (2.5) or Figure 2.3 [20]. Table 2-1and Figure 2.12 show the transition force for various particle sizes and different normal stiffnesses [20].

Table 2-1: Transition force for various particle size samples at different normal stiffness [20].

Normal Stiffness (N/m)	Transition Force for various particle sizes				
	$R = 0.04\ m$	$R = 0.14\ m$	$R = 0.20\ m$	$R = 0.25\ m$	$R = 0.30\ m$
4.80×10^{10}	3.20×10^{3}	4.13×10^{4}	2.10×10^{5}	3.835×10^{5}	5.10×10^{5}
3.20×10^{10}	3.00×10^{3}	4.00×10^{4}	1.90×10^{5}	3.82×10^{5}	3.50×10^{5}

6.40×10^{10}	3.50×10^{3}	4.50×10^{4}	2.5×10^{5}	5.30×10^{5}	8.00×10^{5}
9.60×10^{10}	8.00×10^{3}	7.60×10^{4}	4.80×10^{5}	1.10×10^{6}	1.88×10^{6}
1.11×10^{10}	1.22×10^{4}	1.25×10^{5}	1.025×10^{6}	2.10×10^{6}	3.525×10^{6}

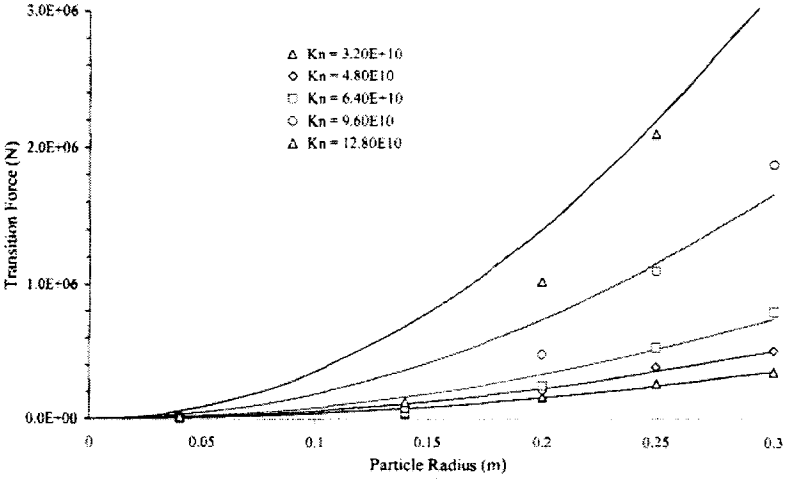

Figure 2.12: Transition force vs. particle radius (models with various normal stiffness) [20].

The exponent of the power function largely determines the damping effect of the model [20]. An suggests Equation (2.44) to adjust the exponent by rock velocity regardless of radius of rock. Figure 2.13 is the best-fit of Equation (2.44) [20].

$$y = 0.0429x^3 - 0.4744x^2 + 2.5508x + 1.1489 \tag{2.44}$$

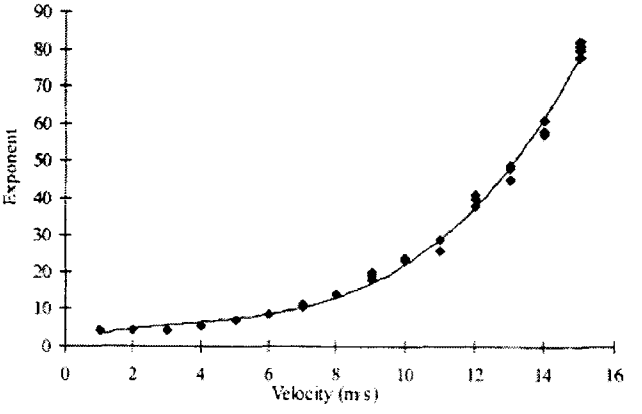

Figure 2.13: exponent vs. impact velocity and various radii [20].

2.4.6.1. Damping and Normal Restitution Coefficient in An Model

Figure 2.14 shows the force-displacement relationship for An's model. In addition to other parameters, in rockfall simulation the normal restitution coefficient depends upon the rock type and slope conditions [20]. Although the energy dissipation in this model mainly depends on the exponent [20], transition force affects on system energy loss after setting the exponent [20]. The exponent is dependent upon the rock impact velocity, and is almost independent of other factors such as particle radius [20]. The numerical model of energy loss in this model is illustrated in Figure 2.14 [20].

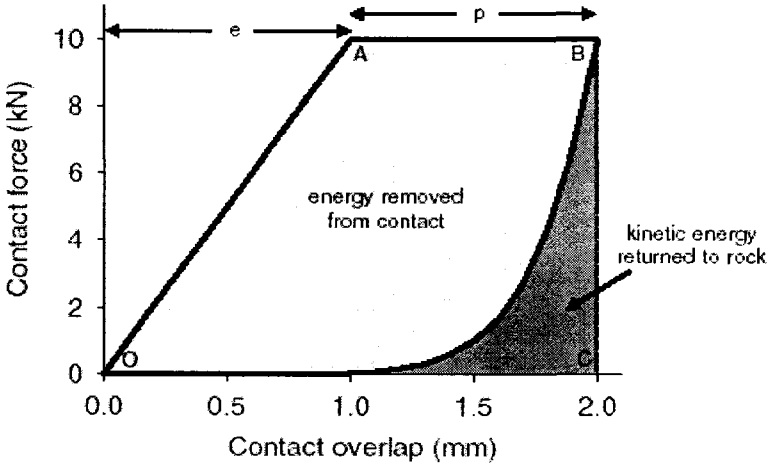

Figure 2.14: Schematic of energy dissipation of elastic-perfectly plastic power function model [20].

The normal restitution coefficient in this model can be found by Equation (2.45) [20].

$$R_n = \sqrt{\frac{2}{b+1}} \times \sqrt{\frac{G+1}{G+2}} \tag{2.45}$$

where:

G is the ratio of elastic to inelastic deformation.

$$G = \frac{e}{p} \tag{2.46}$$

Figure 2.15 illustrates the variations of normal coefficient of restitution versus exponent for different amounts of inelastic deformation. Figure 2.14 shows that normal

coefficient of restitution decreases as the exponent b increases [20]. For an impact with fully elastic deformation ($P=0$), value of b is equal to 7 that gives normal coefficient of restitution of 0.5 [20].

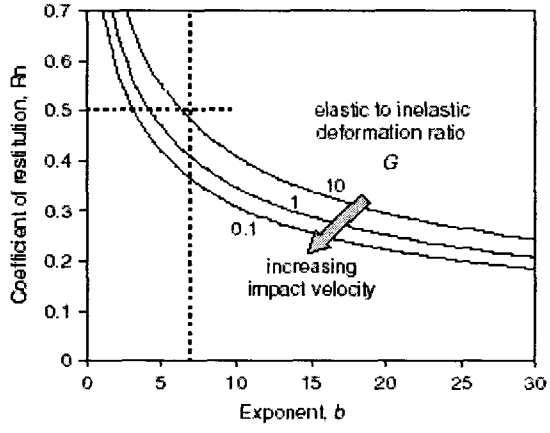

Figure 2.15: Coefficient of normal restitution versus exponent for varying amounts of inelastic deformation [20].

Since inelastic deformation of rocks depends upon impact velocity (increasing mass or velocity, increase of inelastic deformation), the coefficient of normal restitution becomes smaller for higher impact velocities. An adjustment of value of b for impact velocity larger than 4 m/s should be done as in Equation (2.47) [20].

$$b = f(v_i) = 7 + (\frac{v_i}{8})^3 \tag{2.47}$$

where:

v_i is impact velocity.

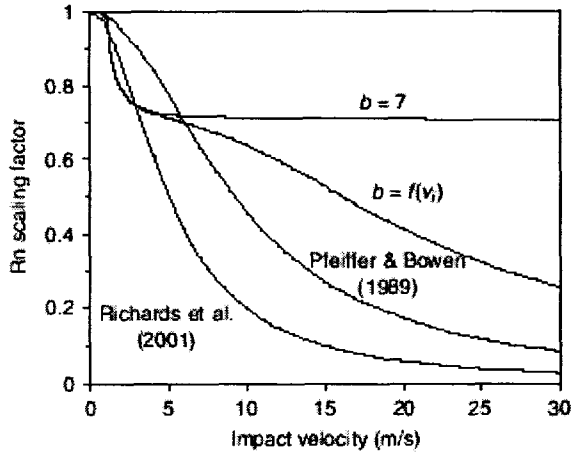

Figure 2.16: Scaling factor for coefficient of normal restitution (as v_i increases R_n decreases) [20].

2.4.7. Modified Discrete Element Model (MDEM)

Ashayer proposed a modified version of DEM called (MDEM) [11]. In MDEM, in order to remove the effect of shock and tensile forces at beginning and end of contact respectively, the normal dashpot is replaced by a nonlinear viscous module as shown in Figure 2.17 [11]. Using nonlinear viscous module makes damping force dependent on velocity and contact indentation [11] and correlates the normal coefficient of restitution with impact velocities [11].

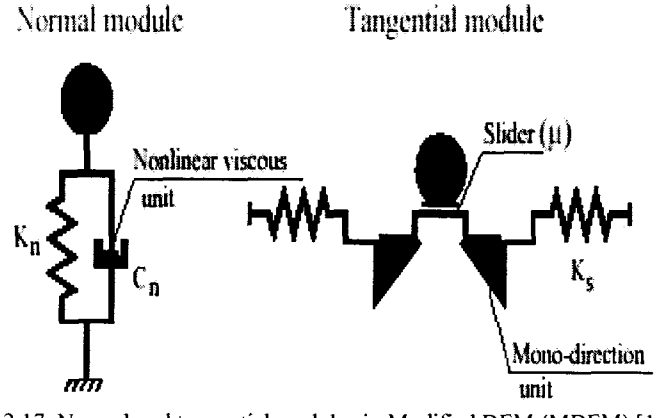

Figure 2.17: Normal and tangential modules in Modified DEM (MDEM) [11].

In this model, tangential dashpot is taken out, and a mono-direction mechanical unit is added. This unit releases the strain energy stored in the tangential direction when

the direction of tangential slip reverses [11]. Since the perfect investigation on application of this model to rockfall simulation has been done by Ashayer [11], this model will not be discussed in this thesis.

3. Review of Current Approaches for Simulation of Rockfall

There are several software packages and codes developed for simulation of rockfall. Table 3-1 shows the list of software representations [11].

Table 3-1: Different computer simulation for rockfalls categorized based on their main Characteristics, after Guzzetti et al. (2002) [11].

Year	Author	Program name	Dimensions	Approach	Probabilistic
1976	Piteau and Clayton	Computer Rockfall model	2D	Lumped -mass	Partly
1982-86	Bozzolo and Pamini	SASS-MASSI	2D	Hybrid	Yes
1985	Bassato el al.	Rotolamento Salto Massi	2D	Lumped- mass	No
1987	Descouedres and Zimmermann	Eboul	3D	Rigid body	No
1989-91	Pfeiffer and Bowen	CRSP	2D	Hybrid	Yes
1990	Kobayashi et al.	-	2D	Rigid body	No
1991-95	Azzoni et al.	CADAMA	2D	Hybrid	Yes
1991	Scioldo	Rotomap	3D	Lumped- mass	NO
1998	Stevens	RocFall ver.4	2D	Hybrid	Yes
1999	Paronuzzi and Artini	Mobyrock	2D	Lumped- mass	Yes
2000	Jones et al.	CRSP 4.0	2D	Hybrid	Yes
2002	Guzzetti et al.	STONE	3D	Lumped -mass	Yes
2007	Ashayer and Curran	GeoRFS	2D	Rigid body	Yes
2007	Nejati	Haraz	3D	Discrete Element Method	Partly

"RocFall" is a 2D probabilistic software for analysis of rockfall, which can be used to simulate rockfall events and design remedial measures and test their effectiveness [12]. It contains two essential objects: a rock which is a disk whose mass is concentrated at a point, and a slope, which consists of any number of 2D line segments with different material properties such as R_n and R_T [12].

Because of availability of software RocFall and its documentations for the author, in this thesis RocFall has been utilized for validation and applying necessary calibration of Haraz. In this chapter, algorithm and formulation of RocFall as well as calculation cycle and formulation of Haraz is presented to have better insight about rockfall simulation with RocFall and to compare the outcomes of RocFall and a code based on 3D Discrete Element Method.

3.1. Calculation Procedure in RocFall

The initial location, velocity, and mass of the rocks must be defined with a value larger than zero. The calculation cycle begins by assigning the initial position of the rock, finding the location of the intersection between the path of the rock (parabola) and a line segment (slope). Once the intersection point is found, the impact is calculated according to the coefficient of restitution. If rock, after the impact still moves fast enough to overcome the present drag force, the process begins again with searching for next intersection point.

$$x = X_1 + (X_2 - X_1)u \tag{3.1}$$

$$y = Y_1 + (Y_2 - Y_1)u \qquad u \in [0,1] \tag{3.2}$$

where:

X_1, Y_1 is the coordinates of the first intersection of rock path and the line segment.

X_2, Y_2 is the coordinates of the second intersection of rock path and the line segment.

The parametric equation for a parabola:

$$x = V_{x0}t + x_0 \tag{3.3}$$

$$y = \frac{1}{2}gt^2 + V_{Y0} + Y_0 \tag{3.4}$$

where:

X_0, Y_0 is the initial position of the rock.

V_{X0}, V_{Y0} is the initial velocity of the rock.

The parametric equations for the velocity of a particle:

$$V_{XB} = V_{X0} \tag{3.5}$$
$$V_{YB} = V_{Y0} + gt \tag{3.6}$$

where:

V_{XB}, V_{YB} is the velocity of a rock at any point along a parabolic path, before impact.

Equating the points of parabola with equations of lines followed by rearranging to the quadratic equation $ax^2 + bx + c = 0$ gives:

$$\left[\frac{1}{2}g\right]t^2 + \left[V_{Y0} - qV_{X0}\right]t + \left[Y_0 - Y_1 + q(X_1 - X_0)\right] = 0 \tag{3.7}$$

where:

q is the slope of line segment.

$$q = \frac{(Y_2 - Y_1)}{(X_2 - X_1)} \tag{3.8}$$

The roots of Equation (3.9) are the times of contact of rock and slope.

$$t = \frac{-b \pm \sqrt{b^2 - 4ac}}{2a} \tag{3.9}$$

The parabola formed by the rock trajectory is checked with every segment of the slope [12]. Once the intersection is detected, the velocity just before the impact is

calculated and transformed into normal and tangential components of the slope according to [12]:

$$V_{NB} = (V_{YB})\cos(\theta) - (V_{XB})\sin(\theta) \quad (3.10)$$

$$V_{TB} = (V_{YB})\sin(\theta) - (V_{XB})\cos(\theta) \quad (3.11)$$

where:

V_{NB}, V_{TB} are the normal and tangential components of the rock velocity, before impact, respectively.

θ is the slope angle of the line segment.

Considering the coefficient of restitution, the impact is calculated according to Equation (3.12) and Equation (3.13) [12]:

$$V_{NA} = R_N V_{NB} \quad (3.12)$$

$$V_{TA} = R_T V_{TB} \quad (3.13)$$

where:

R_N is the coefficient of normal restitution, $R_N \in [0,1]$

R_T is the coefficient of tangential restitution, $R_T \in [0,1]$

The post-impact velocities are transformed back in horizontal and vertical components according to Equation (3.14) and Equation (3.15) [12]: The post-impact velocities are transformed back in horizontal and vertical components according to Equation (3.14) and Equation (3.15) [12]:

$$V_{XA} = (V_{NA})\sin(\theta) + (V_{TA})\cos(\theta) \quad (3.14)$$

$$V_{YA} = (V_{TA})\sin(\theta) + (V_{NA})\cos(\theta) \quad (3.15)$$

where:

V_{XA}, V_{YA} are the velocity components of the rock, after impact, in the horizontal and vertical direction, respectively [12].

3.2. Coefficient of Restitution in RocFall

Typical analysed values in RocFall for the normal coefficient of restitution (R_N) vary from 0.3 to 0.5, and the tangential coefficient of restitution (R_T) ranges from 0.8 to 0.95 [12]. Since coefficient of restitution directly is employed in every cycle to find the new velocity, simulation is very sensitive to any change in the coefficients of restitution [12].

3.3. Discrete Element Method Formulation

The essential parts of a DEM calculation cycle are as follow:

1. Calculation of time step
2. Detection of contacts in each time step
3. Calculation of contact stiffness, contact forces and resultant force on each particle using force-displacement relationship.
4. Updating particle's position using Newton's second law of motion

Note that the following formulation is written the Einstein summation format (the convention that repeated indices are implicitly summed over).

3.3.1. Calculating Time Step

DEM utilizes the central difference time integration method. The system is stable when time step (time increment) is less than critical time.

The critical time corresponding to a point mass with one degree of freedom is given by Equation (3.16)

$$t_{critical} = \frac{T}{\pi} \tag{3.16}$$

where:

T is natural period of a system and can be found by Equation (2.4) [18]:

$$T = 2\pi\sqrt{\frac{m}{k}} \tag{3.17}$$

One approach for estimating the critical time step for assembly of similar disks or spherical particles is to model multiple mass-spring system with infinite series of point masses and springs as is shown in Figure 3.1 [18]. The minimum value of the period of multiple mass-spring system occurs when masses are moving in the synchronized opposing direction such that there is no motion at the center of each spring [18]. The motion of a single mass can be described by two equivalent systems shown in Figure 3.1 [18]. For the general degree of freedom, the translational and rotational stiffnesses are expressed as [18]:

$$k_i^{tran} = (k_n - k_s)n_{(i)}^2 + k_s \tag{3.18}$$

$$k_{(i)}^{rot} = R^2 k_s (1 - n_{(i)}^2) \tag{3.19}$$

where:

k^{tran} is translational stiffness.

k^{rot} is rotational stiffness.

I is moment of inertia.

Therefore, the critical time for the generalized multiple mass-spring system can be expressed as Equation (3.20) [18].

$$t_{critical} = \min\begin{cases}\sqrt{m/k^{tran}} \\ \sqrt{I/k^{rot}}\end{cases} \tag{3.20}$$

where:

$t_{critical}$ is critical time of a system.

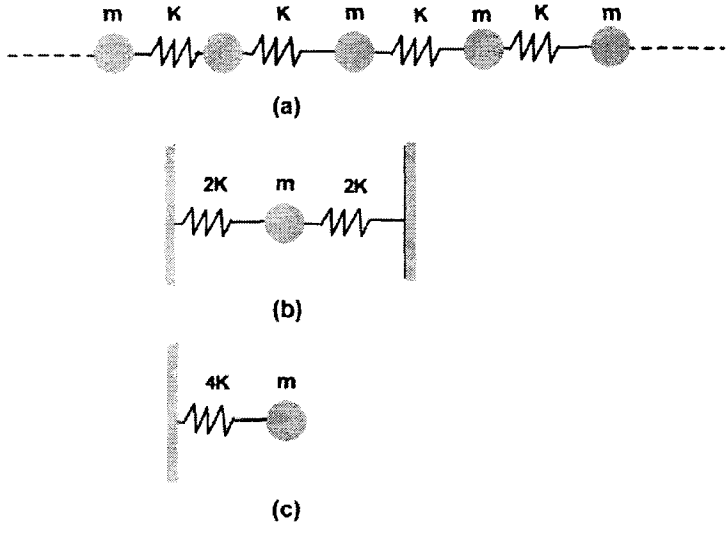

Figure 3.1: Calculation of critical time for multiple mass-spring system [18].

Finally, time step can be determined by the following Equation:

$$\Delta t = \alpha\, t_{critical} \tag{3.21}$$

where:

α is coefficient of critical time which is always $\alpha < 1$.

In this research, the time step is first calculated by determining the maximum stiffness of the possible contacts between objects using linear normal and shear stiffnesses and the minimum mass value of the system. After, the calculated time step is reduced by the value of the coefficient of time step to make sure that time steps are reasonable.

3.3.2. Detection of Contacts

First step in the calculation cycle of DEM is detection of contacts. Contacts can occur between balls, called ball-ball contact, or between a ball and a wall, called ball-wall contact (Figure 3.2). According to definition of contact in DEM, two bodies are in contact when they have an overlap. Hence for every two objects, overlap existence should be checked to detect the contact. Relative normal displacement is determined by Equation (3.22) for ball-ball contact and Equation (3.23) for ball-wall contact.

$$U^n = R^{[A]} + R^{[B]} - d \tag{3.22}$$

$$U_w^n = R^b - d \tag{3.23}$$

where:

U^n is the magnitude of the normal overlap in ball-ball contact.

U_w^n is the magnitude of the normal overlap in ball-wall contact.

$R^{[A]}$ is radius of ball A.

$R^{[B]}$ is radius of ball B.

R^b is radius of ball at ball-wall contact.

d is minimum distance between two contact bodies.

In other words, contact forces are calculated only if U^n or U_w^n are positive [18]. The coordinates of contact points are found by Equations (3.24) and (3.25) [18].

$$x_i^{[c]} = x_i^A + (R^{[A]} - 1/2U^n)n_i \qquad ball - ball \tag{3.24}$$

$$x_i^{[c]} = x_i^{[b]} + (R^{[b]} - 1/2U_w^n)ni \qquad ball - wall \tag{3.25}$$

where:

$x_i^{[c]}(i=1,2,3)$ represents contact point coordinates with respect to the Cartesian system.

$x_i^A(i=1,2,3)$ represents coordinates of centre of ball A at ball-ball contact.

$x_i^{[b]}(i=1,2,3)$ represents coordinates of ball centre at ball-wall contact.

n_i is the normal unit of contact plane.

The unit normal vector for ball-ball contact is calculated by Equation (3.26).

$$n_i = \frac{x_i^B - x_i^A}{d} \tag{3.26}$$

where:

$x_i^A(i=1,2,3)$ represents coordinates of centre of ball A at ball-ball contact.

$x_i^B(i=1,2,3)$ represents coordinates of centre of ball B at ball-ball contact.

The method for determination of unit normal vector for ball-wall contact, considering the plane equation in space is presented in chapter 4.

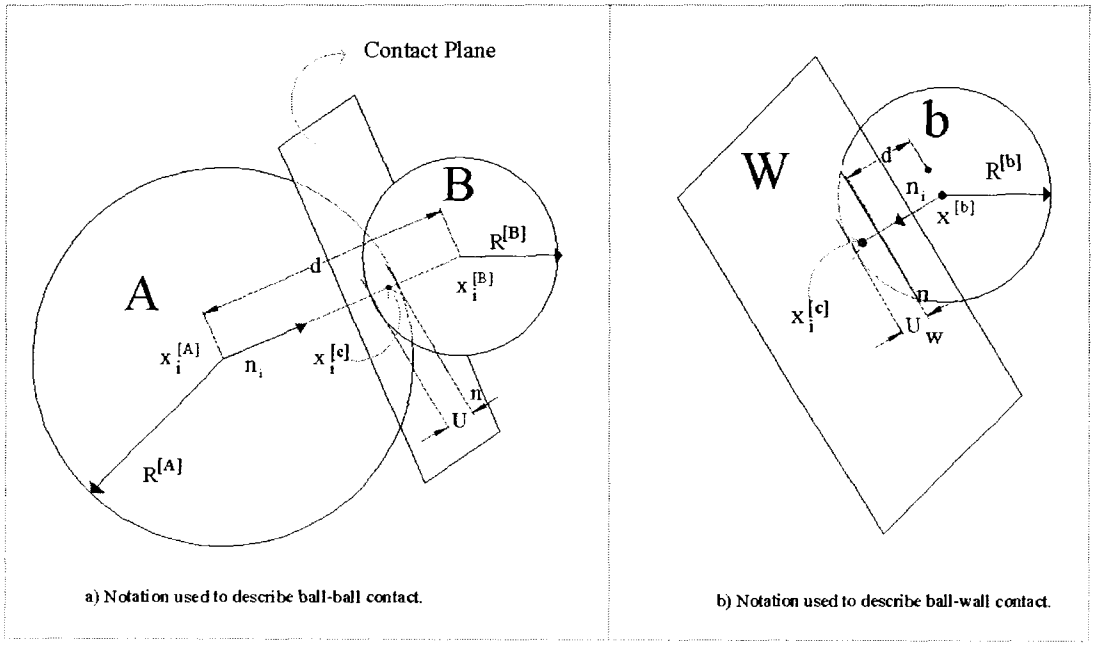

Figure 3.2: Collision notation (a): ball-wall contact. (b): ball-wall contact [18].

3.3.3. Calculation of Contact Forces (Force-Displacement Law)

The contact force with respect to the contact plane (Figure 2.1) can be determined by Equation (3.27) [18].

$$F_i = F_i^n + F_i^s \tag{3.27}$$

where:

$F_i (i = 1,2,3)$ represents the components of contact force with respect to the Cartesian coordinate system.

$F_i^n (i = 1,2,3)$ represents the components of the normal contact force with respect to the Cartesian coordinate system.

$F_i^s (i = 1,2,3)$ represents the components of shear contact force with respect to the Cartesian coordinate system.

3.3.3.1. Calculation of Normal Component of Contact Force

The normal component force of two contact bodies for ball-ball contact and ball-wall contact are calculated by Equations (3.28) and (3.29) respectively.

$$F_i^n = K^n U^n n_i \tag{3.28}$$

$$F_i^n \_ wall = K^n U_w^n n_i \tag{3.29}$$

where:

$F_i^n and F_i^n \_ wall$ are normal contact forces for a ball-ball contact and ball-wall contact, respectively, with respect to the Cartesian coordinates system.

K^n is the ball-ball or ball-wall contact stiffness.

U^n is the normal overlap in ball-ball contact.

U_w^n is the normal overlap in ball-wall contact.

n_i is the unit normal of the contact plane.

3.3.3.2. Calculation of Shear Component Force of Contact Forces

Shear contact force is found by the calculation of two rotations: the first being about the line common to the old and new contact planes, and the second being about the new normal direction. The shear force due to first rotation is determined by Equation (3.30).

$$\{F_i^s\}_{rot.1} = F_j^s(\delta_{ij} - e_{ijk}e_{kmn}n_{kmn}n_m^{[old]}n_n \tag{3.30}$$

where:

$\{F_i^s\}_{rot.1}(i=1,2,3)$ represents the shear force due to rotation about old normal of contact plane with respect to Cartesian system.

n_m^{old} is the old unit normal vector (previous step) to contact.

The shear force due to second rotation is determined by Equation (3.31)

$$\{F_i^S\}_{rot.2} = \{F_j^S\}_{rot.1}(\delta_{ij} - e_{ijk}(\omega_k)\Delta t) \tag{3.31}$$

where:

$\{F_i^s\}_{rot.2}(i=1,2,3)$ represents the shear force components due to rotation about new contact plane with respect to Cartesian system.

(ω_k) is average angular velocity of two contact bodies about the new normal direction (current time step). ω_k can be found by Equation (3.32).

$$\omega_k = 1/2(\omega_j^{[A]} + \omega_j^{[B]})n_j n_i \tag{3.32}$$

where:

$\omega_i^{[B]}(i=1,2,3)$ represents rotational velocity of ball B with respect to the Cartesian system.

$\omega_i^{[A]}(i=1,2,3)$ represents rotational velocity of ball A with respect to the Cartesian system.

$\omega_i^{[B]}(i=1,2,3)$ represents rotational velocity of ball B with respect to the Cartesian system.

The relative motion at contact, contact velocity, V_i is given by:

$$V_i = (\dot{x}_i^{[c]})_B - (\dot{x}_i^{[c]})_A = (\dot{x}_i^{[B]} + e_{ijk}\omega_j^{[B]}(x_k^{[c]} - x_k^{[B]})) - (\dot{x}_i^{[A]} + e_{ijk}\omega_j^{[A]}(x_k^{[c]} - x_k^{[A]})) \quad (3.33)$$

where:

$V_i(i=1,2,3)$ represents the velocity components with respect to the Cartesian system.

$\dot{x}_i^A(i=1,2,3)$ represents the translational velocities of ball A.

$\dot{x}_i^B(i=1,2,3)$ represents the translational velocities of ball B.

$$V_i^s = V_i - V_i^n = V_i - V_j n_j n_i \quad (3.34)$$

where:

$V_i^s(i=1,2,3)$ represents shear components of velocity with respect to the Cartesian coordinate system.

$V_i^n(i=1,2,3)$ represents normal components of velocity with respect to the Cartesian coordinate system.

The shear component of the contact displacement–increment vector, ΔU_i^s, over a time step of Δt, is found by:

$$\Delta U_i^s = V_i^s \Delta t \tag{3.35}$$

Elastic shear force-increment vector is calculated by Equation (3.36).

$$\Delta F_i^s = -k^s \Delta U_i^s \tag{3.36}$$

Finally the shear component of contact force in each time step is determined by Equation (3.37). By summing the old shear force (the shear force calculated at the previous time step) with the shear force- increment in this time step, the contact shear component is determined as follows:

$$F_i^s = \{F_i^s\}_{rot.2} + \Delta F_i^s \tag{3.37}$$

where:

F_i^s $(i = 1,2,3)$ represents shear force with respect to the Cartesian system.

$\Delta F_i^s (i = 1,2,3)$ represents elastic shear force-increments with respect to the Cartesian coordinate system.

3.3.4. Law of Motion

Newton's second law of motion predicts the behaviour of objects for which all existing forces are unbalanced. The presence of an unbalanced force will accelerate a particle that has variable velocity.

$$\sum F = ma \tag{3.38}$$

After finding contact forces, the resultant force on each ball can be determined. Using Newton's second law of motion, the translational and rotational accelerations for each ball at time t with respect to Cartesian coordinate system is calculated as Equation (3.39) [18].

$$\ddot{x}_i^t = \frac{1}{\Delta t}(\dot{x}_i^{(t+\Delta t/2)} - \dot{x}_i^{(t-\Delta t/2)}) \tag{3.39}$$

$$\dot{\omega}_i^t = \frac{1}{\Delta t}(\dot{\omega}_i^{(t+\Delta t/2)} - \dot{\omega}_i^{(t-\Delta t/2)}) \tag{3.40}$$

where:

$\ddot{x}_i^t (i = 1,2,3)$ represents the translation acceleration at time t.

$\dot{\omega}_i^t (i = 1,2,3)$ represent the rotational acceleration at time t.

Integrating above Equations, translational and angular velocities of balls are found at time $(t + \Delta t/2)$ as follow [18]:

$$\dot{x}_i^{(t+\Delta t/2)} = \dot{x}_i^{(t-\Delta t/2)} + (\frac{F_i^t}{m} + g_i)\Delta t \tag{3.41}$$

$$\omega_i^{(t+\Delta t/2)} = \omega_i^{(t-\Delta t/2)} + (\frac{M_i^{(t)}}{I} + g_i)\Delta t \tag{3.42}$$

where:

$\dot{x}_i^{(t+\Delta t/2)} (i = 1,2,3)$ represents the translational velocity at time at mid interval $(t + \Delta t/2)$.

$\dot{x}_i^{(t-\Delta t/2)} (i = 1,2,3)$ represents the translational velocity at time at mid interval $(t - \Delta t/2)$.

$\omega_i^{(t+\Delta t/2)} (i = 1,2,3)$ represents the rotational velocity at time at mid interval $(t - \Delta t/2)$.

Note that, ball velocity in Ng model is updated by Equation (3.43).

$$\dot{x}_i^{(t+\Delta t/2)} = \frac{\dot{x}_i^t (1 - \frac{\beta \Delta t}{2}) + \frac{F_i \Delta t}{m}}{(1 + \frac{\beta \Delta t}{2})} \tag{3.43}$$

Finally, the position of ball's centre (ball's trajectory) is updated by Equation (3.44) [18]:

$$x_i^{(t+\Delta t)} = x_i^{(t)} + (\dot{x}_i^{(t+\Delta t/2)})\Delta t \tag{3.44}$$

where:

$\dot{x}_i^{(t)}(i = 1,2,3)$ represents the position of ball's centre at time t.

$\dot{x}_i^{(t+\Delta t)}(i = 1,2,3)$ represents the new position of ball's centre at time $(t + \Delta t)$. This quantity will use for calculation of force and moment in next calculation cycle.

3.4. Comparison RocFall Algorithm and a Program Based on DEM

DEM potentially can be appropriate for rockfall simulation because of the following reasons:

1- Rocks can be modeled with more detail of their material properties, sizes and shapes.

2- The effect of contact of each rock on other rocks is considered as well as the effect of contacts of rocks on surfaces.

3- Microscopic behaviour of rocks can be tracked as well as macroscopic behaviour.

4- Since a surface can be defined with several triangles and each triangle has its own material properties and stiffness, surface can model very closely to real field conditions.

In contrast with a simulation program based on DEM, RocFall, which is based on the particle model, does not consider the effects of size or shape of each rock and contact of rocks with other rocks, nor the microscopic behaviour of rock and angular momentum of rocks on their trajectories. Also, a freefalling model cannot be modeled using RocFall since according to its algorithm initial velocity should be a non-zero value. In spite of its limitation, RocFall has the following advantages:

1. RocFall is extremely quick to calculate hence, it allows engineers easily find the critical cases by trying different models with different geometries and conditions. Thus, they can take advantage of the analysis of outputs resulting from this software. CPU time for a simulation program based on DEM for complex models would be very high since time steps are very small (the algorithm of RocFall is not based on time step), since according to its algorithm, several parameters are involved and several calculation should be performed.

2. Most of the inputs for RocFall such as slopes' geometry, coefficient of restitution for rock types and friction angle are usually available. Simulation of rockfall using 3D Discrete Element Method requires several inputs. In spite of the RocFall inputs required materials' properties and damping ratio are not available for certain rock types.

3. RocFall is user friendly software and its algorithms are easy to understand; therefore user can be trained fast. A program based on DEM requires series of adjustments and calibration, therefore strong knowledge of rock and dynamics of contacts for analysis of the outputs are required for the user.

4. Some statistical analysis are carried out for output of the rockfall simulation such as distribution of horizontal location of rocks' end points, which provides engineers with necessary information for design efficient remedial measures at appropriate locations.

4. Haraz: Overview and Details

In this chapter, the computer program "Haraz" is presented. The code is based on DEM. "Haraz" is an object oriented program and is written in C++. The main reasons for using C++ are: Codes compiled in C++ are optimal (compared with other high level language codes), which makes them ideal when working on large codes. Furthermore, in C++ there is more control on main memory and this is essential for making a powerful data structure.

In this code there are two main elements, namely ball and wall. Balls are assumed to be spherical rocks with different sizes and materials. Walls are composed from some triangles with different material and stiffness.

4.1. Calculation Cycle

Figure 4.1 shows the general flowchart of computer program Haraz.

4.1.1. Generation of Balls

In this part, balls are generated and their properties are assigned. Balls are spherical rocks with different sizes and materials. First, material properties and radius of each ball are read from an input file, Data.txt. Then, mass, circular section area, moment of inertia and polar moment are calculated according to the following Equations. Finally, after running the program, out put files are printed out.

$$m = 4/3\pi R^3 \gamma / 9.81 \quad (4.1)$$

$$A = \pi R^2 \quad (4.2)$$

$$I = 1/4\pi R^4 \quad (4.3)$$

$$J = 1/2\pi R^4 \quad (4.4)$$

where:

m is mass for each ball.

γ is ball density.

R is ball radius.

I is ball moment of inertia.

J is ball polar moment of inertia.

4.1.2. Ball's Initial Conditions

The initial position of each ball center can be either defined by the user or by randomly generating by uniform distribution over a point assigned by user or equally distributed tangent along a line parallel to impact surface (wall). Note that balls at the initial position should not overlap to avoid initial contact forces. The initial velocity of each ball is also defined by the user.

4.1.3. Generation of Walls

Wall is composed of triangular meshes. The coordinate of vertexes of the triangles are read from input file called "Wallpoints.txt". Also, the linear normal and shear stiffness are read from "Wallstiffness" and are assigned to each mesh. Then, the unit normal of each triangle is calculated.

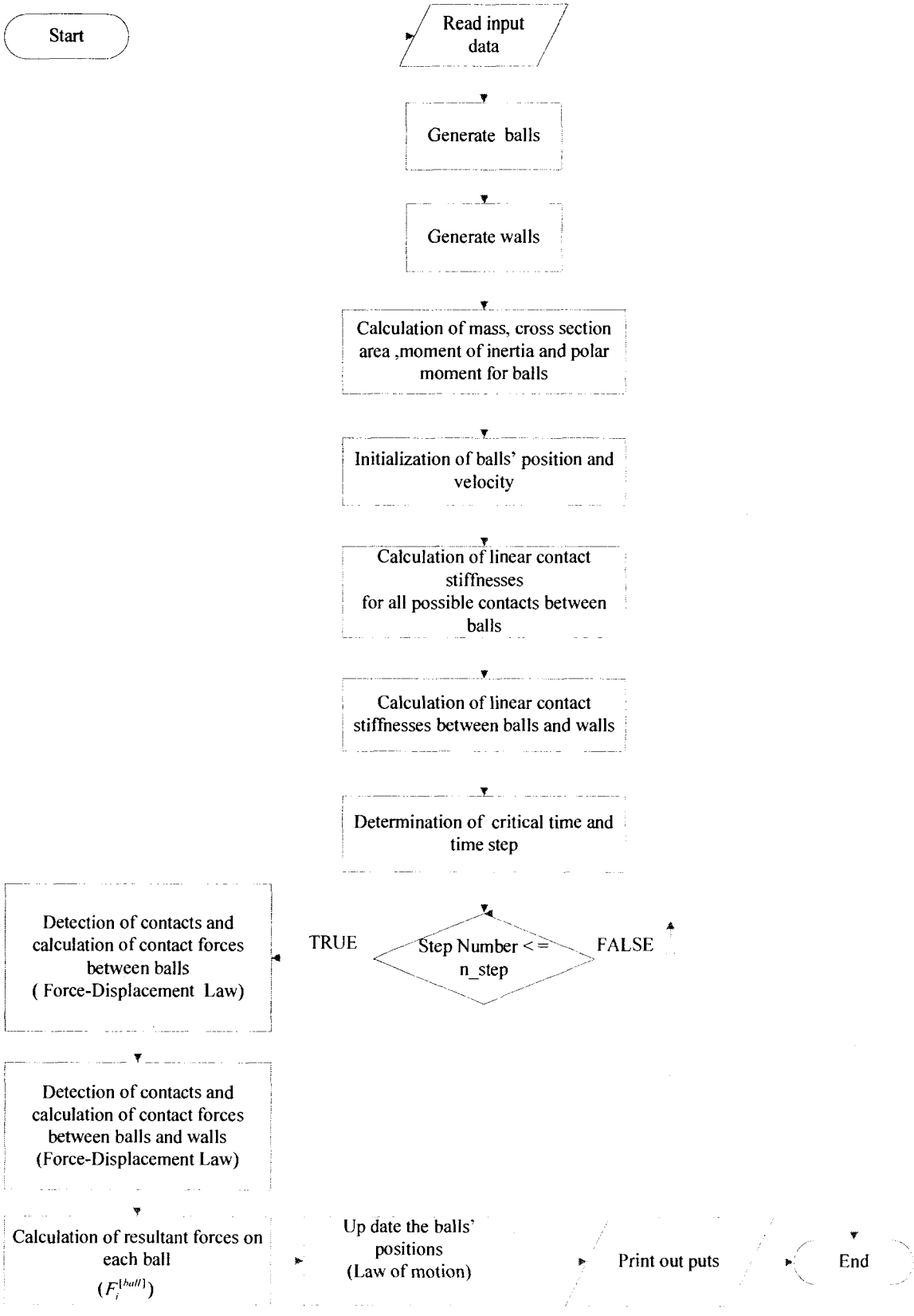

Figure 4.1: Flowchart representation of main block in Haraz.

4.1.4. Determination of the Time Step

For determination of time step, first normal and shear stiffness of each ball and wall are read from related input files and linear normal and shear contact stiffness for all possible ball-ball and ball-wall contacts and the translational and rotational stiffnesses are calculated. After determination of maximum stiffness and minimum stiffness, critical time is calculated using equation (3.20). Finally, by choosing a value for α (coefficient of time step), and multiplying it by the critical time, time step is determined.

4.1.5. Force-Displacement Law

For each ball-ball contact and ball-wall, normal and shear contact forces viscous damping forces are calculated using "CForce" function and "CForce_wall" function, respectively. Figure 4.2 illustrates the calculation procedure of normal and shear stiffness between two balls and Figure 4.3 illustrates the calculation procedure of normal and shear stiffness between a ball and a wall. After calculation of contact force and viscous damping forces, resultant forces acting on each ball are determined. According to contact type contact stiffnesses are calculated.

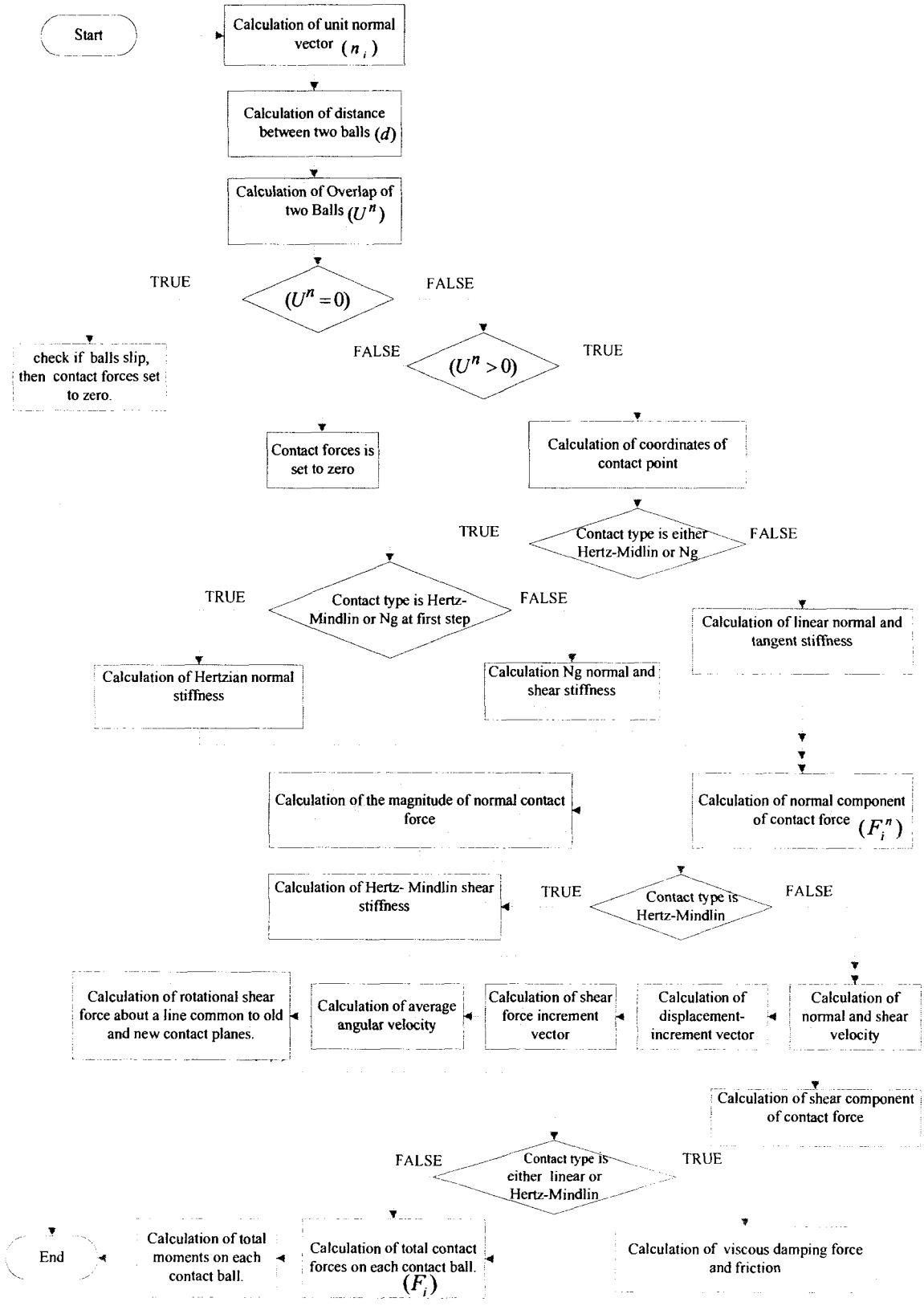

Figure 4.2: Flowchart representation of function CForce: Calculation of contact forces between two balls.

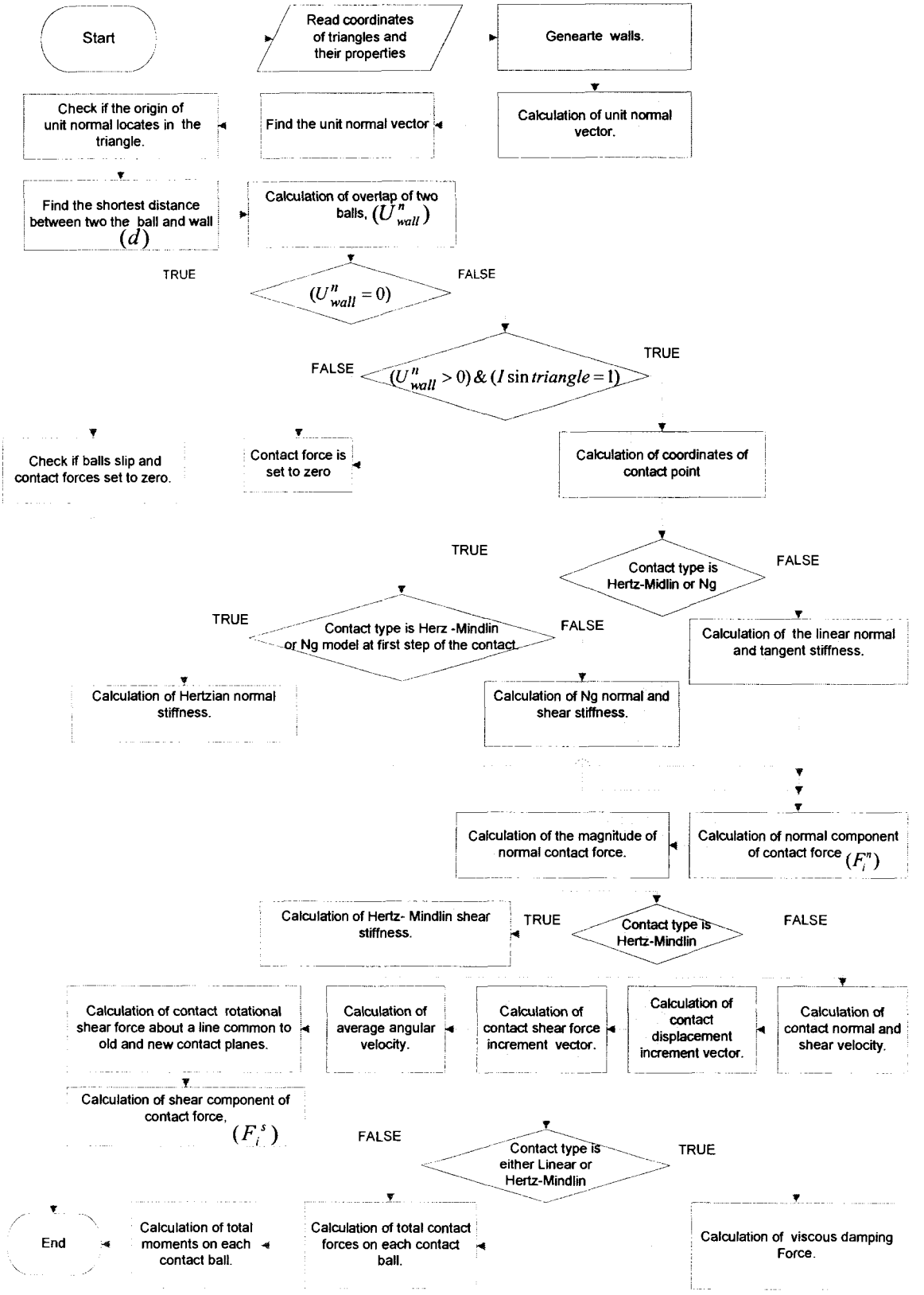

Figure 4.3: Flowchart representation of function CForce_wall: Calculation of contact forces between a ball and a triangle.

4.1.5.1. Calculation of Contact Stiffness for Linear, Hertz-Mindlin and Ng Models

Linear normal and shear stiffness using Equations (2.21) and (2.22). Figure 4.4 and Figure 4.5 illustrate the calculation procedure of normal Hertz-Mindlin stiffnesses and shear Hertz-Mindlin stiffnesses respectively.

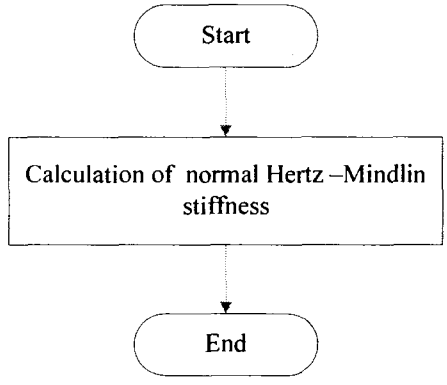

Figure 4.4: Flowchart representation of calculation Hertz-Mindlin normal forces.

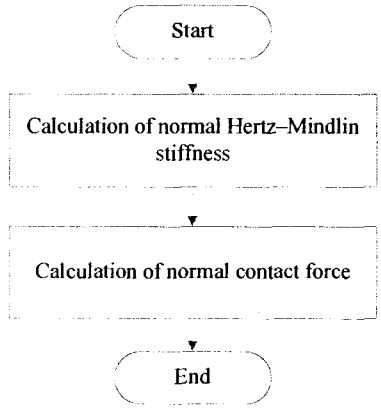

Figure 4.5: Flowchart representations of Hertz-Mindlin shear stiffness.

Figure 4.6 illustrates the calculation procedure of normal and shear stiffness for Ng model.

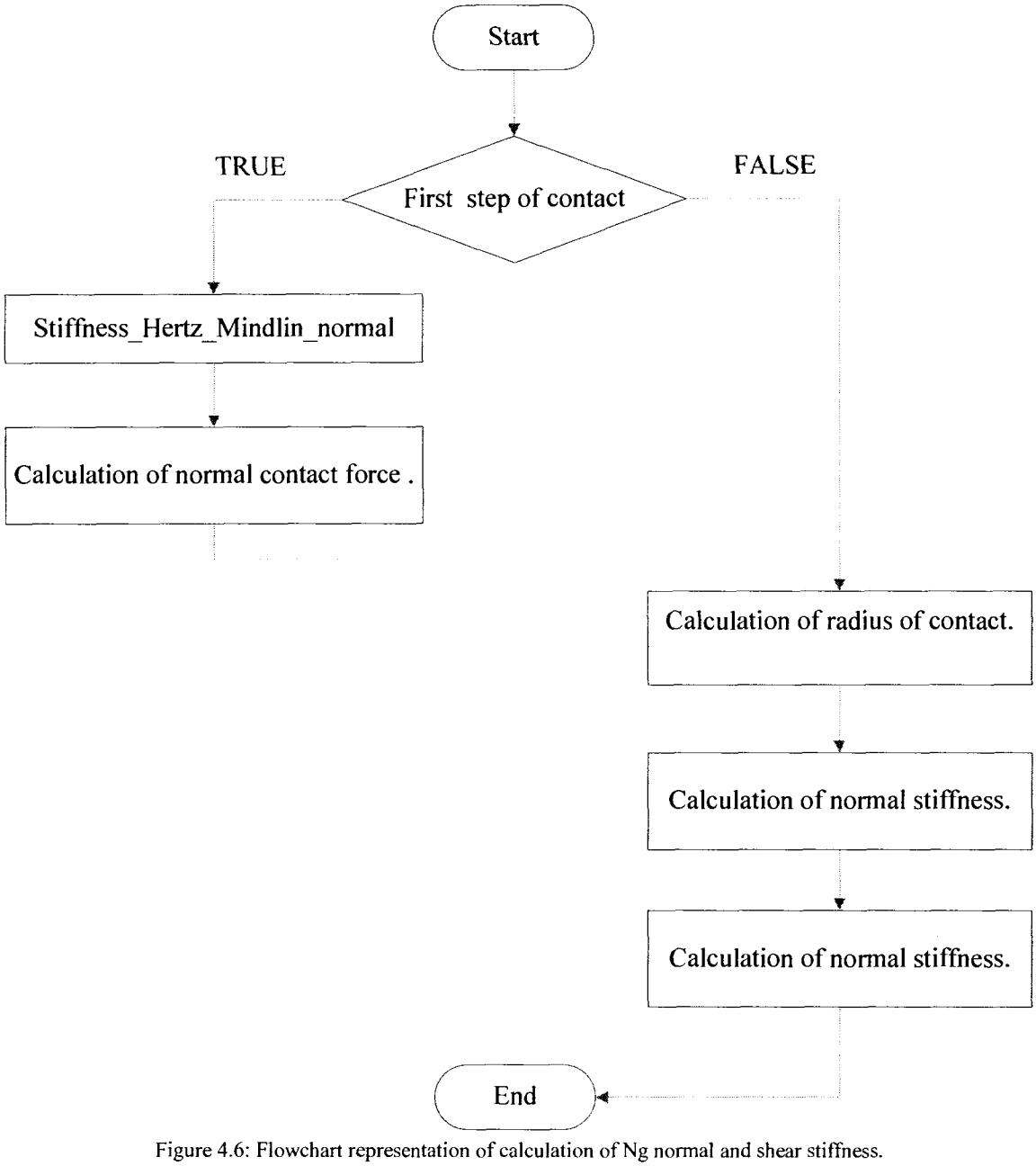

Figure 4.6: Flowchart representation of calculation of Ng normal and shear stiffness.

Figure 4.7 illustrates the procedure of calculation of normal contact forces according to An model.

After calculation of contact stiffnesses, using Equation (3.28) and (3.29), contact forces for linear, Hertz-Mindlin, Ng are calculated.

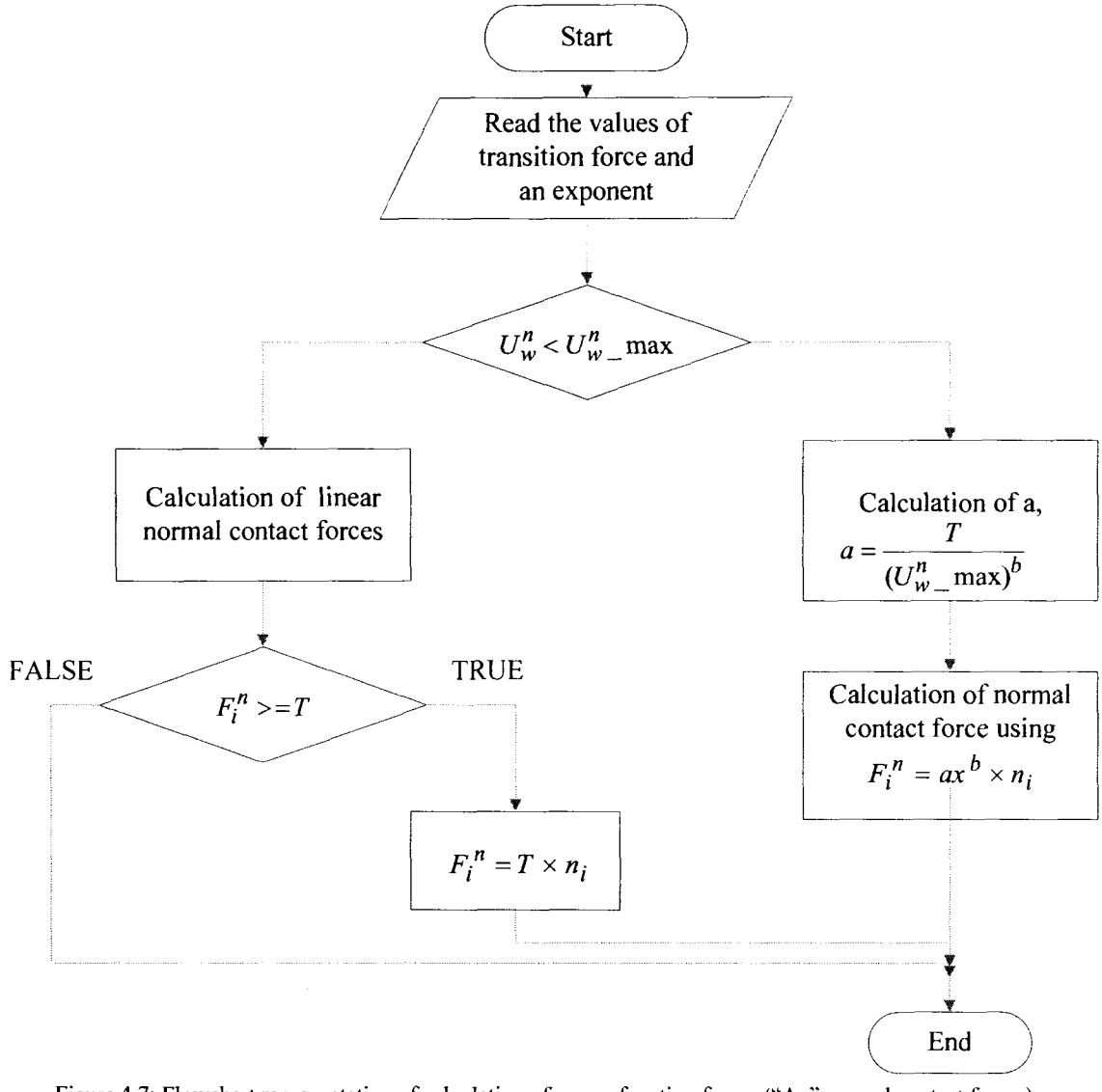

Figure 4.7: Flowchart representation of calculation of power function forces ("An" normal contact forces).

4.1.5.2. Calculation of Viscous Damping Forces

Figure 4.8 illustrates the calculation procedure of viscous damping force.

4.1.5.3. Calculation Unit Normal for Ball-Wall Contact

Equation (4.5) is the standard equation of a plane in 3D space:

$$Ax + By + Cz + D = 0 \tag{4.5}$$

(A, B, C) represent normal vector on the plane. Expanding the above gives:

$$A = y_1(z_2 - z_3) + y_2(z_3 - z_1) + y_3(z_1 - z_2) \quad (4.6)$$

$$B = z_1(x_2 - x_3) + z_2(x_3 - x_1) + z_3(x_1 - x_2) \quad (4.7)$$

$$C = x_1(y_2 - y_3) + x_2(y_3 - y_1) + x_3(y_1 - y_2) \quad (4.8)$$

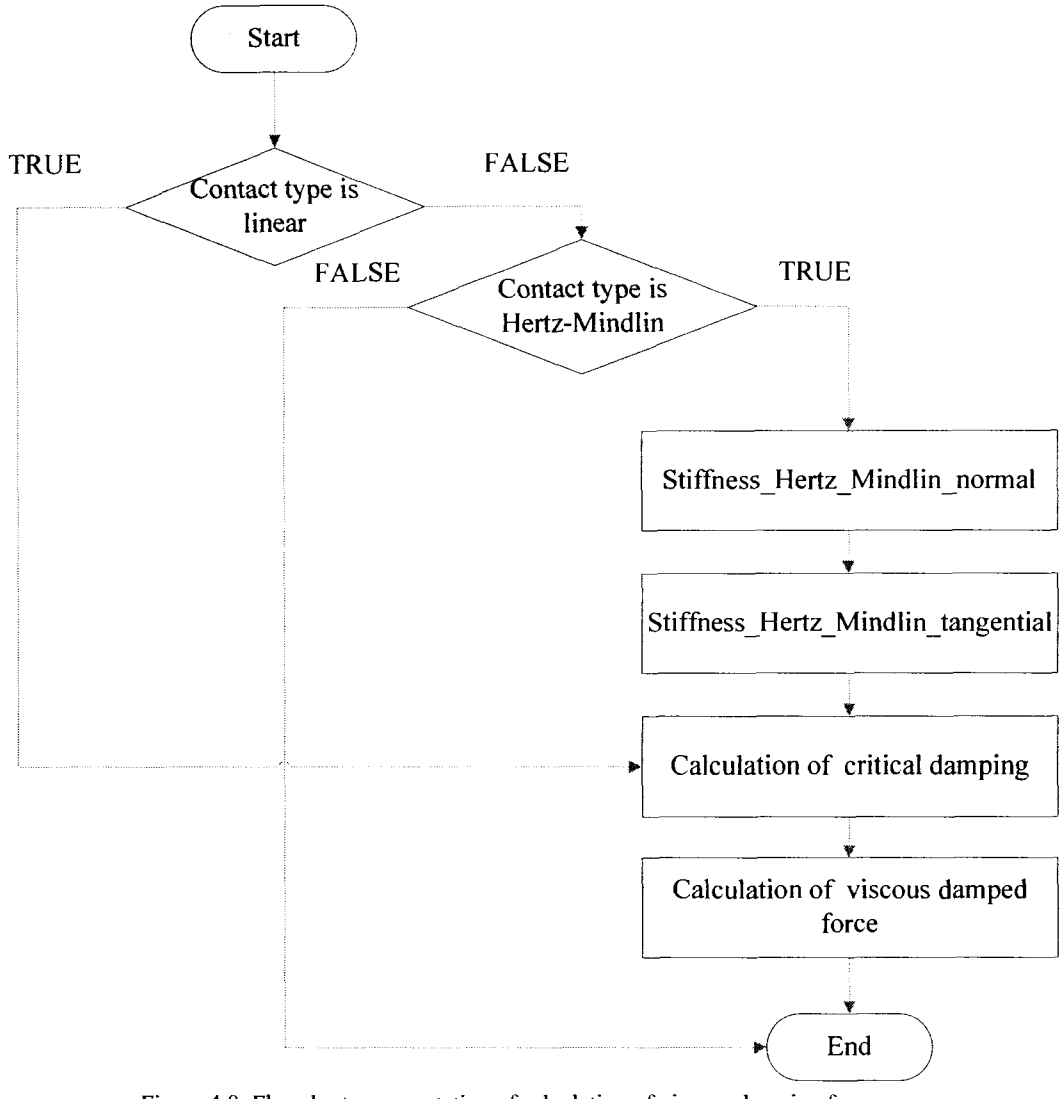

Figure 4.8: Flowchart representation of calculation of viscous damping forces.

4.1.5.4. Perpendicular_ Origin

Equations (4.5), (4.6), (4.7) and (4.8) allow us to calculate the magnitude and the direction of the vector normal to the plane. However, the origin of this vector can be anywhere on the plane of (not necessarily on the mesh). In Haraz,

"Perpendicular_Origin" function determines the coordinates of perpendicular origin on the plane.

4.1.5.5. isInTringle

The "isInTriangle" function checks if the origin of the unit normal vector is located within the mesh.

4.1.5.6. Find_TheShortest_distance: Calculation of the Distance between Ball and Wall

Figure 4.9 illustrates all possible positions of mapped ball centre on the wall. When Ball centre lies in zone (2) or zone (4), distance is the length of normal, and it can be calculated by Equation (4.9)

$$d = \left| x_i^{ball} - x_i^{perpendicu\ lar\ \_\ foot} \right| \tag{4.9}$$

W

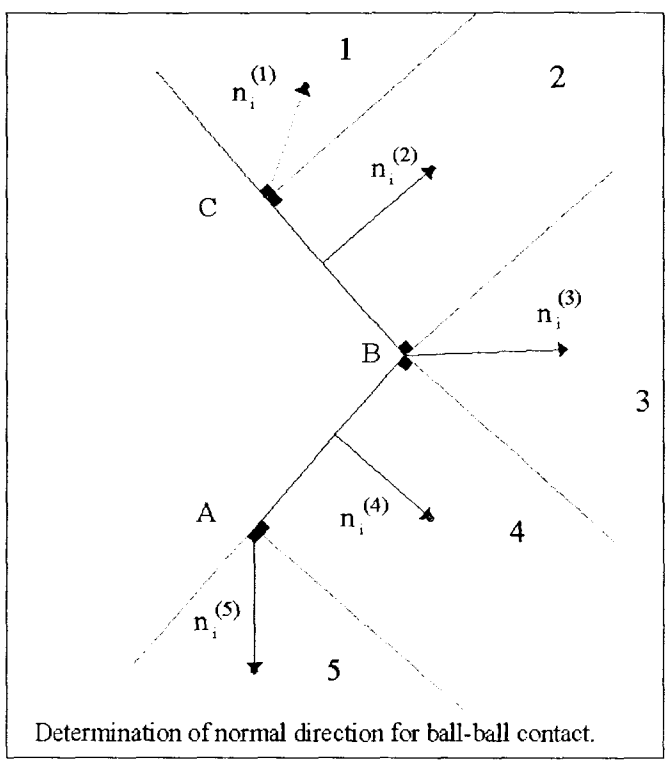

Figure 4.9: Normal unit vector in ball-wall contact [18].

When the ball center located in zone (1), (3) or (5) contact will occur at one of the endpoints. To find out which endpoint, the distance between ball center and three vertexes of triangle is calculated, and the least value would be considered as a distance of ball and the triangle.

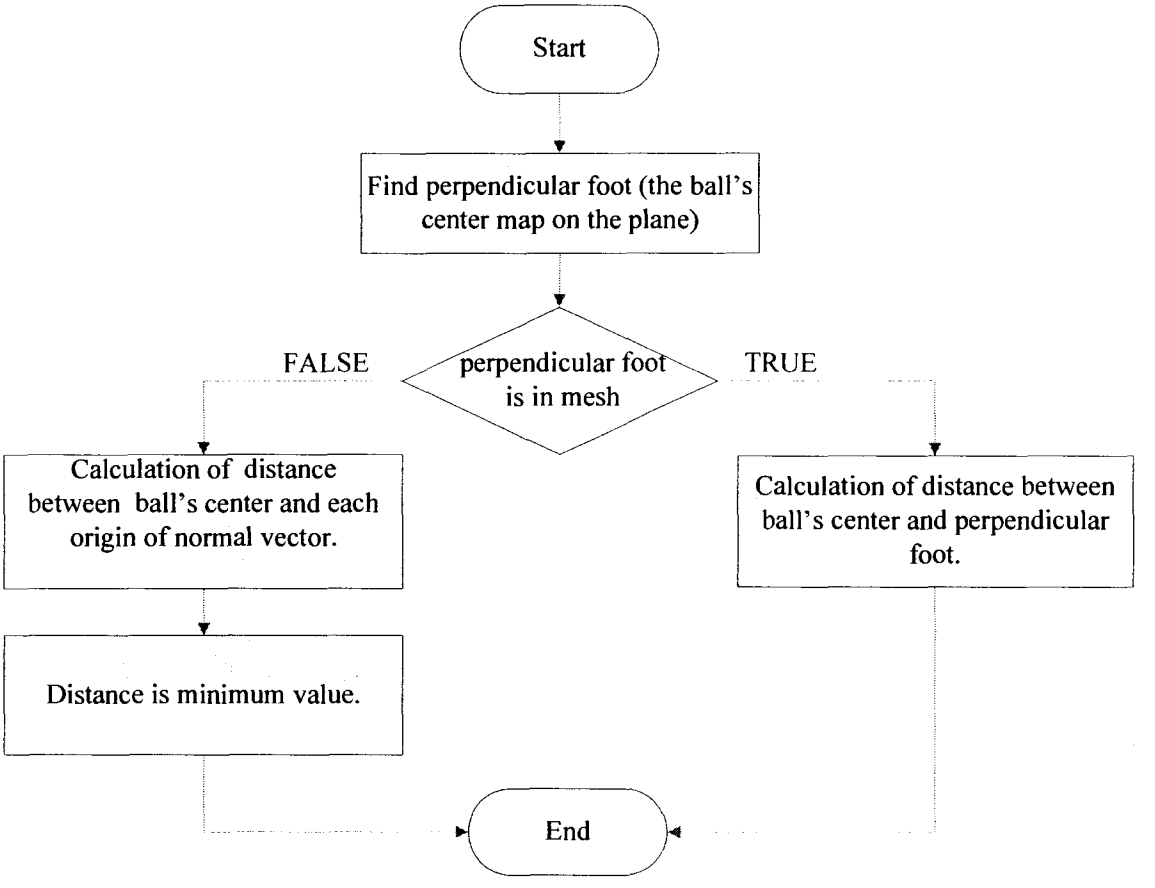

Figure 4.10: Flowchart representation of calculation of the shortest distance between a ball and a triangle.

4.2. Newton's Second Law of Motion

Figure 4.11 represents the procedure of finding new position of each object at the end of the calculation cycle.

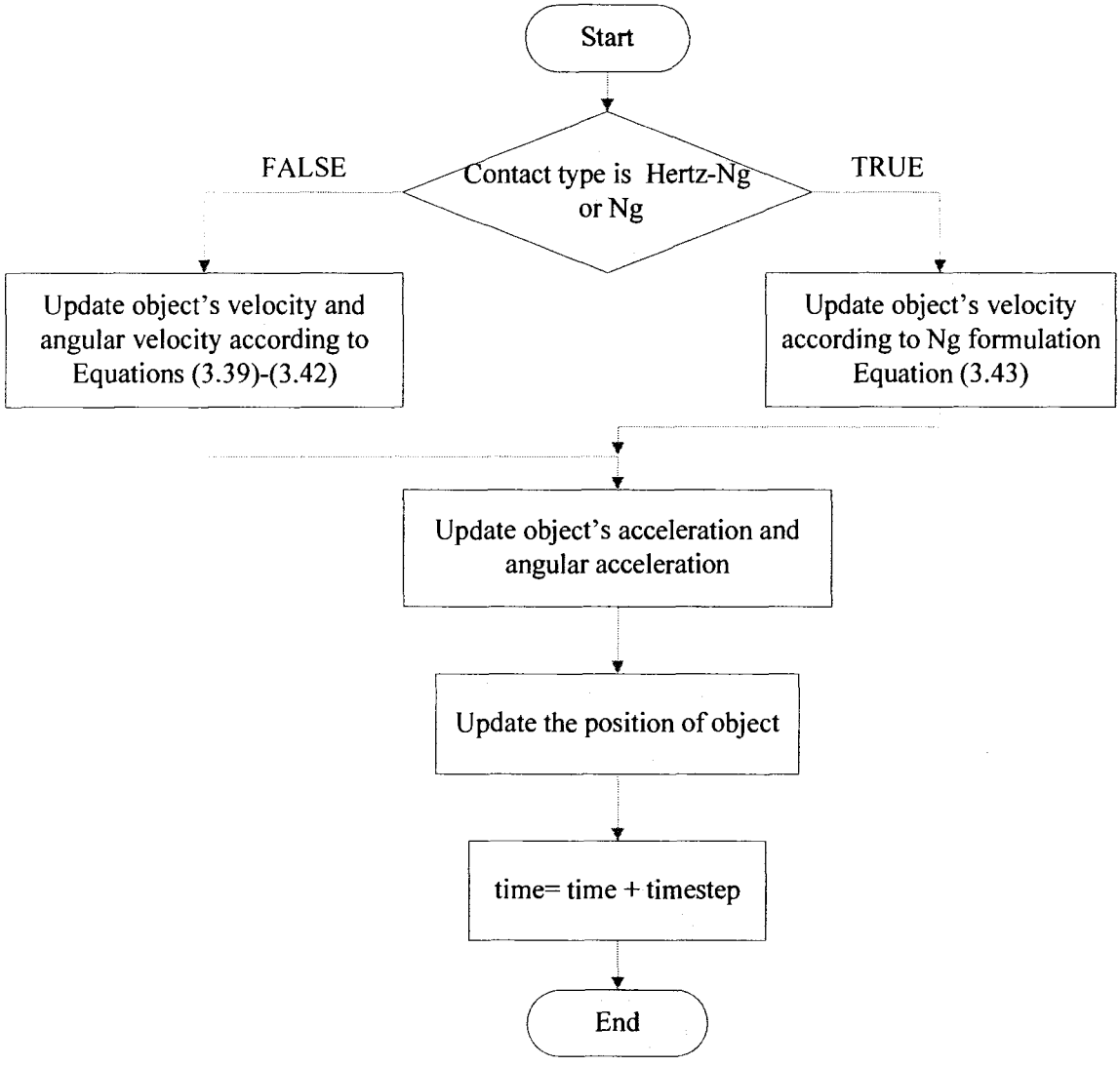

Figure 4.11: Flowchart representation of compute new position of an object using the law of motion.

5. Nonlinear Normal and Shear Stiffness for Different Rock Types

This chapter is concerned with normal and shear stiffnesses, which are produced by Hertz-Mindlin, Hertz-Ng and Ng model. To be able to compare the outcomes of contact models, the ratio of normal stiffness to shear stiffness for different rock types is calculated. Also, variation of normal contact force in respect to time and normal displacement is presented in this chapter. In these models, normal stiffness depends upon objects' material properties: Poisson ratio υ, elastic shear modulus G, and objects' geometry such as radius of ball and contact properties: contact normal overlap. Shear stiffness in addition to material and geometry properties, also depends upon the magnitude of the normal contact force. Table 5-1 illustrates the material's properties of some rock types [40] and Table 5-2 is part of input file for computer program and describes the properties of a ball with *100.8 N* weight (radius of *0.21 m* and density of *2600 kg/m*^{3}) subject to 1.0 m free fall to horizontal wall (Figure 6.1) in ideal situation (damping ratio is equal to zero).

Table 5-1: Properties of some rock types [40].

Rock Type [40]	Young modulus, E (GPa)	Poisson's ratio, υ (dimensionless)	Elastic shear modulus, G (GPa)	Unconfined Compressive Strength (MPa)
Westerly Granite	56	0.11	25.225	229
Lac du Bonnet Granite	69	0.26	27.381	200
Berea Sandstone	19	0.38	6.884	90
Springwell Sandstone	12	0.36	4.412	47
Tournemire Mudstone	23	0.32	8.712	56

Table 5-2: Inputs for the model.

Number of triangles	Number of balls	Number of steps	Contact type code	R (m)	K_n (N/m)	K_s (N/m)	γ (N/m^3)	β
2	1	1×10^7	1,3,4	0.21	6.4×10^{10}	9.6×10^6	2600	0

In order to investigate normal and shear stiffness for Hertz-Mindlin, Hertz-Ng and Ng model, a model of a ball and horizontal wall are modeled. Since in linear model the method to determine the stiffness of individual contact bodies as well as the relation between stiffness and rock properties is not discussed, the comparison of these contact models can be used to find a reasonable range for linear stiffness when a linear model is used. Note that the values of linear stiffnesses are used for determination of time steps in this problem.

5.1. Hertz – Mindlin Model

Normal and shear stiffnesses in Hertz-Mindlin are calculated by Equations (2.24) and (2.25) respectively. Figure 5.1 and Figure 5.2 demonstrate Hertz-Mindlin normal and shear force for some rock types of ball-wall contact. In this case the normal stiffness for all mentioned rock types is about 80% of shear contact stiffness as shown in Table (5-3).

Table 5-3: The ratio of maximum normal stiffness to shear stiffness using Hertz-Mindlin contact model for first impact.

Rock type	$\frac{K^n}{K^s}$
Westerly Granite	0.708
Lac du Bonnet Granite	0.784
Berea Sandstone	0.871
Springwell Sandstone	0.854
Tournemire Mudstone	0.824

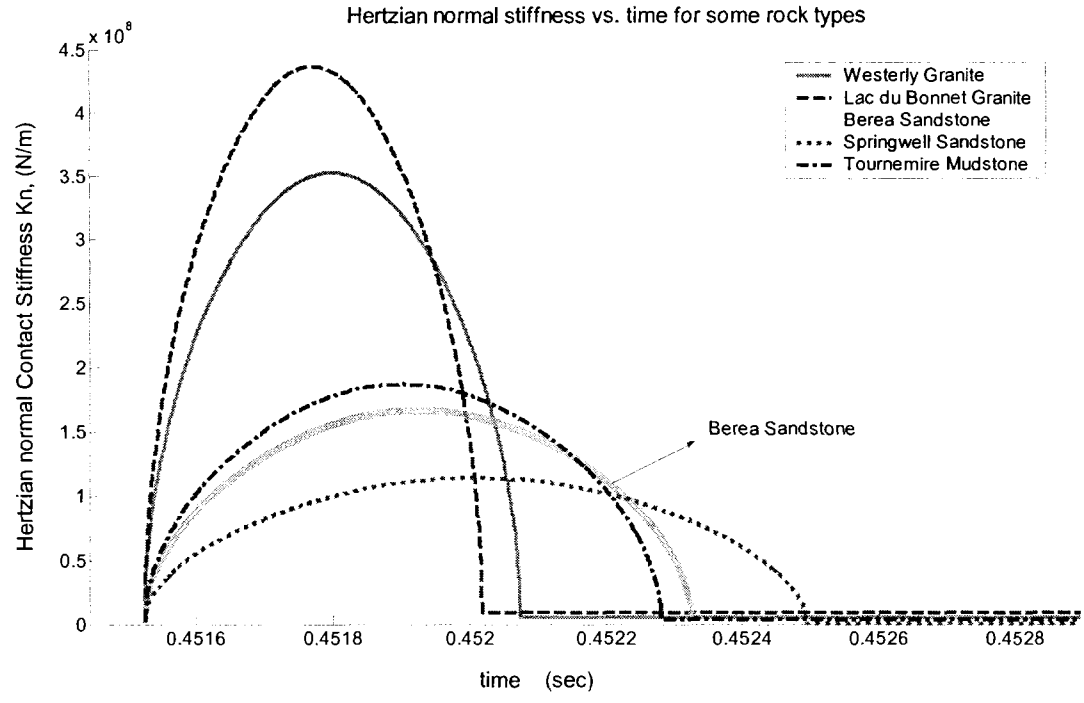

Figure 5.1: The normal stiffness produced by Hertz-Mindlin model for different rock types.

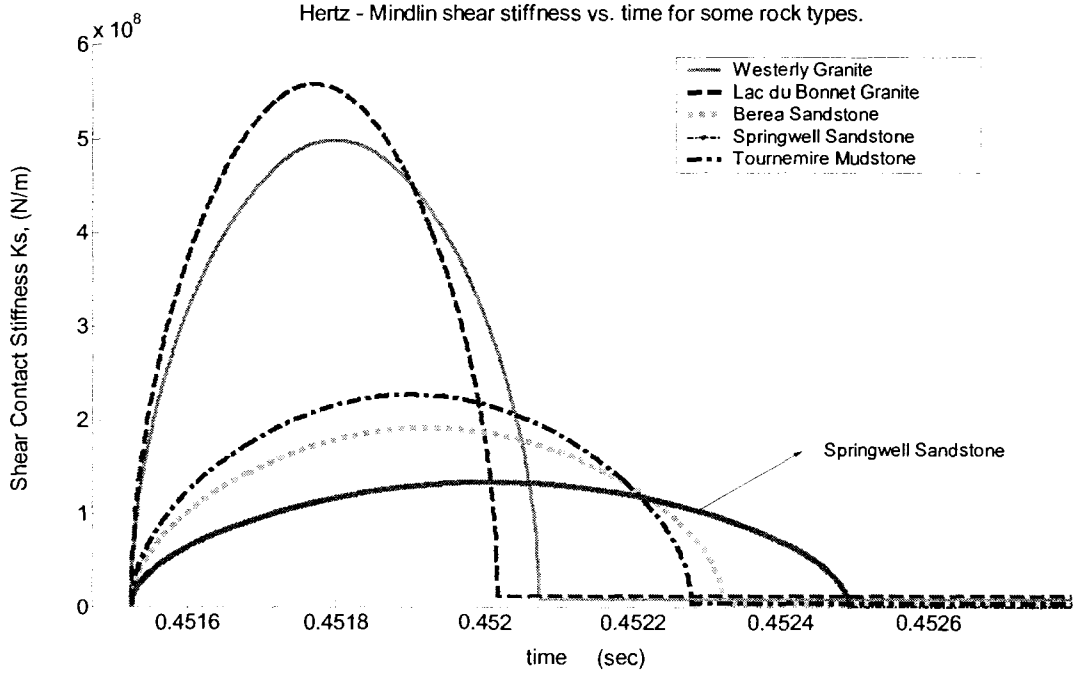

Figure 5.2: The shear stiffness produced by Hertz-Mindlin model for different rock types.

Figure 5.3 illustrates the normal contact forces of the contact model for the mentioned rock types. The value of normal contact forces are calculated by Equation (3.28).

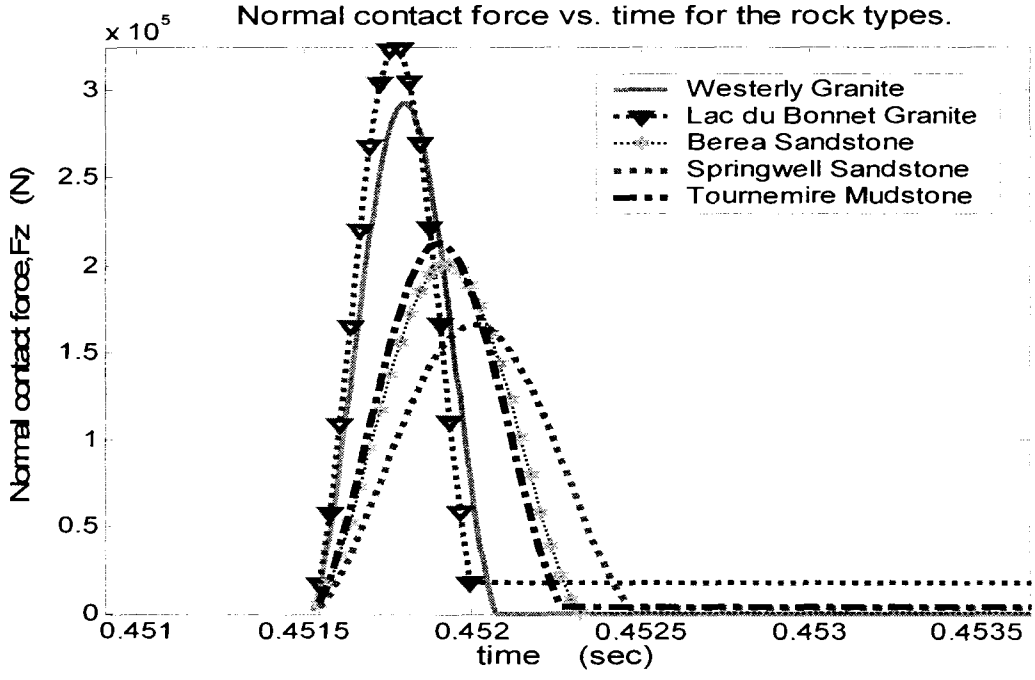

Figure 5.3:The variation of normal contact force versus time.

Figure 5.4 illustrates the variations of normal contact force versus normal overlap for the mentioned rock types. The slope of tangents to curve shows the normal stiffness of the contact.

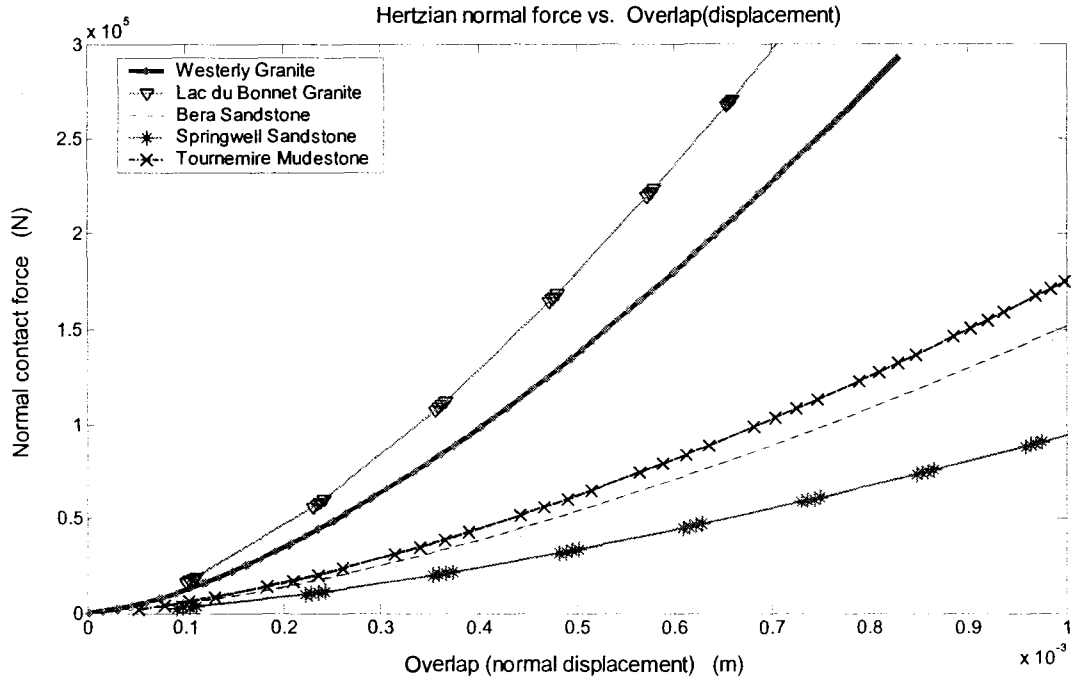

Figure 5.4: The variation of normal contact force versus normal displacement.

5.2. Ng Normal and Shear Stiffness for Different Rock Types

Ng normal and shear stiffness contact for ball-wall contact are calculated by Equation (2.37) and (2.38) respectively. Both normal and shear stiffnesses depend on normal contact force in addition to material and geometry properties. For the first step of contact, when normal contact force is not determined, in this work, the magnitude of normal force is calculated by Hertz-Mindlin formula. Figure 5.5 illustrates the variation of contact normal stiffness versus time for different rock types using Ng model. Figure 5.6 illustrates the variation of contact shear stiffness versus time for the same rock types. Ng normal stiffness is noticeably less than shear stiffness as it is shown in Table 5-4.

Table 5-4: The ratio of maximum normal stiffness to shear stiffness using Ng contact model for first impact.

Rock types	$\frac{K^n}{K^s}$
Westerly Granite	0.0037
Lac du Bonnet Granite	0.0038
Berea Sandstone	0.0057
Springwell Sandstone	0.0063
Tournemire Mudstone	0.0052

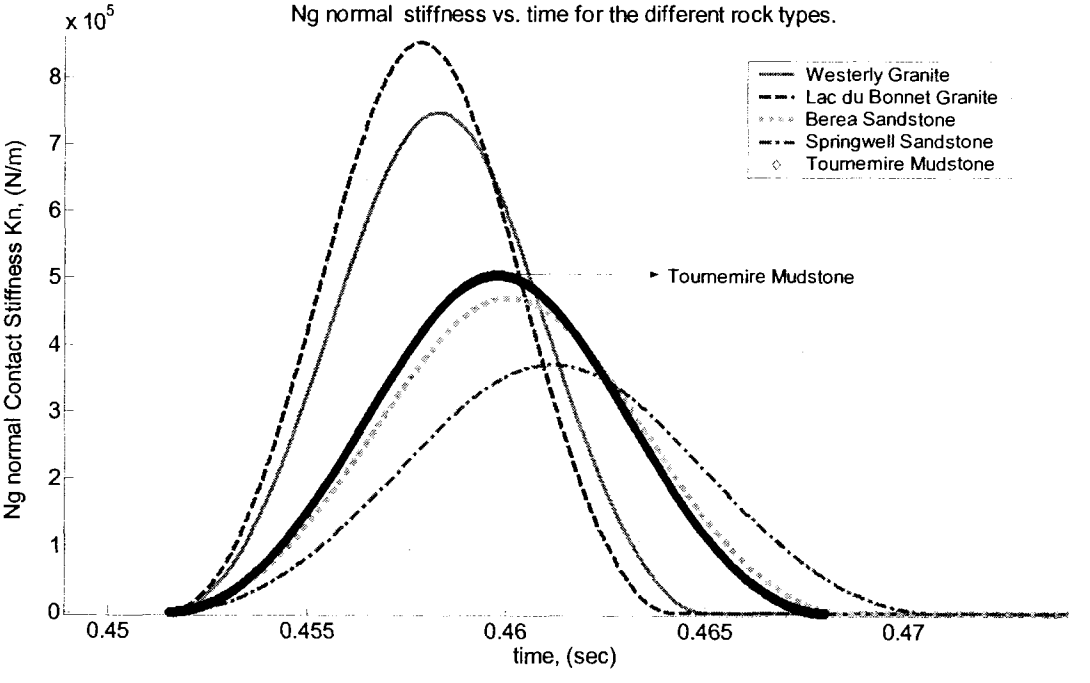

Figure 5.5: The Variation of Ng normal stiffness versus time for different rock types.

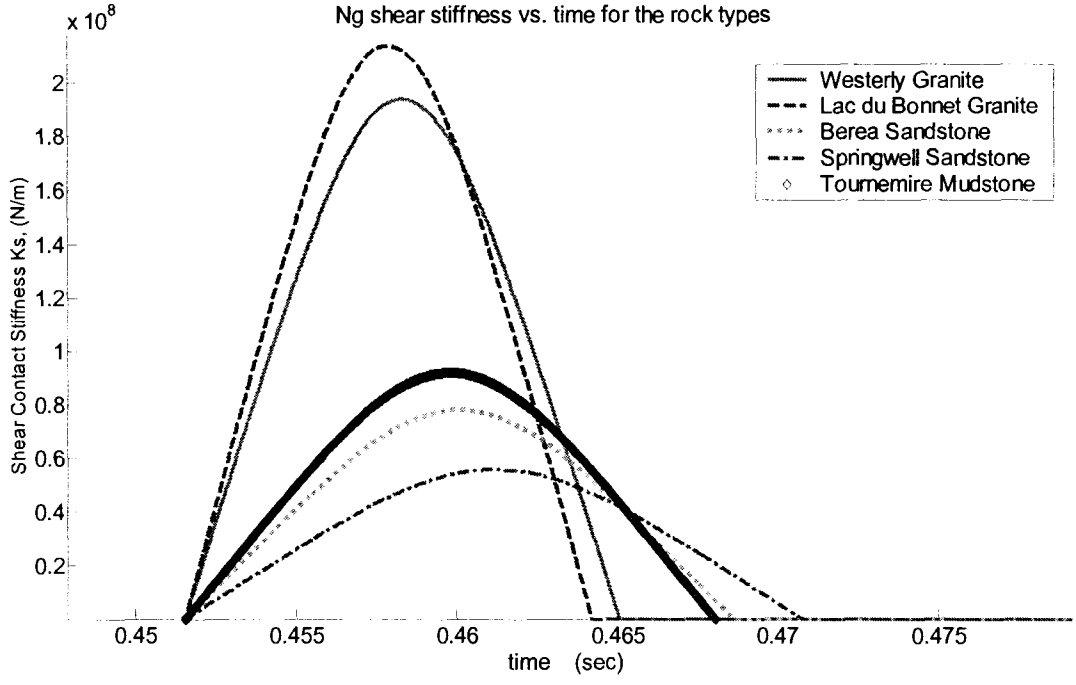

Figure 5.6: The variations of Ng shear stiffness versus time for different material.

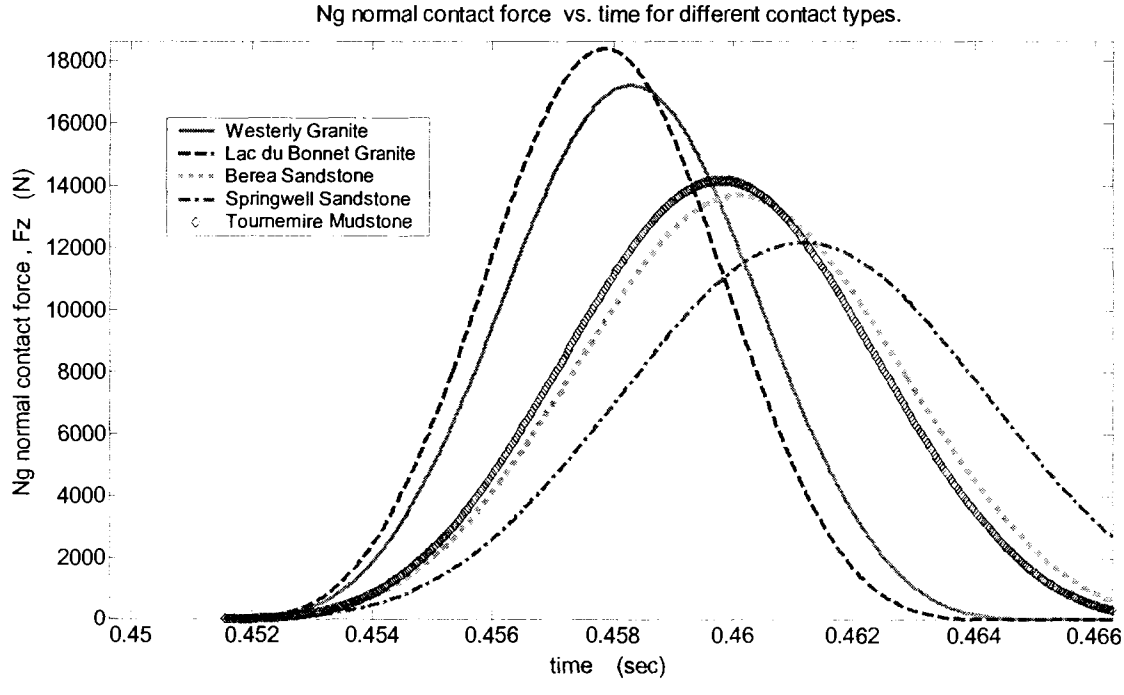

Figure 5.7: The variation of Ng normal forces versus time during first contact.

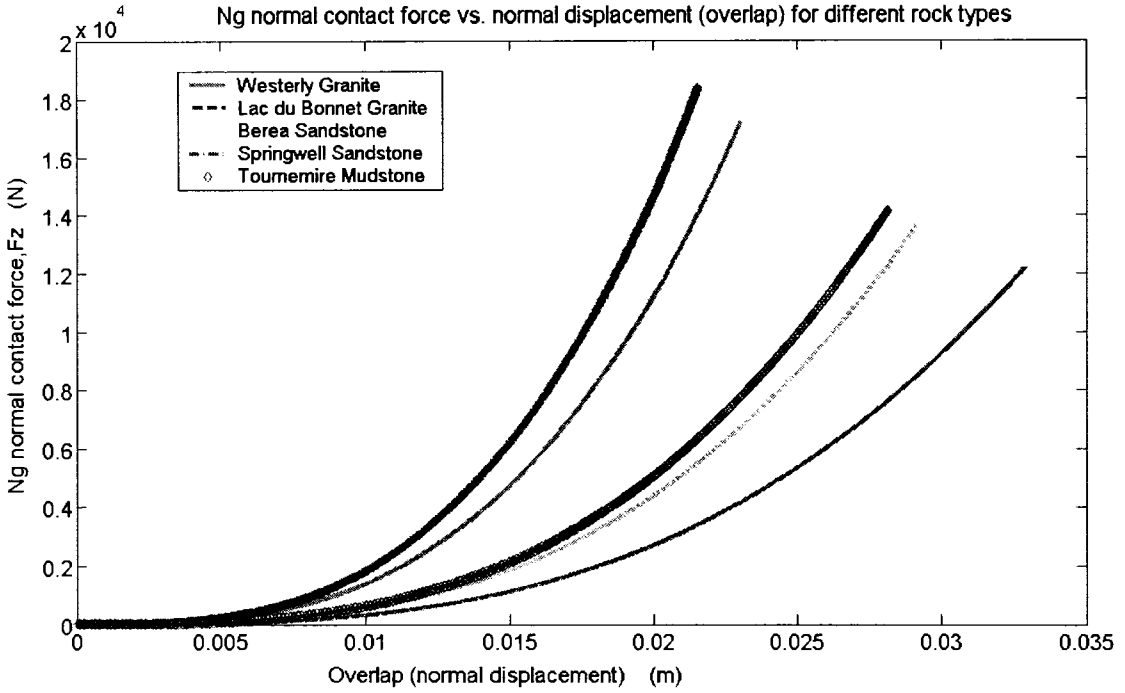

Figure 5.8: The variation of Ng normal forces versus normal displacement for different rock types.

As previously discussed, damping ratio directly affects on calculation of new velocity in Equation (2.41). The relation of damping ratio β in this model and normal coefficient of restitution will be discussed later.

5.3. Hertz-Ng Model

This model combines Hertz-Mindlin and Ng model, i.e., contact stiffness and consequently forces are calculated by Hertz-Mindlin method, at which normal stiffness does not depend upon the value of magnitude of normal force. However, viscous damping used in form of Ng model and the value of damping ratio directly affects the new velocity. As it can be seen in Table 5-5, in this case the ratio of maximum normal stiffness to maximum shear stiffness is greater than Ng model and less than Hertz-Mindlin model.

Table 5-5: Ratio of maximum normal stiffness to shear stiffness using Hertz-Ng contact model for first impact

Rock types	$\frac{K^n}{K^s}$
Westerly Granite	0.0095
Lac du Bonnet Granite	0.0100
Berea Sandstone	0.0144
Springwell Sandstone	0.0152
Tournemire Mudstone	0.0130

Figure 5.9 and Figure 5.10 illustrate the variations of Hertz-Ng contact normal and shear stiffness versus time for above rock types respectively.

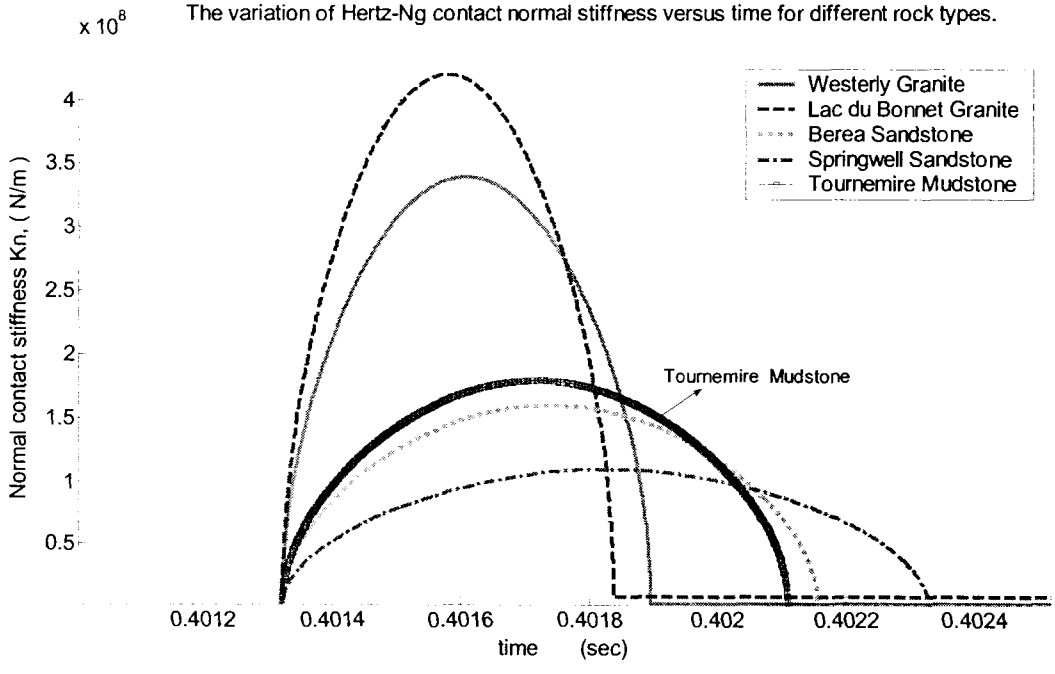

Figure 5.9: The variation of Hertz-Ng contact normal forces versus time for different rock types.

Figure 5.11 illustrates the variations of Hertz-Ng normal contact force versus normal overlap for the mentioned rock types. The slope of tangents to curve shows the normal stiffness of the contact.

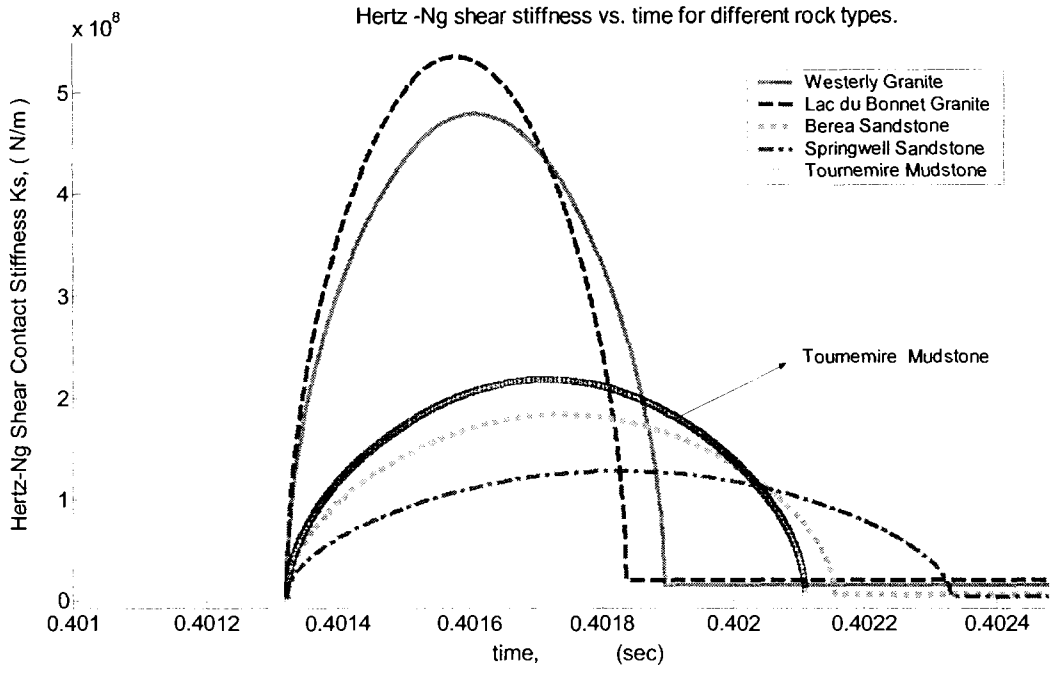

Figure 5.10: The variations of Hertz-Ng shear stiffness versus time for different rock types.

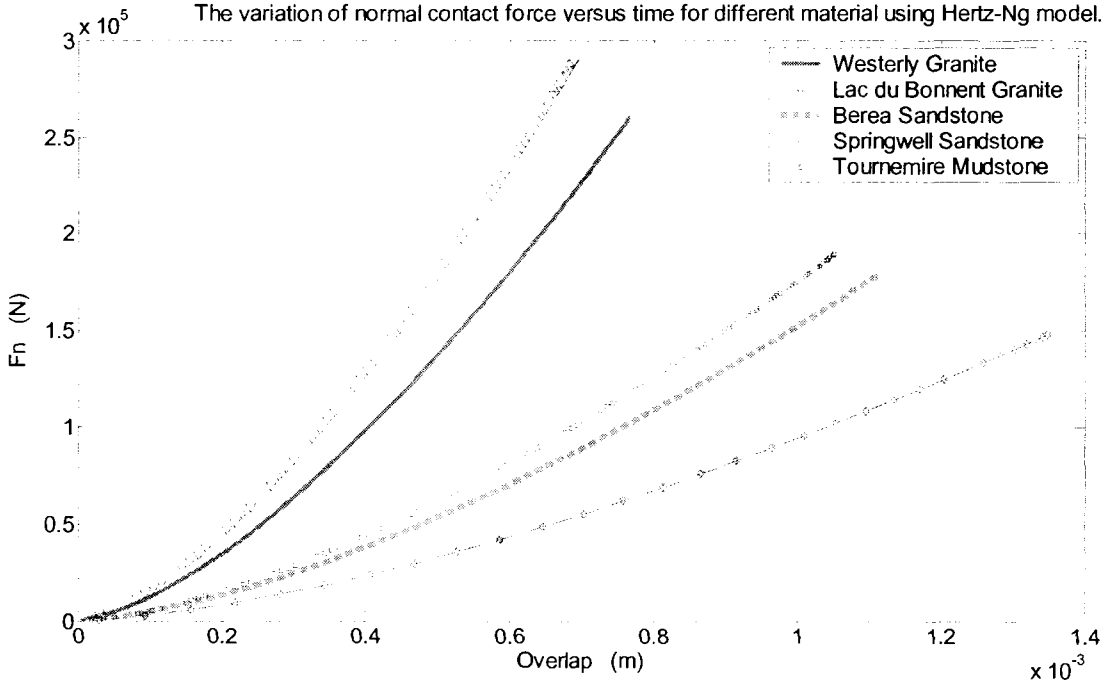

Figure 5.11: The variation of normal contact forces versus normal displacement for different rock types.

5.4. Summary

- Normal and shear stiffnesses and consequently contact forces in Hertz-Mindlin model are larger than the values in Hertz-Ng and Ng models.
- Considering the ratio of normal stiffness to shear stiffness, the ratio of normal stiffness to shear stiffness in Hertz-Mindlin, Hertz-Ng and Ng model are noticeably different. Normal stiffness in Hertz-Mindlin model is about 80 %, in Hertz-Ng model is about 1% and in Ng model less than 1% of shear stiffness.
- Linear, Hertz-Mindlin, Hertz-Ng and Ng contact models only describe the elastic deformation of rocks as force-displacement curves in these models are reversible for different rocks. Therefore, these models do not show the complete presentation of behaviour of colliding rocks and energy loss due to rock fragmentation.

6. Influence of the Contact Models on Dynamic Responses of Falling Ball on a Horizontal Wall

This chapter is concerned with demonstration of microscopic and macroscopic behaviours of a freefall ball colliding with a flat and horizontal wall when different contact models are used. Since collision of a ball and a flat wall can be considered as generalization of the case of collision of two identical spheres [24], the results of this model can be valid for collision of two balls as well. In this chapter, contact of a ball and a horizontal wall is modeled using linear, Hertz-Mindlin, Ng method with and without damping ratio, and the dynamic response of each model is discussed and compared with other contact models. Coefficient of restitution for contact of a 10 kg Berea Sandstone ball and a horizontal wall with different materials is calculated and the correlation of coefficient of restitution and damping ratio is determined for each contact model. Note that the effect of impact velocity on coefficient of restitution is not considered. Moreover, in an ideal system, the contact models Hertz-Mindlin and Hertz-Ng model have the same algorithm.

6.1. Comparison of Contact Models

Table 6-1 is part of the input file named "Data.txt", and it describes the properties of a ball with *100.8 N* weight (radius of *0.21 m* and density of *2600 kg/m*^{3}) subjected to free fall in ideal situation (damping ratio is equal to zero).

Table 6-1: Inputs for the model.

Number of triangles	Number of balls	Number of steps	Contact type code	R (m)	K_n (N/m)	K_s (N/m)	γ (N/m^3)	β
2	1	1×10^7	0,1,4	0.21	6.4×10^{10}	9.6×10^6	2600	0

Wall is a frictionless horizontal plane including two triangles. Figure 6.2 presents the configuration of the wall and arrangements of triangles (mesh).

Table 6-2: wall stiffness of horizontal wall.

Number of triangles	Linear shear stiffness (N/m)	Linear shear stiffness (N/m)
1	10^7	10^7
2	10^7	10^7

Table 6-2 shows the stiffness of each triangle. Note that in ideal situation (where the law of energy conservation is upheld), contact stiffnesses of ball and wall have no effect on the trajectory and velocity of the balls (walls are assumed static). Figure 6.2 shows the trajectory of the ball.

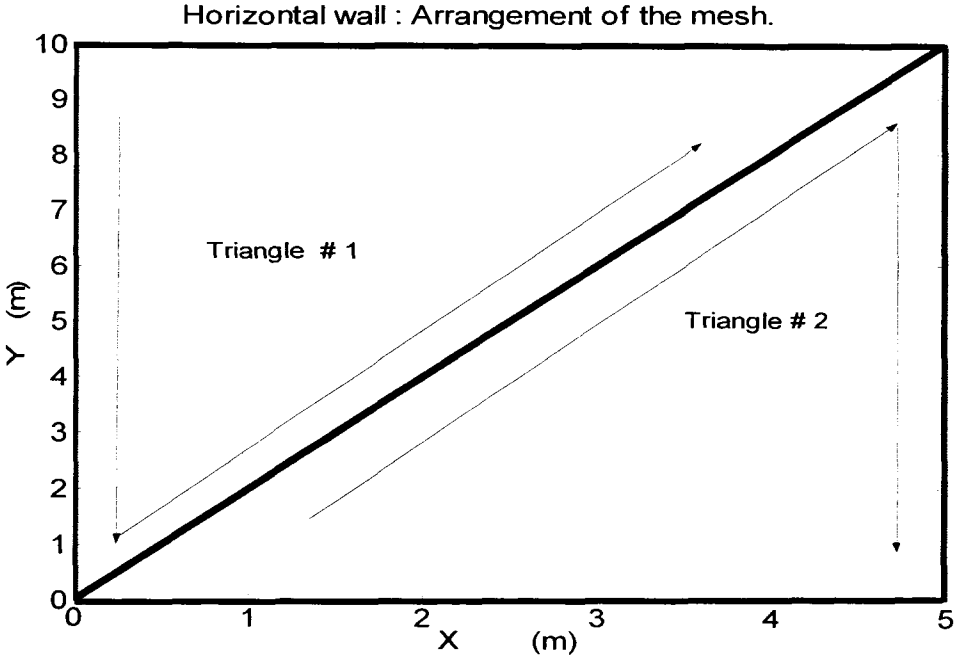

Figure 6.1 : Configuration of the mesh of the horizontal wall.

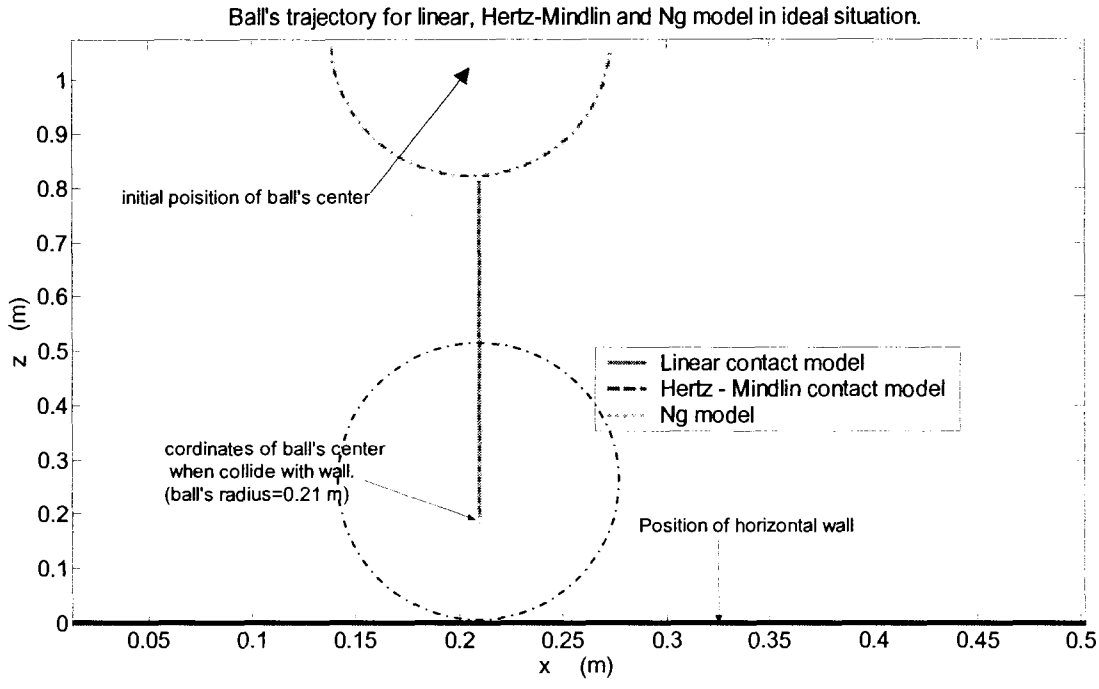

Figure 6.2: Ball trajectory in free fall on horizontal wall when damping ratio equal to zero.

Since the ball is just affected by gravity, the trajectory of ball is vertical. In other words shear forces are equal to zero. According to the law of energy conservation, an object in free fall would have a gradually increasing kinetic energy as the velocity increases as it is drawn closer to ground by gravitational acceleration. Right before the object makes contact with ground, the kinetic energy is at its maximum value, whereas the potential energy is zero. During the contact phase of the object and the wall, the two objects will overlap and potential energy increases. At maximum overlap the potential energy reaches its maximum value. Right after the contact phase, when the object starts to separate from the wall, all the potential energy gradually converts to kinetic energy permitting the object to return to its initial position or elevation. Figure 6.3 shows the ball's motion with respect to time.

Figure 6.4 illustrates the ball's velocity in "Z" direction with respect to time. The fact that all the contact models have similar ball's trajectory and ball's velocity confirms the validity of all the contact methods with respect to the energy conservation law. Also, since the rebound velocity and impact velocity are equal, coefficient of restitution is 1.0, which shows that the collision is perfectly elastic.

Figure 6.5 illustrates the variation of normal force (in the "Z" direction) with respect to the extent of the normal overlap for linear, Hertz-Mindlin, and Ng models. This figure also confirms the conservation of energy in all contact models since the impact and rebound curves coincide, and the ratio of areas under impact and rebound curves is one, meaning there is no energy dissipated.

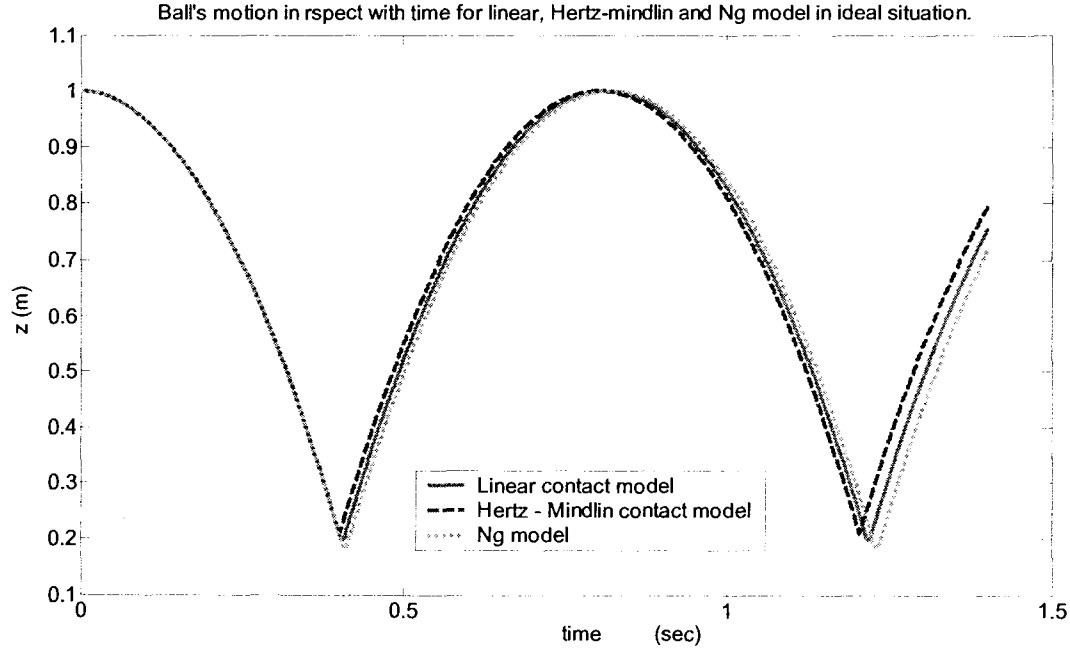

Figure 6.3: Ball's motion in respect with time in ideal situation for different contact model.

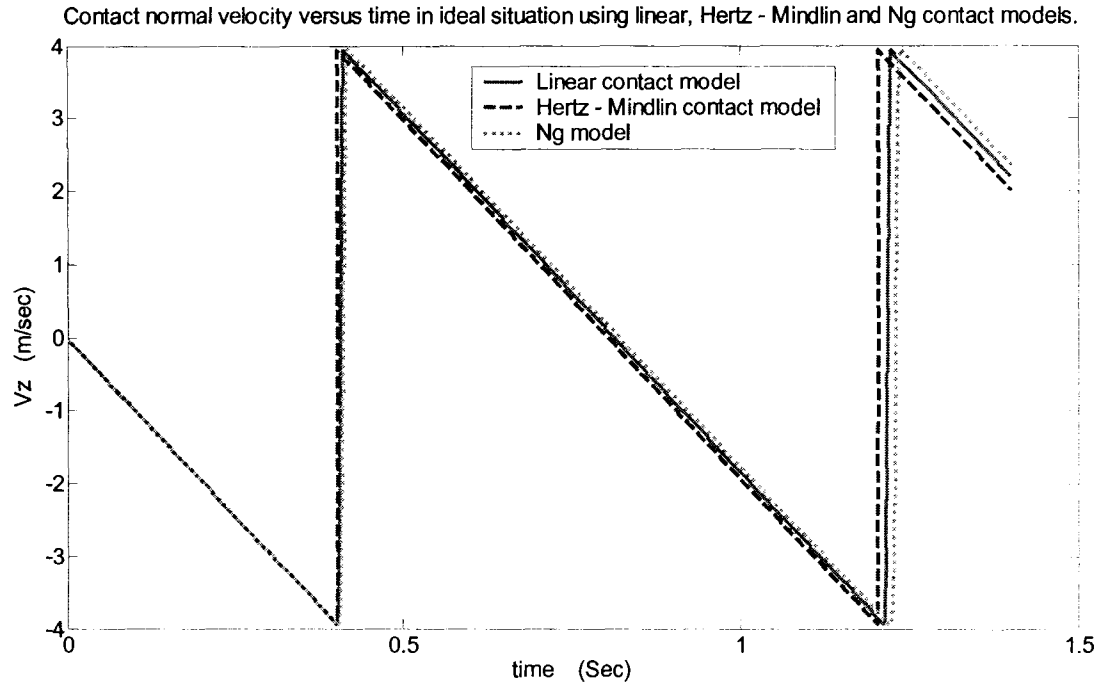

Figure 6.4: Ball's velocity in free fall in ideal situation using linear, Hertz- Mindlin and Ng model.

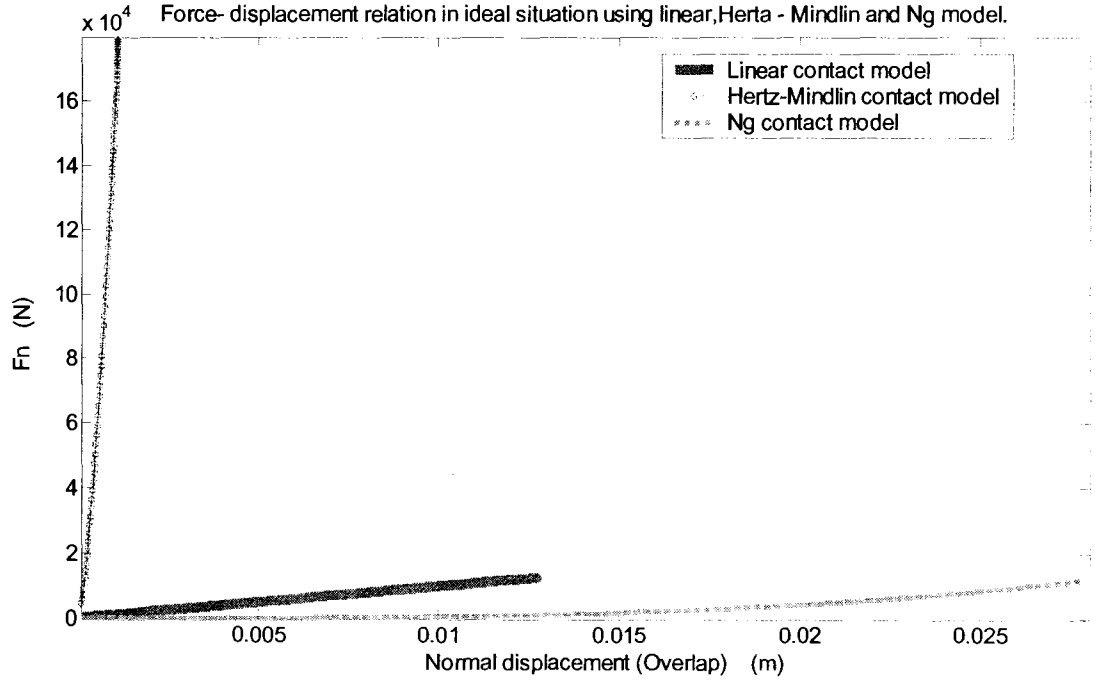

Figure 6.5: Force-displacement relation in ideal situation for different contact models.

The slope of the tangent to each curve in Figure 6.5 represents its stiffness value. As shown in this figure, Hertz-Mindlin model produces larger values for normal stiffness

than other contact models. Also, the area under the loading and unloading curves which are coincided for all the contact models, represent the energy loss of system, which confirms the validity of conservation of energy in this system.

As the Hertz-Mindlin model produces much higher values of the stiffnesses value, normal forces values are larger as well. Figure 6.6 shows the variation of normal force (in the Z direction) with respect to the extent of the overlap of linear, Ng and An models in ideal situation.

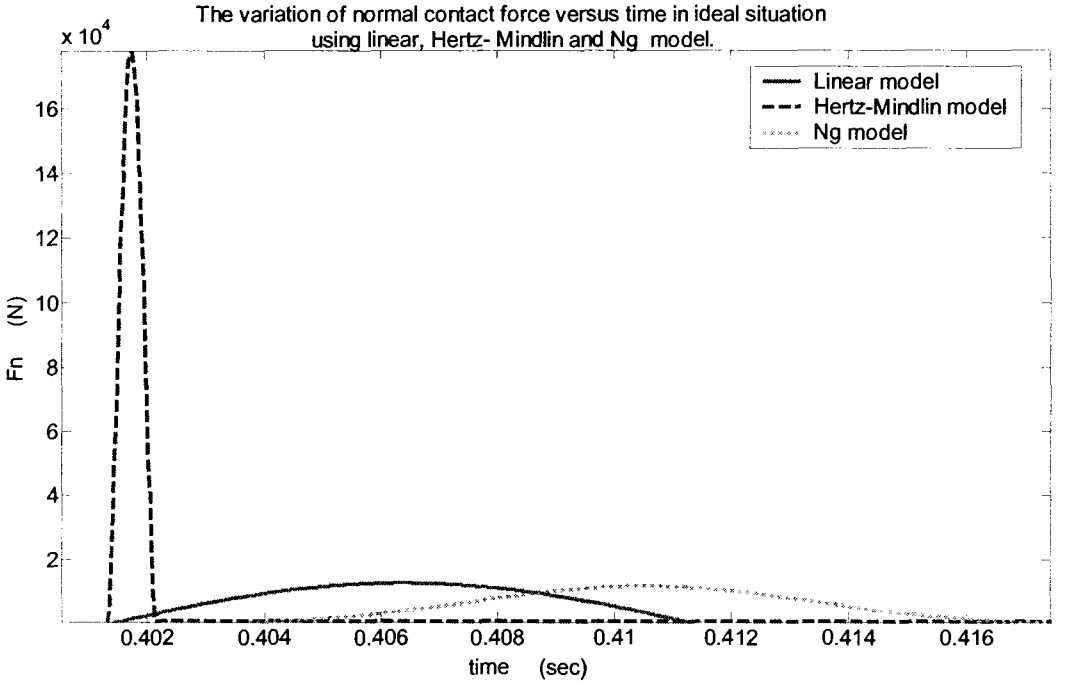

Figure 6.6: Normal contact force versus time in ideal situation for linear, Hertz-Mindlin and Ng contact models at first contact.

The maximum normal forces of Hertz-Mindlin model is about ten times greater than the maximum normal forces of other models and occurs in a much shorter period of time compared to the other contact methods. The linear model and Ng model have almost the same curve configuration as well as the maximum normal force value, but maximum force in Ng model occurs with delay in comparison with linear model

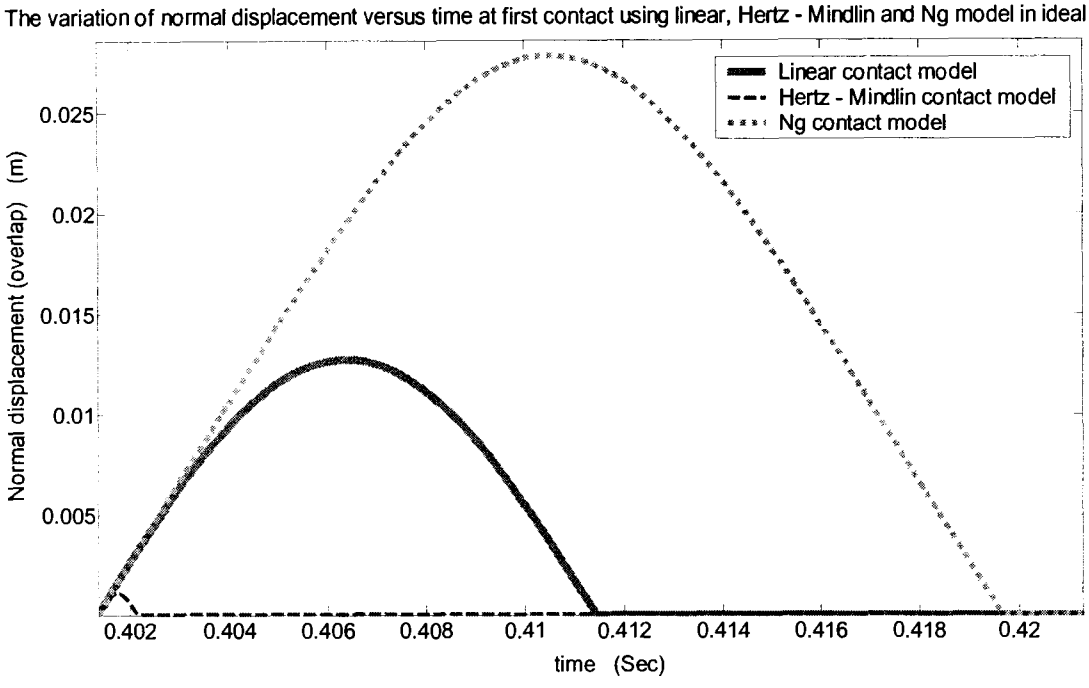

Figure 6.7: The variation of normal displacement versus time at first contact using linear, Hertz –Mindlin and Ng contact models in ideal situation.

Figure 6.7 illustrates the overlap between the ball and the wall over time. Displacement in Ng model is much larger than other models. The minimum displacement occurred with the Hertz-Mindlin method (less deformable method). In fact, it is less than a third of the displacement value of the linear method.

6.2. The Effect of Viscous Damping on Ball Motion

Table 6-3 is part of input file, namely "Data.txt", and describes the properties of a ball (Berea Sandstone), number of triangles and steps. A model including a *10 kg* ball and horizontal ball is built and dynamic of the damped freefall using mentioned contact models which are studied.

Table 6-3: Inputs of simulation

Number of triangles	Number of balls	Number of steps	Contact type code	R (m)	K_n (N/m)	K_s (N/m)	γ (N/m^3)	β	ν	E (Pa)
2	1	1×10^7	0,1,3,4	0.21	6.4×10^{11}	9.6×10^6	2600	various	0.38	6.88×10^9

6.2.1. Ball's Motion

Unlike the freefall system without damping, in damped systems the ball's motion and ball's velocity using different contact models are dissimilar. As seen in Figure 6.8, Figure 6.9, Figure 6.10 and Figure 6.11, for certain damping ratios, the bounce height of the ball using different models is very different. Meaning the effect of the value of damping ratio, in each contact model on macroscopic and microscopic behaviours of ball and also contact time are different. Contact time in Ng and linear models are much longer than Hertz-Mindlin and Hertz-Ng models. Increasing the value of damping ratio increases the contact time in all models except Hertz-Mindlin, which has always a constant contact time.

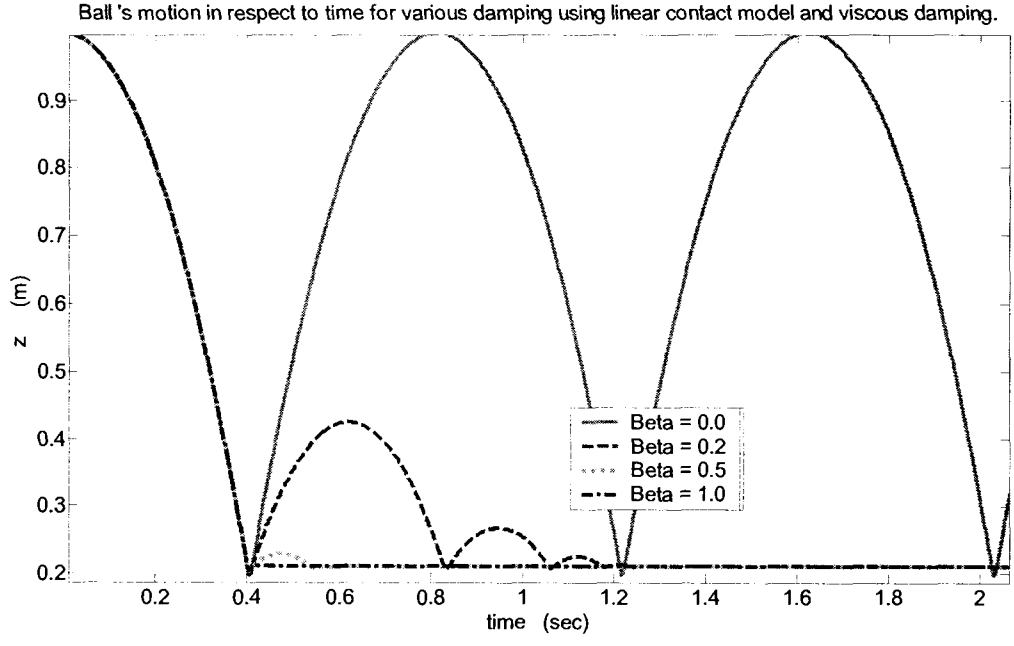

Figure 6.8: Ball's damped motion using linear model.

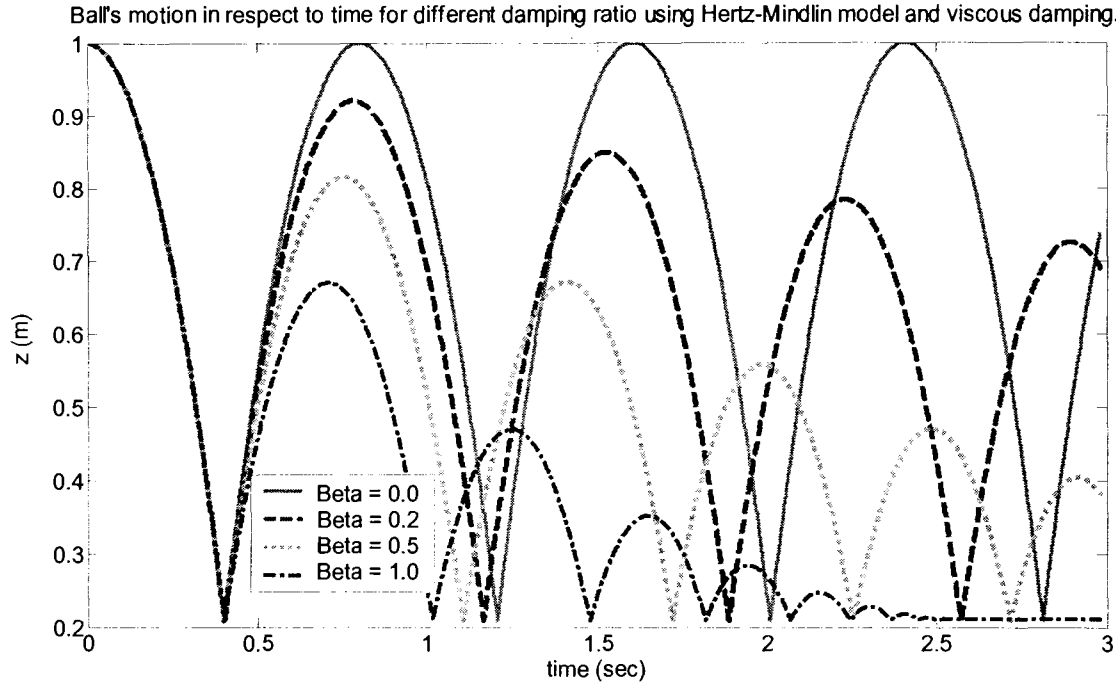

Figure 6.9: Ball's damped motion in respect to time using Hertz-Mindlin model.

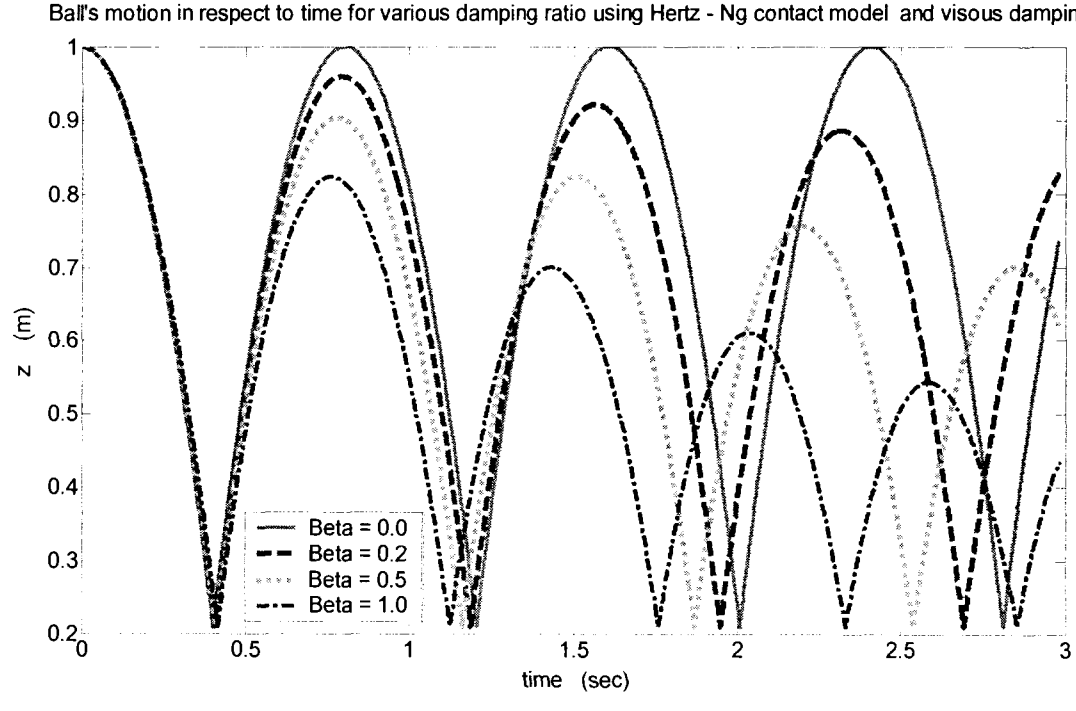

Figure 6.10: Ball's damped motion using Hertz-Ng model.

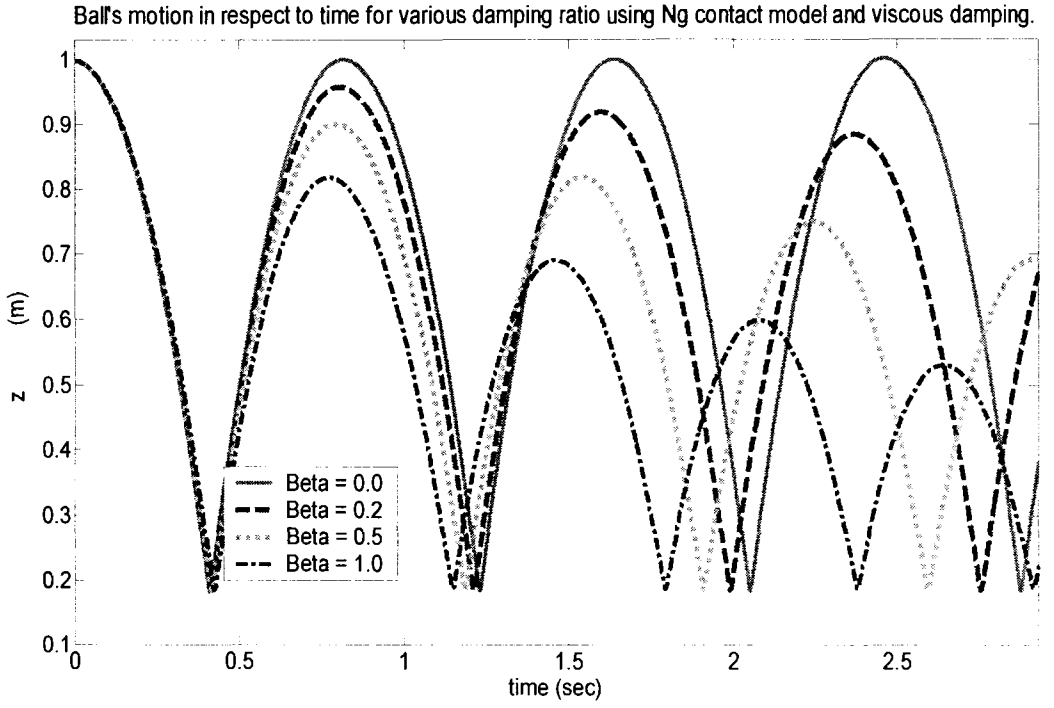

Figure 6.11: Ball's damped motion using Ng model.

6.2.2. Ball's Velocity

The term ball's velocity or contact velocity represents the velocity of the center of ball during contact. Figure 6.12, Figure 6.13, Figure 6.14 and Figure 6.15 illustrate the variation of ball's normal velocity versus time for the different value of the damping ratio for linear, Hertz-Mindlin, Hertz-Ng and Ng model. Similar to ball's trajectory, the effect of the value of the damping ratio is different in each contact model.

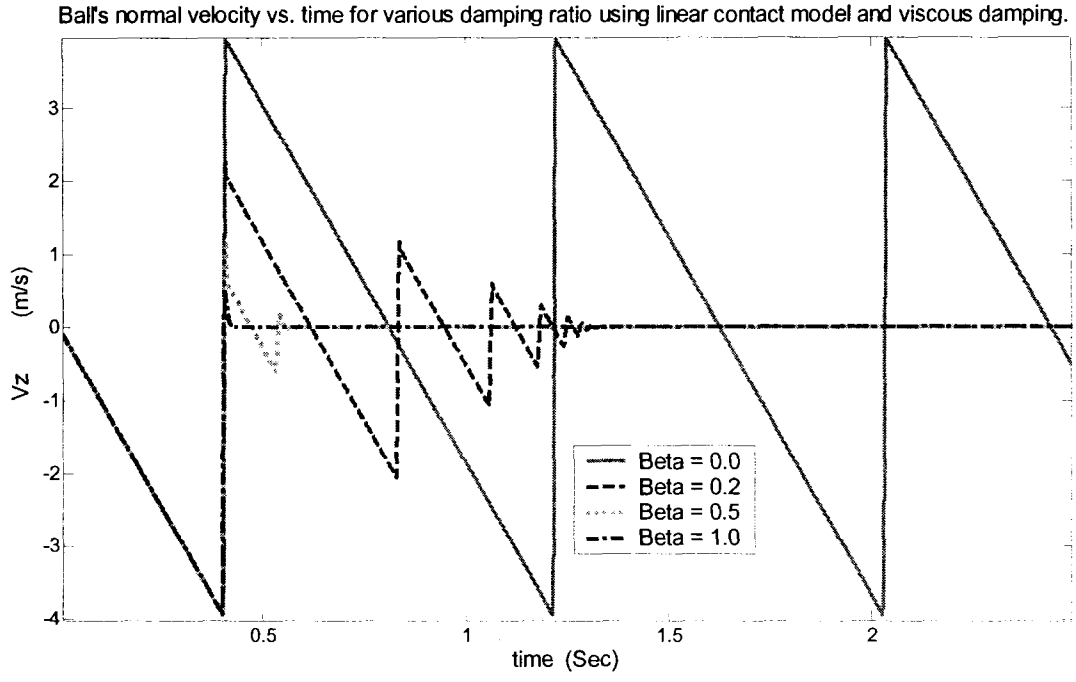

Figure 6.12: The variation of contact velocity versus time for various damping ratio using linear model.

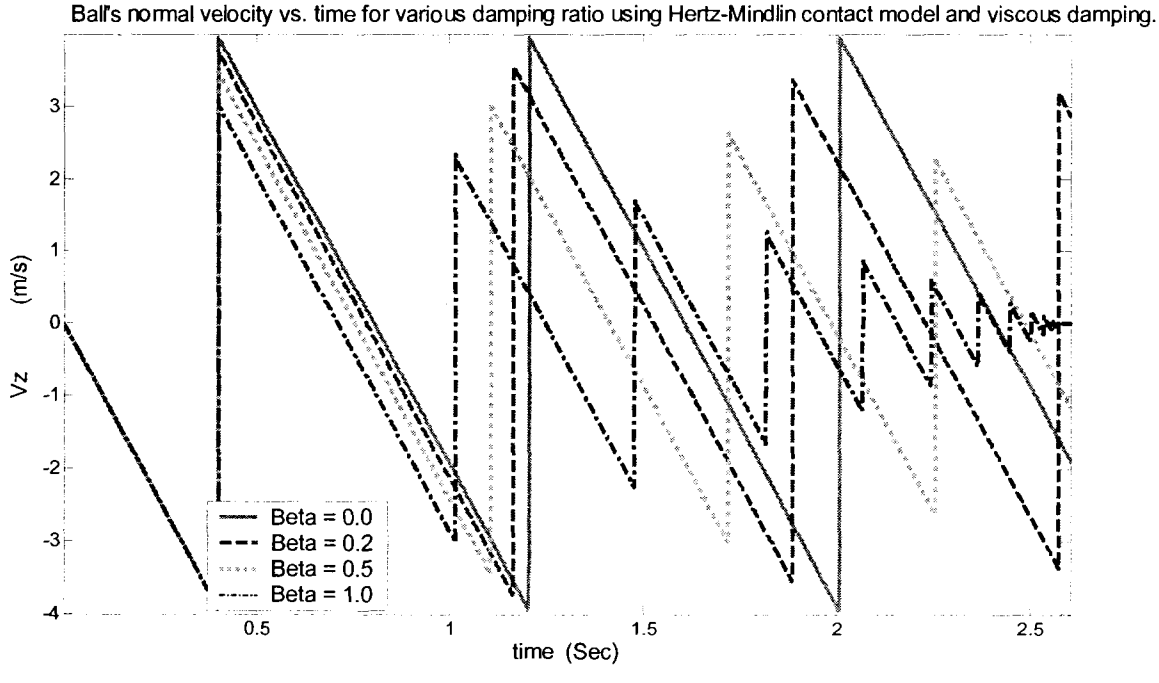

Figure 6.13: The variation of contact velocity versus time for various damping ratio using Hertz-Mindlin model.

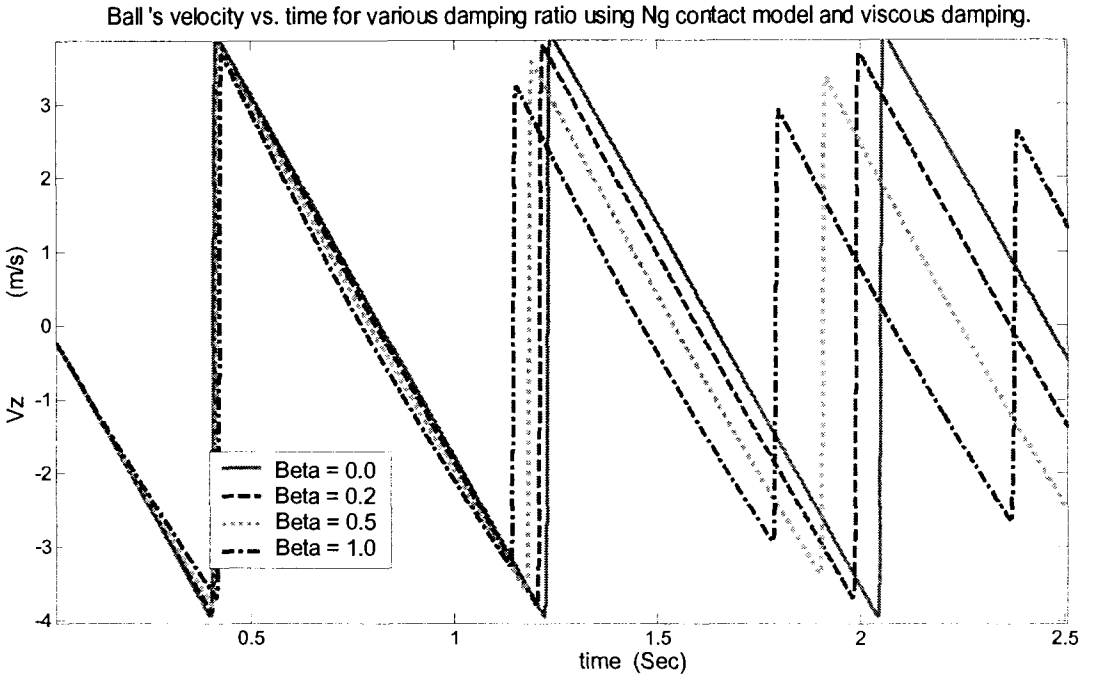

Figure 6.14: The variation of contact velocity versus time for various damping ratio using Hertz-Ng model.

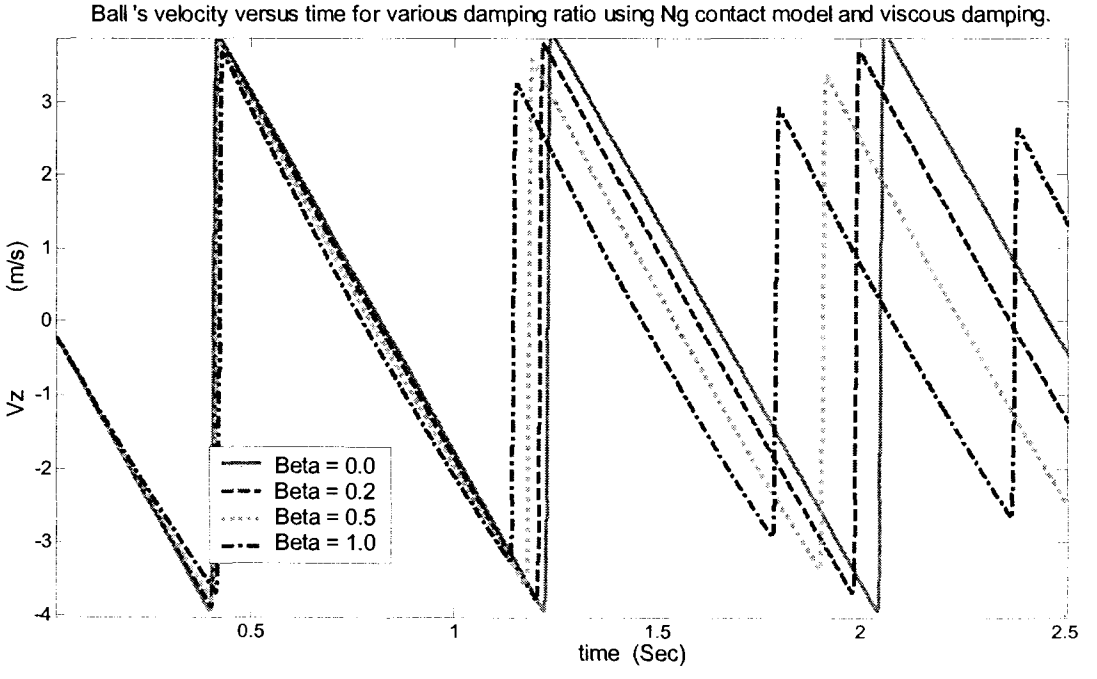

Figure 6.15: The variation of contact velocity versus time for various damping ratio using Ng model.

6.2.3. Contact Normal Force

Figure 6.16, Figure 6.18, Figure 6.20 and Figure 6.22 demonstrate the variations of normal contact forces versus time using linear, Hertz-Mindlin, Hertz-Ng and Ng models respectively. Also Figure 6.17, Figure 6.19, Figure 6.21 and Figure 6.23 illustrate the variations of normal contact force versus time during first contact. As can be seen in force-time figures, is not only the value of maximum normal contact force for different values of damping ratio (β), different in each contact model, but also the configuration of forces, beginning and ending time of contact and the duration of contact forces are different.

In linear model, system for $\beta = 1.0$ is in critically damped condition so ball's motion decays fast but in the other cases, which are in underdamped condition ball's motion oscillate with decreasing bounce height and maximum force, and increasing the damping ratio causes the successive contacts occur faster. For example, as shown in Figure 6.16, second contact for $\beta = 0.5$, occurs about 0.7 (sec) sooner than the second contact when $\beta = 0.0$.

In linear contact model, some tension forces are produced in second phase of contact (rebound). The values of the tension forces decrease with increasing of damping ratio, (β),although for certain value of damping ratio, (β), tension forces decrease in successive contacts.

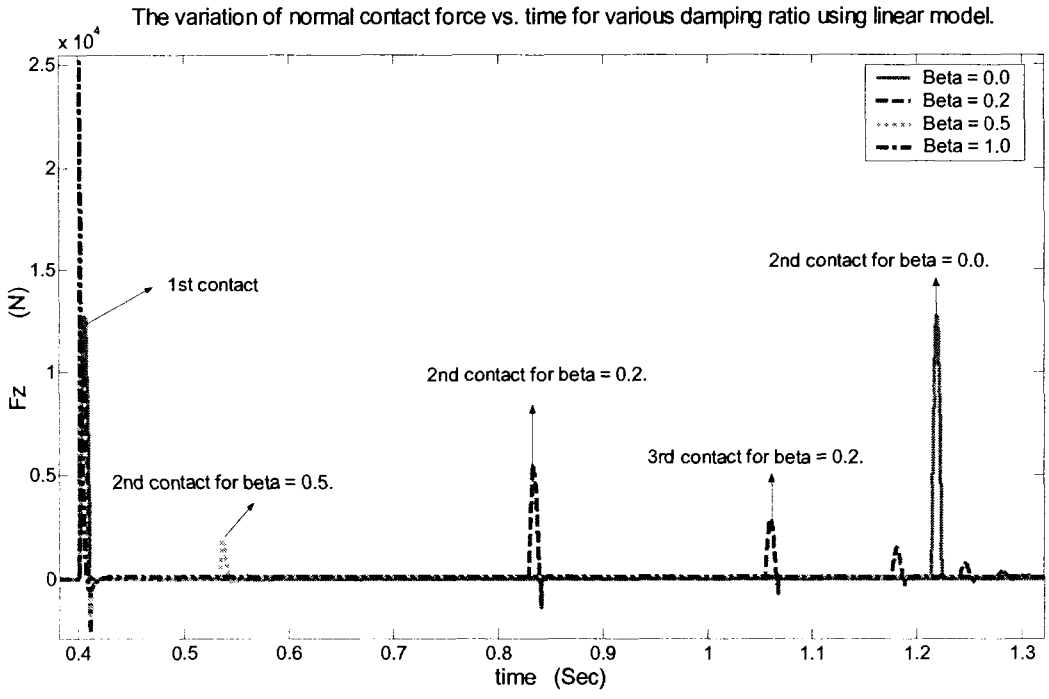

Figure 6.16: The variation of normal contact force versus time using linear model.

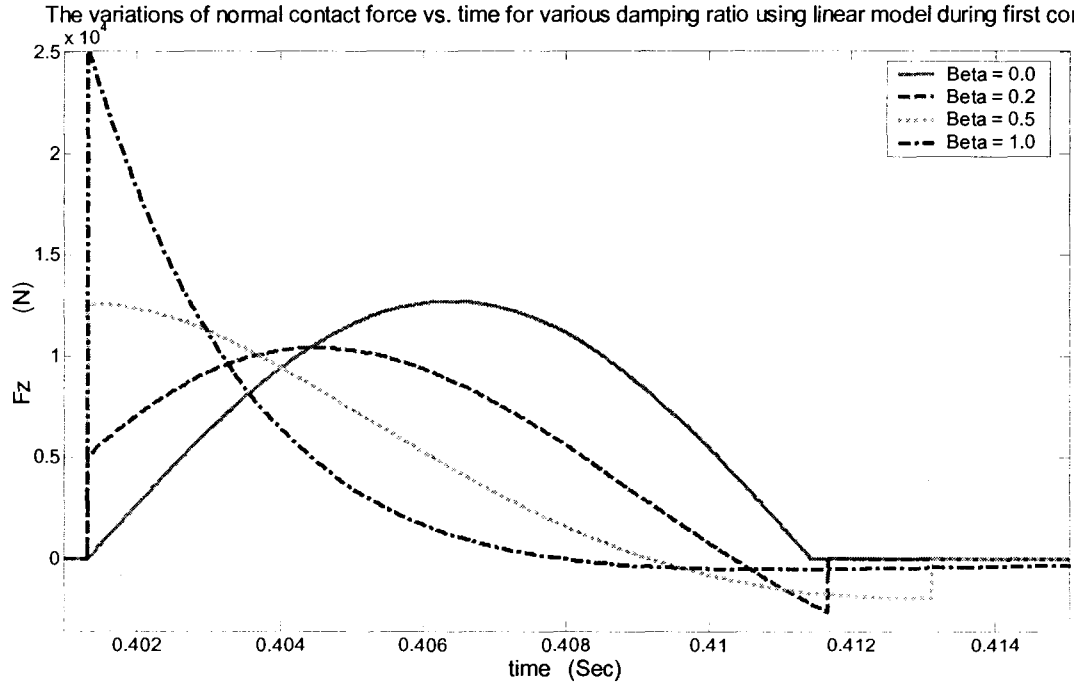

Figure 6.17: The variation of normal contact force versus time using linear model at first contact.

As shown in Figure 6.18 the maximum values of normal contact forces in Hertz-Mindlin model are much higher than the maximum contact force in other models.

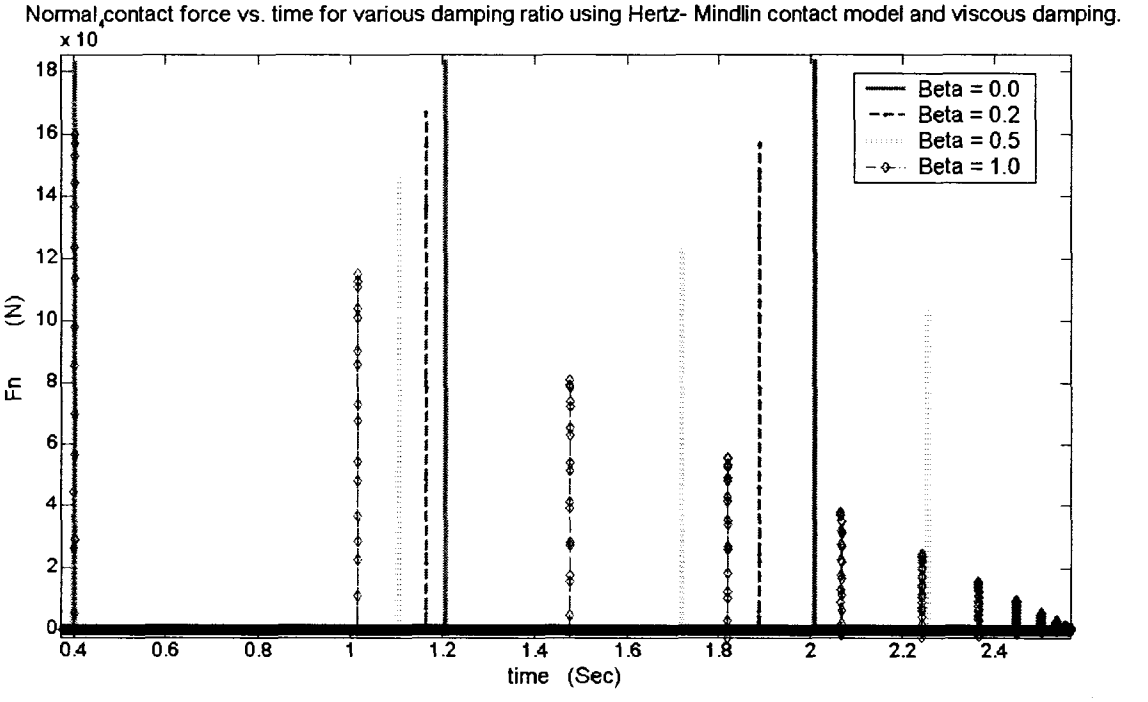

Figure 6.18: The variation of normal contact force versus time using Hertz-Mindlin.

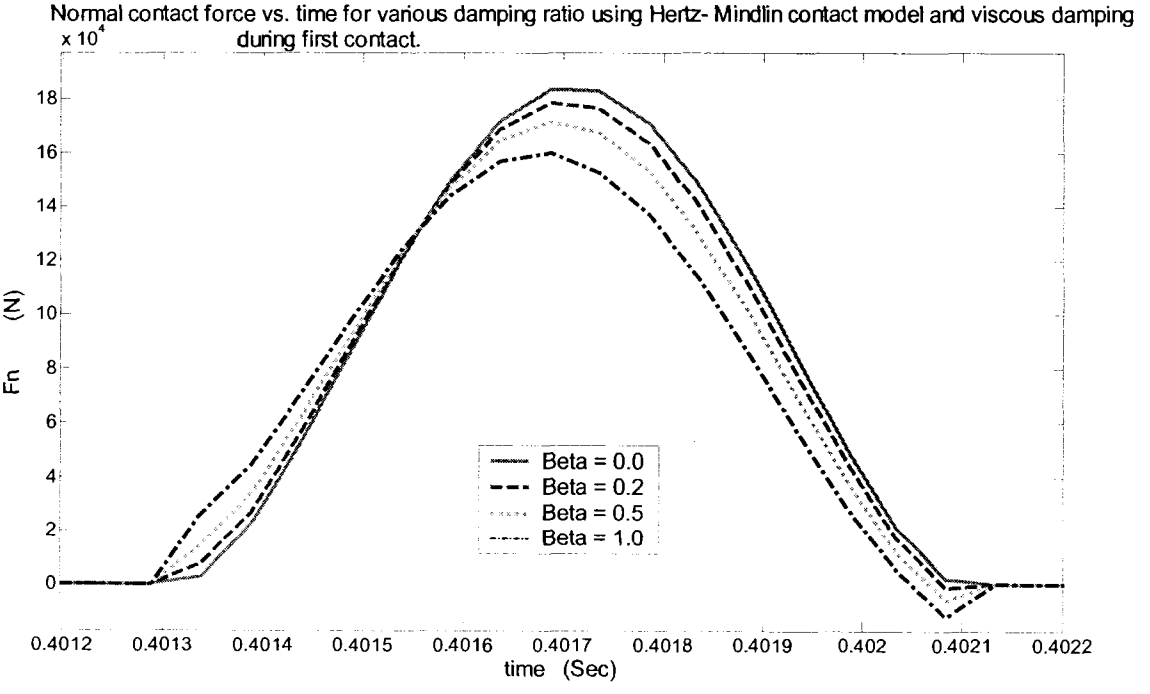

Figure 6.19: The variation of normal contact force versus time using Hertz-Mindlin model at first contact.

At first contact in Hertz-Mindlin contact model (Figure 6.19), the time of maximum contact force for different values of damping ratio (β), is almost the same but for successive contacts, maximum force of contact occurs faster for higher value of damping ratio. As shown in Figure 6.21 and Figure 6.23, at first contact in Hertz-Ng and Ng models, increasing the damping ratio, (β), causes delay in contact. For successive contacts same as Hertz-Mindlin and linear model, contacts with higher value of damping ratio occur faster.

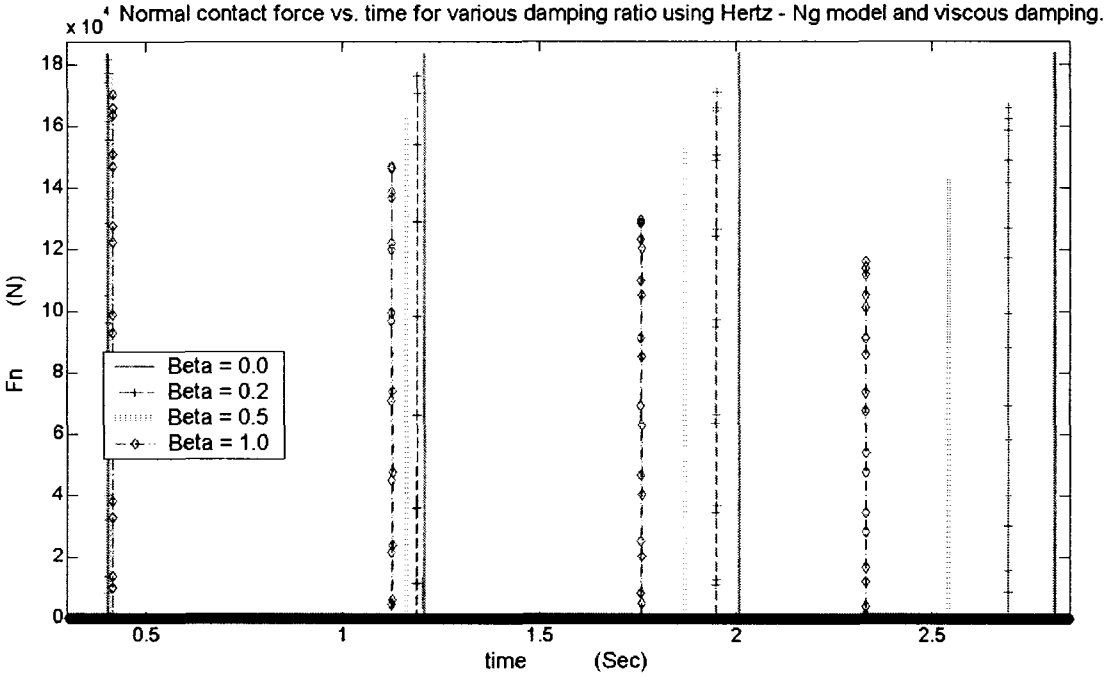

Figure 6.20: The variation of normal contact force versus time using Hertz-Ng model.

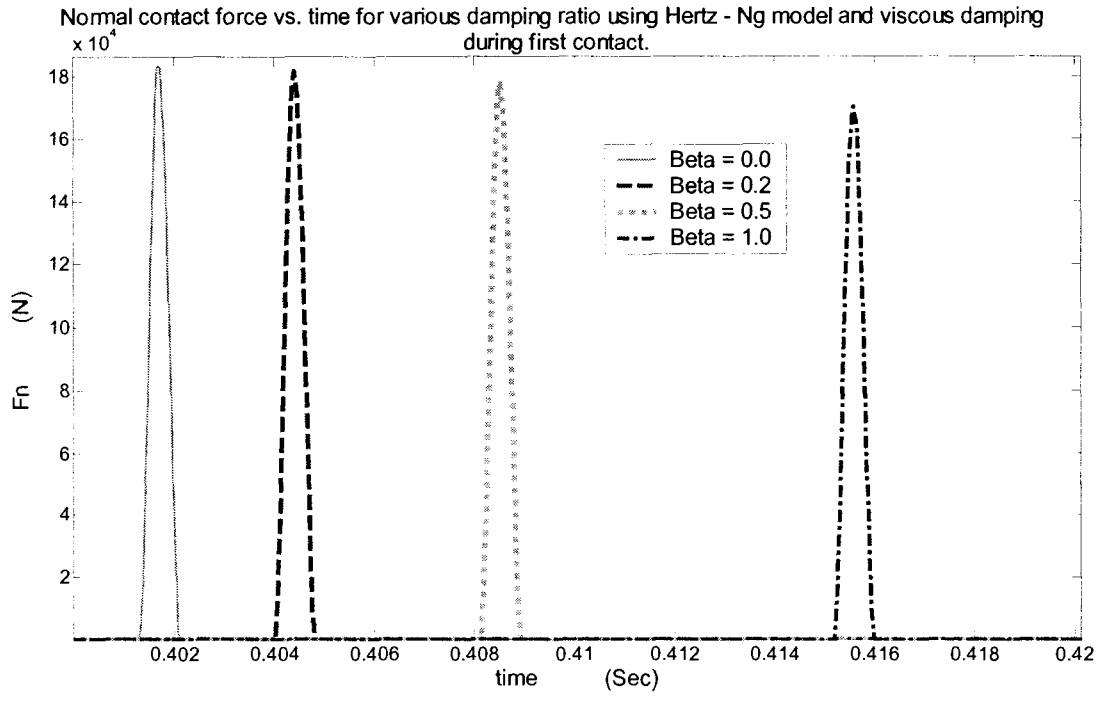

Figure 6.21: The variation of normal contact force versus time using Hertz-Ng model at first contact.

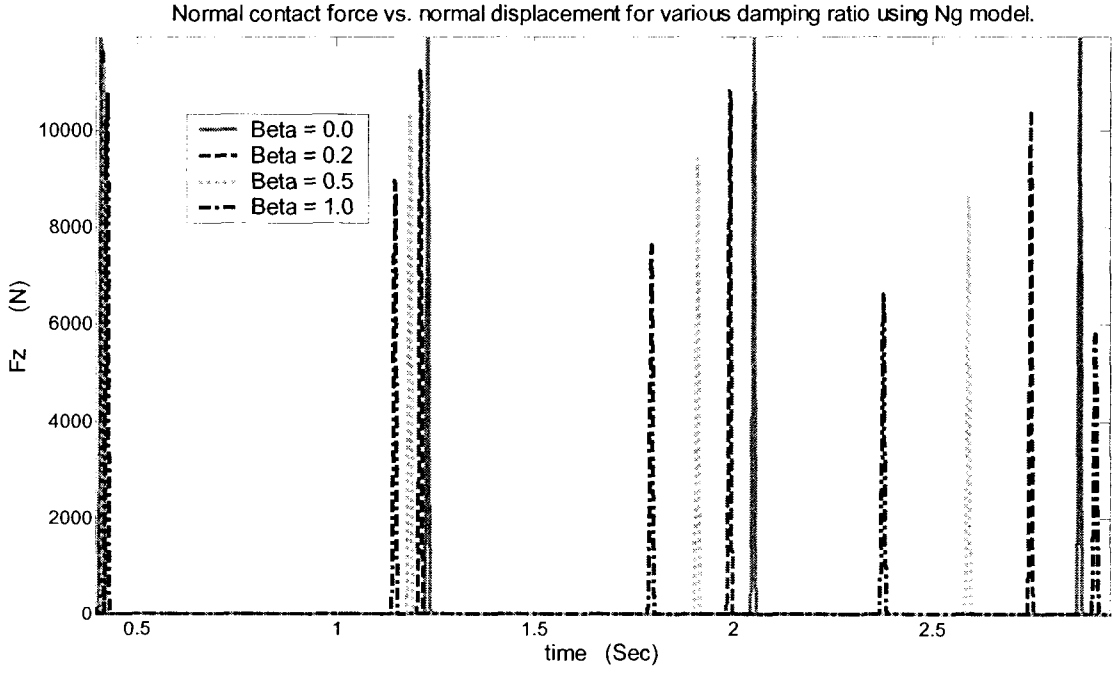

Figure 6.22: The variation of normal contact force versus time using Ng model.

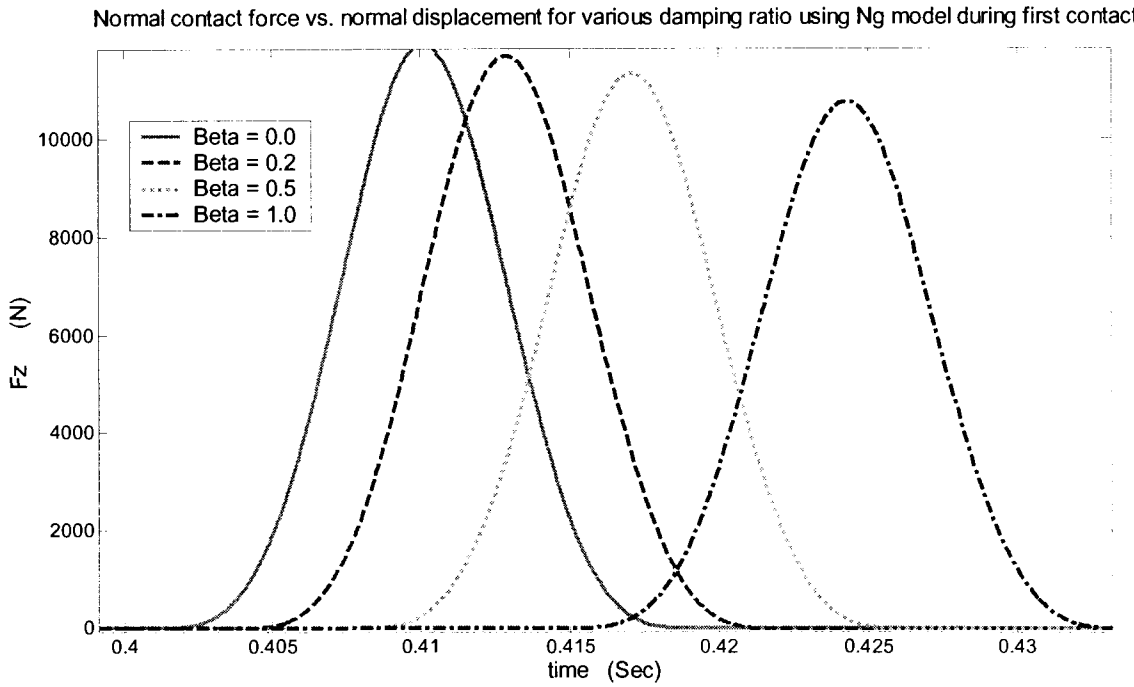

Figure 6.23: The variation of normal contact force versus time using Ng model at first contact.

6.2.4. Normal Displacement (Overlap)

Figure 6.24, Figure 6.26, Figure 6.28 and Figure 6.30 demonstrate the variations of normal contact overlap (displacement) versus time using linear, Hertz-Mindlin, Hertz-Ng and Ng model. Although, configurations of overlaps are different in each contact model, increasing the damping ratio decreases the normal overlap between objects in all the models. Similar to contact forces, the effect of damping ratio on Hertz-Ng and Ng is not noticeable.

At first contact, increasing the value of damping ratio has no effect in contact time in linear and Hertz-Mindlin model in contrast with Hertz-Ng and Ng model since damping ratio is incorporated in updating velocity.

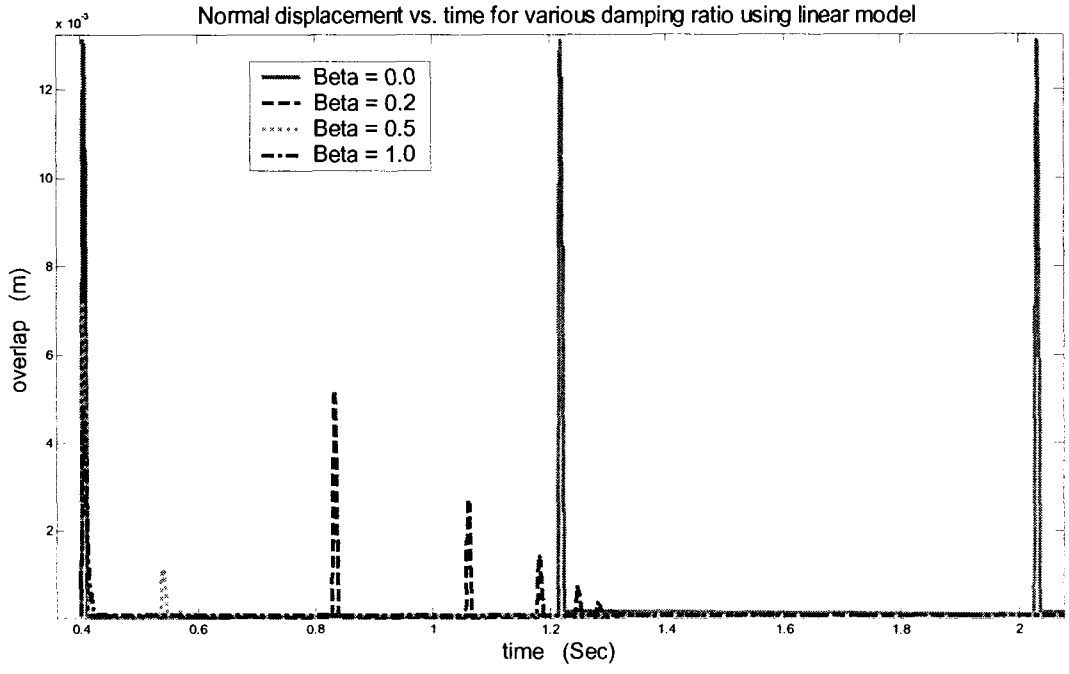

Figure 6.24: The variation of normal displacement versus time using linear model.

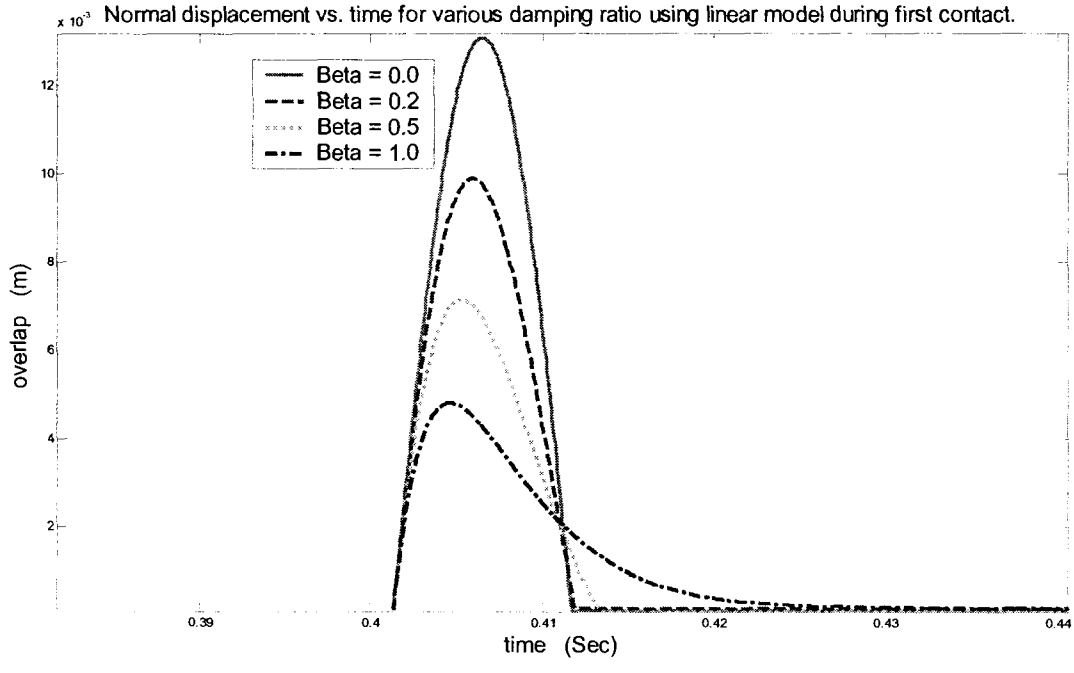

Figure 6.25: The variation of normal displacement versus time using linear model at first contact.

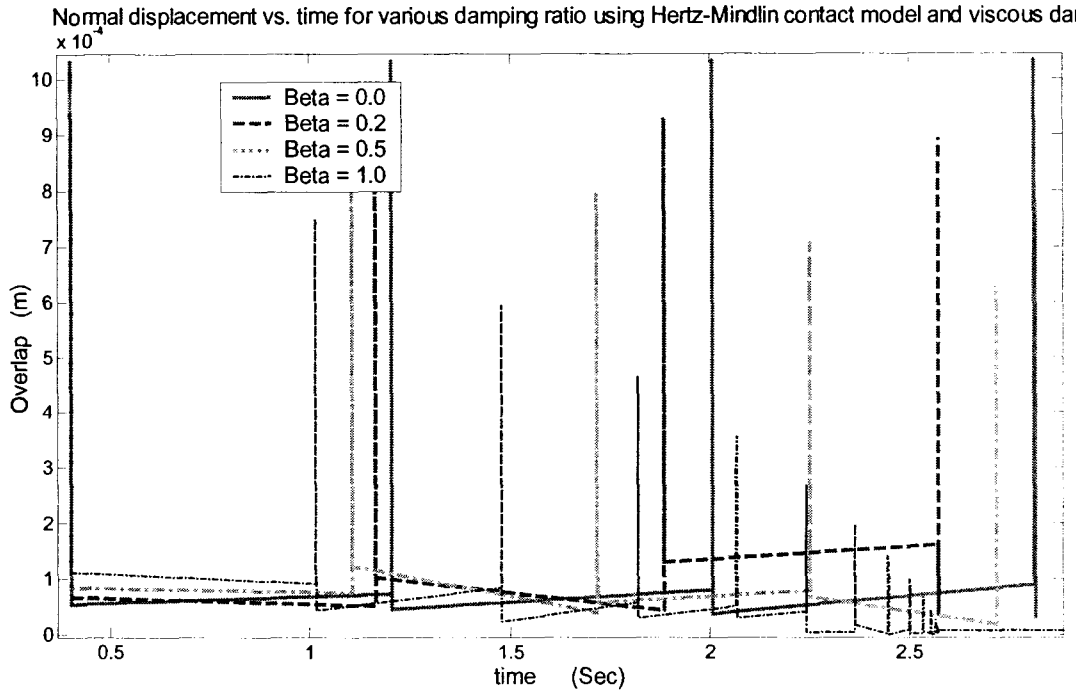

Figure 6.26: The variation of normal displacement versus time using Hertz-Mindlin model.

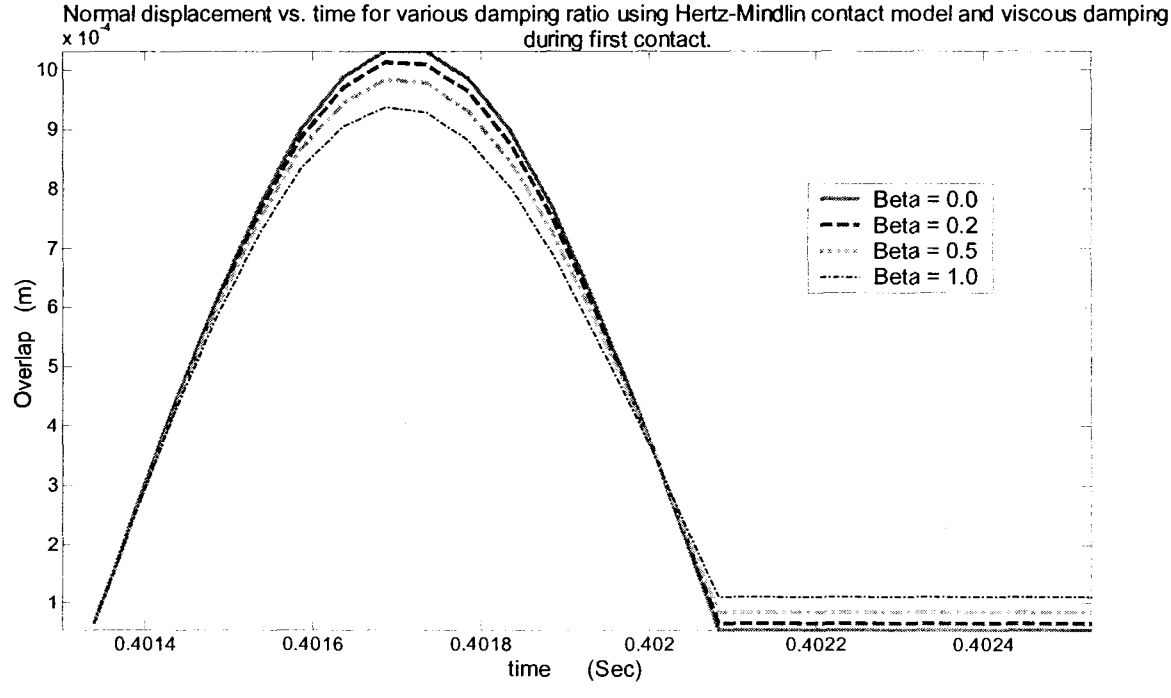

Figure 6.27: The variation of normal displacement versus time using Hertz-Mindlin model at first contact.

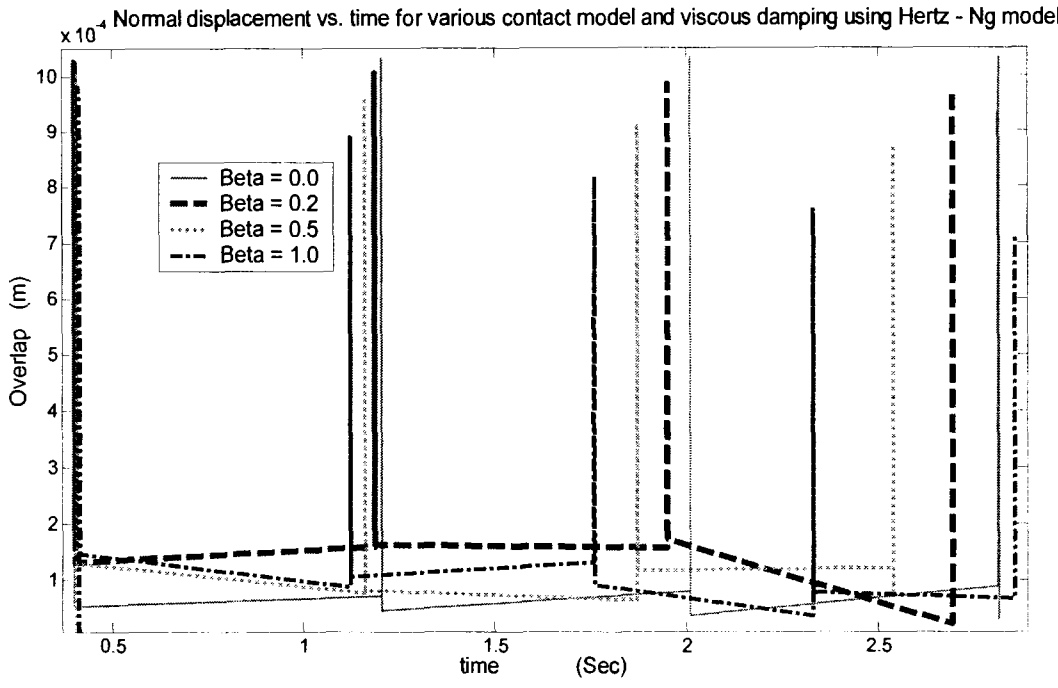

Figure 6.28: The variation of normal displacement versus time using Hertz-Ng model.

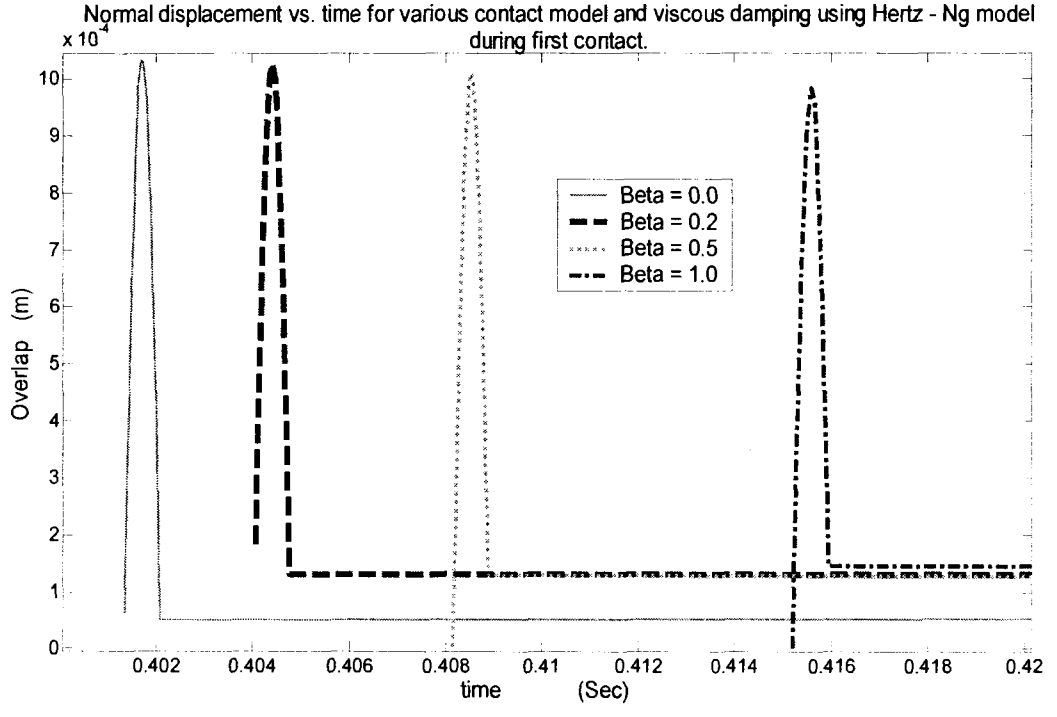

Figure 6.29: The variation of normal displacement versus time using Hertz-Ng model at first contact.

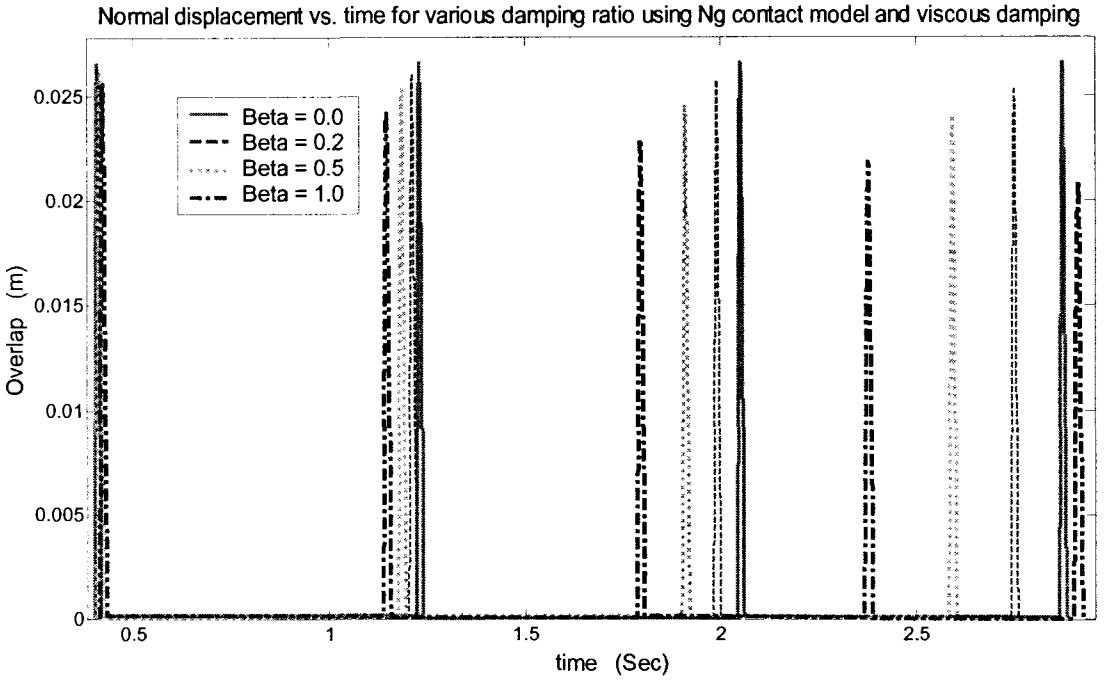

Figure 6.30: The variation of normal displacement versus time using Ng model.

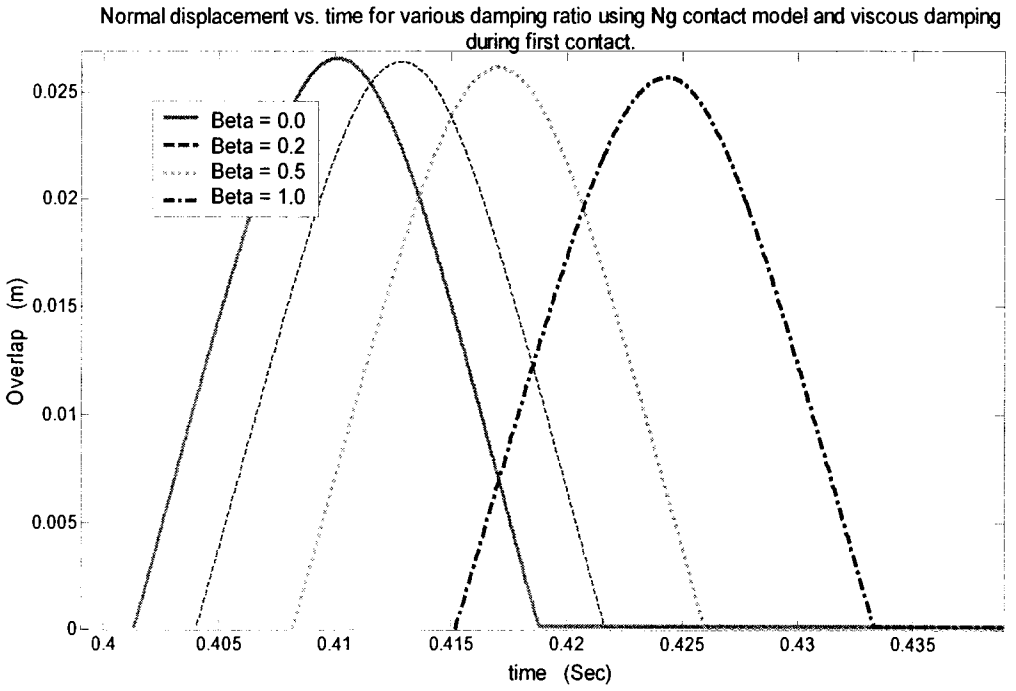

Figure 6.31: The variation of normal displacement versus time using Ng model at first contact.

6.2.5. *Force–Displacement Relation*

Figure 6.32 and Figure 6.33 demonstrate the variations of normal contact force versus normal overlap using linear and Hertz-Mindlin model. Viscous damping is used for dissipation of energy during the contact. Since the linear dashpot (viscous damping) is used, it is expected to see the half elliptic curve with hysteresis behaviour with the maximum damping force at origin [11]. Using viscous damping causes the incorrect hysteresis behaviour [11]. In contrast with experimental tests, the initial contact force is not zero at the beginning of contact in Figure 6.32 and Figure 6.33 [11]. Negative areas in Figure 6.32 and Figure 6.33 represent tension forces that reduce the real amount of energy dissipation which is another error [11]. To cancel the effect of these errors, some nonlinear dashpots were proposed in literature. However these errors in linear and especially in Hertz-Mindlin model can be ignored.

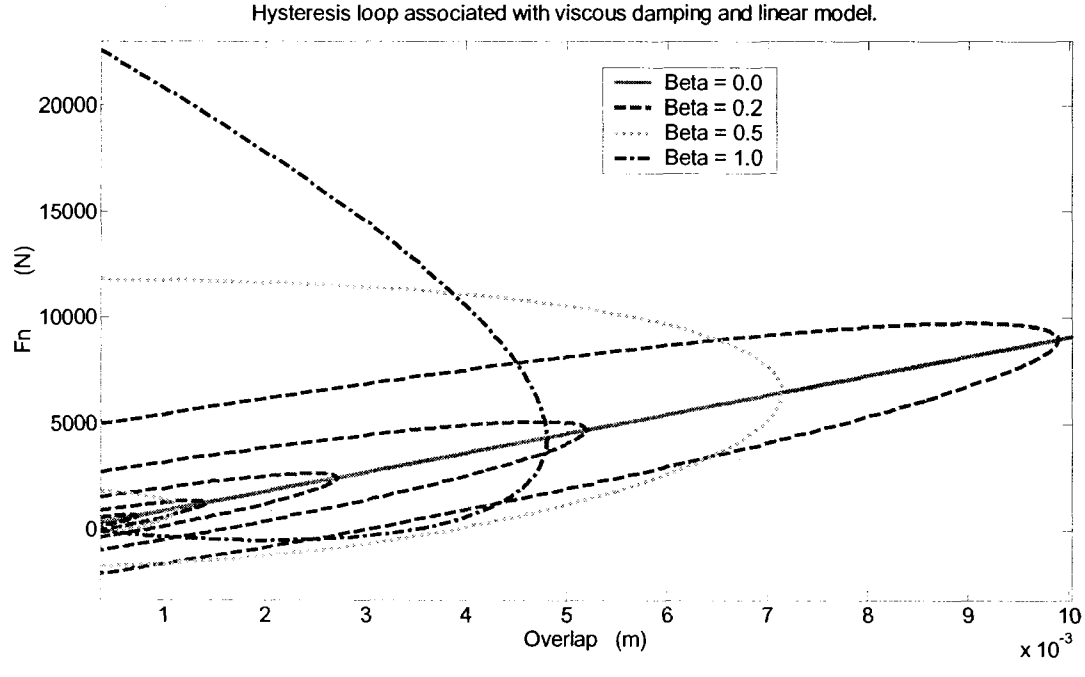

Figure 6.32: The variation of normal contact force versus normal displacement using linear model.

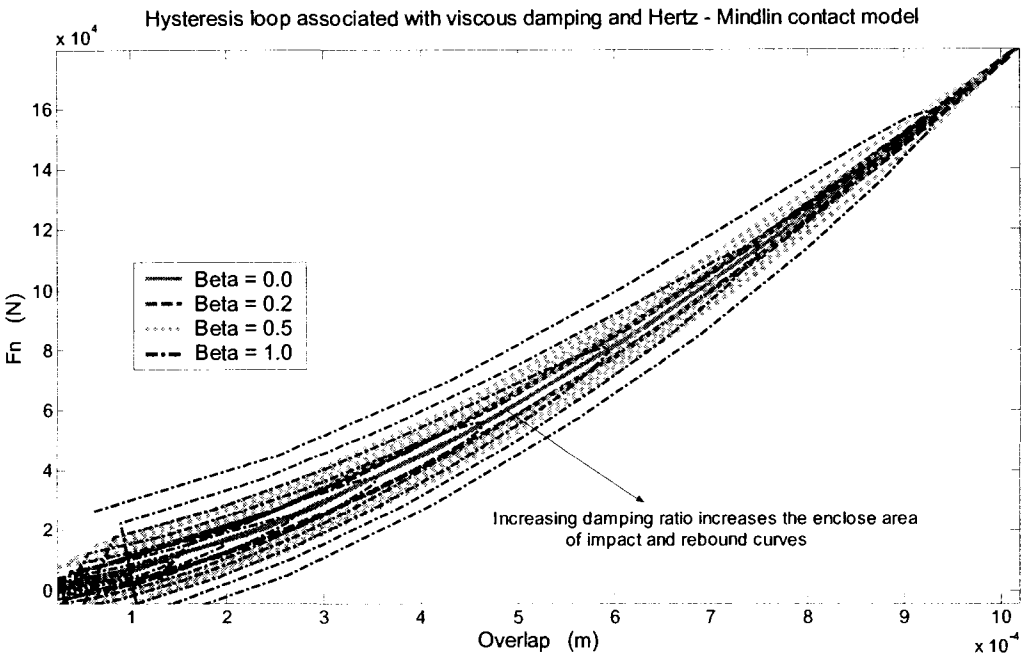

Figure 6.33 : The variation of normal contact force versus normal displacement using Hertz-Mindlin model.

Figure 6.34 and Figure 6.35 demonstrate the variations of normal contact force versus normal overlap using Hertz-Ng and Ng model. In these models the viscous damping ratio is directly applied in Equation (2.40) and directly appears in new velocity formula (Equation (2.41)). The relationship between normal force and normal displacement (overlap) is a nonlinear power law. For both of the models the impact and rebounds curves for the certain damping ratio almost coincide, and for different damping ratio, just maximum force and maximum overlap (the coordinates of end points) differ. Also for both models, the initial force is zero which means that the error in linear and Hertz-Mindlin is cancelled in Ng-Hertz and Ng model.

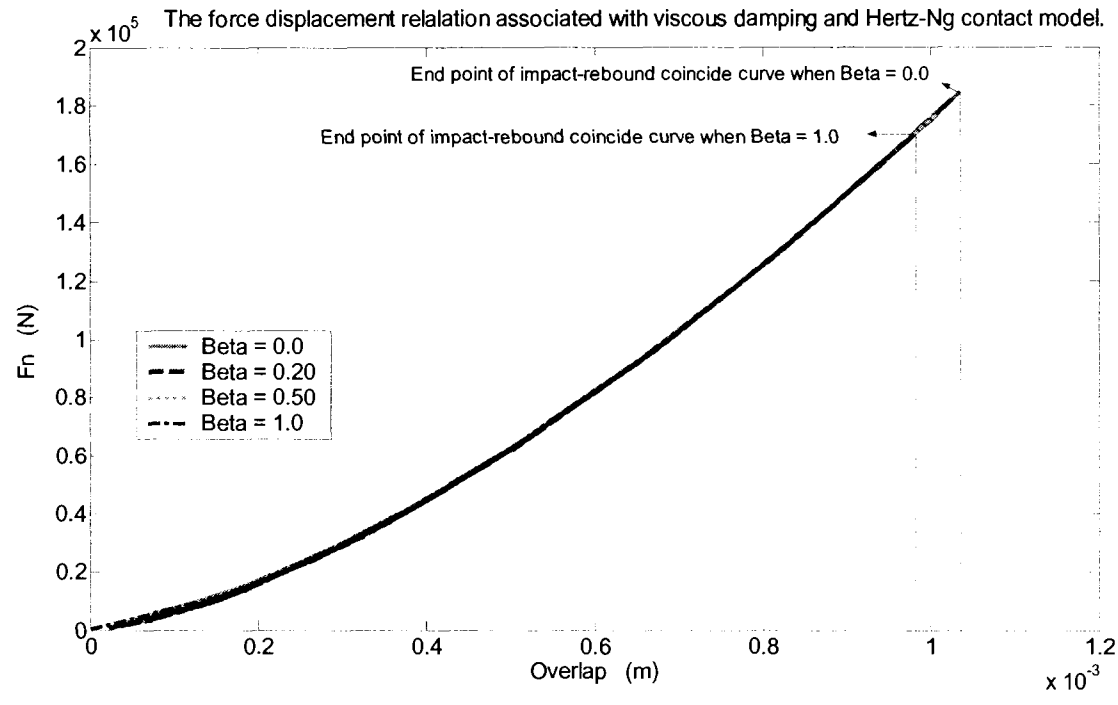

Figure 6.34: The variation of normal contact force versus normal displacement using Hertz-Ng model.

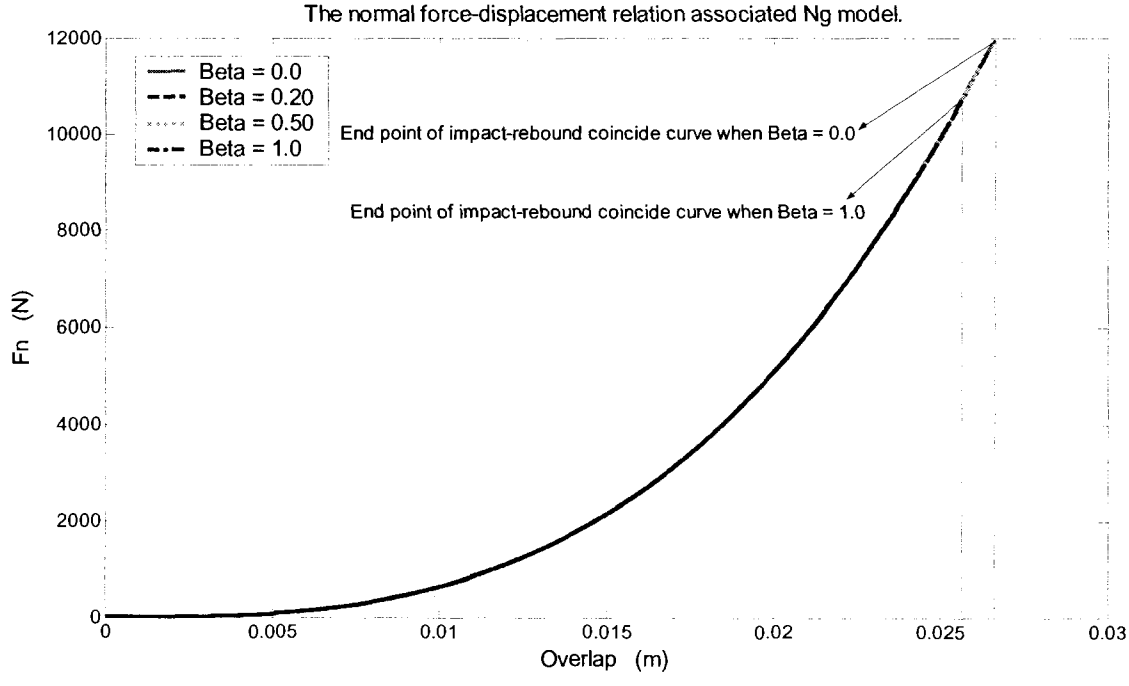

Figure 6.35: The variation of normal contact force versus normal displacement using Ng model.

6.3. Coefficient of Restitution

Table 6-4 shows the values for normal coefficient of restitution for various rock types [11,43] as well as the damping ratio for the mentioned contact models with viscous damping can produce the coefficient of restitution for each material. By definition, coefficient of restitution is the ratio of ball's velocity in last step of contact (when two bodies separate from each other) to ball's velocity in first step of contact when (two bodies start to overlap), as shown in Equation (6.1).

$$R_n = \frac{V_{out}}{V_{in}} \tag{6.1}$$

Where:

R_n is normal coefficient of restitution.

V_{out} is the normal component of velocity, when contact ends (overlap is zero).

V_{in} is the normal component of velocity, at begining to overlap of contact bodies.

As it shown in the table while the values for normal coefficient of restitution range 0.30-0.53, the values for damping ratio for each contact model vary in a different way. For linear model, Hertz-Mindlin and Ng model the values for damping ratio range 0.179-0.364, 2.399-3.76 and 16.1-38.1 respectively. Note that coefficient of restitution depends upon the contact velocity, here no modification is done regarding to the velocity.

Table 6-4: The values of viscous damping ratio for contact of a ball and a wall with different materials.

Wall's materials	Values for $R_n = \frac{V_{rn}}{V_{in}}$	Values for damping ratio (β)			
		Linear	Hertz-Mindlin	Hertz- Ng	Ng
Clean hard bed rock	0.53	0.179	2.399	-	16.10
Asphalt roadway	0.40	0.283	3.169	-	34.90
Bed rock outcrops with hard surface, large boulders	0.35	0.324	3.464	-	36.5
Talus cover	0.32	0.328	3.642	-	37.50
Soft soil	0.30	0.364	3.76	-	38.10

As discussed before, another definition of coefficient of restitution is based on work of indentation approach [11,43]. The areas within the loading (impact) and unloading (rebound) curves define the amount of energy dissipated during impact (energetic definition of coefficient of restitution). Many data about terms of energy dissipation in for different types of rock rockfall studies are presented in terms of coefficient of restitution. To define energy loss in Discrete Element Method and use the previous studies, it is necessary, to find a correlation between coefficient of restitution and damping ratio. Figure 6.36 demonstrates the correlation of coefficient of restitution and damping ratio for first bounce of contact of a ball and horizontal wall, considering above definitions of coefficient of restitutions. For several damping ratios, ratio of relative velocity of ball at end of contact to relative velocity of ball at beginning of contact calculated and linear relation of the coefficient of restitution and damping ratio based on Newton's definition is found. For calculation of energetic coefficient of

restitution, for several damping ratios, the force-displacement curves are drawn and the area within loading and unloading curves of numerically is calculated. With same approach the relation for normal coefficient of restitution and damping ratio for Hertz-Mindlin is found.

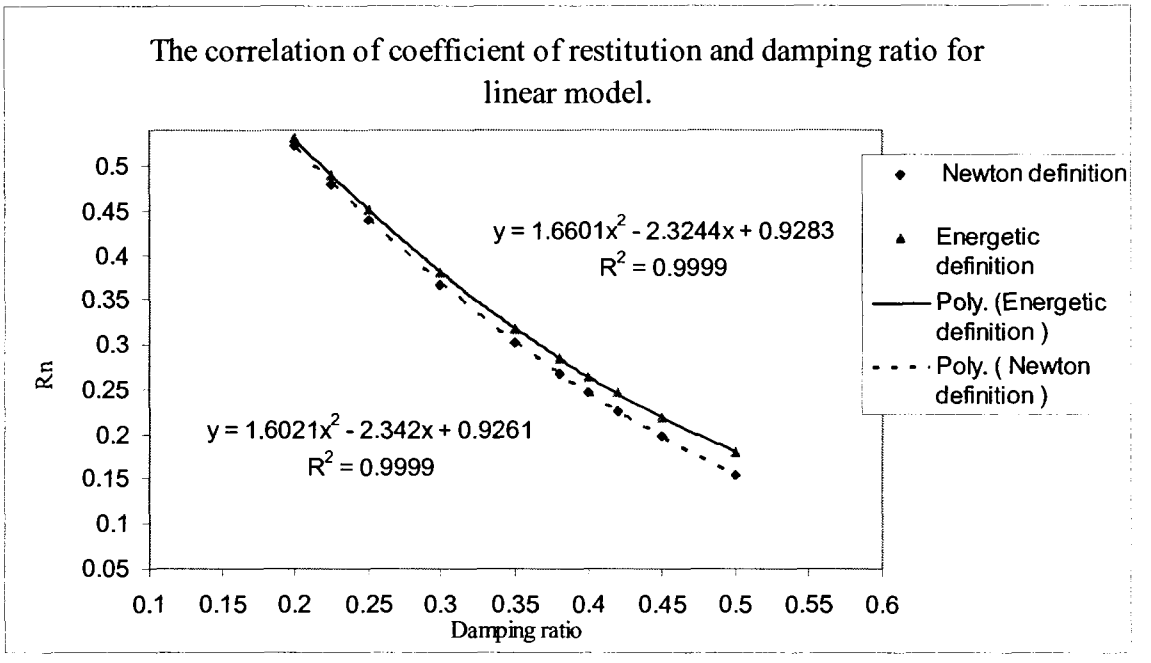

Figure 6.36: The correlation of coefficient of restitution and damping ratio for linear model.

As shown in Figure 6.37 two definition of coefficient of restitution have same representation in linear and especially in Hertz-Mindlin model. For Hertz-Ng model, since increasing the damping ratios, does not change the ratio of end velocity to start velocity of the ball, the relation is not found. In contrast with linear and Hertz-Mindlin model, the relationship between coefficient of restitution and damping ratio are dissimilar (Figure 6.38).

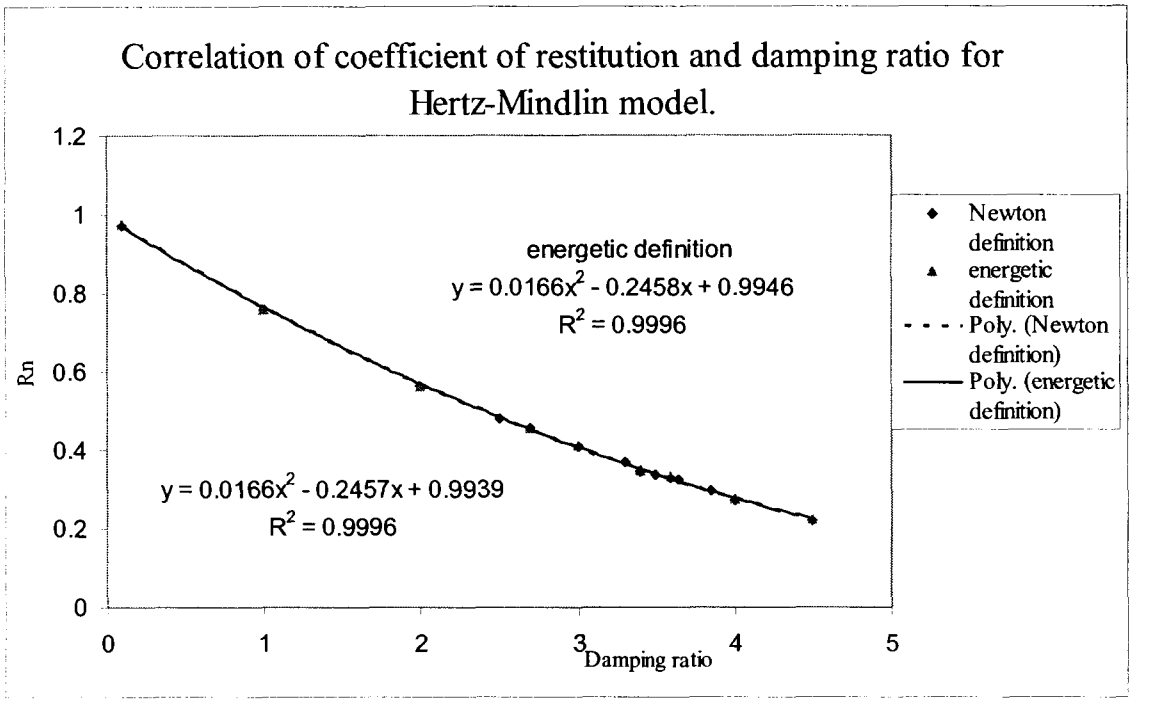

Figure 6.37: The correlation of coefficient of restitution and damping ratio for Hertz-Mindlin contact model.

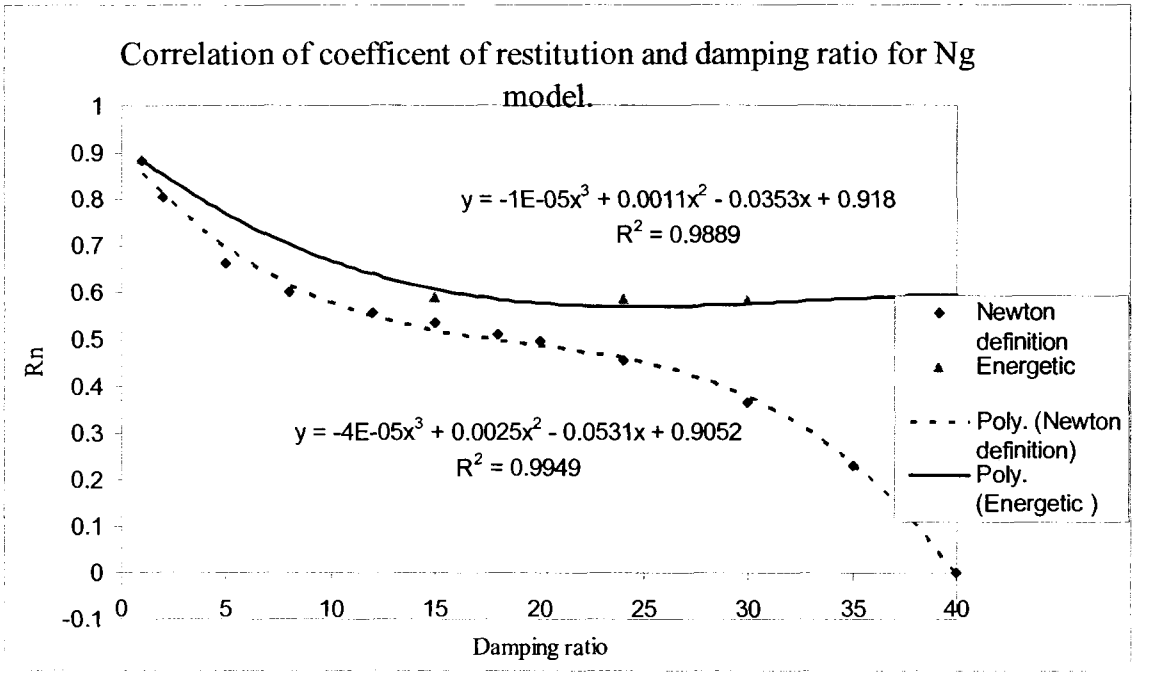

Figure 6.38: The correlation of coefficient of restitution and damping ratio for Ng model.

6.4. Comparing the Ball's Motion in Haraz and RocFall

Figure 6.39 demonstrates the motion of freefall balls with certain set of coefficient of restitution and 10 kg on frictionless surface in RocFall, similar to the model discussed before. Note that since the model is 2D and balls are dimensionless, to obtain maximum height bounce ball's radius should be added to values of this figure. According to RocFall algorithm, balls are moving through the air when their velocities are higher than the certain value. Because of RocFall algorithm, trajectory of ball is very sensitive to this value. Since the effect of air drag (air resistance) is not considered in Haraz model, to be able to compare the results, I reduced initial velocity of ball to 0.001 m/s (minimum possible value).

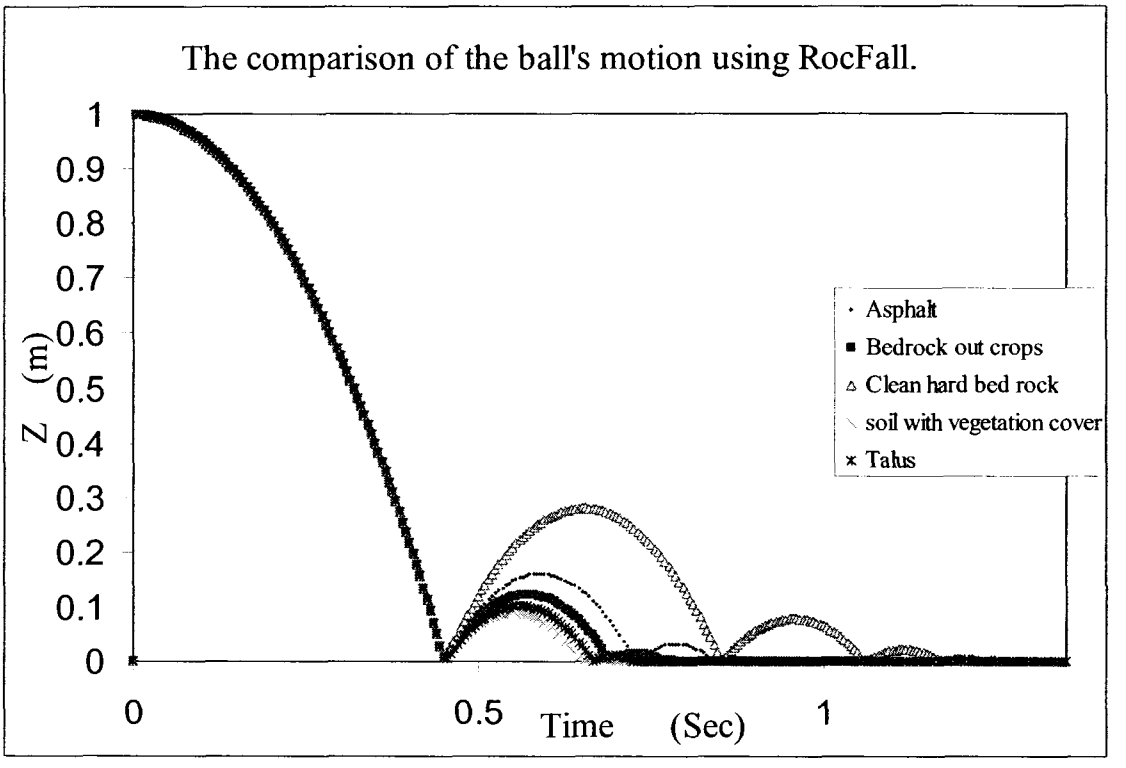

Figure 6.39: Balls trajectories for different wall's material in RocFall.

Figure 6.40 illustrates the motion of a freefall ball with normal coefficient of restitution of 0.53 which is modeled using linear, Hertz-Mindlin and Ng model as well as

a similar model in RocFall. For first contact, adding the ball's radius (0.21m) to maximum bounce height, results in similar configuration of linear and Hertz-Mindlin model in contrast with Ng model. First contact in Ng model occurs with about 0.4 Sec delay in compare with other models. For successive contacts, none of methods are completely similar. However, bounce heights in linear model are much closer to linear model and contact times are different.

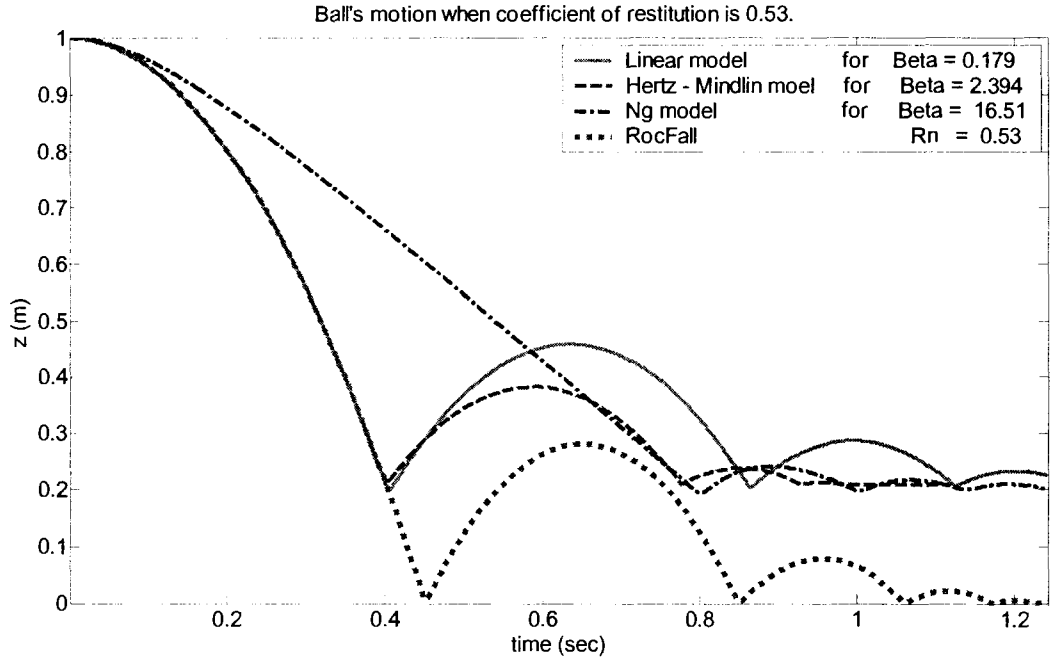

Figure 6.40: Comparison ball's motion comes from linear, Hertz-Mindlin and Ng model and the model in RocFall.

6.5. Summary

- Dynamic behaviour (ball's trajectory, ball's motion and ball's velocity) of Linear, Hertz-Mindlin and Ng contact model in ideal situation are the same and consistent with the law of conservation of energy.

- In ideal situation, force-displacement relationship is nonlinear power function in Hertz-Mindlin and Ng model and force-displacement relationship is linear in contrast with linear model.
- Dynamic behaviour of Linear, Hertz-Mindlin and Ng contact models with viscous damping are dissimilar.
- Force-displacement relationships of linear and Hertz-Mindlin represent the hysteresis loops.
- Force-displacement relationships of Hertz-Ng and Ng model form the power function, and the impact and rebound curves coincide.
- Energetic and Newton coefficient of restitution of linear and Hertz-Mindlin almost coincide.
- Because of dependence of normal and shear contact force to normal force, which does not exist in first contact in Ng model, results of first contact (motion, velocity and etc.) are not reliable.
- Comparison of ball motion when linear, Hertz-Mindlin, Ng model and RocFall shows the similarity of linear model and RocFall model.

7. Study of 3D Elastic-Inelastic Power Function Contact Model and Comparison with Other Contact Models

As previously mentioned, elastic-inelastic power function contact model depends on three factors: initial normal stiffness (K_n), transition force *(T)* and exponent *(b)* [20]. Since each of these elements has a significant effect on macroscopic and microscopic behaviours of falling rocks, effect of each of these parameters are studied and, coefficient of restitution for contact of a *10 kg* Berea Sandston when collides with different walls is determined and correlation of coefficient of restitution and transition force is discussed in this chapter.

7.1. The Effect of the Exponent (b) on Motion of Ball

Using this model, it is necessary to adjust and calibrate the values of initial normal stiffness (K_n), transition force *(T)* and exponent *(b)*, since this model is unstable for some set of values and also, it is possible to get incorrect results. For lower values of linear stiffness, when maximum linear force in first phase of contact (impact or loading) is less than transition force, with any value of exponent, system is unstable. Also, when the value of b is zero the ball's bounce height, the contact velocity and the overlap increase with respect to time (similar to resonance) as shown in. This fact occurs because the value of contact force is equal to value of a, which equal to transition force in each time step; hence, overlap increases causing an increase in the bounce height and the velocity. It is not expected that this case never occurs in reality. When exponent b is

equal to 1.0, the second phase of this model becomes a linear model as shown in Figure 7.1 Equation (7.2). Figure 7.2 shows the motion of ball when transition force has a constant value and value of b is variable. Increasing the value of b decreases the bounce height but effect of exponent on the velocity just appears in first bounces (3-4 first bounces).

$$\begin{cases} F_n = a \\ a = \dfrac{T}{1.0}, \quad b = 0.0 \end{cases} \tag{7.1}$$

$$\begin{cases} F = ax \\ a = \dfrac{T}{B}, \quad b = 1.0 \end{cases} \tag{7.2}$$

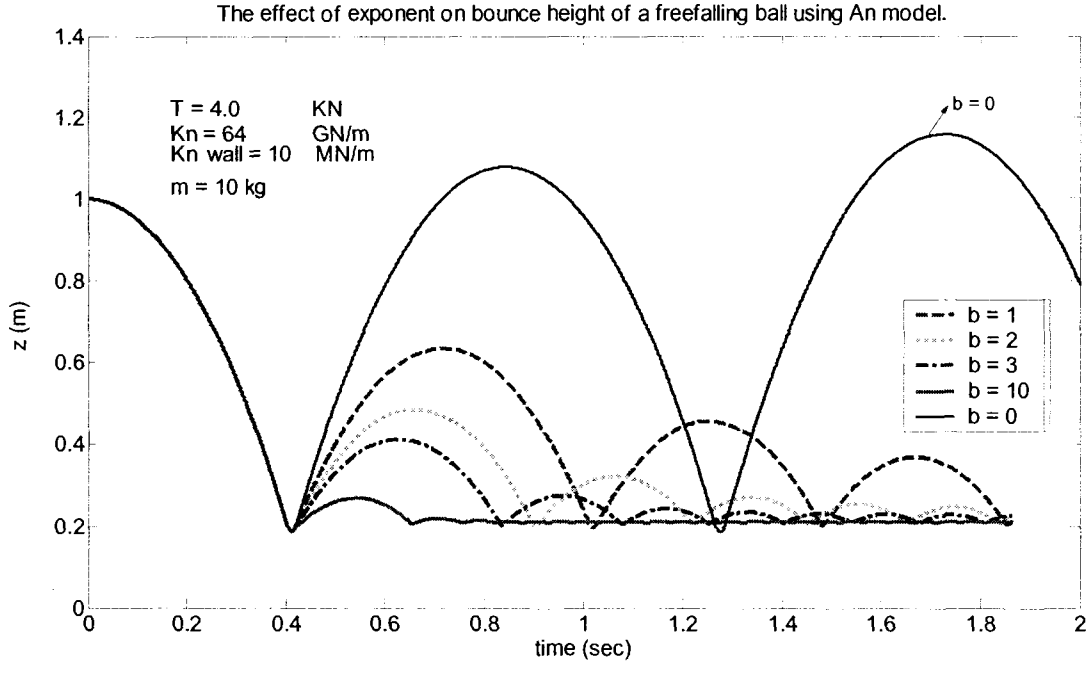

Figure 7.1: Ball's motion in "An" model when exponent is variable.

For adjustment variables of elastic-inelastic power model and also to determine the value of coefficient of restitution, it is necessary to plot the normal contact force versus overlap. Figure 7.2 illustrates the variation of normal contact forces versus normal

overlap (displacement) when exponent b is variable. First phase of first contact of ball and wall (OB) is common for all cases with different exponents, meaning elastic deformation (AB) remains constant for first contact as exponent increases. However, increasing the exponent increases the amount of plastic deformation. Also, increasing the exponent increases the energy loss. For successive contacts, plastic deformation decreases. As shown in Figure 7.2, for *(b=2)*, at first contact plastic deformation (BF) is about 0.020 mm and in second contact decreases to about 0.010 mm (BH) and for third contact plastic deformation is equal to (BG).

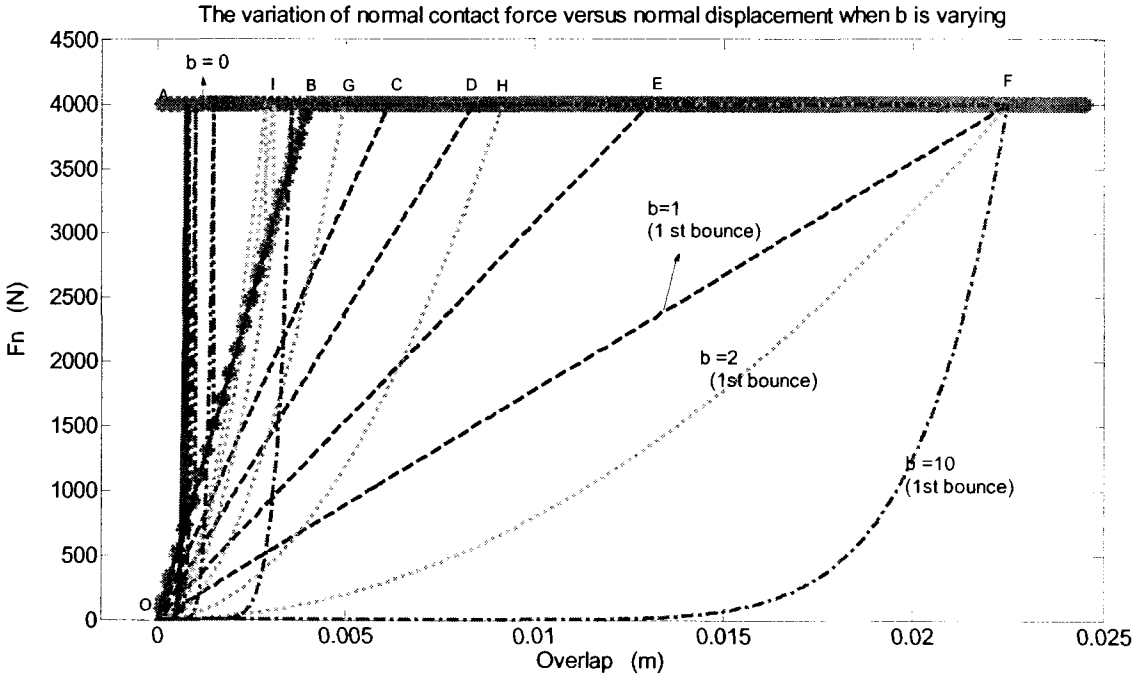

Figure 7.2: The variation of normal contact force versus time when exponent is variable.

7.2. The Effect of the Transition Force on the Motion

As mentioned before transition force is used for determination of the parameter a. The values of Table 7-1 are used to simulate the contact of a *10 kg* freefalling rock from height of *1.0 m* and frictionless horizontal wall for different values of transition force,

constant exponent ($b=8$), and constant normal stiffness of $6.4\times10^{10} N/m$. As is shown in Figure 7.3 and Figure 7.4 increasing the transition force increases the ball's bounce height and the ball's velocity. In addition to that, increasing the value of transition force causes an increase in the contact overlap and consequently an increase in the contact forces.

Table 7-1: the inputs for model a system of a ball and a horizontal wall.

Number of triangles	Number of balls	Number of steps	Contact type code	R (m)	K_n (N/m)	K_s (N/m)	γ (N/m^3)	σ_c (MPa)
2	1	1×10^7	2	0.21	6.4×10^{10}	9.6×10^6	2600	90

Comparing the motion of a *10 kg* freefalling rock from height of *1.0 m* which is modeled with elastic-inelastic power function with the one that is model with linear model, maximum bounce heights and contact normal velocity (first two bounces) of a ball with $T=16\times10^3 N$ and exponent of *(b=8)* is similar to motion of a same ball with 0.2 damping ratio, however contact times and amount of the energy loss for each contact are different. The motion of the balls in linear model ends in about 1.5 sec which is not occurring in the elastic-inelastic power model.

To study the amount of energy loss in each contact in elastic-inelastic power function model, coefficient of restitution for several cases (when transition forces varies from $4\times10^3 N$ to $30\times10^3 N$ and with an exponent of a constant value of 8) is calculated and trend line is drawn as in Figure 7.5.

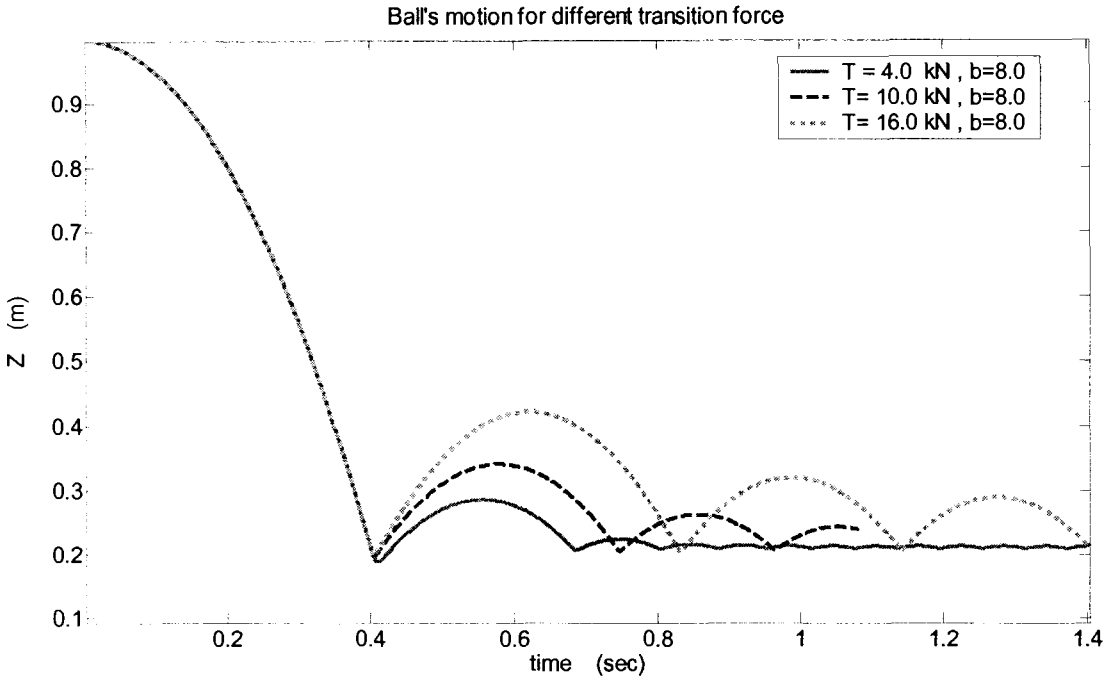

Figure 7.3: The variation of ball's bouncing versus time when transition forces vary from 4.0 KN to 16.0 KN.

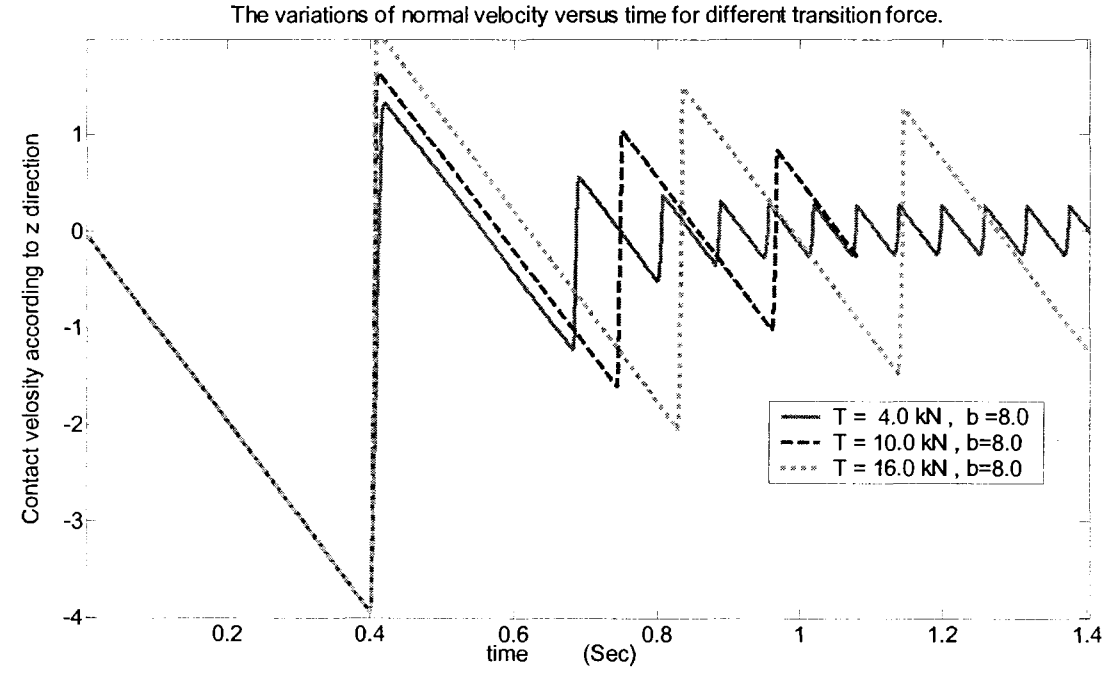

Figure 7.4: The variation of ball's velocity versus time when transition forces vary from 4.0 N to 16.0 N.

The method for calculation of coefficient of restitution is the same as the one used in chapter 6. Considering the values of contact velocities that are printed in the file contact_velocity.txt, the ratio of velocity at beginning of contact and velocity at the end of contact for each contact is calculated (Newton definition).

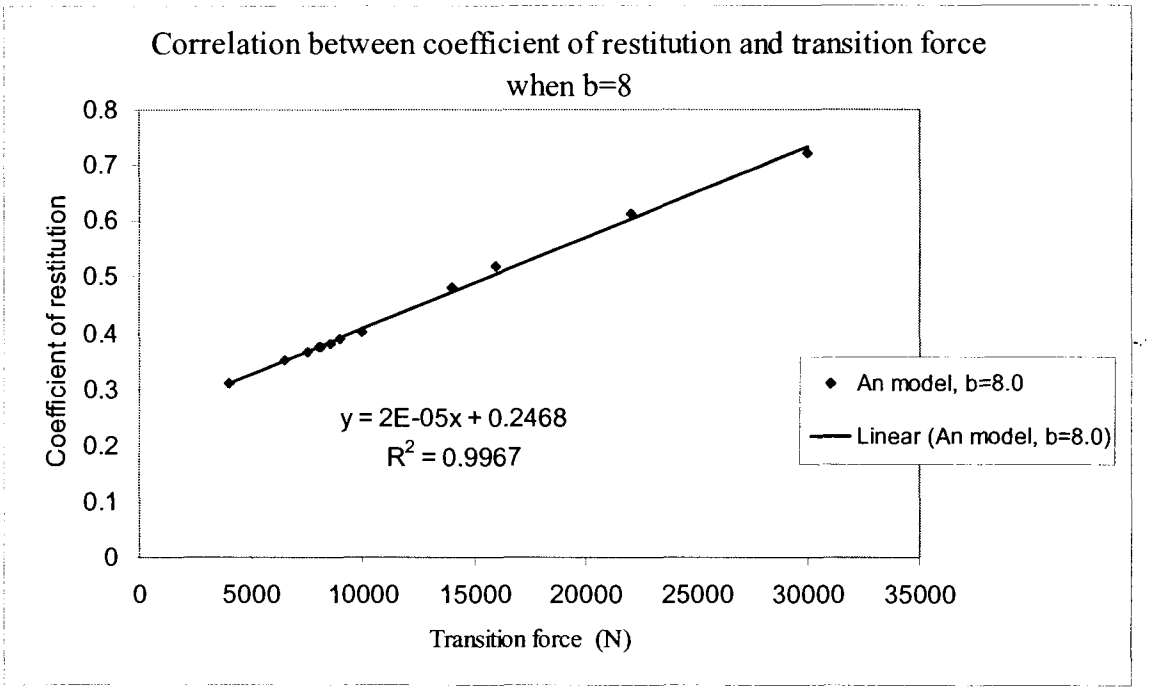

Figure 7.5: The linear relationship between coefficient of restitution and transition force.

As it is shown in Figure 7.5, coefficient of restitution between 0.30-0.53 using Equation (2.1) corresponds to transition forces between $4\times10^3 - 10\times10^3 N$ using Equation (2.1).

Figure 7.6 illustrates the variations of the normal forces versus time. According to algorithm of elastic-inelastic power function model, since contact forces are limited with the values of transition force, as shown in Figure 7.6 maximum contact forces are equal to transition forces and have similar configuration in successive contacts. For lower values of transition force, the number of contacts for certain times is higher. For instance,

during 1.0 sec after first contact, when transition force has a value of $4\times10^3 N$, the ball collides with wall five times, but when transition force has a value of $16\times10^3 N$, only two contacts occur.

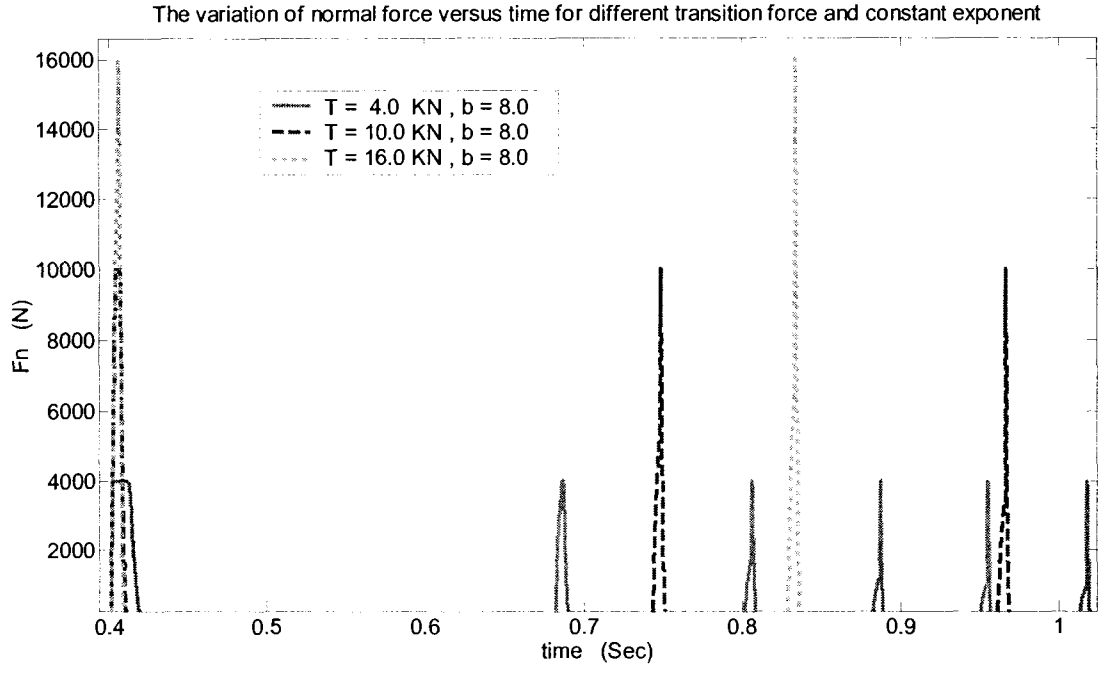

Figure 7.6: The variation of normal contact forces versus time when transition forces vary from 4.0-16.0 KN.

Figure 7.7 illustrates the variations of normal forces and normal displacements (overlaps). For $T=4\times10^3 N$, the ratio of plastic deformation to elastic deformation at the first contact is about 5.55 which seem too much since the rocks are considered brittle. For $T=16\times10^3 N$, plastic deformation does not occur. Force jumps without displacement. This fact is because the final linear contact force (maximum displacement) occurs before reaching to transition force. This fact shows the linear normal stiffness should increase if we need for higher coefficient of restitution. In other words maximum allowable transition force for this set of normal stiffnesses is about $12\times10^3 N$. Also, minimum transition forces should be determined considering the ratio of plastic deformation to total

deformation of the rock. It's important to determine this ratio for different rock types since rocks are brittle and this ratio limits the elastic ratio. The author could not find the values for this ratio for different rock types in the literature.

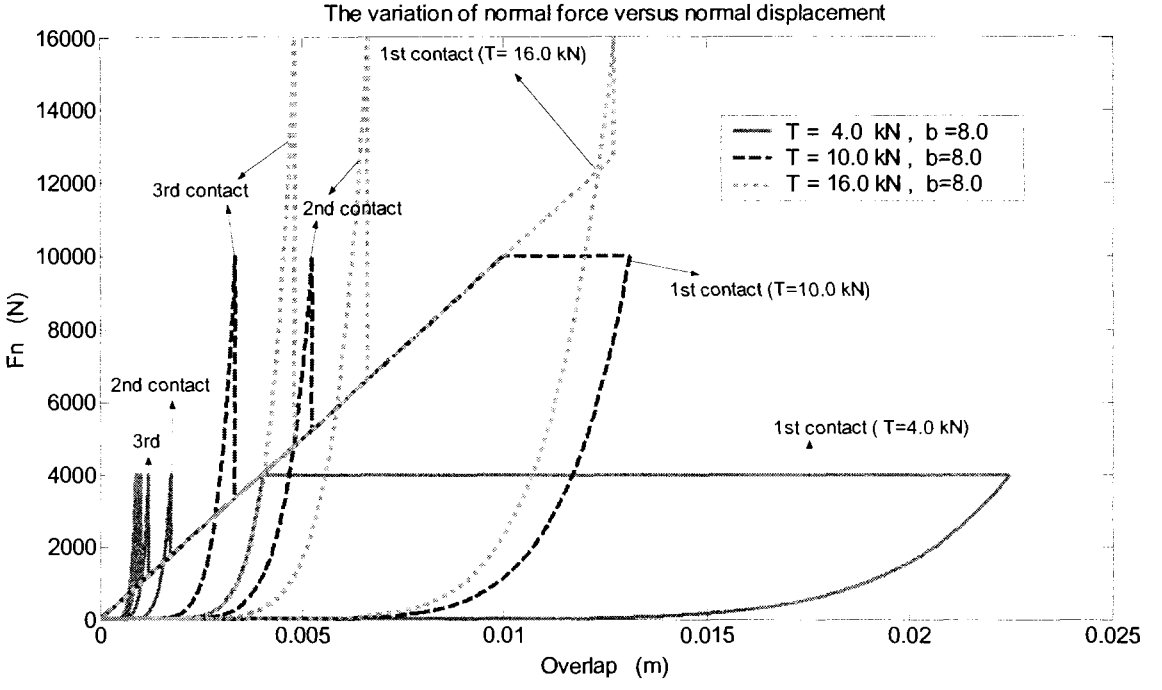

Figure 7.7: The variation of normal contact forces versus normal displacement when transition forces vary from 4.0 to 16.0 KN.

As shown in Figure 7.7, only in first the contact elastic deformation occurs when transition forces are less than $12\times10^3 N$ and for transition forces higher than $12\times10^3 N$ elastic deformation never occurs.

7.3. The Effect of Transition Force and Exponent on Coefficient of Restitution

An suggests a value $250\times10^3 N$ as transition force for a ball with normal stiffness of $6.4\times10^{10} N/m$ for 2D model as mentioned in Table 2-1. According to Equation (2.43), transition force for a rock with properties of Table 7-1 and a scaling factor of 0.078, can

be found $58.0\times10^3 N$ which is about 23 percent of the proposed value. The values of transition forces and exponents that are related to coefficient of restitution of some wall's material are found as it shown in Table 7-2. Using the values of Table 7-2, Figure 7.8 is plotted.

Table 7-2: Coefficient of restitution for some wall's material.

Wall's materials	Values for R_n $R_n = \frac{V_{rn}}{V_{in}}$	Transition force, (N) $T = 58.0\times10^3$	Exponent's values (b)
Clean hard bed rock	0.53	$T/4 = 14.5\times10^3$	7.0
Asphalt roadway	0.40	$T/8 = 7.25\times10^3$	7.0
Bed rock outcrops with hard surface, large boulders	0.35	$T/18 = 3.22\times10^3$	7.5
Talus cover	0.32	$T/20 = 2.9\times10^3$	8.0

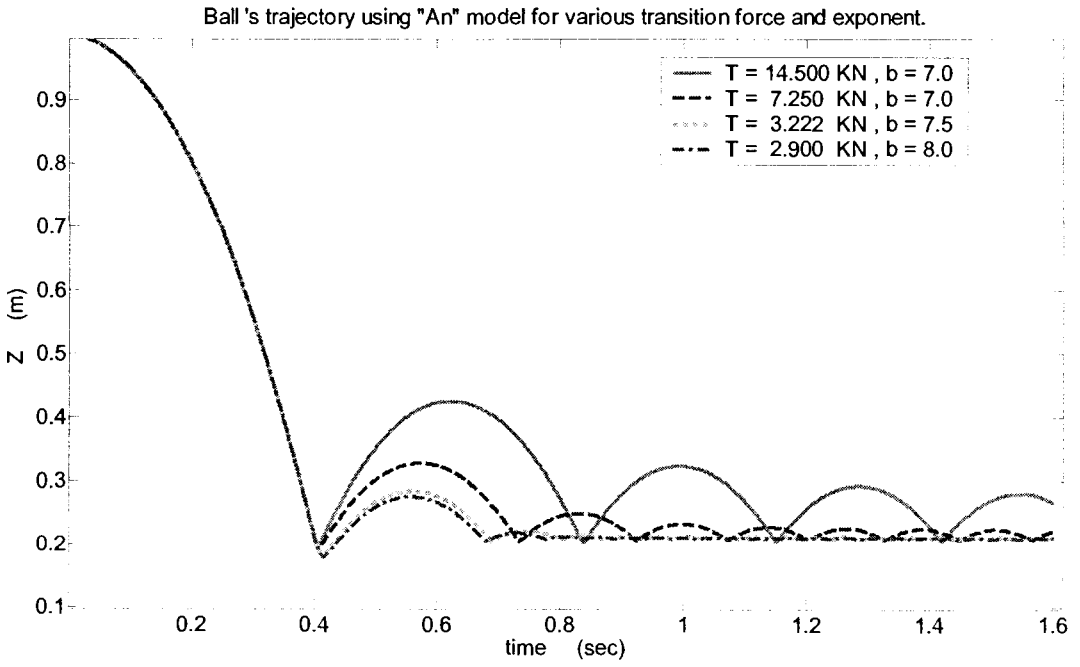

Figure 7.8: Ball's motion in respect to time for various transition forces and exponents.

7.4. Comparison of Elastic-Inelastic Power Function Model and Other Contact Models

Table 7-3 is a combination of Table 6-4 and Table 7-2 that shows the set values for damping ratio, transition forces, and exponents corresponding to coefficient of restitution of different wall's material.

Table 7-3: Coefficient of restitution for some wall

Wall 's material	Values for $R_n = \frac{V_{rn}}{V_{in}}$	Values for damping ratio (β)			An model	
		Linear	Hertz-Mindlin	Ng	Transition force,(N) $T = 58\times10^3$	b
Clean hard bed rock	0.53	0.179	2.399	16.10	$T/4 = 14.5\times10^3$	7.0
Asphalt roadway	0.40	0.283	3.169	34.90	$T/8 = 7.25\times10^3$	7.0
Bed rock outcrops with hard surface, large boulders	0.35	0.324	3.464	36.5	$T/18 = 3.222\times10^3$	7.5
Talus cover	0.32	0.328	3.642	37.50	$T/20 = 2.9\times10^3$	8.0
Soft soil	0.30	0.364	3.76	38.10	-	-

To compare the macroscopic behaviour of a ball freefalling on a horizontal wall (made of above materials) using different contact models, the variation of ball's motion and ball's contact velocity with respect to time are plotted in Figure 7.9 and Figure 7.10. It seems that the elastic-inelastic model is similar to linear model however energy dissipation in each contact is less than linear model.

Figure 7.9 demonstrates the difference in ball's motion with respect to time and also maximum bounce height of the ball using different contact models. It can be seen that energy dissipation in Hertz-Mindlin model is faster than other models. In other words

the ball's motion in Hertz-Mindlin model ends before the motion in other contact models. First contact in Ng model and Hertz-Ng model occurs with a delay in comparison with other models. Maximum bounce heights are noticeably less than other models, also.

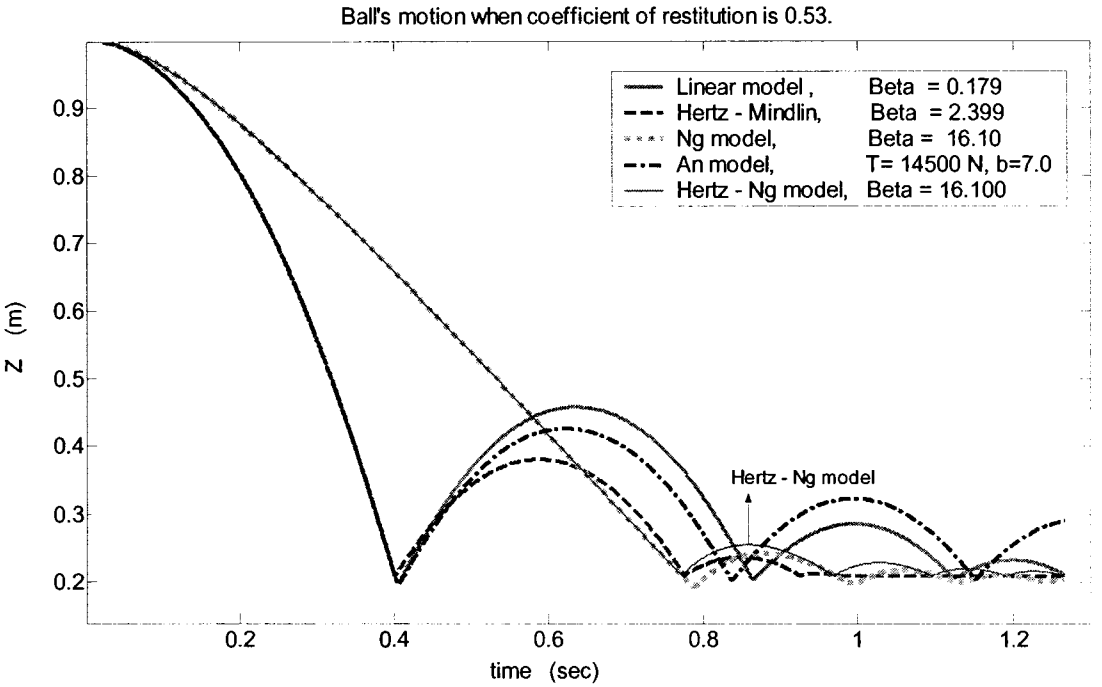

Figure 7.9:Ball's motion using different contact model when coefficient of restitution is 0.53.

Although, as it's shown in Figure 7.10 coefficient of restitution is the same (the ratio of rebound velocity to impact velocity) for all the contact models, the magnitude of rebound and impact velocity are different. Also, contact times are different. Obviously, these small differences in a simple model can be noticed in complex models.

This study provides some analytical data of microscopic and macroscopic behaviours of contact of a ball and wall; it is recommended that the validation of data, examined by performing sets of experimental test in future researches. To be able to distinguish which contact model is more appropriate for rockfall simulation, comparison and calibration of analytical results is necessary.

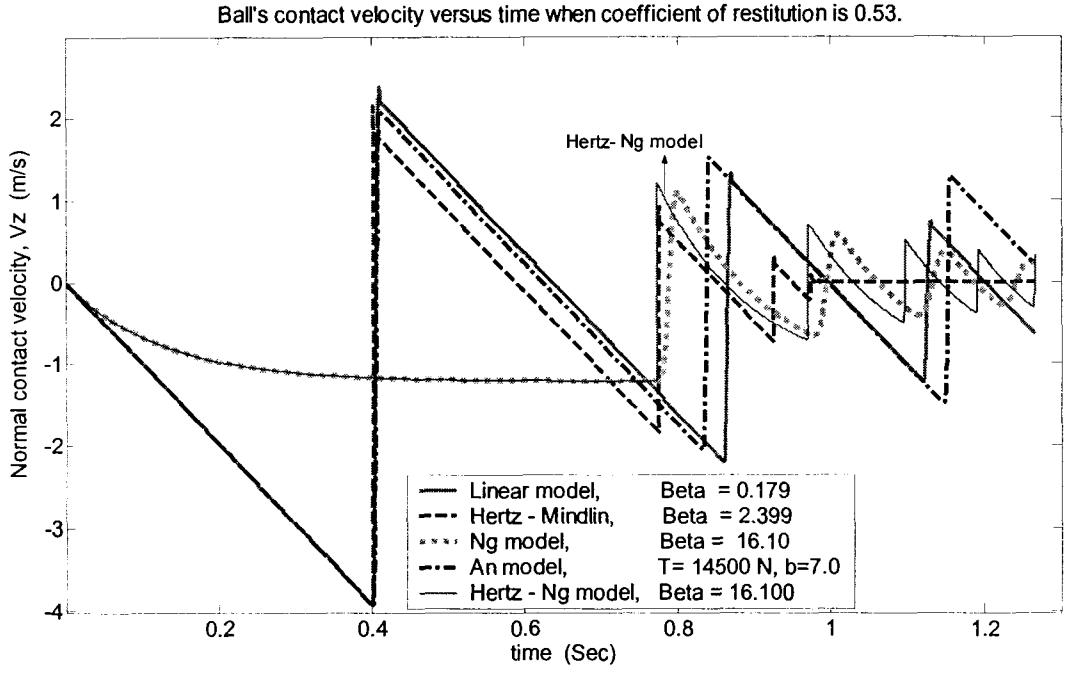

Figure 7.10: The variation of contact velocity versus time using different contact models when coefficient of restitution is 0.53.

7.5. Summary

- Adjustment of variables and calibration for this model is necessary. Several sets of input parameters were observed, whose results are not acceptable. Adjustments can be done by plotting the force-displacement relationship.

- Rocks fragments can be modeled using elastic–inelastic power Function (An) model; however the value of transition force should be studied through analytical and experimental tests in future researches.

- Minimum value of the transition force should be determined in order to limit plastic deformation considering the ratio of plastic deformation to total deformation of the rock.

- An's suggested values for transition force in 2D models are not valid for 3D models.
- For successive contacts, elastic deformation remains constant since it is only dependent on linear stiffness for first contact as exponent increases, but increasing the exponent increases plastic deformation in further researches.
- Increasing the exponent noticeably increases the energy loss.
- For successive contacts, plastic deformations decrease as the exponent increases.
- The macroscopic behaviour of a ball which is modeled by elastic-inelastic power function model is similar to linear model however energy dissipation in each contact is less than the energy loss of each contact in linear model.
- Using the Ng model and Hertz-Ng model is not recommended in application of rockfall, as macroscopic and microscopic behaviours are far from expectations.

8. Coefficient of Restitution of Slopes Using Linear Model

Normal coefficient of restitution of freefall ball on horizontal, flat wall using different contact models are studied in chapter 6 and 7. Since trajectory of a freefall ball on horizontal, flat wall is vertical as shown in Figure 6.2; hence, coordinates of the ball's contact velocity in respect with "X" and "Y" are equal to zero. This chapter is concerned with determination of normal and tangential coefficient of restitution for slopes and the variation of coefficient of restitution versus slope angle as well as the variation of normal and tangential coefficient and coefficient of restitution of resultant velocity (COR) of during the successive contacts. For this purpose two slopes with slope ratio of -1:1.73 and -1:1 are modeled and normal and tangential coefficient of restitution as well as COR for a freefall ball (Berea Sandstone ball) (Table 8-1) for various damping ratio are calculated. For calculation of Newton coefficient of restitution, same method as method of chapter 6 and chapter 7 is utilized.

Table 8-1: Inputs for the model.

Number of triangles	Number of balls	Number of steps	Contact type code	R (m)	K_n (N/m)	K_s (N/m)	γ (N/m^3)	β	ν	E (Pa)
4	1	1×10^7	0	0.21	1×10^7	1×10^7	2500	various	0.38	6.88×10^9

The ratio of the magnitude of velocity when contact ends (overlap of ball-wall ends) to magnitude of velocity of the ball when overlap starts (ball and wall start to overlap) represent Newton definition for coefficient of restitution. Since most of the studies of coefficient of restitution are conducted in 2D, traditionally coefficient of

restitution is calculated with respect to extent of normal and tangent of the slope. However, Cartesian system can be more appropriate when 3D DEM is used since ball's trajectory and ball's velocity are determined with respect to extent of Cartesian Axes.

Figure 8.1 illustrates the ball's trajectory on a slope with slope ratio -1:1.73 when different values of damping ratio are used. When damping ratio is higher than 0.1 ball's motion ends after some contact with slope but for the values less than o.1, ball collide with horizontal wall as well. For damping ratio equal to 0.01, the ball collides with a slope twice then several times collides with horizontal wall. For damping ratios less than 0.1, ball's trajectory ends in different distance in horizontal wall. Figure 8.2 illustrates the ball's trajectory on a slope with slope ratio -1:1.73 for different values of damping ratio.

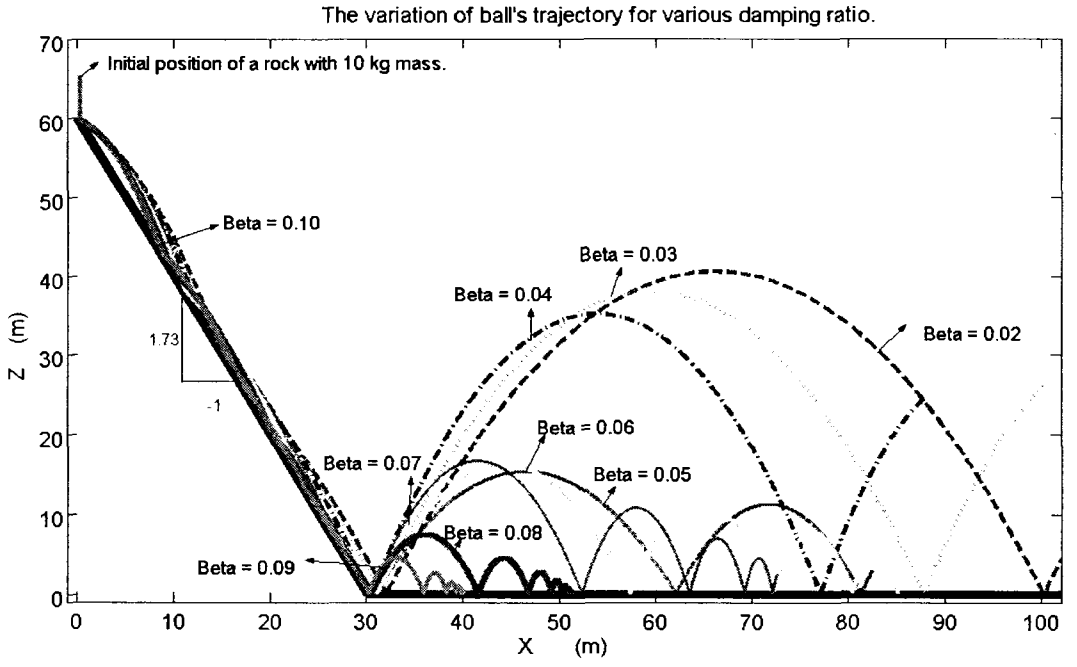

Figure 8.1: The variation of ball's trajectory for various damping ratio for a 120 degree slope angle.

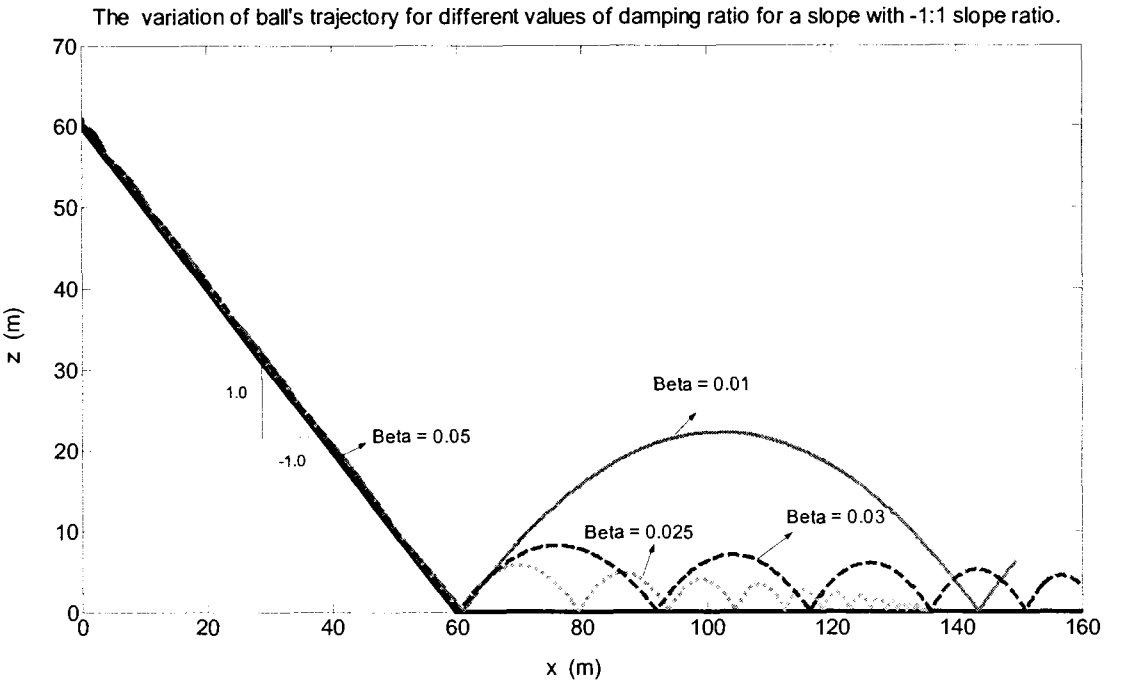

Figure 8.2: The variation of ball's trajectory for various damping ratio for a 135 degree slope angle.

8.1. Coefficient of Restitution for a 120 Degree Slope Angle (slope ratio -1:1.73)

Figure 8.3 illustrates the correlation of normal and tangential coefficient of restitution and damping ratio as well as correlation of coefficient of restitution (COR) and damping ratio for a 120 degree slope. COR is the ratio of the magnitude of resultant velocity at end of the contact to magnitude of velocity at beginning of the contact. The values of normal, tangential coefficient of restitution, and also COR are almost the same in successive contacts.

Table 8-2 shows the values of coefficient of restitution with respect to "Z" when a ball collides with a slope with -1:1.73 slope ratio (a 120 degree slope). As shown in Table 8-2, for a certain value of damping ratio, the coefficient of restitution increases in successive contacts. In order to find a coefficient of restitution for a slope, average value is calculated. Figure 8.4 illustrates the variation of coefficient of restitution versus

damping ratio for this slope. Also trend line for average values of coefficient of restitution versus damping ratio is plotted and its linear equation is displayed.

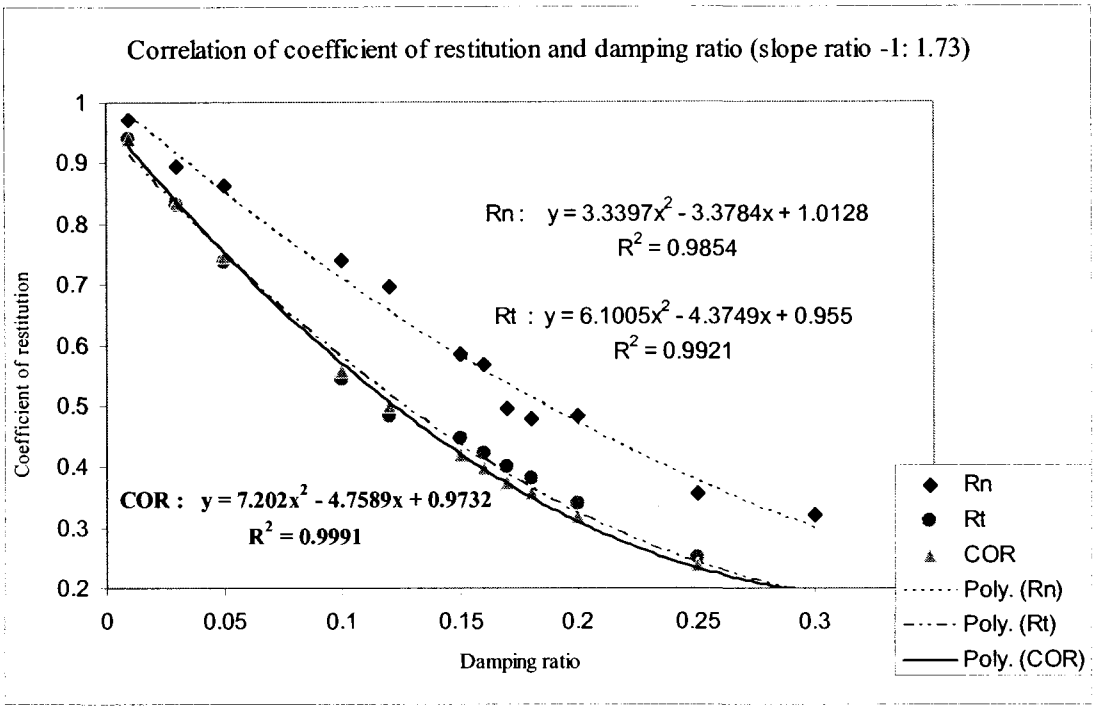

Figure 8.3: The variation of coefficient of restitution versus damping ratio for a slope with slope ratio of -1:1.73.

Table 8-2: Coefficient of restitution with respect to "Z" for different damping ratio for a 120 degree slope.

Damping ratio	Normal coefficient of restitution						
	First bounce	Second bounce	Third bounce	Forth bounce	Fifth bounce	Sixth bounce	Average
0.01	0.557	0.786	-	-	-	-	0.671
0.02	0.518	0.734	-	-	-	-	0.626
0.03	0.481	0.686	-	-	-	-	0.583
0.04	0.446	0.641	-	-	-	-	0.544
0.05	0.414	0.599	0.641	-	-	-	0.551
0.06	0.384	0.559	0.599	-	-	-	0.514
0.07	0.355	0.522	0.559	-	-	-	0.479
0.08	0.329	0.487	0.522	0.537	-	-	0.469
0.09	0.304	0.454	0.487	0.501	0.509	-	0.451
0.10	0.281	0.424	0.455	0.468	0.475	0.479	0.448
0.15	0.186	0.297	0.320	0.334	0.339	0.343	0.300

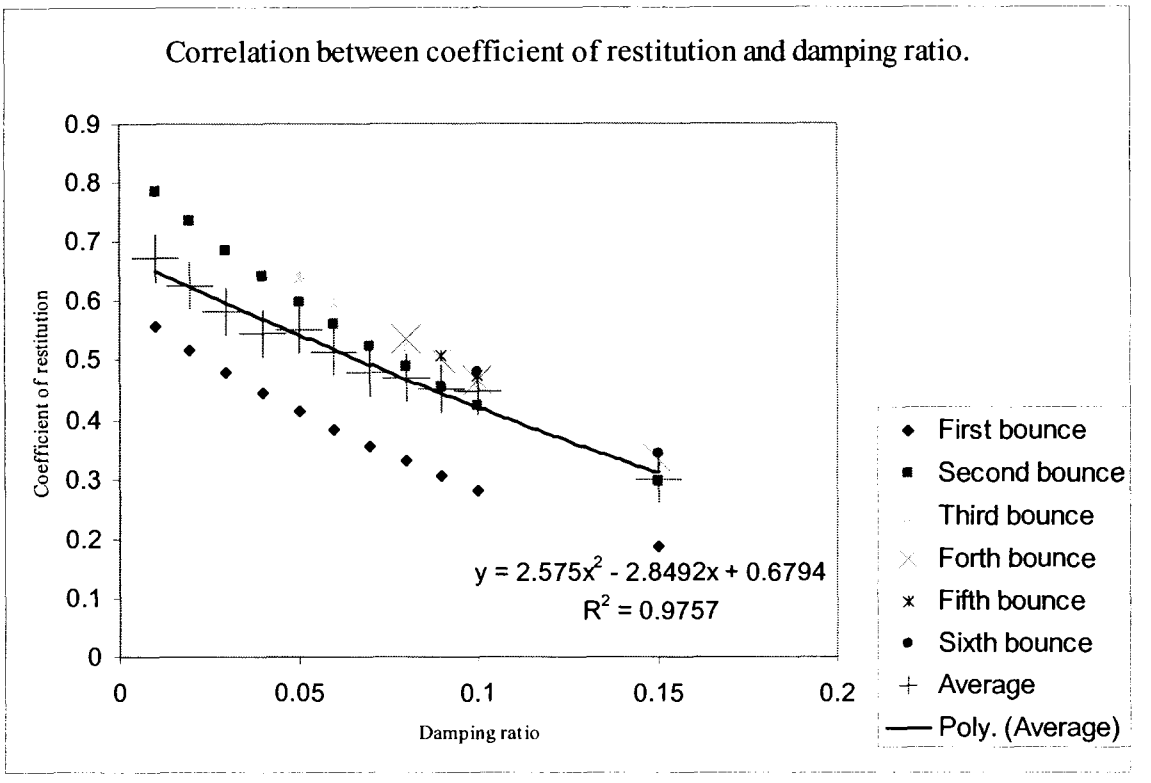

Figure 8.4: The variation of coefficient of restitution with respect to "Z" versus damping ratio for a slope with slope ratio of -1 : 1.73.

Table 8-3 shows the values of coefficient of restitution with respect to "Z" for different values of damping ratio for a horizontal wall after the slope. Coefficients of restitution with respect to "Z", which are normal to surface as well, are almost constant for successive contacts (bouncing). Since for damping ratio equal to 0.1 ball's trajectory ends before in slope and the range of calculated coefficient of restitution ranges between 0.970-0.76 which is not in range coefficient of restitution of rocks which is 0.3-0.53, stiffness of horizontal ball should be modified and lower values of stiffness should be assigned to horizontal walls in compare with sloped walls. Figure 8.5 shows the correlation of coefficient of restitution and damping ratio for a horizontal wall after the slope.

Table 8-3: Coefficient of restitution for different damping ratio for horizontal wall.

Damping ratio	Coefficient of restitution						
	First bounce	Second bounce	Third bounce	Forth bounce	Fifth bounce	Sixth bounce	Average
0.01	0.971	0.969	-	-	-	-	0.970
0.02	0.931	0.939	-	-	-	-	0.935
0.03	0.911	0.910	-	-	-	-	0.911
0.04	0.882	0.882	-	-	-	-	0.882
0.05	0.849	0.855	0.854	-	-	-	0.853
0.06	0.833	0.828	0.828	0.828	0.828	-	0.829
0.07	0.807	0.802	0.802	0.802	0.802	-	0.803
0.08	0.788	0.777	0.777	0.776	0.776	0.775	0.777
0.09	0.758	0.758	0.753	0.759	0.759	0.754	0.756

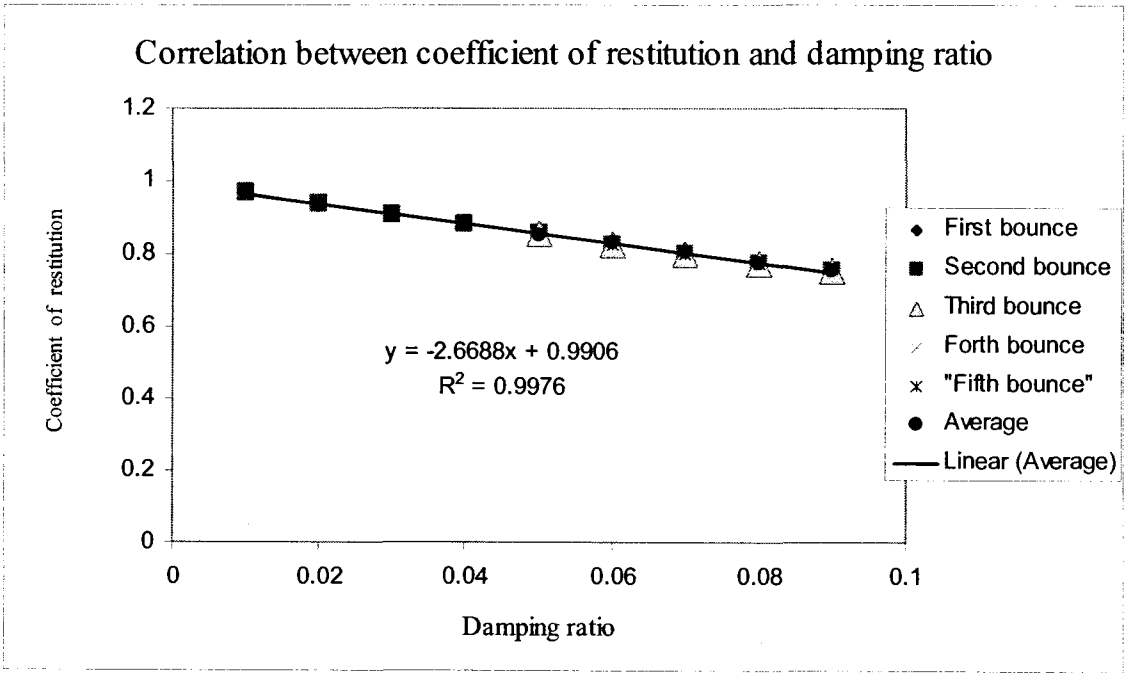

Figure 8.5: Correlation of coefficient of restitution and damping ratio for horizontal wall after a 120 degree slope.

8.2. Coefficient of Restitution for a 135 Degree Slope Angle (slope ratio -1:1)

Using same method as chapter 6 and chapter 7, coefficient of restitution for the various damping ratio for collisions of a freefalling ball and a slope with slope ratio of

-1:1 are calculated. Figure 8.6 demonstrates the correlation of normal and tangential coefficient of restitution and damping ratio for a 135 degree slope as well as the correlation of COR and damping ratio.

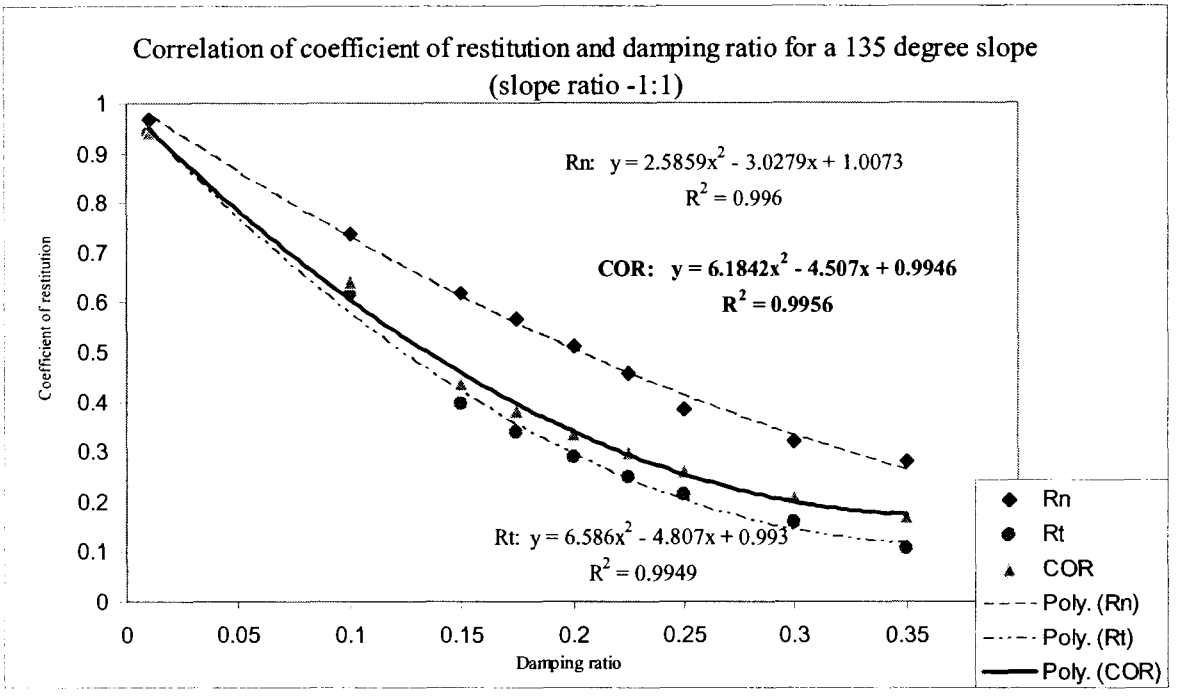

Figure 8.6: Correlation of coefficient of restitution and damping ratio for a slope with slope ratio -1:1.

As shown in Table 8-4, similar to a slope with slope ratio of -1:1.73, for a certain value of damping ratio coefficient of restitution increases in successive contacts. In order to find a coefficient of restitution for the slope, average value of coefficient of restitution is calculated as well. Comparing the values of coefficient of restitution of 120 degree slope angle (first model) and the 120 degree slope (second one) result in that coefficient of restitution depends on slope angle. Increasing the slope increases the value of coefficient of restitution. Figure 8.7 illustrates the variation of coefficient of restitution with respect to "Z" and damping ratio for a slope with slope ratio -1:1.

Table 8-4: Coefficient of restitution with respect to "Z" for different damping ratio for a 135 degree slope.

Damping ratio	Normal coefficient of restitution						
	First bounce	Second bounce	Third bounce	Forth bounce	Fifth bounce	Sixth bounce	Average
0.01	0.311	0.664	0.759	0.802	0.828	-	0.673
0.02	0.282	0.617	0.705	0.770	0.785	-	0.632
0.03	0.256	0.573	0.656	0.695	0.717	0.731	0.605
0.04	0.232	0.533	0.611	0.646	0.667	0.680	0.561
0.05	0.209	0.496	0.569	0.603	0.622	0.633	0.522
0.06	0.189	0.464	0.530	0.561	0.549	0.600	0.482
0.07	0.169	0.455	0.488	0.524	0.541	0.552	0.455
0.08	0.151	0.397	0.463	0.486	0.502	0.513	0.419

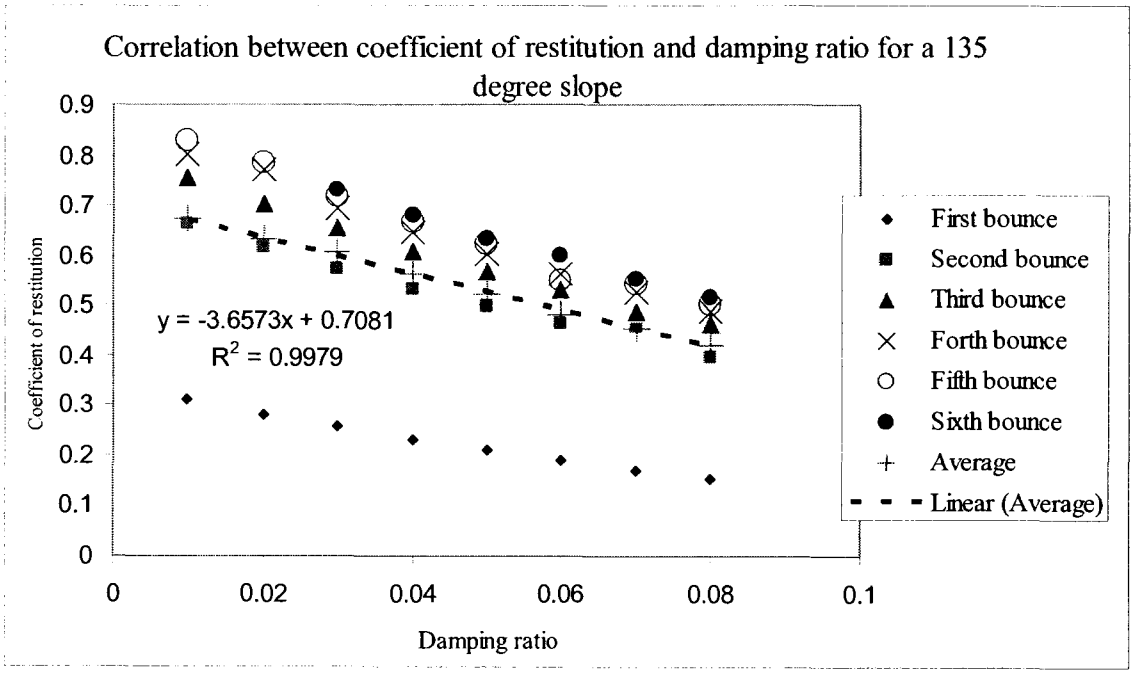

Figure 8.7: Correlation of coefficient of restitution with respect to "Z" and damping ratio for a 135 degree slope.

Figure 8.8 demonstrates the variation of coefficient of restitution versus damping ratio for a horizontal wall after the slope. Similar to previous case (horizontal wall after the a 120 degree slope), coefficients of restitution with respect to "Z", which are normal to surface as well, are almost constant for successive contacts.

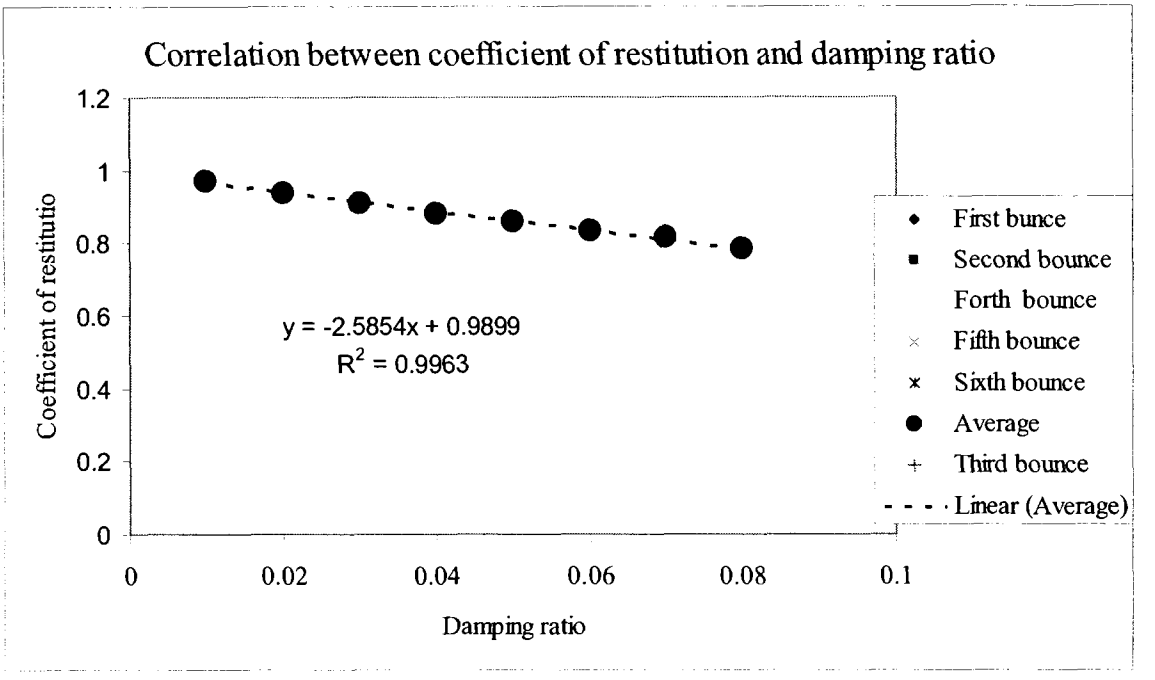

Figure 8.8: Correlation of coefficient of restitution and damping ratio for horizontal wall after a slope with slope ratio - 1:1.

Table 8-5: Coefficient of restitution for different damping ratio for a horizontal wall after a 135 degree slope.

Damping ratio	Normal coefficient of restitution						
	First bounce	Second bounce	Third bounce	Forth bounce	Fifth bounce	Sixth bounce	Average
0.01	0.969	-	-	-	-	-	0.969
0.02	0.939	0.939	0.939	-	-	-	0.939
0.03	0.910	0.910	0.910	-	-		0.910
0.04	0.881	0.881	0.881	0.881	-	-	0.881
0.05	0.858	0.858	0.858	0.858	0.855	0.858	0.857
0.06	0.836	0.835	0.834	0.829	0.836	0.835	0.834
0.07	0.828	0.812	0.820	0.808	0.809	0.810	0.814
0.08	0.787	0.786	0.779	0.787	0.786	0.779	0.784

The calculated normal coefficient of restitution for horizontal wall after slope, which defined by same property of the slope are higher than the expected value (0.53). To avoid this error, for walls with same material, horizontal walls should be define by lower values of stiffness.

8.3. Summary

- The values of coefficient of restitution for a certain value of damping ratio increases in successive bounces when are calculated with respect to Cartesian axes, for contact of a ball and a slope.
- The values of normal and tangential coefficient of restitution as well as COR, for a certain value of damping ratio are almost constant.
- Normal, tangential coefficient of restitution and COR depends upon slope angle.
- Increasing the slope angle (120 to 135 degree) increases the values of normal coefficient of restitution and COR.
- For damping ratio of less than 0.1, increasing the slope angle (120 to 135 degree) increases the values of tangential coefficient of restitution.
- For certain value of damping ratio, coefficient of restitution remains almost constant in successive contacts.
- Stiffness of horizontal walls should be modified and lower values of stiffness in compare with the values of stiffness for sloped walls should be assigned to horizontal walls since the values of coefficient of restitution which produced with similar values of stiffness, are higher than range of coefficient of restitution of rock types.

9. Estimation of the Horizontal Travel Distance of a Rock Using Artificial Neural Networks (ANN)

Finding the trajectories and endpoints (horizontal travel distance) of rocks of a probable rockfall are important outcomes of the rockfall simulation. Having information of balls' trajectory as well as the kinetic energy level of the rock at location of remedial measures for rockfall allows engineers to design appropriate remedial measures with reasonable factor of safety at appropriate position.

Figure 9.1 shows some of the possible trajectories for a falling rock from top of the slope. Endpoint of a rock by definition is where rock stops and velocity is zero $(Vx = 0, Vy = 0, Vz = 0)$. For analysis of rockfall and determination of horizontal travel distance of a falling rock, several models should be prepared since many factors are involved in rockfall such as geometry of slope, slope angle, number of rocks, mass (radius and density), initial position, initial velocity, coefficient of restitution, which is related to materials and stiffness of walls and materials and damping ratios of rocks. Figure 9.2 shows the effect of damping ratio of a ball on the ball's trajectory. Also Figure 9.3 shows the effect of mass on a rock's trajectory in rockfall. This chapter is concerned with determination of a ball's horizontal travel distance considering different conditions of rocks and walls.

For this purpose, in this chapter, 122 sets of data are collected for various conditions of a ball using linear contact model. The corresponding data can be found in Appendix 2. Since the results of DEM based code are strongly sensitive to time steps and at same time CPU time is high, coefficient of time steps are chosen between 0.085-0.001

in order to keep time steps reasonable (in order of 1×10^{-6} sec or less). Then an intelligent model (the Artificial Neural Network model) is built. After validation of the model, a sensitivity analysis is performed for seven factors of DEM which are ball's radius, ball's density, damping ratio, initial position of the ball (horizontal and vertical coordinates with respect to X and Z) and initial velocity of the ball (horizontal component of the velocity with respect to "X" direction and vertical component of the velocity with respect to "Z" direction). Finally, the effect of mentioned parameters on horizontal travel distance of a spherical rock is discussed.

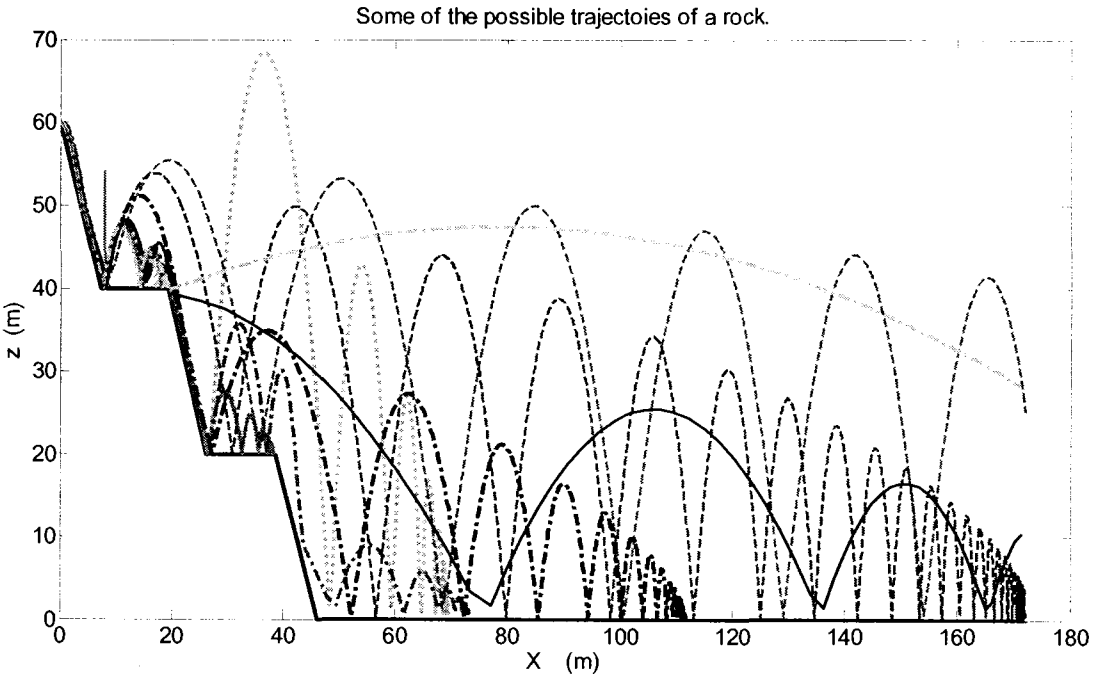

Figure 9.1: Some of the possible trajectories for a rock at top of the slope.

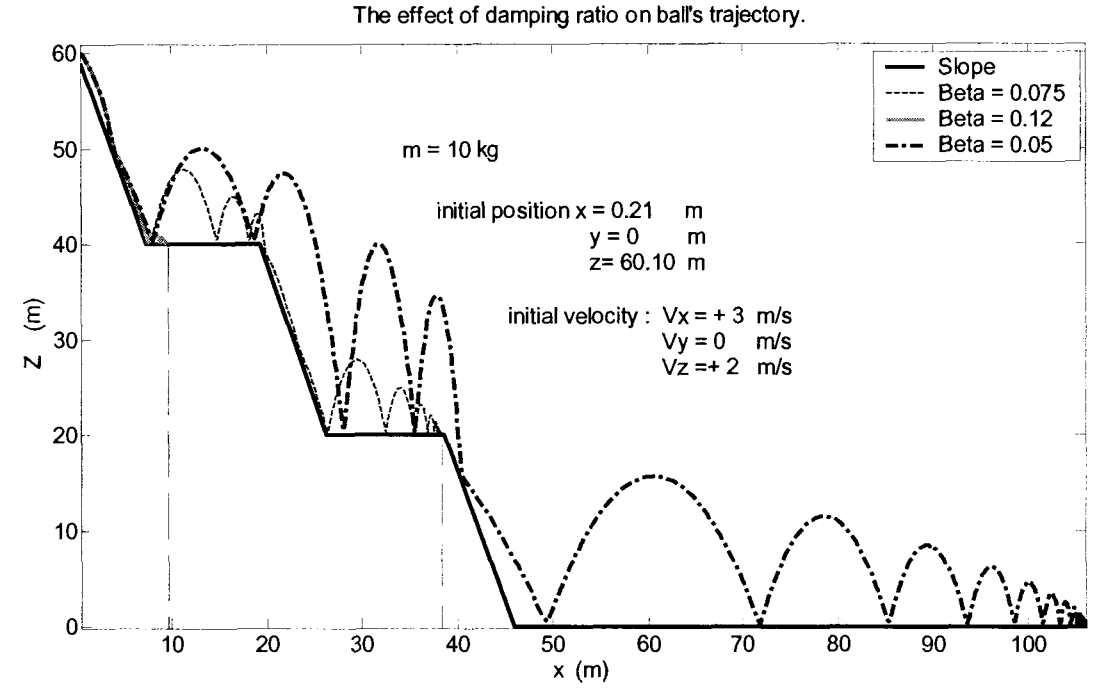

Figure 9.2: The variation of ball's trajectories when ball's damping ratio is variable using linear model.

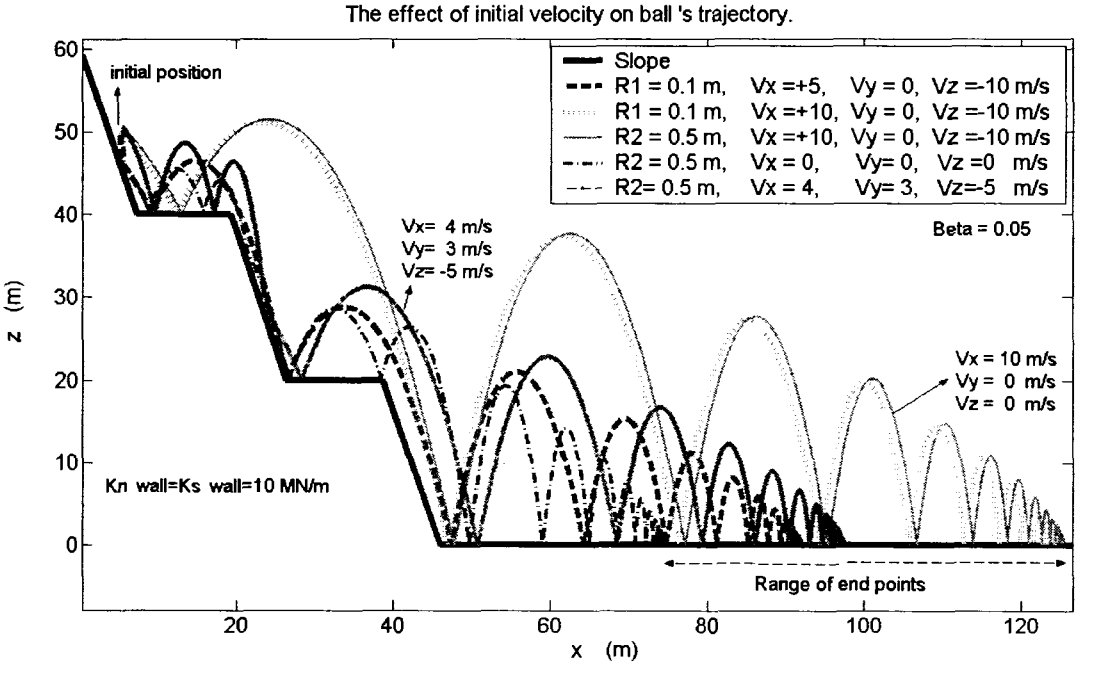

Figure 9.3: The variation of ball's trajectort when ball's damping ratio change using linear model.

9.1. Intelligent Modeling

In this chapter, Artificial Neural Networks method is used to model the horizontal travel distance of a rock as a function of various parameters. Using this method, we can find the horizontal travel distance of a rock for an arbitrary set of parameters in order to overcome the time consumption of running the code.

9.1.1. Basics of Artificial Neural Network

A methodology for modeling procedural and reflexive functions is using the Artificial Neural Networks, which can be described as non-linear multivariable function approximators and are motivated by input-output and learning properties of biological neural systems [44]. "Artificial Neural Networks consist of processing elements interconnected by weighted links that simulate the neurons and synapses of biological nervous systems (see Figure 9.4)" [44]. "Their knowledge is acquired by learning, which can be either supervised or unsupervised "[44].

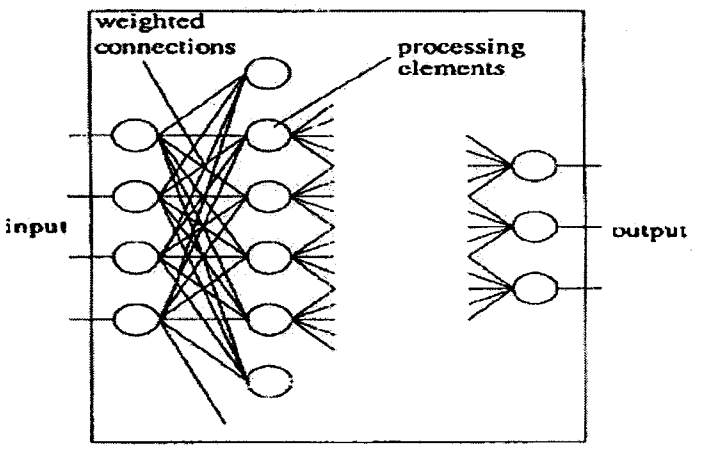

Figure 9.4: Basic structure of Artificial Neural Network [44].

The method presented here takes advantage of the fact that Artificial Neural Networks organize themselves while learning experience [44]. In this thesis, an Artificial

Neural Networks model is designed for estimation of horizontal travel distance of a ball based on supervised training method.

9.1.2. Artificial Neural Network Based Approximation

The (ANN) based model is developed with 7 inputs, 1 output, with 5 layers, each layer has 7, 5, 7, 2, 1 neurons respectively. Also, "tansig" and "logsig" excitation functions are used. *122* sets of data are obtained from the code to train the network. The training history of the network is depicted in Figure 9.5. As seen after about *1000* epochs the training error reaches *0.01= 1cm* which is satisfactory for our purpose. The simulation results show that the developed model provides a good performance for estimation of horizontal travel distance of a ball.

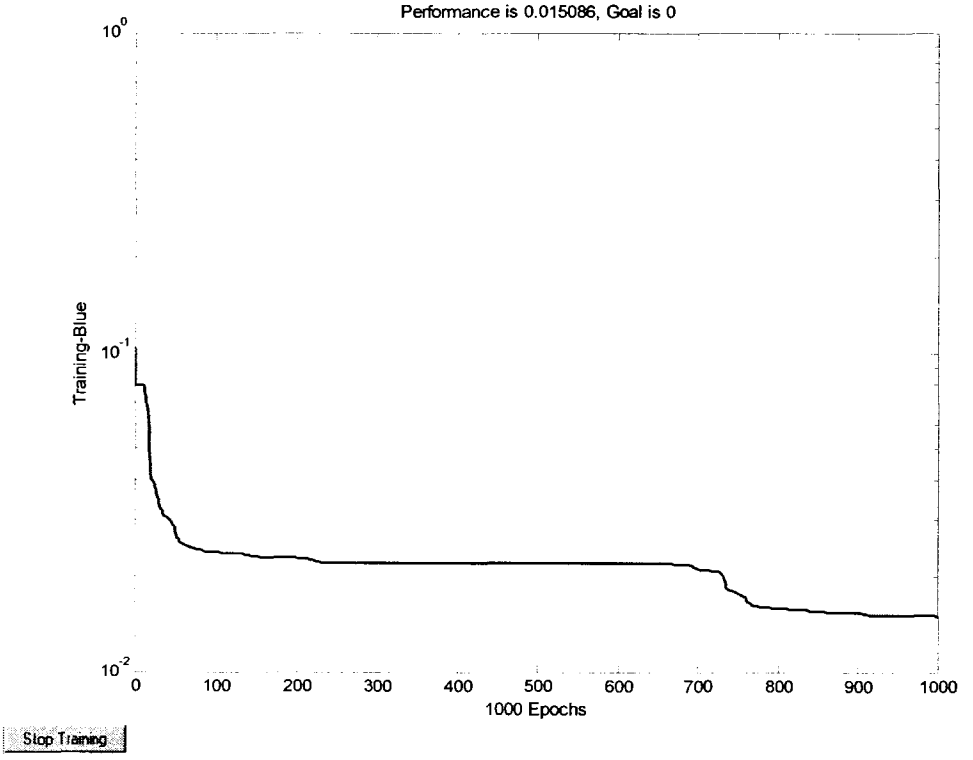

Figure 9.5: Training of Neural Network Estimator

9.2. Sensitivity Analysis Based on Neural Network Model

After developing and training the (ANN) model, the model is validated with some 20 sets of data. Since the values of horizontal travel distance of the Neural Network match with the out put of the simulation, the (ANN) model is used for sensitivity analysis. To study the effect of each of the factors such as ball's radius, density of the rock, damping ratio, initial position and initial velocity of the ball, the trained Neural Network model is used for a wide range of inputs. The results are plotted in Figure 9.6 through Figure 9.12. For each case, one parameter varies within range of interest and other parameters preserved constant.

The effect of the mass of the ball in simulation rockfall using DEM is considerable because mass affects the value of time step, new velocity of the ball and gravity as an external force. Mass of a spherical ball depends on ball's density and ball's radius. Figure 9.6 shows the effect of density on horizontal travel distance of the freefalling of ball and Figure 9.7 shows the effect of the ball's radius and on horizontal travel distance. As shown in Figure 9.6, the effect of density of a ball is negligible. This fact allows the researchers to choose any value for density (within a range of rock types density) when density of ball is not determined exactly.

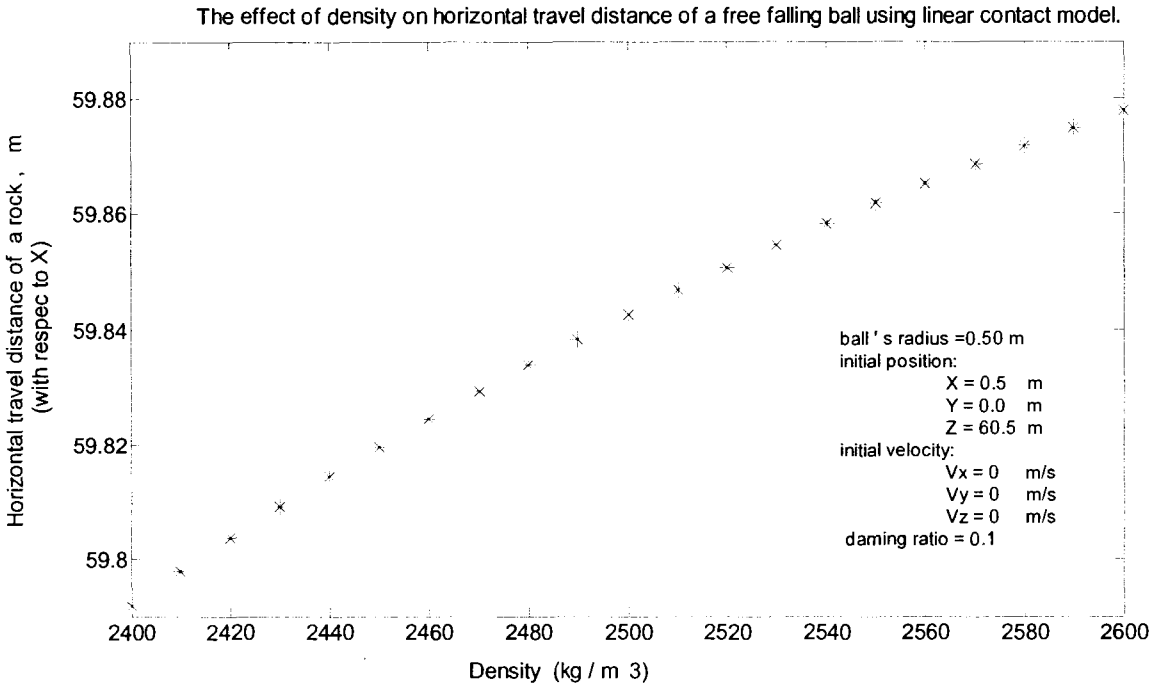

Figure 9.6: The effect of density of a freefalling ball on horizontal travel distance using linear model.

The effect of the ball's radius on horizontal travel distance of a ball is considerable. For ball's radius of smaller than *0.5 m*, increasing the value of radius increases the horizontal travel distance, but for ball's radius larger than 0.9 m, the horizontal travel distance decreases. As mentioned in previous chapters, damping ratio has noticeable effect on macroscopic and microscopic behaviours of a falling ball such as ball's trajectory. Figure 9.8 demonstrates the effect of damping ratio on horizontal travel distance. As shown in Figure 9.8, the range of 0.01 to 0.20 for damping ratio has a considerable effect on horizontal travel distance using linear contact model. Noticeable effects of damping ratio on ball's trajectory and ball's horizontal distance indicates the importance of study of energy loss concept and more specific determination of damping ratio for rock types in rockfall simulation.

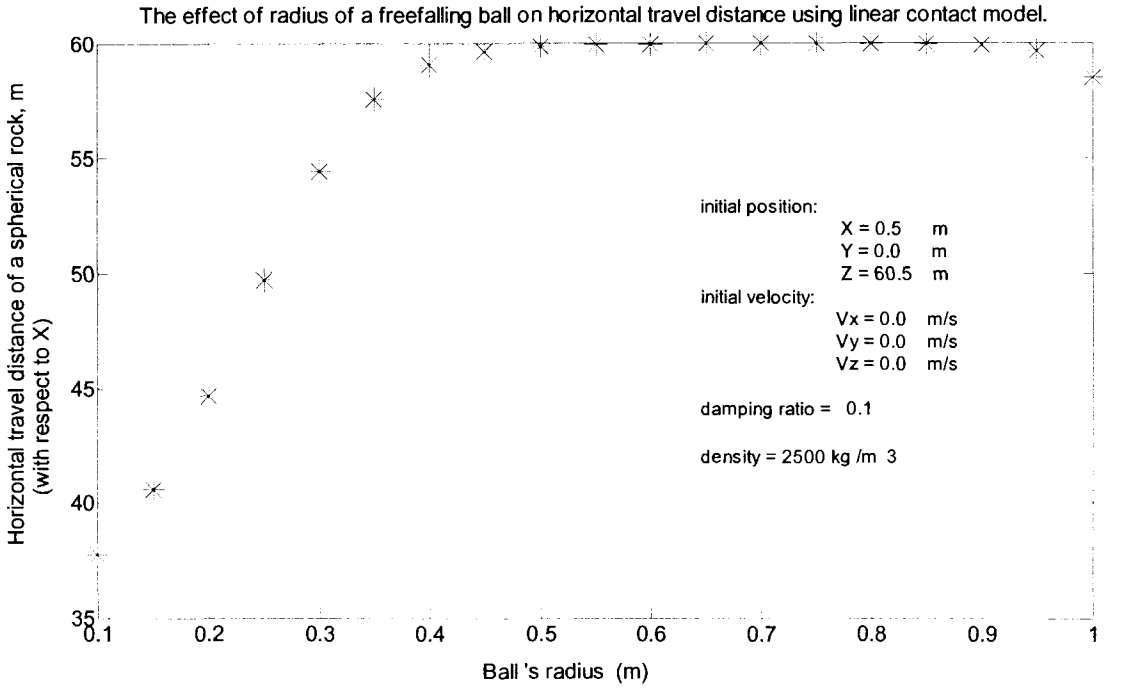

Figure 9.7: The effect of radius of a freefalling ball on horizontal travel distance using linear model.

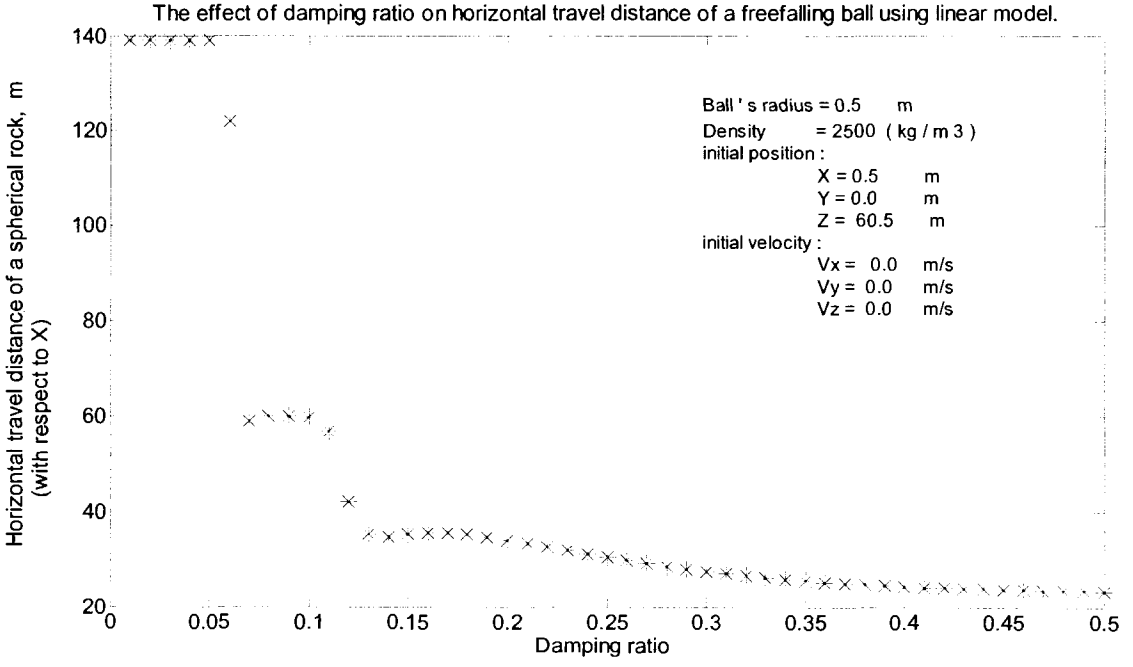

Figure 9.8: The effect of damping ratio of a freefalling ball on horizontal travel distance using linear model.

Figure 9.9 and Figure 9.10 show the effect of initial position of the ball on horizontal travel distance. In spite of the small effect of horizontal coordinate alone on ball's trajectory, initial height of the freefalling ball affects ball's trajectory considerably due to dependence of potential energy upon the height of falling. Figure 9.10 shows at location horizontal wall *(x=45)*, where the height of falling is about *60 m,* how the height of the falling ball dramatically affects on the horizontal travel distance.

Figure 9.11 and Figure 9.12 show the influence of initial velocity on horizontal travel distance of the ball. Kinetic energy of the system depends upon velocity; hence horizontal and vertical component of velocity affect the ball's motion. Also, velocity affects the damping force and energy loss of the system. Furthermore, initial velocity is participating for updating velocity and has an effect on impact of contact particles; hence the effect of velocity in multiple contacts can be significant.

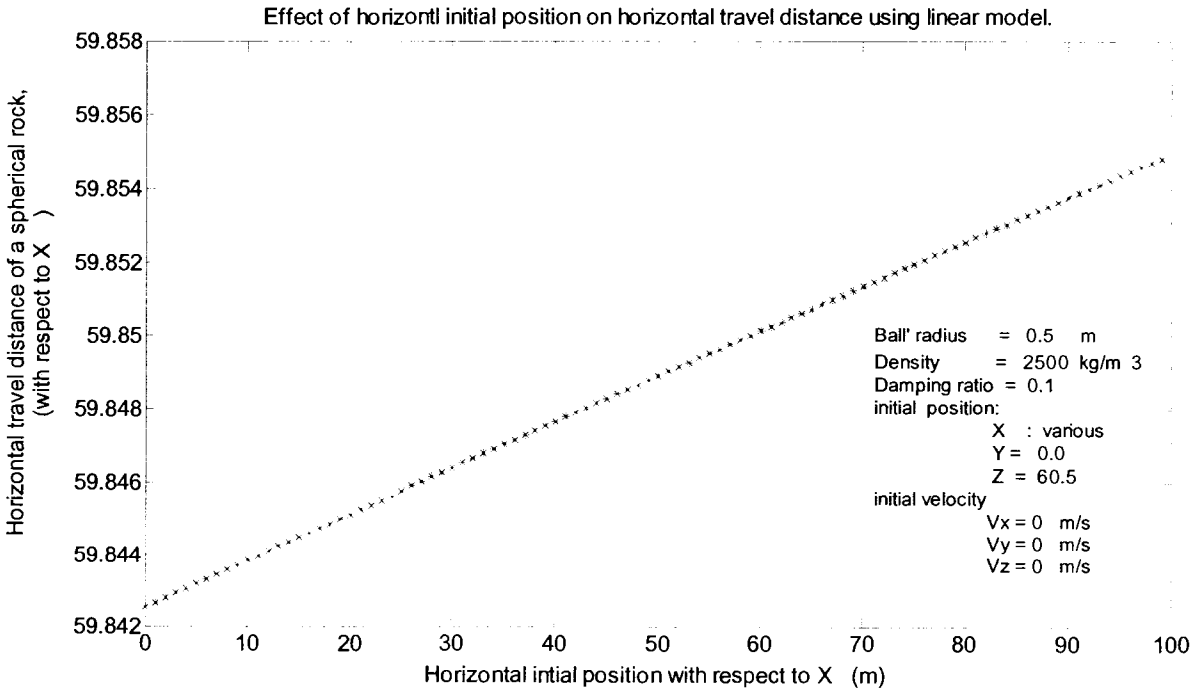

Figure 9.9: The effect of horizontal initial position of a freefalling ball on horizontal travel distance using linear model.

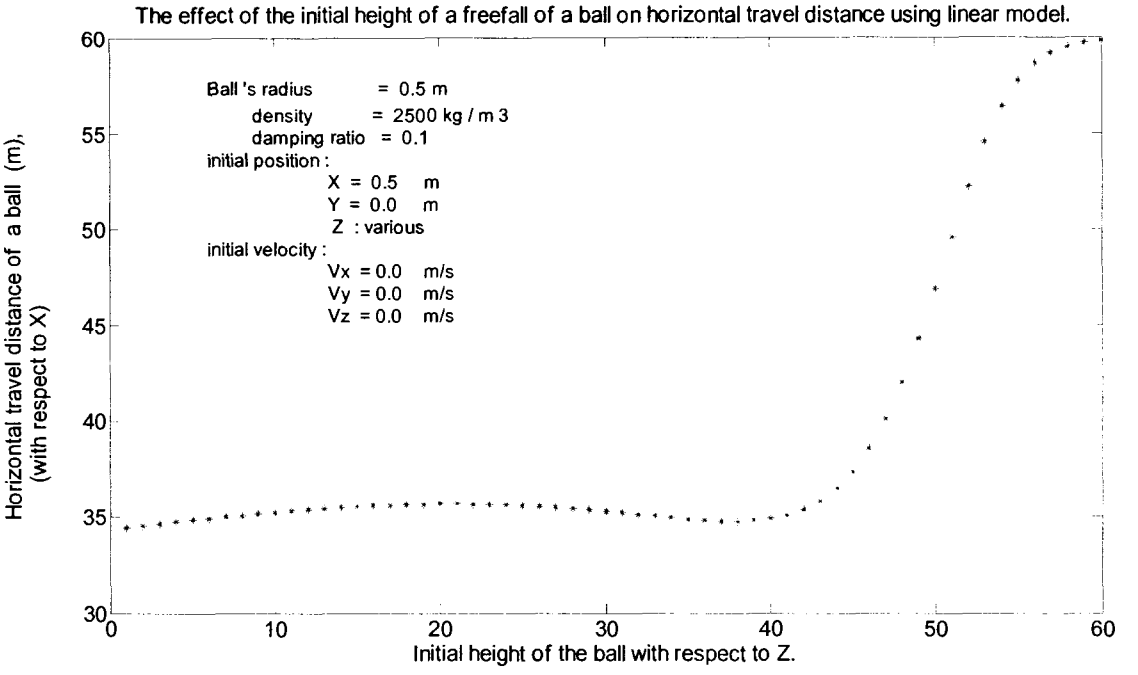

Figure 9.10: The effect of vertical initial position (Z) of a freefalling ball on horizontal travel distance using linear model.

In comparison between horizontal and vertical component of the velocity, effect of the vertical velocity on ball's trajectory and horizontal travel distance is greater.

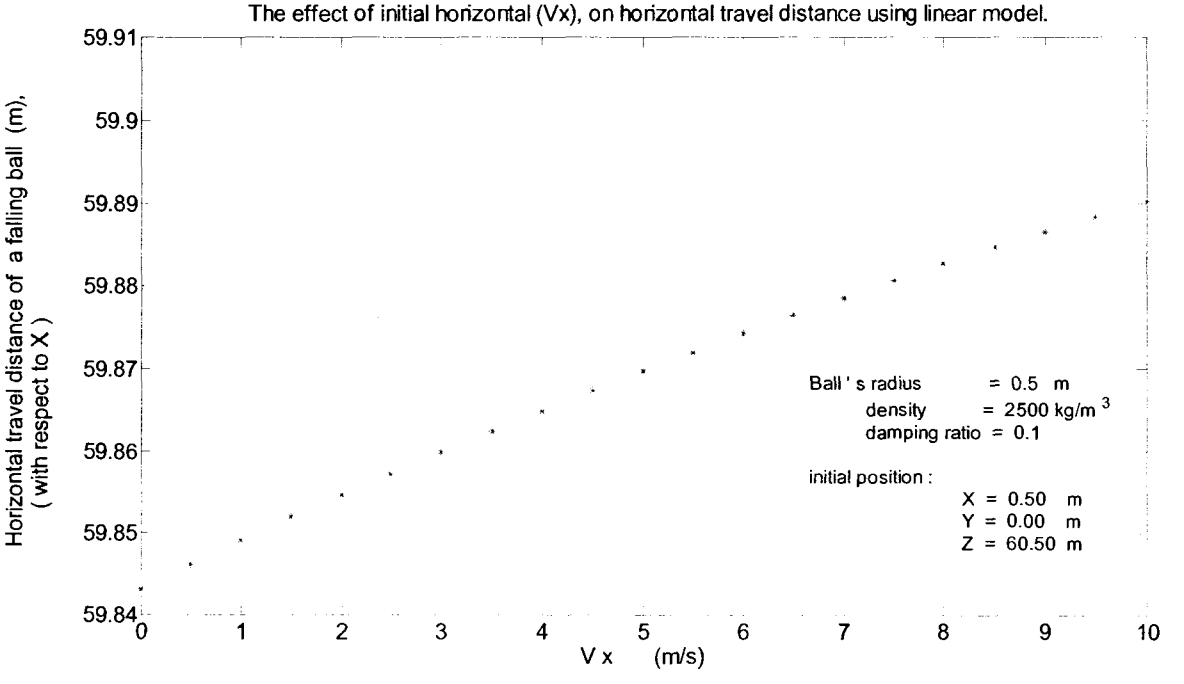

Figure 9.11: The effect of initial velocity (with respect to X) of a freefalling ball on horizontal travel distance using linear model.

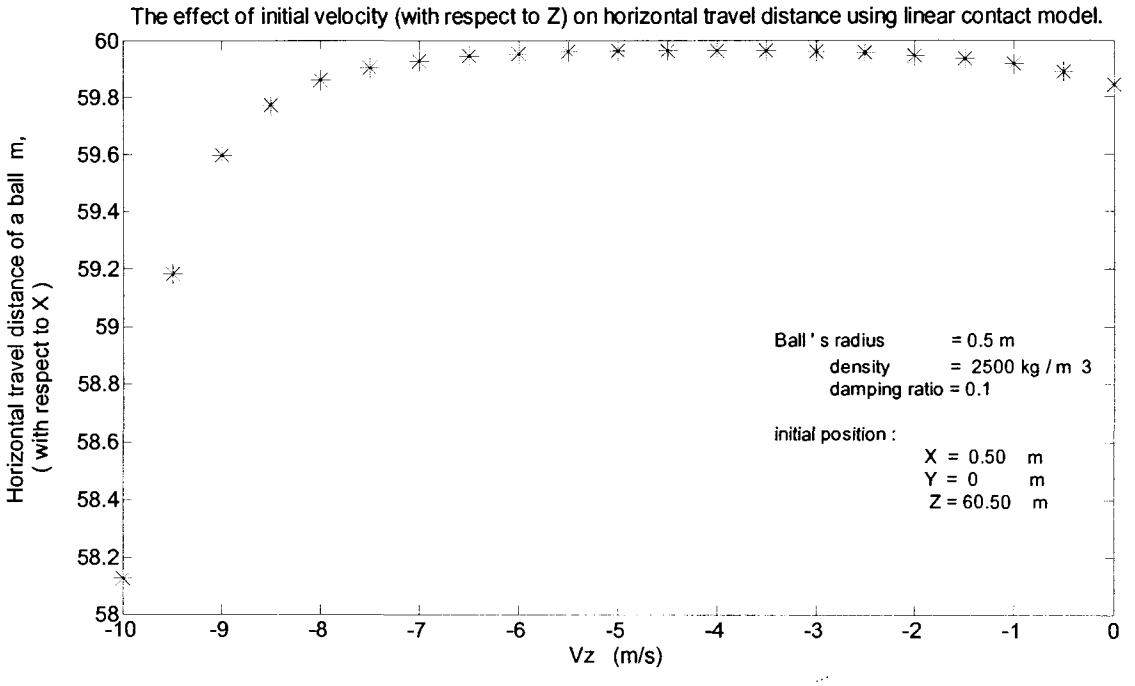

Figure 9.12: The effect of vertical initial position (Z) of a freefalling ball on horizontal travel distance using linear model.

9.3. Summary

- The effect of the radius, damping ratio and vertical initial condition (position and velocity) of ball on ball's trajectory on horizontal travel distance of a ball are considerable.

10. Summary and Recommendations for Further Research

DEM potentially can be powerful tool for rockfall simulation although CPU time is high and more experimental data for calibration of simulation is required. It is expected the data in this research, provides necessary information about contact models in DEM and some better insight about mechanism of contacts in rockfall.

10.1. Conclusion

To find the most appropriate contact model for rockfall analysis, five models have been chosen. Three contact models obtained through DEM, which were successfully used for the modeling of soil grains (linear model, Hertz-Mindlin, Ng model), elastic-inelastic power function, a contact model which originally was developed by An for simulation of rockfall and also combination of Hertz model and Ng model (Hertz-Ng model) that have been modeled to investigate the effect of each contact model on dynamic of rocks contacts. In this research, simple model containing a spherical ball and a horizontal plane was built to study the outcomes of each contact model and dynamic behaviour of a rock in normal direction.

Linear contact model contains normal and shear linear springs. Hertz-Mindlin, Ng and Hertz-Ng have nonlinear springs in normal and shear directions. Elastic-inelastic power function, (An) model has a linear spring for shear stiffness also a linear spring for first phase of normal contact (phase of loading). When two bodies collide, the resultant stiffness of two bodies is calculated. Although the resultant stiffness due to contact is

established, for linear model in contrast with other models, the method to determine the stiffness of individual contact bodies as well as the relation between stiffness and rock properties was not discussed in previous studies.

Hertz-Mindlin, Hertz-Ng and Ng model directly depends upon material properties of each contact bodies. In this research the contact stiffness of Hertz-Mindlin, Hertz-Ng and Ng model contact models has been compared. The comparison of the contact models can assist researchers to select better values for stiffness when a linear model is used. However, this research showed that the effect of the magnitude of stiffness of linear springs on the macroscopic behaviour (trajectories and velocities) of rocks is negligible when the time steps are very small.

Microscopic and macroscopic behaviours of a freefall ball when collide with a flat and horizontal wall has been studied when different contact models are used. Since collision of a ball and flat wall can be considered as generalization of the case of collision of two identical spheres, the results would be also valid for ball-ball contact as well.

Normal coefficient of restitution of freefall ball on a orizontal and flat wall using different contact models has been studied and coefficient of restitution for contact of a *10 kg* Berea Sandstone ball and a horizontal wall with different materials has been calculated, and the correlation of coefficient of restitution and damping ratio is determined for each contact model.

As previously mentioned, elastic-inelastic power function contact model depends on three factors: initial normal stiffness (K^n), transition force (T) and exponent *(b)* [20]. Each of these elements has a significant effect on macroscopic and microscopic behaviours of falling rocks. In this research, the effect of each of these parameters has

been studied for a 10 kg Berea Sandstone ball, and furthermore coefficient of restitution for contact of a 10 kg Berea Sandstone when collide with different walls' material is determined and correlation of coefficient of restitution and transition force has been determined.

Result of this research have indicated that the Ng, Hertz-Ng contact models are not appropriate for rockfall simulation.

Trajectory of a freefall ball on a horizontal and flat wall is vertical. Hence, the magnitudes of the contact velocity in respect with "X" and "Y" are equal to zero. Two slopes (120 degree slope and 135 degree slope) have been modeled to investigate normal and tangential coefficient of restitution and COR for slopes and the variation of coefficient of restitution versus slope angle as well as the variation of coefficient of restitution during the successive contacts.

Finding the trajectories and endpoints (horizontal travel distance) of the rocks of a probable rockfall are important outcomes of the rockfall simulation. Having information of balls trajectory as well as the kinetic energy level of the rock, allows engineers to design appropriate remedial measures for rockfalls with reasonable factor of safety at appropriate position. In this research, 122 sets of data have been collected for a single contact (a ball and a slope) using the computer program "Haraz" and an intelligent model (the Artificial Neural Networks model) has been built. After validation of the model, a sensitivity analysis is performed for seven factors of DEM and the effect of seven parameters on horizontal travel distance of the falling ball has been investigated: ball's radius, ball's density, damping ratio, initial position of the ball (horizontal and vertical coordinates with respect to X and Z), and initial velocity of the ball (horizontal

component of the velocity with respect to " X" direction and vertical component of the velocity with respect to "Z" direction).

10.2. Future Work

Some parameters such as rock's geometry and friction are not considered in this research, which may have noticeable effect on outcomes of the simulation of rockfall. Some studies have shown a considerable effect of rocks' geometry on coefficient of restitution [11]. As a result, the author suggests a vast study of the effect of the mentioned parameters on energy loss of the system and rockfall simulation.

Since rock's fragments are source of energy loss in rockfall modeling that affect the overall behaviour of rocks in rockfall simulation, author suggests a vast study of rocks' fragments, rock's fractures and plastic deformations of rocks using DEM.

Furthermore, knowing the minimum and maximum values of deformation (elastic and plastic deformation) or the ratio of maximum plastic to total deformation for rock types can be useful for calibration and validation of elastic-inelastic power contact model as a model which was the only contact model within this research that considers both plastic and elastic deformations.

Multiple contacts, contact of rocks (ball-ball) together and several contacts to walls (ball-ball) during rockfall, are possible. Contacts of balls together can change their velocity, momentum and impact and can affect on energy loss since coefficient of restitution is a velocity dependent parameter. It also can break the rocks to smaller pieces. It is strongly recommended to carry out a study of multiple contacts in rockfall.

Recommended future of this research can be listed as:

1. Investigation on the effect of rock's shapes (rock's geometry) and friction in rockfall simulation.
2. Investigation on modeling of the rock fragments during contacts.
3. Modeling and investigation of multiple contacts.

APPENDIX 1

Inroduction to Computer Program "Haraz"

"Haraz" mainly contains two classes: ball and wall associated main elements mentioned previously. Several functions are applied to generate the simulation. In this chapter the functions and their tasks are illustrated. Table 2 shows some of the math and functions which are used in this program. Table1, Table 2 and Table 3 represent of classes and functions which are used in the program.

Table1: List of classes in Haraz.

Class list	Objectives
Ball	Presents spherical rocks properties and their mechanical behaviour
Wall	Presents wall surfaces' properties (mesh) and their mechanical properties.

Table 2: Complementary functions in Haraz.

Math Function list	Task
Dot_product	Implementation of dot product
Cross_product	Implementation of cross product

Table 3: The list of functions in Haraz.

Functions list	Task	Class
CForce	Find contact force for a ball-ball contact.	Ball
CForce_wall	Find contact force for a ball-wall contact.	Wall
Stiffness_linear	Calculation of normal and tangential linear contact stiffness (constant values) for ball-ball contact.	Ball
Stiffness_linear_wall	Calculation of normal and tangential linear contact stiffness (constant values) for a ball-wall contact	Wall
Stiffness_Hertz_Mindlin_normal	Calculation of normal contact stiffness for ball-ball contact	Ball
Stiffness_Hertz_Mindlin_tangent	Calculation of normal contact stiffness for ball-ball contact	Ball
Stiffness_Hertz_Mindlin_normal_wall	Calculation of normal contact stiffness for ball-wall contact	Wall
Stiffness_Hertz_Mindlin_tangent_wall	Calculation of normal contact stiffness for ball-wall contact	Wall
Force_power_function_contact_Model_An_ball	Calculation of normal component of contact force for ball-ball contact	Ball
Force_power_function_contact_Model_An	Calculation of normal component of contact force for ball-ball contact	Ball

Viscous_damping	Calculation of viscous damping and normal and shear damping- forces for ball-ball contact	Ball
Viscous_damping_wall	Calculation of viscous damping and normal and shear damping- forces for ball-wall contact.	Wall
Local damp	Calculation of local damping and normal and shear damping- forces for ball-ball contact.	Ball
Local damp_wall	Calculation of local damping and normal and shear damping- forces for ball-wall contact	Wall
Sim	This function simulates the motion of single particle using Newton's second law of motion. Centered finite difference involving Δt is used for solving the differential equations	Ball and Wall
Stiffness_cr	Calculation of translational and rotational stiffness and find the maximum value	Ball
Time_cr	Calculation of critical time	Ball
Find_TheShortest_distance	Find the distance between a ball and each triangle	Wall
Perpendicular _Origin	Find the perpendicular origin	Wall
isInTringle	Checking if perpendicular origin is in mesh	Wall

List of Input and Output Files in Haraz

Input files are text files. "Microsoft Excel" is used to build the input and outputs.

Data

The first input file is named "Data.txt". Data contains the number of triangles, the number of balls, the number of steps, the contact model type and also ball properties. It introduces the balls with their properties such as radius (R), linear normal stiffness (K^n), linear shear stiffness (K^s), density (γ), damp ratio (β), coefficient of friction (μ) and elastic shear modulus. Table 4 illustrates an example of data.txt for one ball and 12 triangles. Table 5 shows the code for each contact model type.

Table 4: An example of " Data.txt"

Number of triangles	Number of balls	Number of steps	Contat type code	R (m)	K_n (N/m)	K_s (N/m)	γ (N/m^3)	β	ν	E (Pa)
12	1	6×10^7	1	0.21	6.40×10^{10}	9.60×10^6	2600	various	0.38	6.88×10^9

Table 5: the code for each contact model type.

Contact Model Type	code
Linear model	0
Hertz- Mindlin model	1
Elastic-inelastic power function model (An)	2
Ng-Hertz model	3
Ng model	4

Wallpoints

"Wallpoints" is a text file which contains the coordinates of mesh. Points should be in the order of counter clockwise starting from the highest or the lowest point of wall. For example, Table 6 illustrates the input data to for the wall is shown in following figure.

Table 6: An example for Wallpoints input file format

Vertex's Number	X (m)	Y (m)	Z (m)
1	0	10	60
2	10	0	60
3	7.3	10	40
4	7.3	0	40
5	19.3	10	40
6	19.3	0	40
7	26.2	10	20
8	26.2	0	20
9	38.6	10	20
10	38.6	0	20
11	46	10	0
12	46	0	0
13	170	10	0
14	170	0	0

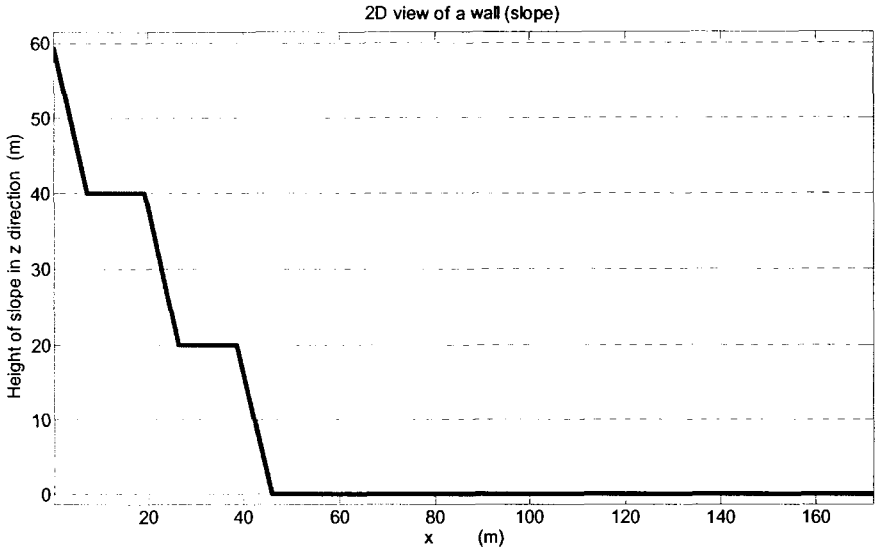

Figure 1: 2D view of a wall.

Wallstiffness

"Wallstiffness" is a text file which contains linear normal and linear shear stiffness for each mesh. Table 7 shows the normal and shear stiffness of each triangle.

Table 7: Normal and shear stiffness for the wall.

Triangle Number	Kn (N/m)	Ks (N/m)
1	1×10^6	7×10^6
2	1×10^7	7×10^6
3	1×10^7	7×10^6
4	4×10^6	7×10^6
5	7×10^6	7×10^6
6	7×10^6	7×10^6
7	1×10^6	7×10^6
8	1×10^6	7×10^6
9	1×10^6	1×10^6
10	1×10^6	1×10^6
11	1×10^6	1×10^6
12	1×10^6	1×10^6

Points

This file contains the coordinate of meshes and is used for "Matlab for drawing purpose.

Location_out

After running the file for each ball an out put file is built is named location_out (the ball number) for example for three balls location_out1 for 1st ball , location_out2 for Newton's second law of motion ball and location_out3 for third ball will build automatically by program. Table 8 demonstrates some part of Location_out1.txt.

Table 8: Part of file called "Location_out1".

Time (sec)	X (m)	Y (m)	Z (m)	Vx (m/s)	Vy (m/s)	Vz (m/s)	Ax (m/s^2)	Ay (m/s^2)	Az (m/s^2)
0	0.454	0	60.454	0	0	0	0	0	0
0.00025	0.454	0	60.454	0	0	-2.45×10^{-3}	0	0	-9.81
0.0005	0.454	0	60.454	0	0	-4.9×10^{-3}	0	0	-9.81
0.000749	0.454	0	60.454	0	0	-7.35×10^{-3}	0	0	-9.81
0.000999	0.454	0	60.454	0	0	-9.8×10^{-3}	0	0	-9.81
0.001249	0.454	0	60.454	0	0	-1.223×10^{-2}	0	0	-9.81
0.001499	0.454	0	60.454	0	0	-1.147×10^{-2}	0	0	-9.81

Force_out.txt

Same as location_out files, after running the file for each ball an out put file is built is named Force_out(the ball number) for example for three balls Force_out1 for 1st ball , Force _out2 for Newton's second law of motion ball and Force _out3 for third ball will build automatically by program. Importing the data to "Matlab" allows the user to plot the graphs. Table 9 demonstrates some part of Force_out1.txt.

Table 9: Part of Force_out1 file.

time	ball-ball contact forces			ball-wall contact forces			Resultant forces acting on each ball		
Sec	Fx (N)	Fy (N)	Fy (N)	Fx_wall (N)	Fy_wall (N)	Fz_wall (N)	Fx_total (N)	Fy_total (N)	Fz_total (N)
3.16101	0	0	0	2.058×10^{3}	0	-3.098×10^{3}	-2.058×10^{3}	0	3.098×10^{3}
3.17095	0	0	0	1.783×10^{3}	0	-268×10^{3}	-1.783×10^{3}	0	268×10^{3}
3.18089	0	0	0	0	0	0	0	0	0
3.19083	0	0	0	0	0	0	0	0	0

Fn_Un_wall.txt

"Fn_Un_wall.txt" files represent normal forces and normal overlaps of each ball during contact for each time step.

Table 10: An example of output file called "Force_out1.txt " file.

Time (Sec)	Fn (N)	Un (m)
0.401331	5.238×10^{3}	6.32×10^{-5}
0.401347	5.382×10^{3}	2.58×10^{-4}
0.401363	5.521×10^{3}	4.51×10^{-4}

Contact_velocity.txt

"Contact_velocity.txt" files represent normal velocity of each ball during contact for each time step.

Table 11: Part of "Contact_velocity.txt" file.

time	Normal contact velocity
0.401331	3.91819
0.401347	3.87927

APPENDIX 2

List of Samples for Estimation of Horizontal Travel Distance of a Rock

Table A.2.1: Values of samples for a rock and 12 triangles of the mesh.

Radius of a rock R_1	Density of a rock γ kg/m^3	Damping ratio β	Normal stiffness of a ball (N/m)	Normal stiffness of a ball (N/m)	x_0 (m)	y_0 (m)	z_0 (m)	v_{x0} (m/s)	v_{y0} (m/s)	v_{z0} m/s	Normal stiffness of a wall (N/m)	Normal stiffness of a wall (N/m)	End point X coordinate (m)
0.1	2600	0.075	6.410^7	$9.6*10^5$	0.1	0	60.1	3	0	-2	10^7	10^7	38.365
0.2	2600	0.075	$6.4*10^7$	$9.6*10^5$	0.2	0	60.2	3	0	-2	10^7	10^7	38.312
0.3	2600	0.075	$6.4*10^7$	$9.6*10^5$	0.3	0	60.3	3	0	-2	10^7	10^7	38.344
0.4	2600	0.075	$6.4*10^7$	$9.6*10^5$	0.4	0	60.4	3	0	-2	10^7	10^7	38.356
0.5	2600	0.075	$6.4*10^7$	$9.6*10^5$	0.5	0	60.5	3	0	-2	10^7	10^7	38.404
0.6	2600	0.075	$6.4*10^7$	$9.6*10^5$	0.6	0	60.6	3	0	-2	10^7	10^7	69.502
0.7	2600	0.075	$6.4*10^7$	$9.6*10^5$	0.7	0	60.7	3	0	-2	10^7	10^7	70.010
0.8	2600	0.075	$6.4*10^7$	$9.6*10^5$	0.8	0	60.8	3	0	-2	10^7	10^7	73.200
0.9	2600	0.075	$6.4*10^7$	$9.6*10^5$	0.9	0	60.9	3	0	-2	10^7	10^7	172.00
1.0	2600	0.075	$6.4*10^7$	$9.6*10^5$	1.0	0	61.0	3	0	-2	10^7	10^7	172.00
0.7	2600	0.01	$6.4*10^7$	$9.6*10^5$	0.7	0	60.7	3	0	-2	10^7	10^7	172
0.7	2600	0.03	$6.4*10^7$	$9.6*10^5$	0.7	0	60.7	3	0	-2	10^7	10^7	112.861
0.7	2600	0.05	$6.4*10^7$	$9.6*10^5$	0.7	0	60.7	3	0	-2	10^7	10^7	106.917
0.7	2600	0.07	$6.4*10^7$	$9.6*10^5$	0.7	0	60.7	3	0	-2	10^7	10^7	91.760
0.7	2600	0.1	$6.4*10^7$	$9.6*10^5$	0.7	0	60.7	3	0	-2	10^7	10^7	15.300
0.7	2600	0.2	$6.4*10^7$	$9.6*10^5$	0.7	0	60.7	3	0	-2	10^7	10^7	8.973
0.7	2600	0.3	$6.4*10^7$	$9.6*10^5$	0.7	0	60.7	3	0	-2	10^7	10^7	8.090
0.7	2600	0.4	$6.4*10^7$	$9.6*10^5$	0.7	0	60.7	3	0	-2	10^7	10^7	8.014
0.7	2600	0.5	$6.4*10^7$	$9.6*10^5$	0.7	0	60.7	3	0	-2	10^7	10^7	7.99
0.7	2600	0.6	$6.4*10^7$	$9.6*10^5$	0.7	0	60.7	3	0	-2	10^7	10^7	7.98
0.21	2600	0.02	$6.4*10^7$	$9.6*10^5$	0.21	0	60.21	3	0	-2	10^7	10^7	172
0.21	2600	0.04	$6.4*10^7$	$9.6*10^5$	0.21	0	60.21	3	0	-2	10^7	10^7	111.701
0.21	2600	0.06	$6.4*10^7$	$9.6*10^5$	0.21	0	60.21	3	0	-2	10^7	10^7	74.753
0.21	2600	0.08	$6.4*10^7$	$9.6*10^5$	0.21	0	60.21	3	0	-2	10^7	10^7	172
0.21	2600	0.12	$6.4*10^7$	$9.6*10^5$	0.21	0	60.21	3	0	-2	10^7	10^7	9.405

0.21	2600	0.14	$6.4*10^7$	$9.6*10^5$	0.21	0	60.21	3	0	-2	10^7	10^7	8.967
0.21	2600	0.25	$6.4*10^7$	$9.6*10^5$	0.21	0	60.21	3	0	-2	10^7	10^7	7.090
1	2600	0.35	$6.4*10^7$	$9.6*10^5$	1	0	61	3	0	-2	10^7	10^7	8.370
1	2400	0.35	$6.4*10^7$	$9.6*10^5$	1	0	61	3	0	-2	10^7	10^7	8.380
1	2400	0.1	$6.4*10^7$	$9.6*10^5$	1	0	61	3	0	-2	10^7	10^7	15.628
1	2400	0.4	$6.4*10^7$	$9.6*10^5$	1	0	61	3	0	-2	10^7	10^7	116.418
1	2400	1	$6.4*10^7$	$9.6*10^5$	1	0	61	3	0	-2	10^7	10^7	39.943
1	2400	0.01	$6.4*10^7$	$9.6*10^5$	5	0	50.1	3	0	-2	10^7	10^7	8.567
0.1	2500	0.1	$6.4*10^7$	$9.6*10^5$	4.1	0	50.1	3	0	-2	10^7	10^7	172
0.1	2500	0.01	$6.4*10^7$	$9.6*10^5$	4.1	0	50.1	3	0	-2	10^7	10^7	13.019
0.4	2500	0.03	$6.4*10^7$	$9.6*10^5$	4.4	0	50.1	3	0	-2	10^7	10^7	153.111
0.7	2500	0.075	$6.4*10^7$	$9.6*10^5$	4.7	0	50.1	3	0	-2	10^7	10^7	16.089
0.8	2500	0.2	$6.4*10^7$	$9.6*10^5$	4.8	0	50.1	3	0	-2	10^7	10^7	9.824
0.8	2500	0.05	$6.4*10^7$	$9.6*10^5$	20.1	0	40.8	3	0	-2	10^7	10^7	172
0.8	2500	0.2	$6.4*10^7$	$9.6*10^5$	20.1	0	40.8	3	0	-2	10^7	10^7	27.686
0.2	2500	0.15	$6.4*10^7$	$9.6*10^5$	19.5	0	40.2	3	0	-2	10^7	10^7	29.061
0.3	2500	0.16	$6.4*10^7$	$9.6*10^5$	19.6	0	40.3	3	0	-2	10^7	10^7	28.677
0.5	2500	0.15	$6.4*10^7$	$9.6*10^5$	19.8	0	40.5	3	0	-2	10^7	10^7	29.462
0.5	2500	0.05	$6.4*10^7$	$9.6*10^5$	19.8	0	40.5	3	0	-2	10^7	10^7	68.283
0.5	2500	0.03	$6.4*10^7$	$9.6*10^5$	19.8	0	40.5	3	0	-2	10^7	10^7	117.242
0.5	2500	0.01	$6.4*10^7$	$9.6*10^5$	19.8	0	40.5	3	0	-2	10^7	10^7	172
0.1	2500	0.01	$6.4*10^7$	$9.6*10^5$	26.3	0	20.1	3	0	-2	10^7	10^7	35.357
0.6	2500	0.01	$6.4*10^7$	$9.6*10^5$	26.3	0	20.6	3	0	-2	10^7	10^7	36.58
0.6	2500	0.08	$6.4*10^7$	$9.6*10^5$	39.2	0	20.6	3	0	-2	10^7	10^7	59.422
0.3	2500	0.075	$6.4*10^7$	$9.6*10^5$	38.9	0	20.3	3	0	-2	10^7	10^7	60.404
0.2	2500	0.03	$6.4*10^7$	$9.6*10^5$	45.2	0	20.2	3	0	-2	10^7	10^7	83.54
0.2	2500	0.03	$6.4*10^7$	$9.6*10^5$	50.2	0	20.2	3	0	-2	10^7	10^7	88.547
0.2	2500	0.3	$6.4*10^7$	$9.6*10^5$	100.2	0	20.2	3	0	-2	10^7	10^7	109.086
0.2	2500	0.2	$6.4*10^7$	$9.6*10^5$	100.2	0	20.2	3	0	-2	10^7	10^7	111.06
0.75	2400	0.1	$6.4*10^7$	$9.6*10^5$	105.75	0	10.75	3	0	-2	10^7	10^7	114.801
0.4	2400	0.06	$6.4*10^7$	$9.6*10^5$	0.4	0	60.4	3	0	-2	10^7	10^7	76.666
0.4	2400	0.06	$6.4*10^7$	$9.6*10^5$	1.4	0	60.4	3	0	-2	10^7	10^7	118.504
0.4	2400	0.06	$6.4*10^7$	$9.6*10^5$	2.4	0	60.4	3	0	-2	10^7	10^7	84.078
0.4	2400	0.06	$6.4*10^7$	$9.6*10^5$	3.4	0	60.4	3	0	-2	10^7	10^7	172
0.4	2400	0.06	$6.4*10^7$	$9.6*10^5$	4.4	0	60.4	3	0	-2	10^7	10^7	73.310
0.4	2400	0.06	$6.4*10^7$	$9.6*10^5$	5.4	0	60.4	3	0	-2	10^7	10^7	79.330
0.4	2400	0.06	$6.4*10^7$	$9.6*10^5$	6.4	0	60.4	3	0	-2	10^7	10^7	83.409
0.4	2400	0.06	$6.4*10^7$	$9.6*10^5$	7.4	0	60.4	3	0	-2	10^7	10^7	139.168

0.4	2400	0.06	$6.4*10^7$	$9.6*10^5$	8.4	0	60.4	3	0	-2	10^7	10^7	81.97
0.4	2400	0.06	$6.4*10^7$	$9.6*10^5$	9.4	0	60.4	3	0	-2	10^7	10^7	86.309
0.4	2400	0.06	$6.4*10^7$	$9.6*10^5$	10.4	0	60.4	3	0	-2	10^7	10^7	89.364
0.4	2400	0.06	$6.4*10^7$	$9.6*10^5$	11.4	0	60.4	3	0	-2	10^7	10^7	90.725
0.4	2400	0.06	$6.4*10^7$	$9.6*10^5$	12.4	0	60.4	3	0	-2	10^7	10^7	132.287
0.4	2400	0.06	$6.4*10^7$	$9.6*10^5$	13.4	0	60.4	3	0	-2	10^7	10^7	77.608
0.4	2400	0.06	$6.4*10^7$	$9.6*10^5$	14.4	0	60.4	3	0	-2	10^7	10^7	85.111
0.4	2400	0.06	$6.4*10^7$	$9.6*10^5$	15.4	0	60.4	3	0	-2	10^7	10^7	90.523
0.4	2400	0.06	$6.4*10^7$	$9.6*10^5$	16.4	0	60.4	3	0	-2	10^7	10^7	94.076
0.4	2400	0.06	$6.4*10^7$	$9.6*10^5$	17.4	0	60.4	3	0	-2	10^7	10^7	95.648
0.4	2400	0.06	$6.4*10^7$	$9.6*10^5$	18.4	0	60.4	3	0	-2	10^7	10^7	112.064
0.4	2400	0.06	$6.4*10^7$	$9.6*10^5$	19.4	0	60.4	3	0	-2	10^7	10^7	98.589
0.4	2400	0.06	$6.4*10^7$	$9.6*10^5$	20.4	0	60.4	3	0	-2	10^7	10^7	96.995
0.4	2400	0.06	$6.4*10^7$	$9.6*10^5$	21.4	0	60.4	3	0	-2	10^7	10^7	172
0.4	2400	0.06	$6.4*10^7$	$9.6*10^5$	22.4	0	60.4	3	0	-2	10^7	10^7	109.107
0.4	2400	0.06	$6.4*10^7$	$9.6*10^5$	23.4	0	60.4	3	0	-2	10^7	10^7	109.107
0.4	2400	0.06	$6.4*10^7$	$9.6*10^5$	24.4	0	60.4	3	0	-2	10^7	10^7	108.018
0.4	2400	0.06	$6.4*10^7$	$9.6*10^5$	25.4	0	60.4	3	0	-2	10^7	10^7	106.081
0.4	2400	0.06	$6.4*10^7$	$9.6*10^5$	26.4	0	60.4	3	0	-2	10^7	10^7	102.723
0.4	2400	0.06	$6.4*10^7$	$9.6*10^5$	27.4	0	60.4	3	0	-2	10^7	10^7	88.665
0.4	2400	0.06	$6.4*10^7$	$9.6*10^5$	28.4	0	60.4	3	0	-2	10^7	10^7	62.444
0.4	2400	0.06	$6.4*10^7$	$9.6*10^5$	29.4	0	60.4	3	0	-2	10^7	10^7	63.444
0.4	2400	0.06	$6.4*10^7$	$9.6*10^5$	30.4	0	60.4	3	0	-2	10^7	10^7	64.444
0.4	2400	0.06	$6.4*10^7$	$9.6*10^5$	31.4	0	60.4	3	0	-2	10^7	10^7	123.213
0.4	2400	0.06	$6.4*10^7$	$9.6*10^5$	32.4	0	60.4	3	0	-2	10^7	10^7	122.900
0.4	2400	0.06	$6.4*10^7$	$9.6*10^5$	33.4	0	60.4	3	0	-2	10^7	10^7	121.584
0.4	2400	0.06	$6.4*10^7$	$9.6*10^5$	34.4	0	60.4	3	0	-2	10^7	10^7	119.394
0.4	2400	0.06	$6.4*10^7$	$9.6*10^5$	35.4	0	60.4	3	0	-2	10^7	10^7	128.031
0.4	2400	0.06	$6.4*10^7$	$9.6*10^5$	36.4	0	60.4	3	0	-2	10^7	10^7	97.123
0.4	2400	0.06	$6.4*10^7$	$9.6*10^5$	37.4	0	60.4	3	0	-2	10^7	10^7	72.965
0.4	2400	0.06	$6.4*10^7$	$9.6*10^5$	38.4	0	60.4	3	0	-2	10^7	10^7	73.965
0.4	2400	0.06	$6.4*10^7$	$9.6*10^5$	39.4	0	60.4	3	0	-2	10^7	10^7	74.965
0.4	2400	0.06	$6.4*10^7$	$9.6*10^5$	40.4	0	60.4	3	0	-2	10^7	10^7	75.965
0.4	2400	0.06	$6.4*10^7$	$9.6*10^5$	41.4	0	60.4	3	0	-2	10^7	10^7	76.965
0.4	2400	0.06	$6.4*10^7$	$9.6*10^5$	42.4	0	60.4	3	0	-2	10^7	10^7	77.965
0.4	2400	0.06	$6.4*10^7$	$9.6*10^5$	46.7	0	60.4	3	0	-2	10^7	10^7	81.965
0.4	2400	0.06	$6.4*10^7$	$9.6*10^5$	47.7	0	60.4	3	0	-2	10^7	10^7	82.965
0.4	2400	0.06	10^5	10^5	0.4	0	60.4	3	0	-2	10^7	10^7	40.392

0.4	2400	0.06	$5*10^5$	$5*10^5$	0.4	0	60.4	3	0	-2	10^7	10^7	83.58
0.4	2400	0.06	10^6	10^6	0.4	0	60.4	3	0	-2	10^7	10^7	81.933
0.4	2400	0.06	$5*10^6$	$5*10^6$	0.4	0	60.4	3	0	-2	10^7	10^7	81.86
0.4	2400	0.06	10^7	10^7	0.4	0	60.4	3	0	-2	10^7	10^7	81.967
0.4	2400	0.06	10^8	10^8	0.4	0	60.4	3	0	-2	10^7	10^7	82.300
0.8	2400	0.03	10^7	10^7	0.8	0	60.8	5	0	0	10^7	10^7	116.923
0.8	2400	0.03	10^7	10^7	0.8	0	60.8	5	1	0	10^7	10^7	116.923
0.1	2400	0.05	10^7	10^7	0.1	0	60.1	10	0	-10	10^6	10^6	124.4
0.1	2400	0.05	10^7	10^7	0.1	0	60.1	5	0	-10	10^6	10^6	94.000
0.5	2400	0.05	10^7	10^7	0.5	0	60.5	10	0	-10	10^6	10^6	125.435
0.5	2400	0.05	10^7	10^7	0.5	0	60.5	10	1	-20	10^6	10^6	137.411
0.5	2400	0.05	10^7	10^7	0.5	0	60.5	0	0	0	10^6	10^6	74.464
0.5	2400	0.05	10^7	10^7	0.5	0	60.5	4	3	-5	10^6	10^6	97.393
0.5	2400	0.1	10^7	10^7	0.5	0	60.5	5	6	-8	10^6	10^6	67.990
0.5	2400	0.2	10^7	10^7	0.5	0	60.5	3.5	2	-9	10^6	10^6	10.331
0.5	2400	0.3	10^7	10^7	0.5	0	60.5	8	4	-1	10^6	10^6	8.934
0.5	2400	0.4	10^7	10^7	0.5	0	60.5	8	4	-1	10^6	10^6	8.480
0.5	2400	0.4	10^7	10^7	0.5	0	60.5	6.2	4	-13	10^6	10^6	9.858
0.5	2400	0.4	10^7	10^7	0.5	0	60.5	6.2	4	-13	10^6	10^6	9.860
0.9	2400	0.5	10^7	10^7	0.9	0	60.9	6.2	4	-13	10^6	10^6	10.082
1	2400	0.6	10^7	10^7	0.1	0	61.0	10	2.3	-15	10^6	10^6	12.059

Appendix 3

Matlab Code for Artificial Neural Network

```
clear all;
% Reading Inputs
load data4.txt;
a=data4;
r1=a(:,2);
Gama=a (:,3);
Beta=a (:,4);
X=a (:,5);
Y=a (:,6);
Z=a (:,7);
Vx=a (:,8);
Vy=a (:,9);
Vz=a (:,10);
Kx=a (:,11);
Ky=a (:,12);
Endpoint=a (:,17);

% %Setting Inputs
InputRange1 = [0.1  1; 2400 2600; 0.01 1; 0.1 105.75;10.75 61;0 10;-20
0];

%setting outputs
net11 = newff(InputRange1, [7,5,7,2,1], {'tansig' 'tansig' 'tansig' 'tansig'
'logsig' }, 'trainlm');
net11.trainParam.epochs = 1000;
% Here are learning examples
%% Filling Array
```

```
InputSet1 = [r1';Gama';Beta'; X'; Z';Vx';Vz'];    % Getting Data
% The targets for learning examples
%%Filling Array
 Target1 =[Endpoint'];

% Scaling
[m,n]=size(InputSet1);

for i=1:m
   Scale(i)=max(abs(InputRange1(i,1)),abs(InputRange1(i,2)));
end
Scale_Target=max(abs(Target1));

for i=1:m
   for j=1:n
      InputSet2(i,j)=InputSet1(i,j)/Scale(i);
   end
end
Target2=Target1./Scale_Target;
% training
net11=train(net11, InputSet2, Target2);
%simulation
 Y1 = sim(net11,InputSet2);
 %figure(2); plot((Target1-Y1)./Target1*100)
 figure(2); plot(Target1-Y1*Scale_Target)
 %figure(3); plot((Target2-Y1)./Target2*100)
figure(3); plot(InputSet1(2,:),Y1*Scale_Target,'*');
%//////////Gamatest
Gama_test1=2400:10:2600;
r1_test1=0.5*ones(1,21);
Beta_test1=0.1*ones(1,21);
```

```
X_test1=0.5*ones(1,21);
Z_test1=60.5*ones(1,21);
Vx_test1=0*ones(1,21);
Vz_test1=0.0*ones(1,21);

Input_test1
=[r1_test1/Scale(1);Gama_test1/Scale(2);Beta_test1/Scale(3);X_test1/Scale(4);Z
_test1/Scale(5);Vx_test1/Scale(6);Vz_test1/Scale(7)];
Y2 = sim(net11,Input_test1);
figure(4); plot(Gama_test1,Y2*Scale_Target,'*')
%/////////r1
Gama_test1=2500*ones(1,19);
r1_test1=0.1:0.05:1;
Beta_test1=0.1*ones(1,19);
X_test1=0.5*ones(1,19);
Z_test1=60.5*ones(1,19);
Vx_test1=0*ones(1,19);
Vz_test1=0.0*ones(1,19);
Input_test1
=[r1_test1/Scale(1);Gama_test1/Scale(2);Beta_test1/Scale(3);X_test1/Scale(4);Z
_test1/Scale(5);Vx_test1/Scale(6);Vz_test1/Scale(7)];
Y3 = sim(net11,Input_test1);
figure(5); plot(r1_test1,Y3*Scale_Target,'*')
%/////////beta
Gama_test1=2500*ones(1,50);
r1_test1=0.5*ones(1,50);
Beta_test1=0.01:0.01:0.5;
X_test1=0.5*ones(1,50);
Z_test1=60.5*ones(1,50);
Vx_test1=0*ones(1,50);
Vz_test1=0.0*ones(1,50);
```

```
        Input_test1
=[r1_test1/Scale(1);Gama_test1/Scale(2);Beta_test1/Scale(3);X_test1/Scale(4);Z
_test1/Scale(5);Vx_test1/Scale(6);Vz_test1/Scale(7)];
        Y4 = sim(net11,Input_test1);
        figure(6); plot(Beta_test1,Y4*Scale_Target,'*')

        %//////////X
        Gama_test1=2500*ones(1,100);
        r1_test1=0.5*ones(1,100);
        Beta_test1=0.1*ones(1,100);
        X_test1=0.1:1:100;
        Z_test1=60.5*ones(1,100);
        Vx_test1=0*ones(1,100);
        Vz_test1=0.0*ones(1,100);

        Input_test1
=[r1_test1/Scale(1);Gama_test1/Scale(2);Beta_test1/Scale(3);X_test1/Scale(4);Z
_test1/Scale(5);Vx_test1/Scale(6);Vz_test1/Scale(7)];
        Y5 = sim(net11,Input_test1);
        figure(7); plot(X_test1,Y5*Scale_Target,'*')
        %//////////z
        Gama_test1=2500*ones(1,60);
        r1_test1=0.5*ones(1,60);
        Beta_test1=0.1*ones(1,60);
        X_test1=5*ones(1,60);
        Z_test1=1:60;
        Vx_test1=0*ones(1,60);
        Vz_test1=0.0*ones(1,60);
        Input_test1
=[r1_test1/Scale(1);Gama_test1/Scale(2);Beta_test1/Scale(3);X_test1/Scale(4);Z
_test1/Scale(5);Vx_test1/Scale(6);Vz_test1/Scale(7)];
```

```
Y6 = sim(net11,Input_test1);
figure(8); plot(Z_test1,Y6*Scale_Target,'*')
%/////////Vz
Gama_test1=2500*ones(1,21);
r1_test1=0.5*ones(1,21);
Beta_test1=0.1*ones(1,21);
X_test1=5*ones(1,21);
Z_test1=60.5*ones(1,21);
Vx_test1=0*ones(1,21);
Vz_test1=-10:0.5:0.0;
Input_test1
=[r1_test1/Scale(1);Gama_test1/Scale(2);Beta_test1/Scale(3);X_test1/Scale(4);Z
_test1/Scale(5);Vx_test1/Scale(6);Vz_test1/Scale(7)];
Y7 = sim(net11,Input_test1);
figure(9); plot(Vz_test1,Y7*Scale_Target,'*')
%/////////Vx
Gama_test1=2500*ones(1,21);
r1_test1=0.5*ones(1,21);
Beta_test1=0.1*ones(1,21);
X_test1=5*ones(1,21);
Z_test1=60.5*ones(1,21);
Vx_test1=0:0.5:10;
Vz_test1=0.0*ones(1,21)
Input_test1
=[r1_test1/Scale(1);Gama_test1/Scale(2);Beta_test1/Scale(3);X_test1/Scale(4);Z
_test1/Scale(5);Vx_test1/Scale(6);Vz_test1/Scale(7)];
Y8 = sim(net11,Input_test1);
figure(10); plot(Vx_test1,Y8*Scale_Target,'*')
```

References

[1] Evans GE, Mugnozza GS, Storm A, Hermanns RL. Lanslides from Massive Rock Slope Failure. In proceeding of NATO Advanced Research Workshop on Massive Rock Slope Failure, New Models for Hazard Assessment; Springer published in cooperation with NATO public Diplomacy Division: Celano(Italy), June 2002, pp. xi

[2] Perret S, Dolf F, Kienholz H. Rockfalls in to forests: Analysis and simulation of rockfall trajectories- considerations with respect to mountainous forests in Switzerland. *Lanslides* 2004; 1:123-130.

[3] Evans SG. *Landslides: in A Synthesis of Geological Hazards in Canada.* (ed.) G.R. Brooks, Geological Survey of Canada, Bulletin 548, 2001; 43–79.

[4] Transportation Safety Board of Canada. Report Number R95V0017. Sources: http:// www.tsb.gc.ca/en/reports/rail/1995/r95v0017/r95v0017.asp (Acceded 1/July/2008).

[5] Statement of Allegations of Staff of the Ontario Security Commission. In the Matter of the Securities ACT, R.S.O. 1990, c. S.5, as Amended and in the Matter of AGNICO-EAGLE Mines Limited. 2003. (Acceded 4/Feb/2008).Source: http://www.osc.gov.on.ca/ Enforcement/Proceedings/SOA/soa_20050422_agnico-eagle-mines.pdf

[6] Transport Canada. Transport Development Centre Report. Source:http://www.tc.gc.ca /TDC/publication/updates/v17n1.htm (Acceded 1/July/2008).

[7] Dorrena LKA, Maierb B, Puttersa US, Seijmonsbergen AC. Combining field and modelling techniques to assess rockfall dynamics on a protection forest hill slope in the European Alps. *Geomorphology 2004*; 57:151–167.

[8] Nevada Department of Transportation. Geotechnical Policies and Procedures manual, chapter 14; 2005,Source:http://www.nevadadot.com/reports_pubs/Geo_PPManual/pdfs/ Geo_PPM_Chapter14.pdf (Acceded 1/July/2008).

[9] Baillifard F, Jaboyedoff M, Sartori M. Rockfall hazard mapping along mountainous road in Switzerland using GIS-based parameter rating approach. *Natural Hazards and Earth System Science* 2003; 3:431-438.

[10] Ghazipour N, Orumiey A, Entezam Soltani I, Pirouz M. The hazard zonation of rockfall along Chalus road in north of Iran . *Geophysical Research Abstract* 2007; 7: 423.

[11] Ashayer P. Application of Rigid Body Impact Mechanics and Discrete Element Modeling to Rockfall Simulation. PhD thesis, Department of Civil Engineering Department of University of Toronto; 2007

[12] Stevens WD. RocFall: A Tool for Probabilistic Analysis, Design of Remedial Measures and Predication of Rockfalls. Master's thesis, department of Civil Engineering of University of Toronto; 1998.

[13] Chau KT, Wong RHC, Wu JJ. Coefficient of restitution and restitution and rotational motions of rockfall impacts. *International Journal of Rock Mechanics & Mining Sciences* 2002; 39:69-77.

[14] Stead D, Eberhardt E, Coggan J, Benko B. Advanced Numerical Techniques in Rock Slope Stability Analysis-Application and Limitations. in *Proceeding of Landslides-Causes, Impacts and Countermeasures, Davos, Switzerland*, June 2001,pp. 615-624.

[15] Gunzburger Y, Merrien-Soukatchoff V, Guglielmi Y. Influence of daily surface temperature fluctuations on rock slope stability: case study of the Rochers de Valabres slope (France). *International Journal of Rock Mechanics & Mining Science* 2005; 42: 331-349.

[16] Coggan JS, Stead D, Eyre JM. Evaluation of techniques for quarry slope stability assessment . *Trans. Institute Min. Metall. Sect. B*, 1998 ; 107:139-147.

[17] Cundall PA. .Discontinuous Future for Numerical Modeling in Soil and Rock. In proceeding of third International Conference on Discrete Element Method- *Geotechnical Special publication*, 2002; No. 117

[18] Itasca Consulting Group; Inc. 1999; PF3D Manuals.

[19] Ng TT. Input Parameters of Discrete Element Methods. *Journal of Engineering Mechanics* 2006; 132(7):513-521.

[20] An B. A study of energy loss during rock impact using PFC2D. *M.Sc.* thesis submitted to University of Alberta: *Edmonton ;*2006.

[21] Gilardi G , Sharf I. Literature survey of contact dynamics modeling. *Mechanism and Machine Theory* 2002; 37(10): 1213-1239.

[22] Pedrami R. Hybrid Modeling and Simulation of Bodies in Contact Bodies in Contact. MASc. thesis ,department of mechanical & industrial of *Concordia University*; 2005.

[23] Strong WJ. *Impact mechanics*. Cambridge University Press: Cambridge; 2000.

[24] Goldsmith W. *Impact: The Theory and Physical Behaviour of Colliding Solids*. Edward Arnold Publishers Ltd: London, 1960;

[25] Pfeiffer TJ, Bowen, TD. Computer simulation of rockfall. Bulletin of the Association of Engineering Geologist 1989; XXVI (1):135-146.

[26] Hertz H. On the contact of elastic solids. *Journal Reine und Angewandte Mathematik* 1882; 92: 156-171.

[27] Mindlin RD. Compliance of Elastic Bodies in Contact. *ASME Journal of Applied Mechanics* 1949; 16: 259-268.

[28] Vu-Quoc L, Zhang X, Lesburg L. Normal and tangential force-displacement relations for frictional elasto-plastic contact of spheres. *International journal of Solids and Structures* 2001; 38:6455-6489.

[29] Johnson DL, Norris AN. Rough elastic spheres in contact: memory effects and the transverse force. *Journal of Mechanics and Physics Solids* 1997; 45(6):1025-1036.

[30] Mindlin RD, Deresiewicz H. Elastic Spheres in Contact under Varying Oblique Forces. *ASME Journal of Applied Mechanics* 1953; 20: 327-344.

[31] Cundall PA, Strack ODL. A discrete numerical model for granular assemblies. *Geotechnique* 1979; 29:47-65.

[32] Elata D, Berryman JG. Contact force-displacement laws and the mechanical behaviour of random packs of identical spheres. *Mechanics of Materials* 1996; 24: 229-240.

[33] Cundall, PA .Computer Simulations of Dense Sphere Assemblies, Micromechanics of Granular material. *Elsevier Science Publishers,* 1988.

[34] Fu Y. Experimental quantification and DEM simulation of micro-macro behaviours of granular materials using X-Ray tomography imaging. PhD thesis, Depatment of civil and environmental of Louisiana State University and Agricultural and Mechanical College; 2005.

[35] Azzoni A, de Freitas MH. Experimentally gained parameters, decisive for rockall analysis. *Rock Mechanics and Rock Engineering* 1995, Springer-Verlag; 28(2):111-124.

[36] Huang H. Discrete Element Modeling of Tool-Rock Interaction. PhD thesis submitted to University of Minnesota; 1999.

[37] An B, Tannant DD. Discrete element method contact model for dynamic simulation of inelastic rock impact. *Computers & Geosciences* 2007; 33: 513-52.

[38] O"Sullivan C, Bray JD. Selecting a suitable time step for discrete element simulations that use the central difference time integration scheme. *Engineering Computations* 2004; 21(2/3/4): 278-303.

[39] Di Renzo A, Di Maio FP. An improved integral non-linear model for contact of particles in distinct element simulations. *Chemical Engineering science* 2005; 60:1303-1312.

[40] The Applied Seismology Laboratory and professor Young's group. *Useful information for seismology and rock mechanics. Liverpool.* Source: http://www.liv.ac.uk/ seismic /links/info.html (accessed June 2007)

[41] Potyondy D, Cundall PA. A Bonded-Particle model for Rock. *International Journal of Rock Mechanics and Mining Sciences* 2004; 41:1329-1364.

[42] Fakhimi A, Villegas T. Application of dimensional analysis in calibration of a Discrete Element Model for rock deformation and fracture. *Rock Mechanics and Rock Engineering* 2007; 40(2):193-211.

[43] RocFall Verification manual, rocscience Inc., 2002

[44] Izadi HA, Pakmehr M, Moghaddam MM . Designing autolanding Neuro-Controller using PID and optimal strategies. *Journal of Aircraft* 2006; 43(1):91-101.